Local Physical and Hydraulic Factors affecting Leaf Retention within Streams

Laura Rh. B. Trodden M.A.(Oxon) M.Sc

This thesis is submitted to Cardiff University in accordance with the requirements for the degree of Doctor of Philosophy.

April 2012

ABSTRACT

Annual allochthonous leaf litter inputs to temperate headwater streams provide a major contribution to the energy and carbon dynamics of the system, with whole seasonal cycles being determined by leaf litter inputs. Although a number of different physical and hydraulic factors have been linked to leaf retention, the mechanism of leaf retention has not been fully quantified.

A series of flume experiments investigated how leaf retention and the flow structure varied with bed heterogeneity, boulder submergence and boulder density. Two set-ups were used; a flat bed consisting of two physically different substrates, sand and pebbles, under the same 'global' conditions and an idealised situation using uniformly sized concrete hemispheres placed in a staggered array directly on the flume bed, where the boulder submergence and density was varied systematically for a constant discharge. Saturated leaves were added, with retention number and locations being recorded. Detailed three-dimensional velocity measurements were taken throughout a control volume.

Significantly higher retention was observed on the larger substrate and the presences of protrusions were found to be important. Boulder density was significantly related to both the retention efficiency and retention per boulder with an optimum density occurring at the intermediate density. Flow depth was found not to be significantly related to any measure of retention.

The presence of the boulders generated a number of previously identified coherent structures within the flow. Increase in boulder density produced larger wakes, stronger cross-streamwise and vertical velocities and increased TKE within the boulder flow layer. The flow structure did not change with boulder submergence but with increasing boulder density it changed from isolated boulders with separate wakes to wake-interfering flow where the wakes of adjacent boulders were observed to 'overlap'. A strong relationship was exhibited between the spatially-averaged near-bed shear stress immediately upstream of the boulder and retention. Retention increased as the shear stress neared zero, and decreased with both large negative and positive shear stresses.

Maximum retention occurred under isolated flow conditions, with an increase in density providing increased retention due to a greater number of retention locations. However, a change in flow conditions to wake-interaction resulted in a decrease in retention.

DECLARATION

This work has not previously been accepted in substance for any degree and is not concurrently submitted in candidature for any degree.

Signed: .... (Candidate) Date:.......................................

Statement 1

This thesis is being submitted in partial fulfilment of the requirements for the degree of Doctor of Philosophy.

Signed: .... (Candidate) Date:.......................................

Statement 2

This thesis is the results of my own independent work/investigation, except where otherwise stated. Other sources are acknowledged by explicit references.

Signed: .... (Candidate) Date:.......................................

Statement 3

I hereby give consent for my thesis, if accepted, to be available for photocopying and for inter-library loan, and for the title and summary to be made available to outside organisations.

Signed: .... (Candidate) Date:.......................................

ACKNOWLEDGEMENTS

I would like to thank both my supervisors, Catherine Wilson and Steve Ormerod, for their guidance, help and support over the course of my PhD, and for their invaluable comments on this thesis.

I would especially like to thank my wonderful husband for making the completion of this PhD possible and bearable, and allowing me to complain at length on a daily basis. I really appreciate him reading the many drafts and am now sure he probably knows it better than me.

Lastly to all my family and friends that have supported me through this process, thank you, and I now promise you will no longer have to hear the words thesis and PhD.

CONTENTS

LIST OF FIGURES

LIST OF TABLES

NOTATION

The following symbols are used throughout this thesis;

β	Proportionality constant of mixing length
δ	Boundary layer thickness
κ	von-Karman constant
μ	Dynamic viscosity
ν	Kinematic viscosity
ρ	Density
τ	Bed shear stress
ϕ_{xyz}	Boulder volume fraction (referred to as volume boulder density on the graphs)
A	Cross-sectional area
b	Width
C_D	Drag Coefficient
d, D	Object diameter
D_{50}	Median particle size
E_R	Retention Efficiency for individual test, calculated as the number of leaves retained divided by the number added
$\bar{E}_R$	Mean Retention Efficiency
$\bar{E}_{RB}$	Mean Retention Efficiency per Boulder
F_D	Drag force
Fr	Froude number
g	Gravity
h	Boulder height
k	Roughness height
k_R	Retention coefficient (m^{-1})
L	Characteristic length (used in the calculation of Reynolds number)
L_0	Total number of leaves
L_i	Leaves retained at distance i
n	number of boulders
n	Mannings n

$P_R(x)$	Probability of leaf retention at distance x
$P_R(i)$	Probability of leaf retention at distance between zero and x
$P_T(x)$	Probability of leaf transport to distance x
q	Discharge per unit width
Q	Discharge
Q_M	Measured discharge
Q_A	Calibrated discharge
R	Hydraulic Radius
Re	Reynold Number
Re_d	Stem Reynold Number
s	Standard deviation
S, S_o	Bed slope
S_f	Energy slope
S_w	Water surface slope
S_x	Longitudinal boulder spacing
S_y	Lateral boulder spacing
T_m	Mean transport distance $(1/k_R)$
T_T	Distance required for 99% of leaves to be retained
T_x	Transport distance
u, v, w	Instantaneous velocities in the three dimensions (longitudinal, transverse and vertical)
$\bar{u}, \bar{v}, \bar{w}$	Time-averaged velocities in the three dimensions
u', v', w'	Fluctuating velocity components in the three dimensions
$Urms, Vrms, Wrms$	Turbulence intensities in the three dimensions
$\bar{U}_z, \bar{V}_z, \bar{W}_z,$	Depth-averaged velocities in the three dimensions
$\bar{U}_{BL}, \bar{V}_{BL}, \bar{W}_{BL}$	Boulder layer depth-averaged velocities in three dimensions
$< \bar{U} >, < \bar{V} >, < \bar{W} >$	Spatially-averaged velocities in the three dimensions
$\bar{U}_{xyz}, \bar{V}_{xyz}, \bar{W}_{xyz}$	Globally-averaged velocities in the three dimensions
$\bar{U}$	Area Mean Velocity
$\bar{U}_{Blockage}$	Area Mean Velocity taking into consideration the area reduction due to the presence of the boulders
$\bar{U}_{bed}$	Near-bed streamwise velocity (within 10mm of the bed)
U_*	Shear Velocity
U_∞	Free Stream Velocity
V	Velocity
x	Distance in longitudinal direction
y	Distance in transverse direction
z	Distance in vertical direction
z_0	Flow depth
z_c	Critical flow depth
z_n	Normal flow depth

BIOLOGICAL TERMS

The following biological terms are used throughout this thesis;

Abscission	The process whereby a plant drops one or more parts, e.g. leaves.
Allochthonous	Material that originates somewhere other than where it is found.
Autotrophic	Organisms with the ability to create organic compounds from inorganic sources of energy, such as light, e.g. plants.
Collectors	Organisms within a stream that are capable of removing and collecting fine particles from the water as a source of food.
Colonisation	The process whereby microorganisms move onto a leaf.
Ecosystem	The community of organisms that interact with each other and the environment within which they live and interact.
Heterotrophic	Organisms that are not capable of fixing carbon and are therefore reliant on organic sources of carbon for energy.
Metabolism	The sum of the physical and chemical reactions that occur in a living organism, that allow the creation of molecules required for growth.
Organic Matter	Matter that has come from a living organism and that is capable of decay.
Pre-conditioning	Physical or biological activity that has occurred prior to the leaf being broken down within a stream.
Processed	The leaf has been subject to biological and physical processing and all nutrients have been released
Producers	Organisms that are capable of fixing carbon and therefore create the base of the foodweb.
Protozoans	Group of single-cell mobile organisms.
Scrapers	Organisms within streams that are able to remove algae from surfaces as a source of food.
Shredders	Organisms within streams that process organic material, such as leaves, as a source of food and reduce them to smaller particles.

1

INTRODUCTION

Interdisciplinary research has received considerable attention and support over the past decade. The key advantage is that it allows problems present within a research area to be investigated using the combined knowledge of different subjects. Researchers from a different subject area might be able to shed new light on a problem by investigating it from a different angle. The effect of the flow on the ecology present within a stream is not a new area of research (e.g. Edington, 1968; Hynes, 1970; Young et al., 1978), however focus on it from biologists, engineers and geomorphologists has increased in recent years, leading to the coining of the name 'Ecohydraulics' (Lancaster and Downes, 2010*b*). Despite this increased recognition in the overlap between the research of environmental engineers and stream ecologists, there is still separation of the research and the publication of results.

Concern has been raised (Lancaster and Downes, 2010*b*,*a*) over the quality of the research in the field, and whether enough stall is put on the presence of 'strong ecological content'. Research has focused on the creation of habitat preference models created by relating survey data to physical or hydraulic variables, referred to as abundance-environmental relationships (AERs). However, these models are then used to predict the changes in populations in response to a change in environmental conditions. The limitations of these models must be understood in order for them to be used correctly, and care must be taken when inferring relationships between hydraulic and ecological factors. Most importantly, both ecological and hydraulic factors must be given equal weight and consideration when conclusions are drawn.

Stream ecosystems are unique habitats, with specialised organisms designed to live within them (Giller and Malmqvist, 1998). The unidirectional nature gives them a unique spatial linkage, with upstream regions affecting downstream regions, but not vice versa (Tank et al., 2010). Variation in the flow conditions due to seasonal variation results in a changeable channel morphology, creating spatial variation at a number of scales. This spatial variation of the bed within itself will then affect the flow conditions present, making it hard to separate the effects of the physical and hydraulic characteristics on the ecology. The development of the River Continuum Concept (RCC) suggested that the physical changes that occur along the length of river are responsible for defining changes in the biological communities and dominant organic matter, generating testable hypotheses that research could focus on (Vannote et al., 1980).

The generalised structure and function of a stream ecosystem has been well documented (e.g. Hynes, 1970; Cummins, 1974; Cummins et al., 1995; Giller and Malmqvist, 1998). For over four decades, the dependence of temperate stream ecosystems on inputs of allochthonous organic matter, primarily leaves, to provide energy and carbon has been well recognised (Fisher and Likens, 1973; Cummins, 1974; Young et al., 1978; Webster et al., 1987). Leaf litter within streams provides a direct source of food for the numerous heterotrophs present, however their processing of the material into smaller constituents also releases nutrients and energy, for use by other organisms. The dependence is so strong that seasonal cycles exist which are determined by the input of leaf litter (Hladyz et al., 2011). However, in order for the processing to occur, the leaves must be retained within the system, otherwise they are lost and downstream organisms derive the benefit. The processing of the leaf litter can be used as an indicator of the function and health of a stream, therefore it generates continued interest. But despite the importance of leaf litter inputs, the exact hydraulic or physical factors that determine the retention of leaves have not be fully quantified.

Both physical and hydraulic factors, such as characteristics of the leaves (e.g. Webster et al., 1987; Hoover et al., 2010), flow depth (e.g. Webster et al., 1994), gradient (e.g. Larrañaga et al., 2003), stream discharge (e.g. Young et al., 1978; Webster et al., 1999; Larrañaga et al., 2003) and instream structures or protrusions (e.g. Webster et al., 1987, 1994; Ehrman and Lambert, 1992; Hoover et al., 2010), have been linked to retention of leaves, but the mechanism of retention has not been identified. The importance of hydraulic factors has been suggested in relation to other ecology distributions, such as fish habitats (Shamloo et al., 2001), macro-invertebrate distributions (Hart et al., 1996) and predator-prey relationships (Lacey and Nikora, 2008) within streams and therefore it is logical that these same factors will control the retention of leaves.

Without knowledge of how these important sources of carbon and nutrients are retained within streams, the consequences of changes to the physical structure and hydraulic characteristics of a stream, or even the removal of riparian vegetation, can not be fully understood. Sustainable river management and river restoration needs to be based on strong scientific theory (Rice et al., 2010a). Satisfactory maintenance of a river or the restoration of those that have been damaged or altered requires a firm understanding of how the stream ecosystem is created by, and maintained by, both the physical and hydraulic characteristics. If leaf litter can not be retained within temperate headwater streams, then the ecosystem and food-web structure will suffer. Comparisons between restored and natural streams have illustrated that the knowledge at present is not sufficient to restore a stream, once changed, back to its natural state (Muotka and Laasonen, 2002).

It is well established that the effects of a changing climate will result in temperate regions receiving increases in temperature and rainfall. Variation in the temperature will change the timing of the seasonal progression, which could result in a delayed or more rapid leaf drop within the autumn. The seasonal dependence of stream ecosystems on leaf litter inputs is documented, and therefore without an understanding of how the leaves are retained, the effects of a shift in this seasonal cycle can not be suggested. Increased rainfall will have major consequences on the discharge of streams; it could result in more exaggerated seasonal patterns, or the increased frequency of low return period discharges. Increases in discharge and storm events are known to negatively affect the retention of leaves, with leaf transport distances being related to the peak discharge during a storm (Webster et al., 1987). However increased discharges are also associated with increased streamwise velocities and increased flow depth, the exact effect of which has yet to be identified. The combined effects of a narrow leaf drop window and increased frequency and magnitude of storm events could have serious effects on the health of streams due to the inability to retain the organic material. Without full understanding of the mechanisms of leaf retention, action can not be taken to prevent the effects of the changing climate.

The retention of leaves at particular locations allows organisms within the stream to breakdown the leaves, releasing carbon and nutrients for use by other organisms, and therefore creating local regions of high nutrient status. The breakdown rates of leaves under various conditions have been well researched. The knowledge of retention locations, or the factors that created a retention location, and the number of leaves that a particular location could retain, would allow the retentiveness of a stream reach to be analysed, and therefore the calculation of carbon capture, and nutrient availability, purely from leaf litter input. This information could also be used in nutrient modelling for streams and rivers, to allow for the bulk nutrient status of a reach or even to create small local input locations within the model.

1.1 Aims

This thesis investigates the local physical and hydraulic factors affecting leaf retention and therefore aims to improve the understanding of the mechanism of leaf retention within streams therefore allowing improvements to be made to river management and restoration methods, and reducing any undesirable effects of future climate change. This will be achieved through a series of flume experiments, which will allow the systematic investigation of the effects of bed heterogeneity, protrusion submergence and the density of protrusions in isolation from other factors. The specific aims of this thesis are:

- To identify whether there is a difference in retention between two physically different bed materials under the same 'global' conditions.
- Identify the effect of boulder submergence and density on leaf retention.
- Identify to what extent retention is defined by the probability of contact with a protrusion.
- Identify whether the interacting effect of adjacent boulders is related to leaf retention.
- Identify the flow structures present within an array of boulders.
- Identify how the wake size and structure of a boulder is affected by boulder submergence and density.

1.2 Thesis Outline

This thesis presents a series of flume experiments that investigate the method of leaf retention within streams, examining both physical and hydraulic factors. A key factor of this research is that the physical and hydraulic characteristics of a stream are intrinsically linked, making the separation of the causing factors difficult. **Chapter 2** presents an overview of a stream ecosystem, describing the input of energy to the system, and its use. The importance of leaf inputs is discussed along with the importance of the retention of this material to enable the system to benefit. Previously researched links between both hydraulic and physical parameters and leaf retention are presented. Active retention on different structures is an important feature, and therefore how these structures, influence the flow is discussed. The methods of characterising the flow within a stream are discussed along with the scale of which measurements can be taken and parameters can be applied.

Chapter 3 describes the consistent methods and equipment that will be used to investigate the factors involved in leaf retention, such as the flume and its setup, how velocity measurements will be taken, and the description of bed material that will be used. Full details of each piece of equipment are given along with the results of any calibration carried out, and the details of how measurements will be taken in Chapters 4, 5 and 6.

Chapters 4, 5 and 6 present the experiments carried out, the results and their discussion and the conclusions that were drawn. **Chapter 4** investigates the retention characteristics of two physically different substrates, sand ($D_{50} = 0.93$mm) and pebbles ($D_{50} = 28$mm), under the same 'global' conditions. The use of a flat bed allows the effect of the size of the substrate to be isolated from the effects of the bedforms they create in natural systems. Saturated leaves were added to the flume and the settlement locations recorded to allow the patterns of retention to be examined. Four locations of high retention were chosen where more detailed analysis was carried out by measuring the bed profile, and taking detailed three-dimensional velocity measurements, the results of which could be used to examine the method of retention.

Chapter 5 investigates how the retention of leaves is affected by both boulder submergence and density in an idealised situation. Concrete hemispheres, used as an analogue to boulders, were placed in a regular staggered array, where the lateral and longitudinal spacing was changed to vary the density. Saturated leaves were added, with the distribution and number of retained leaves being recorded. The variation in the retention characteristics of the different combinations of boulder density and flow depth are compared through the presentation of the retention efficiencies, coefficients and distributions.

Chapter 6 investigates the effect of the boulders on the flow and how this effect changes with boulder densities and submergence. The range of densities used allows the effect of both isolated and interacting boulders to be examined. Visualisation of the flow was carried out using detailed three-dimensional velocity measurements within a control volume, and through the calculation of mean velocities and turbulence statistics, which allow comparison between the different boulder densities and flow depths. The results of the flow visualisation are then linked to the results presented in Chapter 5, linking the ecological to the hydraulics.

Chapter 7 summarises the conclusions presented within this thesis and presents the ideas for further research.

2

FLOW AND LEAF RETENTION WITHIN STREAMS

Temperate headwater streams require terrestrial sources of organic material to provide energy to support the ecosystem. Inputs of organic matter have two possible fates; retention or export. Retention of the organic matter allows it to be directly used as a food source by a range of heterotrophs, while their actions release energy and nutrients for use by other organisms. Therefore the presence of retentive structures or protrusions, such as boulders, and pebble clusters are an important stream feature. The rate of retention of organic matter has been related to discharge, flow depth and bed complexity within streams; however the variation within flow conditions and experimental methods makes comparison between studies difficult. Streams are governed by free surface flow, and therefore open channel flow parameters can be used to define conditions at both 'local' and cross-sectional averaged scales. Researchers have simplified bed forms and protrusions to examine the effects on flow conditions in laboratory experiments, with boulders being approximated to hemispheres in flume experiments. Examination of the flow around a hemisphere has identified the presence of a horseshoe vortex immediately upstream of the base of the hemisphere. Separation of the boundary layer near the crest of the hemisphere creating 'arch' shaped separation vortices that rotate down towards the reattachment point from which they are shed as hairpin vortices, which then travel towards the water surface. The size of the wake has been seen to be affected by the level of upstream turbulence and obstacle density and can be characterised as a fraction of the flow volume.

2.1 Introduction

There has been a large promotion of interdisciplinary research over the past decade. One such area is the subject of this thesis, which lies at the interface between the engineering principles of fluid mechanics, and the biological field of stream ecology, in particular investigating the impact of physical and hydraulic aspects of a stream on the ecology present. Although research examining the effects of flow on stream organisms is not a new concept, the research area has expanded in recent years (Rice et al., 2010b), and the name 'Ecohydraulics' has been coined (Lancaster and Downes, 2010*b*).

Analysis of research in this area has led to what some consider (e.g. Lancaster and Downes, 2010*b*; Rice et al., 2010a) a number of worrying discoveries, and the initiation of a debate. There is discontinuity in the research despite the interdisciplinary nature, with a distinct lack of cross over when it comes to the publication of research. Researchers are continuing to publish in journals specifically related to their discipline, with engineers and biologists publishing separately despite the similarity of the subject matter. In particular, the predominant number of papers using the word 'Ecohydraulics' have been published in engineering journals (Rice et al., 2010b), however this does not suggests that this research is not published within biological journals, just that if it is then this phrase is not used.

The second concern involving Ecohydraulics research has been raised by Lancaster and Downes (2010*b*) in a recent review paper produced for a special issue of 'River Research and Application'. Lancaster and Downes (2010*b*) suggest that a substantial proportion of the research in this field lacks the 'strong ecological content' that is expected from the nature of the discipline, a concern that is shared by Rice et al. (2010a). However Rice et al. (2010a) suggest that collaborations need to occur not only between hydraulic engineers and stream ecologists but also fluvial geomorphologists, due to the overlap in expertise and research areas.

Lancaster and Downes (2010*b*) suggested that too much emphasis is placed on habitat preference models, generated from survey data, collectively referred to as abundance-environmental relationships (AERs), which correlate small-scale species densities to some physical or hydraulic variable. These models are then used to generate habitat association models (HAMs), which in turn are used to predict changes in populations in relation to changing conditions, such as the impacts of climate change, and therefore develop management strategies (Lancaster and Downes, 2010*b*). However, it is suggested (e.g. Lancaster and Downes, 2010*b*; Rice et al., 2010a) that the use of AER to predict population densities, and the change to those densities under changing environmental conditions, is ultimately flawed as population dynamics need to be described by four vital rates, birth, death, immigration and emigration, which if not included makes population assumptions invalid.

Lancaster and Downes (2010*b*) discuss a number of limitations of AERs, such as causation of relationships, generalisation of models and biological interaction, suggesting that their usefulness, if not carried out correctly, is limited. Care must be taken when assuming causation; it is necessary that causation is proved and not assumed merely due to the presence of a relationship between a variable and abundance. It is often assumed that organisms that are present within a stream live under optimum conditions, and that their tolerance is limited to a narrow range. Although some organisms have a well defined response to, for example, velocity, others operate on a threshold relationship, above or below which they can not survive (Lancaster and Downes, 2010*b*). Therefore instead of fitting 'optimal' relationships represented as best-fit lines, relationships with chemical or physical gradients should be described as limiting relationships, for example maximum and minimum tolerances.

To allow the application of AER's to the management of streams, generalised AER models need to created across model sites, and from multiple experiments. It is assumed that the shape of the relationship to a variable is consistent for all situations; however Lancaster and Downes (2010*b*) suggest that the response of the organisms to a specific variable can change between different situations, due to the interaction between the number of physical and chemical gradients present within the ecosystem. The last limitation is ignoring the presence of biological interactions. The spatial distribution of one species can have a direct effect, due to competition or predation, on the spatial distribution of another species, which if ignored makes the assumptions of an AER incorrect. Lancaster and Downes (2010*b*) do not state that AERs are of no use, merely that all assumptions and relationships that are developed need to be based on sound and detailed ecological theory, as well as sound hydraulics, to allow them to be of use.

As would be expected, the suggestions of Lancaster and Downes (2010*b*), in particular the criticism of AERs, were not taken favourably and were dismissed in a discussion paper response by Lamouroux et al. (2010), who accused Lancaster and Downes (2010*b*) of going "too far in their criticism". Lamouroux et al. (2010) used the study of Dolédec et al. (2007) to illustrate the existence of generalisation. They state that out of 151 taxa the fact 14 taxa have a generalised AER that explains greater than 50% of their log-density variations among the microhabitats, and 41 taxa where the generalised AER explains greater than 30% of the variation, illustrates that generalised AER are valid and that many taxa have repeatable AERs. However, looking at these statistics from another perspective shows that 72.8% and 90.7% of the taxa had site-averaged AERs that explained less than 30% and 50% of the density variation respectively. However it could be suggested that for a model to be deemed successful, more variation should be explained than unexplained (50%), but this is not true for the majority of taxa cited in the study by Dolédec et al. (2007).

Lancaster and Downes (2010*b*) themselves provided two examples of what they deemed to be good practice, where there was a good synthesis of biology and hydraulics. Lamouroux et al. (2010) deemed these examples to both neglect the complexity of ecological processes, and be too complex to be of any use to stream management. However Lancaster and Downes (2010*a*) defend their examples, and suggest that Lamouroux et al. (2010) criticism of their review failed to address the concerns that were raised and merely defended the 'status quo'. This is an on going debate, however, the author believes that the concerns of Lancaster and Downes (2010*b*) are valid, and that care must be taken to ensure that ecology and hydraulics are given equal standing within this field of research. Engineers must ensure they consider the biological implications of the relationships they suggest, and biologists need to ensure they take hydraulic measurements to the same standard and detail as hydraulic engineers.

The introduction to this chapter has been presented to provide context to the interdisciplinary nature of this research, and stress the need to treat each subject within the field with equal care. This chapter will outline both the ecological and hydraulic knowledge and research that is relevant to the subject of this thesis. First, stream ecosystems will be discussed so that the role of leaves within the ecosystem can be identified, and it will be illustrated why their retention is of interest. The current research relating to the retention of leaves will be discussed, providing the context for the research that will be presented in later chapters. As we are concerned with the effect of the physical and hydraulic conditions on the leaves, the flow within streams will be discussed along with the parameters that can be used to quantify conditions at a local scale, as well as how the physical characteristics might influence the local hydraulic conditions. In particular we will focus on obstacles within the flow, and how the flow changes with proximity of boulders, investigating the turbulent development of a wake, and how at dense configurations of boulders the multiple wakes interact.

2.2 Stream Ecosystem

A stream ecosystem is a unique habitat in a number of ways; it has a changeable channel morphology, a large degree of spatial variation at all scales, there are specialised organisms designed to live in this habitat, and there is a large degree of variability between streams (Giller and Malmqvist, 1998). Streams also have a unique spatial linkage that links the upstream and downstream ecosystems throughout a stream network, however this is a unidirectional link, in which upstream material is transported downstream (Tank et al., 2010). A river system consists of a pattern of tributaries that come together to form the main stream, where the location of an individual stream within this hierarchy can be described by the order of the stream (Hynes, 1970). First order streams are unbranched headwater, with no tributaries and are the smallest of a stream network. When two first-order streams meet and join they form a second-order stream, and when two second-order streams join they become a third order, and so on (Hynes, 1970; Giller and Malmqvist, 1998).

All streams and rivers experience general longitudinal changes, the most obvious is the increase in size, e.g. width and depth, from source to mouth. Moving downstream, the bed slope of the channel generally decreases, and the width, depth and discharge increase (Giller and Malmqvist, 1998). The increase in discharge occurs due to the addition of more tributaries, despite the marked decrease in slope (Hynes, 1970). The increase in size is associated with a decrease in the influence of material from the surrounding area on the functioning of the stream (Giller and Malmqvist, 1998). Variation within the velocity field throughout the river has an effect on the river bed, with high velocities creating regions of scour and lower velocities leading to deposition of bed material. An alternating pattern of habitats is established, consisting of shallow, high velocity 'riffles' where coarse material is present and deeper, slower velocity 'pools' dominated by finer particles (Hynes, 1970; Giller and Malmqvist, 1998).

The River Continuum Concept (RCC) was developed by Vannote et al. (1980), providing for the first time testable hypotheses relating to stream ecosystems towards which research could be focused. The RCC views streams as ecosystems that change along a longitudinal template, with biological adaptations. Although the RCC was developed for temperate forested catchments (Tank et al., 2010), this general concept has been shown, with some degree of modification, to fit a range of settings (Cummins et al., 1995). The template suggests that there are changes in the dominant type of organic matter and biological communities present, in response to physical changes that occur in the river from the headwaters to the river mouth (Cummins et al., 1995). The RCC predicted that in low-order streams, those that are forested headwaters, allochthonous inputs are dominant, while mid-order streams would be dominated by autotrophic production when significant cover was not present, and in high order larger streams, heterotrophic metabolism would dominate as primary production would be light limited (Tank et al., 2010). This in turn will have an effect on the range and dominance of organisms present, for example low order streams will require species categorised as ‘shredders’ to process the coarse particulate organic matter, whereas high order streams will be dominated by ‘collectors’ due to the high levels of fine particulate organic matter (Cummins et al., 1995).

The generalised structure and function of a stream ecosystem is well known, and can be found in a number of freshwater biology and stream ecology textbooks and papers (e.g. Hynes, 1970; Cummins, 1974; Cummins et al., 1995; Giller and Malmqvist, 1998). Although streams contain organisms that have the ability to photosynthesise, temperate headwater streams gain the majority of their organic matter, and therefore energy, from terrestrial sources making them heterotrophic (Cummins, 1974). The majority of the organic matter is processed during autumn and winter, a time period associated with the lowest temperature, demonstrating that the organisms that carry out this process are adapted to work at lower temperatures (Cummins, 1974). The importance of leaf litter inputs is so great that whole seasonal cycles within rivers are defined by them, (Hladyz et al., 2011).

The organic matter from terrestrial environments enters in the form of either Particulate Organic Matter (POM), in particular Coarse Particulate Organic Matter (CPOM), particles greater than 1mm in diameter, or Dissolved Organic Matter (DOM), particles less than 0.45μm in diameter (Cummins, 1974; Tank et al., 2010). CPOM consists of whole and fragments of leaves, twigs, needles, and larger particles such as logs and branches (Cummins, 1974). DOM enters the stream in the form of leachate from surface run-off and groundwater, for example nutrients from fertilisers used in adjacent farmland. Figure 2.1 illustrates the fate of the organic matter within a stream ecosystem. The organic matter has two possible fates; it is either directly exported out of the system, or is processed within the stream reach (Webster et al., 1999). The processing either reduces the organic matter to the constituent compounds or is used directly for biological growth. Loss of organisms from the system, through drift or dislodgement also leads to export of the organic matter. Figure 2.1 also shows that there is some degree of production of matter within the stream from macro and micro primary producers through photosynthesis.

Fisher and Likens (1973) produced one of the first quantified energy budgets for a headwater forested temperate stream in New Hampshire, USA, where they demonstrated that allochthonous material provided greater than 99% of the stream energy, where 44% came from litter and throughfall from the adjacent forest, confirming the idea that stream

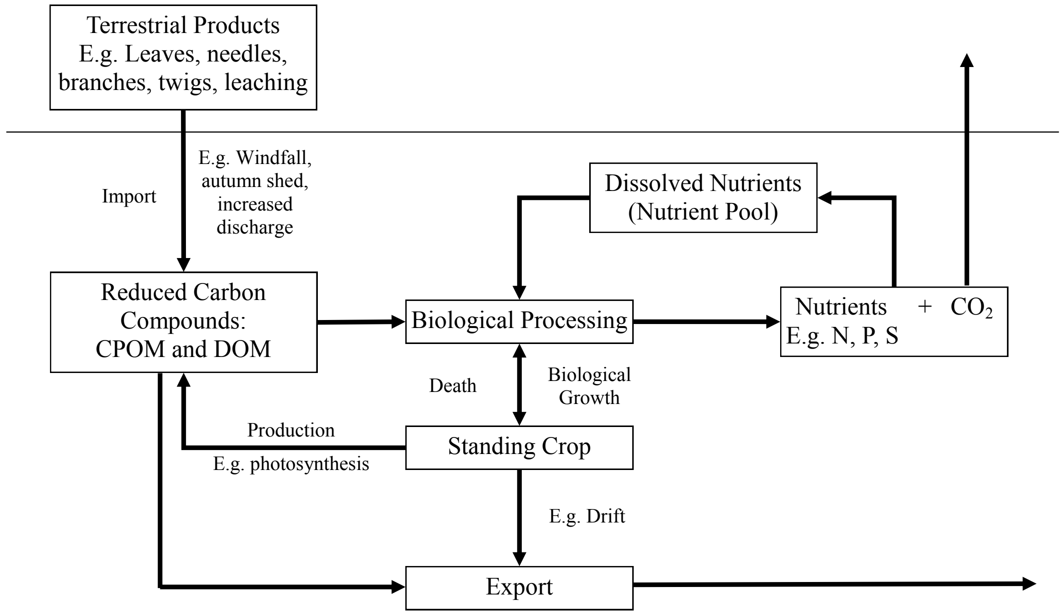

Figure 2.1. The origin and fate of carbon compounds within stream, adapted from Cummins (1974)

ecosystems are dependent on terrestrial imports for their major source of energy. However, 66% of this material was seen to be transported directly out of the system (Fisher and Likens, 1973). Tank et al. (2010) suggested that the conclusion of dependency on external energy sources is drawn because of the bias towards research within headwater streams surrounded by deciduous forest. Low instream production would be expected in these cases due to reduced light availability, suggesting that in lesser vegetated areas internal energy would become more important.

The biological processing of the CPOM, or the food web of the system, can be examined in more detail, an illustration of which is given in Figure 2.2. The majority of processing is the reduction of the CPOM to Fine Particulate Organic Matter (FPOM), particles between 1mm and 0.5μm in diameter, and the extraction of nutrients and energy. On initially entering a stream the terrestrial CPOM is subject to two processes: leaching of soluble components and colonisation of the CPOM by microorganisms, such as bacteria, spores of aquatic fungi and protozoans (Cummins, 1974). After leaching the CPOM consists of a high carbon, low nitrogen substrate. CPOM is then converted to FPOM, through physical and biological means; the action of the water leads to physical abrasion, and the biological action of microbial metabolism and feeding by shredders (coarse particle feeders) (Cummins, 1974). The rate of conversion to FPOM is dependent on the degree of pre-conditioning of the leaves and the conditions of the stream (Cummins, 1974).

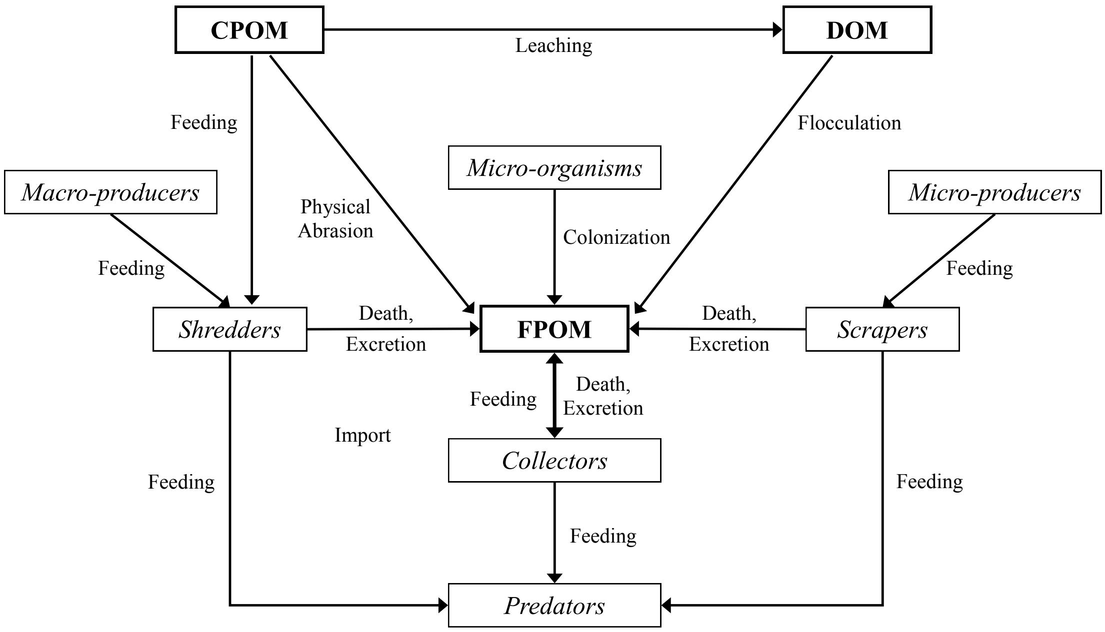

Figure 2.2. Illustration of a stream food web, adapted from Cummins (1974); Cummins et al. (1995), resources are shown in bold and organisms are shown in italics).

Although primary production is low within streams, it does occur via photosynthetic organisms; that is organisms that contain chlorophyll. These can be divided into two groups, microproducers such as algae, and macroproducers such as vascular plants (Cummins et al., 1973). Algae are fed on by specialist organisms, referred to as scrapers, that have the ability to remove algae that is firmly attached to surfaces within the stream (Cummins, 1974). Macroproducers are important for the cycling of nutrients (Cummins et al., 1973), but they do not enter the stream energy system until times of dieback, when they are fed on by shredders, and therefore their energy input follows a similar pathway to that of terrestrial CPOM (Cummins, 1974).

Most FPOM present in streams is the result of the breakdown of larger organic matter (Webster et al., 1999). However, FPOM is also created through the physical flocculation of DOM, and colonies of microbes themselves are referred to as FPOM as they can not be separated from the material they feed on (Cummins, 1974). The organisms that feed on the FPOM are referred to as collectors, as they have the ability to aggregate the particles. The macroconsumers, e.g. shredders, scrapers and collectors, present are dominated by macro-invertebrates, about 3 to 5mm in size (Cummins, 1974). Predators, for example fish, form the top of the food chain, controlling the populations of macroconsumers (Cummins, 1974), and maintaining the balance within the stream ecosystem.

Three parameters are of particular importance for organisms within a stream and therefore the breakdown of organic matter; temperature, oxygen and light (Giller and Malmqvist, 1998; Tank et al., 2010). Temperature varies much more in streams than in lakes, however the variation is over a smaller range (Hynes, 1970). Temperature follows both seasonal and diurnal cycles, with maximum temperatures seen during the afternoon, and minimum temperatures in the very early morning (Hynes, 1970). The physiological processes of freshwater organisms are dependent on the ambient temperature of the water (Giller and Malmqvist, 1998), therefore temperature has a complex effect on stream ecosystems, having an indirect effect on the organisms themselves and a direct effect on the chemical constituents of the stream. Increased temperatures lead to increased feeding and digesting, and therefore increased metabolism and respiration (Giller and Malmqvist, 1998), which in turn increases the biological oxygen demand (BOD). Large amounts of biological activity, e.g. metabolism, decomposition of organic matter, occur at the low temperatures present from later autumn to early spring within streams, however there is still thermal control, e.g. leaf litter is processed 20% quicker at 10°C compared to 5°C. This ability for metabolism to be carried out at low temperatures is not parallelled in terrestrial systems (Cummins, 1974). Another important effect of temperature is that it changes the viscosity of the water, this in turn affects the Reynolds number of the flow and the rate at which sediment settles out (Hynes, 1970), however to have a significant effect it requires a larger change in temperature than is necessary to effect metabolism.

Oxygen is required by organisms for respiration and enters the water through diffusion from the air (Giller and Malmqvist, 1998). The dissolved gases within the stream tend to be in equilibrium with the atmosphere (Hynes, 1970). The solubility of oxygen in water is inversely correlated with temperature, and is therefore affected by the seasonal and diurnal variation. The degree of turbulence within a stream, which is dependent on the Reynolds number, affects the dissolved oxygen concentration, with an increase in turbulence increasing the dissolved oxygen concentration within the water. If plant growth is present then photosynthesis will also increase the dissolved oxygen during the day, and respiration decreases the dissolved oxygen during the night.

Light is necessary for photosynthesis and therefore primary production. The amount of light available is dependent on the time of year, and geographic location (Giller and Malmqvist, 1998). The light available increases with altitude and decreases with the increased presence of riparian vegetation (Giller and Malmqvist, 1998). The turbidity of the water also affects the ability of light to penetrate the water and therefore the degree of light available at different depths. When the flow depth is low, streams are relatively clear, however spates (increased discharge events) increase the amount of suspended material and therefore increase the turbidity and affect light penetration (Hynes, 1970).

A number of factors affect the rate at which leaves are processed within a steam, such as the level of preconditioning and degree of colonisation (Cummins, 1974), where the time required for microbial-animal succession to start and be completed varies for different species (Cummins et al., 1973). Cummins et al. (1995) showed that the processing rate of leaves also varies between leaf species, and therefore suggested that some species would need to be retained longer in order to be processed. As leaf packs occur naturally within streams and generally consist of a number of different species, the decomposition of leaves within a single leaf pack will vary (Tank et al., 2010), but if some species are processed quicker this could lead to destabilisation of the leaf pack, and cause other leaves to be transported before being fully processed. However, transport rates, defined as the inverse of transport turnover time (the time organic matter was retained on stream bed between movements) were found to be substantially higher than the breakdown rates for all sizes of organic matter (Webster et al., 1999). Therefore organic matter is more likely to be transported on from a location than be fully broken down at the location (Webster et al., 1999). Not all reduction in organic matter is associated with organism growth, with some species losing mass despite a reduction in leaf mass (Cummins et al., 1973). Cummins et al. (1973) showed that when shredders and collectors were present together, loss of leaf mass could be primarily due to the feeding of shredders, showing a negligible effect of the collectors on the processing of CPOM. Investigation of the metabolism of leaves under controlled conditions showed processing of organic material to be equally due to mircoorganism metabolism and invertebrate metabolism (Cummins et al., 1973).

The maintenance of water quality within a stream depends on a balance between CPOM, FPOM and DOM, and the organisms that convert the organic matter between the different particle sizes (Cummins, 1974). A stream that travels through an undisturbed woodland is characterised by high productivity (Cummins, 1974). The ability to retain the organic matter, such as leaf litter, affects the ability to process the organic matter and obtain the energy from it; for example retentive structures have been used to reduce the movement and export of the CPOM, in order to increase productivity (Cummins, 1974). A stream of good water quality has the ability to process at least a third of the total organic matter that inputs into the stream. The composition of the riparian zone, the terrestrial ecosystem that borders the stream, can have an overriding effect on the biological response. More information about the literature regarding the dynamics and the metabolism of allochthonous organic matter within streams can be found in the review by Tank et al. (2010).

The recycling of materials within streams is affected by both abiotic factors, e.g. temperature, pH, light, and biotic factors, e.g. feeding rates and excretion. However the major factors are the pattern and properties of the flow and the availability of retentive structures (Cummins et al., 1995). If an upstream section of steam is inefficient at processing or storing material, there is ‘leaching’ to a downstream portion (Cummins et al., 1995). For example, if a region of stream has high retention and high biological activity, then it will recycle nutrients quickly and the effect of the flow moving the organic matter and nutrients downstream is reduced, import of energy and nutrients is greater than export, resulting in a stable ecosystem. However, if retention and biological activity is low, then nutrients are recycled slowly; import matches or is less than export resulting in a less stable ecosystem due to greater competition for resources (Cummins et al., 1995).

The presence of retentive regions or obstacles within the flow will have an effect on the velocity field, and therefore in turn the bed mobility and river morphology. But these regions are also biologically important, providing habitats for organisms or shelter in times of higher discharges (Hynes, 1970). Streams that have many obstacles, or deposition areas, will be able to retain material for longer, which has consequences for the diversity and abundance of organisms present (Giller and Malmqvist, 1998). Leaf packs formed against obstacles, can support greater abundance and diversity of benthic invertebrates than the surrounding substrate (Giller and Malmqvist, 1998).

2.3 Retention of Organic Matter

As discussed in the previous section, the input of terrestrial organic matter provides the majority of a temperate low-order stream’s energy source (Cummins, 1974), the processing of which adds nutrients to the DOM pool (Webster et al., 1987), and the energy allows growth of stream organisms and provides the base of the food chain (Figure 2.2) (Young et al., 1978). The major source of terrestrial input is in the form of CPOM ($>$ 1mm), such as logs, twigs, plant parts, bark, etc, where the largest component is generally riparian leaves (Webster et al., 1999). After entering the stream OM it is either retained, where it can be biological processed, or it is exported from the system, therefore being transported further downstream (Figure 2.1) (Cummins, 1974; Webster et al., 1999).

The ability of the stream to retain the terrestrial material directly affects how much energy the ecosystem can derive from the material (Cummins, 1974; Young et al., 1978; Webster et al., 1987; Tank et al., 2010). Therefore the stream ecosystem is dependent on both passive and active methods of retention, such as backwaters, pools, bank vegetation, rocks, and woody-debris (Webster et al., 1994). Once the material is retained, then the leaves tend to stay where they are retained and be subject to biological and physical processing; however, storm events can dislodge the material, and transport it downstream (Webster et al., 1999). As shown in the previous section, the breakdown of the CPOM leads to the creation of FPOM, and DOM, which is then transported more easily (Webster et al., 1994). The rate of organic matter breakdown is affected by its retention location. Macro-invertebrates have been shown to have strong preferences for certain flow conditions (Bouckaert and Davis, 1998), and therefore material retained in locations accessible to invertebrates can be processed more readily (Hoover et al., 2006). Understanding the mechanisms of retention within a stream will not only allow predictions of resource availability for organic matter budgets, but might also provide insight into the spatial variation of different organisms seen in stream ecosystems (Hoover et al., 2006). The retention of particulate organic matter within streams has been investigated for a number of different sized particles, FPOM (Webster et al., 1987, 1999), CPOM such as leaves (Young et al., 1978; Webster et al., 1987; Ehrman and Lambert, 1992; Webster et al., 1994, 1999; Muotka and Laasonen, 2002; Larrañaga et al., 2003; James and Henderson, 2005; Hoover et al., 2006; Cordova et al., 2008; Hoover et al., 2010) and woody-debris (Ehrman and Lambert, 1992; Webster et al., 1994; James and Henderson, 2005; Cordova et al., 2008).

As leaves are the largest component of the CPOM input (Webster et al., 1999), we will focus on the literature related to their presence within streams. The largest input of leaves to temperate forested streams, occurs at autumn, due to leaf abscission (Fisher and Likens, 1973). Initially on falling, these unconditioned leaves float on the surface, and therefore can be actively retained only on retentive structures that break the water's surface, such as debris-dams, emergent vegetation or protruding boulders (Hoover et al., 2006). Leaves then rapidly absorb water, decreasing their buoyancy, and causes them to enter the water column where they are retained more easily on retentive structures, which could be due to the greater number of obstacles present below the water surface. Webster et al. (1999) suggest that the smaller the OM particle then the more closely related one would expect its movement and transport to be to the movement of sediment. The transport of leaves has not been investigated in the same detail as sediment transport; however, the shape and size of leaves, such as the large surface area, would suggest that they would not behave in the same way.

Although the research into the retention of leaves is limited, a number of field experiments have been carried out to investigate their retention using both real leaves (e.g. Young et al., 1978; Webster et al., 1987; Ehrman and Lambert, 1992; Hoover et al., 2006; Cordova et al., 2008) and artificial leaves (e.g. Webster et al., 1994; Muotka and Laasonen, 2002; Larrañaga et al., 2003; James and Henderson, 2005; Cordova et al., 2008), which have been shown to be effective mimics (Larrañaga et al., 2003; James and Henderson, 2005; Cordova et al., 2008). However very few experiments (e.g. Webster et al., 1987; Hoover et al., 2006, 2010) have been carried out in the controlled environment provided by a flume, where hydraulic and physical characteristics can be manipulated in isolation. There are two suggested methods of retention; either passive retention where leaves settle out in deeper regions where the velocities are decreased, such as dead zones, or deep pools (Hoover et al., 2010), or active retention where the leaves are retained on obstacles or 'retentive structures' within the flow (Ehrman and Lambert, 1992; Cordova et al., 2008).

A number of physical characteristics of a stream have been linked to the retention of leaves; discharge (e.g. Young et al., 1978; Muotka and Laasonen, 2002; Larrañaga et al., 2003), depth (e.g. Webster et al., 1994), bed gradient (e.g. Larrañaga et al., 2003), retentive structures (e.g. Webster et al., 1987, 1994; Ehrman and Lambert, 1992; Larrañaga et al., 2003; Cordova et al., 2008) and substrate type (e.g. Webster et al., 1987; Hoover et al., 2010). Most studies have indicated a negative correlation between discharge and retention (Young et al., 1978; Webster et al., 1994; Muotka and Laasonen, 2002; Larrañaga et al., 2003; Hoover et al., 2006). However, the precise nature of the relationship has been seen to vary with leaf type (Young et al., 1978; Webster et al., 1994), and channel types (Muotka and Laasonen, 2002; James and Henderson, 2005).

Muotka and Laasonen (2002) found that the heterogeneity of the bed affected the degree to which the retention of the system was affected by increases in discharge. The heterogeneity of the bed is inherently linked to discharge as this affects the degree of submergence of protrusions and bed forms. Retention in simplified 'channelised' streams (streams that had been heavily dredged for log transport) did not significantly decrease with discharge, but the natural streams were seen to have the most severe reduction in retention with increase in discharge, (Muotka and Laasonen, 2002). This suggests that the locations available for retention in a simpler channel are more stable locations unaffected by discharge; however, in a natural stream there are regions that can retain leaves when the force on the leaf is low but when the discharge increases the leaves can not remain retained. It is therefore possible that at low discharges leaves can be retained on smaller 'retentive structures', but increased discharges require larger 'retentive structures'. Although the channel type, i.e. surrounding vegetation or bed complexity, was seen to affect the relationship with discharge, Larrañaga et al. (2003) showed that the relationship did not change for the order of the stream, although only streams of orders 1-3 were tested.

The relationship between retention and discharge is also shown in the seasonal variation seen in transport distances and retention, with greater retention in summer and autumn within streams in North Carolina, USA (Webster et al., 1994), which they link to the seasonal variation in discharge. However, Webster et al. (1994) suggest that the greater retention in autumn is related to the larger quantities of leaves that enter streams at that time, suggesting that the formation of leaf packs is increased by the increased volume of leaves within the water column. Higher discharges present within the autumn months will also be associated with higher mean flow depths, which will result in a greater proportion of the bank being in contact with the water, leading to leaves present on the banks also entering the water. Spates (increased discharge events) increase the transport of leaves downstream, with the length of transport being related to the peak discharge of the spate (Webster et al., 1987). However, the volume of matter that is transported during a spate is correlated to the rate of increase of discharge, not the absolute discharge (Webster et al., 1987). This relationship to discharge would be expected, as higher discharges are associated with higher velocities, and it is known that higher velocities are capable of moving larger sized sediment particles. Hoover et al. (2006) suggests that the relationship between discharge and retention could actually indicate a more direct relationship with a variable that varies in relation to discharge, such as flow depth, velocity, or channel width.

A relationship to flow depth, as suggested by (Webster et al., 1994), where leaf analogues travelled further when the depth increased, suggests that the retention is not just affected by the flow of the water, but that it is also dependent on the probability of leaves coming into contact with a 'retentive structure'. This is shown in the difference in retention between riffles and pools, where shallower riffles retained more leaves (Hoover et al., 2006, 2010); however this effect can not be isolated from the greater presence of 'retentive structures' that would be expected in a riffle. The effect of flow depth is more likely to be the effect of relative protrusion, defined as the height of a protrusion or the bed roughness divided by the flow depth, which describes the degree to which the substrate elements protrude into the flow, (Hoover et al., 2006). Despite the investigation of the effect of retentive structures in the retention of leaves, the effect of relative protrusion has not been significantly investigated. Hoover et al. (2006) reported relative protrusions of 0.56–0.92 for riffles and 0.17–0.37 for pools, with greater transport distances in riffles. However, there was a large difference in velocity, with the velocity measured in the riffle approximately five times that measured in pools, and therefore these very low velocities in pools could be responsible for the higher retention observed (Hoover et al., 2006). Muotka and Laasonen (2002) observed an increase in relative roughness from channelised, to restored and natural stream types. Greater retention was seen in the natural streams, where the relative roughness was the highest (0.38), however this was associated with a decrease in discharge compared to the other two stream types.

Larrañaga et al. (2003) found that the majority of analogue leaves were retained on the first obstacle they came into contact with and Hoover et al. (2010) suggested that in riffles leaves were retained when they encountered a protrusion from the bed, with the flexibility of leaves allowing them to wrap around the upstream face. Both Ehrman and Lambert (1992) and Hoover et al. (2010) suggest that the degree of retention is related to the number of obstacles present. But this is contradicted by Webster et al. (1987), who found the presence of obstacles to be significant but the number of obstacles not to be significant.

The obstacles in question were 8cm diameter concrete boulders, however the number used only varied from 1 to 5, which might not have been a great enough range for the number to have a significant effect on retention.

Young et al. (1978) suggested that the number of leaves transported a given distance could be fitted to a negative exponential model;

$$L(x) = L_0 e^{-k_R x} \tag{2.1}$$

where $L(x)$ is the number of leaves in transport at a length x, L_0 is the total number of leaves and the regression coefficient (k_R), or the slope of the relationship, represents the instantaneous rate of entrainment of leaves, or retention coefficient as used by Hoover et al. (2010). This relationship can also be used to generate expected transport distance for the organic matter; for instance, the inverse of the retention coefficient gives the mean transport distance, T_m, the distance at which 63.2 % of the material would have been retained (Webster et al., 1987). This inverse relationship can also be used to calculate the total retention distance (T_T), the distance required to retain 99% of the material (Young et al., 1978). The negative exponential model has been applied in a number of experiments (Ehrman and Lambert, 1992; Webster et al., 1994, 1999; Muotka and Laasonen, 2002; Larrañaga et al., 2003), providing a parameter that allows the retentive characteristics to be compared between streams and experiments. However, as most experiments have been carried out in streams, the hydraulic and physical characteristics of which vary considerably, it would be difficult to isolate the reason for any differences seen in the retentiveness. Under the controlled conditions of a flume, where factors can be varied in isolation, this model of retention could provide a useful tool to compare results.

Young et al. (1978) showed that wet leaves were seen to travel shorter mean distances than dry leaves (192 and 226m respectively) over all their experiments within streams. This is as expected due to the differences in which wet and dry leaves are transported and retained. Wet leaves are much more flexible and able to wrap around obstacles but inflexible dry leaves need obstacles that protrude the water surface to be retained. The importance of flexibility was seen by Hoover et al. (2010), who found the retention of stiff material, such as needles, to be related to the settling velocity of the particle and the turbulence in the stream; however this was not true for leaves, suggesting that their flexibility has an effect on their movement and retention. This was illustrated by the different retention locations of leaves compared to stiff needles, with needles settling in the deeper intersections between protrusions, whereas the leaves were retained by 'wrapping' themselves around the protrusions (Hoover et al., 2010). A difference in transport distance is also seen between leaf species (Young et al., 1978; Webster et al., 1987; Larrañaga et al., 2003). For example, within natural streams Young et al. (1978) found oak leaves travelled further than beech or maple leaves, and Webster et al. (1987) saw dogwood leaves travel further than oak leaves (15.7 and 5.7m respectively). Webster et al. (1994) found the size of the leaves affected their movement, using smaller triangular artificial leaves in smaller streams, because larger rectangular artificial leaves were found to have restricted movement. This difference between species was more significantly tested by Larrañaga et al. (2003) who tested seven leaf species, and plastic strips as an analogue. They found that abscised alder leaves were most easily retained, travelling a mean distance of only 11.2m across 21 reaches, and that sycamore leaves travelled the furthest (50m) with the difference between the two species being significant.

Larrañaga et al. (2003) used the investigation of different leaf species to also investigate the effect of leaf size and shape on transport distances, by analysing the retention. The sycamore leaves were found to be the largest, widest and heaviest leaf species, which could explain their greater transport distance, however the alder leaves were not the smallest (in any measurement) of the leaf species. Although weak trends were observed, evaluating length, width, surface area, perimeter and dry weight, for larger leaves to travel further, a significant relationship was not identified (Larrañaga et al., 2003) . A relationship between size and transport distance has been seen in wood analogues, where dowel length was negatively related to transport distance, suggesting that the increase in length increases the probability of coming into contact with an obstacle (Bocchiola et al., 2006; Cordova et al., 2008). All these experiments (Young et al., 1978; Webster et al., 1987; Ehrman and Lambert, 1992; Larrañaga et al., 2003) suggest that leaves travel only relatively short distances (10-100m) before they are retained and processed, however the variation in the transport distances suggests that there are many factors that influence their transport.

Analysis of transport lengths of organic matter also showed that the degree to which leaves were retained was affected by the complexity of the bed. A simple comparison was carried out by Webster et al. (1987) in a series of flume experiments, where the retention of leaves and their uptake length was measured using the different substrates of pea gravel and artificial turf under the same conditions. The greater complexity or roughness of the gravel resulted in a higher retention of leaves and a shortened transport distance of 7m compared to 12.3m; however, the difference was not found to be significant. The effect of retentive structures was also tested by the presence and absence of obstacles, where the presence of obstacles more than doubled retention, and nearly quartered the mean transport distance. Although the presence and absence of obstacles was significant, the number of obstacles was not found to be significant, however as previously stated the number of obstacles was only varied from one to five (Webster et al., 1987), which is not a significantly large range over which to test the effect of varying obstacle density. However, Webster et al. (1987)

showed that both the presence of obstacles and the complexity of the bed are important factors in aiding retention of leaves, indicated by reduced mean transport distances.

The role of bed complexity in increasing the retention of leaves was confirmed in later research. Ehrman and Lambert (1992) investigated the effects of the presence of woody-debris, and therefore bed complexity, within a stream on retention and transport lengths. Where at least one woody debris dam was present, significantly more leaves were retained than for reaches where there was no woody-debris present or where it was only present within the margins of the stream. The retentiveness of the debris-dam reaches was also shown in the mean transport distances calculated from fitting the negative exponential model, where leaves only travelled a mean distance of 109m, compared to the 125m for edge wood reaches, and 168m for reaches where wood was absent. These experiments were carried out under similar discharges (0.250-0.278 m^3/s) with similar flow depths , however the reaches containing less wood (edge-wood and absent reaches) were reported to have greater velocities ($\approx$ 0.7m/s compared to 0.44m/s), a difference that is not explained by the variation in discharge. Although the flow depth was similar among the reaches, the widths are not given. The discharge was estimated from dye diffusion, and the mean velocity was estimated from the nominal transport time of dye over 50m. The greater volume of wood present at debris-dam reaches could be responsible for the lower estimated velocity due to the retardation of the dye by the presence of the wood, illustrated by the greater hydraulic retention that was measured (Ehrman and Lambert, 1992). It could be suggested that the higher velocities are the reason for the reduced retention in the reduced wood reaches rather than the decreased presence of obstacles, however, more detailed velocity measurements would be needed to confirm this.

The effects of bed complexity were nicely illustrated in a study by Muotka and Laasonen (2002) who compared the retentiveness of three channel types; those that had been 'channelised' or heavily dredged, the same streams after they had been restored, and natural streams that had not been altered. Restoration of the streams endeavoured to reinstate the original heterogeneous bed structure. The bed roughness, relative roughness and mean stone size were seen to increase from channelised to restored to natural streams. Plastic strips were used in the place of leaves, as mimics have been shown to behave similar to real leaves. However, plastics can not absorb water so are therefore more likely to behave like newly fallen leaves rather than saturated leaves that have entered the water column. The authors found that the retention efficiency (number strips retained divided by the number added) of the streams was improved ($\approx$ 25% compared to 8%) after restoration but that natural streams still retained significantly more ($\approx$ 60-75%). The variation in retention matches the variation in relative roughness with higher retention related to higher relative roughness. The data for the channelised and restored streams was comparable due to very similar discharges, mean velocities and flow depths, however in the natural streams the discharge was lower, along with a shallower flow depth and lower mean velocity which could be responsible for the greater retention observed. Futhermore, the restoration was associated with a decrease in the presence of moss, which in natural streams was the most retentive structure. The importance of different retentive structures will be discussed later in this section. The negative exponential model was applied, finding that the retentive coefficients were significantly higher for the natural streams. However, in applying the model the authors did not fix the intercept of the model so that 100% of the leaves were in transport at the release point, making the retention coefficients not comparable to those calculated in later chapters of this thesis.

When retention is compared between riffles and pools within a stream, Hoover et al. (2006) found the pools to be more retentive, as shown by much shorter mean transport distances, despite the greater bed complexity associated with riffles. However in these experiments, like in most streams, the pools were deeper and had much slower mean velocities. It can therefore be suggested that the retention in these regions was passive, whereas retention in the faster riffles requires the presence of retentive structures, suggesting that the spatial distribution and density of these structures might be important. This idea was supported by less variation being seen in the transport distances of pools than riffles, suggesting that the passive retention is more consistent, the distance being controlled by the weight of the leaf and velocity of the water (Hoover et al., 2006). Larrañaga et al. (2003) could not distinguish a difference in retention between pools and riffle in base flows, however in high flow situations, such as a flood, riffles became much more retentive, and the retentiveness of pools decreased.

Numerous 'retention structures' have been identified within the literature; protrusions, such as boulders and pebble clusters (Ehrman and Lambert, 1992; Muotka and Laasonen, 2002; Larrañaga et al., 2003; James and Henderson, 2005; Hoover et al., 2006), woody-debris (Ehrman and Lambert, 1992; Muotka and Laasonen, 2002; Larrañaga et al., 2003), debris-dams (Ehrman and Lambert, 1992), backwaters or pools (Ehrman and Lambert, 1992; James and Henderson, 2005), and instream and bank vegetation (Ehrman and Lambert, 1992; Muotka and Laasonen, 2002; James and Henderson, 2005); however the effectiveness of these structures varies between streams and is dependent on the presence of other structures. Ehrman and Lambert (1992) found debris-dams, when present, to be the most important retentive structure; however when these were not present large wood debris became important, with roots and backwaters being the most important in a non-wooded stream. Backwaters were highly retentive structures in each of the three reaches (debris-dams, edge wood, and non-wooded), it could be suggested that this is not a retentive structure *per se*, instead it would be expected that retention in pools and backwater is a passive process due to the increased flow depth and reduced velocities, and therefore the presence of wood would have little effect on the ability of this region to retain leaves. Rocks were not found to be an important structure in any of the tested streams (Ehrman and Lambert, 1992), however the relative submergence (flow depth divided by the height of the structure) of these rocks was not stated, but flow depths ranged from 0.36 to 0.44m. However Larrañaga et al. (2003) found boulders and cobbles to retain the greatest proportion of leaf analogues under baseflow conditions, but their importance did decrease with an increase in discharge, with woody-debris and gravel increasing in importance.

Larrañaga et al. (2003) calculated a relative retentive efficiency for each structure, this described the percentage of retention attributed to a particular structure relative to the percentage area of the stream bed that that structure covered. Cobbles were highly retentive, retaining 2.7 times, under base flow conditions, the number of leaves than would be estimated from their aerial coverage if all retentive structures are assumed to behave equally. Snags, a term used to cover both bank and instream vegetation, roots and overhanging branches, were found to be the most retentive structures by James and Henderson (2005), with riffles retaining very few natural and analogue leaves. This difference in importance of retentive structures to retain leaves was also seen by Muotka and Laasonen (2002), in their comparison of different channel types. Where the stream had been ‘channelised’, moss and cobbles retained the most leaves. After restoration, moss was not important and the retention by cobbles increased, but in natural streams moss and boulders were the most important structures. The usefulness of woody debris and stream margins in the retention of leaves remained constant in the three stream types suggesting their presence or there mechanism of retention did not change between stream types (Muotka and Laasonen, 2002). The study of Muotka and Laasonen (2002) was the only study of those discussed to show the importance of moss as a retentive structure within streams.

2.4 Flow in Streams

Within streams, flow characteristics are governed by the dynamics of open channel flow, in which the flow type and behaviour can be rigidly defined. Open channel flow is characterised by the presence of a free surface that is subject to atmospheric conditions. The presence of the free surface complicates the flow, in contrast to flow through pipes, due to its ability to change position with time and space. Conditions within natural channels are highly variable in terms of both the geometric shape and the roughness of the bed material (Chow, 1959), which makes the characterisation more empirical. Variation can be seen at every spatial level, from sequences of riffles and pools, to millimetre variation caused by the variation on the surface of the substratum (Hart and Finelli, 1999).

Within open channel flow, the type of flow can be categorised as steady, uniform, or a combination of both, to define how parameters of the flow vary with time and space. In the context of open channel flow the hydraulic factor of importance is flow depth (Chow, 1959). These two categories give rise to the following flow types (Chow, 1959; Chadwick et al., 2004):

- Steady Uniform - Fundamental type of flow in open channels, where the flow depth does not vary in time and is uniform over the channel
- Steady Non-uniform - The flow depth does not change in time, but it does change either gradually or rapidly over the channel. This is also know as varied flow.
- Unsteady Non-uniform - The flow depth changes in both time and space.

In natural streams, uniform flow is unlikely to be present, as the flow depth will generally vary along the channel. However, steady flow can be seen if the discharge remains constant.

The behaviour of the flow, as opposed to the flow type, is controlled by the viscous and gravitational forces relative to the inertial forces (e.g. Chow, 1959; Douglas et al., 2001). The viscous forces arise from the friction created as the fluid particles move relative to each other, whereas the inertial forces come from the acceleration of the fluid. The ratio of these forces defines whether the flow is laminar, transitional or turbulent. In laminar flow, the viscous forces are much stronger than the inertial forces. The particles of the fluid move in an orderly fashion, with parallel thin layers sliding over each other but without mixing. However, in turbulent flow the inertial forces are much stronger than the viscous forces. Turbulent flow is characterised by mixing between the layers, with the velocity of the particles fluctuating in both magnitude and direction, and often resulting in the formation of eddys. Transitional flow is the phase between the two, where the flow is becoming turbulent but is not fully developed.

Two dimensionless ratios are used to describe the flow by relating the gravitational or viscous forces to the inertial forces. The ratio of the viscous forces to the inertial forces is represented by the Reynolds number, Re, defined as,

$$Re = \frac{UL}{\nu} \text{ , where } \nu = \frac{\mu}{\rho} \tag{2.2}$$

where U is the velocity of the flow, L is a characteristic length, (in open channel flow this is the hydraulic radius or flow depth), ν is the kinematic viscosity, μ is the dynamic viscosity and ρ is the density of the fluid. Whereas the ratio of the gravitational forces to the inertial forces is given by the Froude number, Fr, defined as,

$$Fr = \frac{U}{\sqrt{gL}} \tag{2.3}$$

where U is the velocity of the flow, L is a characteristic length, and g is gravity. The Froude number can be used to describe whether the flow is sub- or super-critical (Chow, 1959). If $Fr < 1$, then the gravitation forces are stronger, the velocity is low, and the flow is subcritical. However if $Fr > 1$, then the inertial forces have become dominant, resulting in a higher velocity flow, and therefore it is supercritical.

The Reynolds number, as a representation of the ratio of viscous and inertial forces, is used as an indicator of the behaviour of the flow, whether it is laminar, transitional or turbulent. In open channel flow, the threshold values for each flow type differ depending upon whether the flow is in a smooth or rough channel. Within natural streams, the rough bed will cause friction with the water, and therefore the inertial forces would generally be higher than the viscous forces, implying turbulent flow. Chow (1959, Fig. 1.4) shows the variation seen in Reynolds number for the different types of flow in rough channels, and suggests that the flow becomes turbulent in a rough channel at a Reynolds number of approximately 2000.

2.4.1 Uniform and Gradually Varied Flow

A major assumption of the parameters within open channel flow hydraulics is that the flow is uniform. Under uniform flow conditions the flow depth, and therefore the cross-sectional area, are constant throughout the length of the channel, and the energy slope, S_f, (the change in specific energy over length), is equal to the water surface slope, S_w, and the bed slope, S_0 (Chow, 1959). Under these conditions the gravitational weight of the water along the plane of the direction of flow is balanced by the frictional force of the boundaries acting in the opposite direction, resulting in a balance of the energy within the system.

When the conditions of uniform flow are not met the flow is considered to be gradually varied. A number of different flow profiles, which describe the water surface profile within gradually varied flow, have been identified, the type of which is dependent on the flow depth relative to the critical (z_c) and normal (z_n) flow depths. The critical and normal depth lines divide the flow into three zones, (1) the space above the upper line, (2) the space between the two lines and (3) the space below the lower line.

The flow is classified as subcritical if $z_0 > z_c$ and supercritical if $z_0 < z_c$. The steepness of the channel is seen to affect the type of water surface profile and can also be described by the relationship of z_c to z_n;

- Mild channel (M) - $z_n > z_c$
- Critical channel (C) - $z_n = z_c$
- Steep channel (S) - $z_n < z_c$

For each of these channel types there are three profile types dependent on the zone in which the profile is present.

2.4.2 Boundary Layer

When a real fluid meets a stationary surface then the layer of fluid directly in contact with that surface also becomes stationary due to the the boundary shear stress, which is the friction of the surface. This effect causes shearing between the layers of fluid: the layer adjacent to the surface creates shear stress between it and the next layer, causing deceleration, with this continuing through the fluid (Chadwick et al., 2004). As the fluid moves further over the surface the thickness of fluid that is affected by the surface increases, forming the boundary layer. At some height above the surface, the flow will experience no effect of surface and the velocity reaches that of the free fluid. The edge of the boundary layer and therefore the thickness, δ, can be defined as where the velocity is 99% of the free stream velocity (U) (Chadwick et al., 2004).

When fluid first flows over a surface a completely laminar boundary layer is created; however as the flow travels further along the surface it becomes turbulent (Chow, 1959), shown in Figure 2.3. In the turbulent zone the presence of eddys and mixing creates a steeply sheared profile near the surface that becomes more uniform as it reaches the edge of the boundary layer (Chadwick et al., 2004).

The formation and thickness of the boundary layer is affected by the roughness of the surface over which the fluid is flowing. If the channel or surface that the fluid is travelling over is relatively smooth then the velocities on the surface are very low and a laminar layer is created below the turbulent flow; this is the laminar sub-layer (see Figure 2.3) (Chow, 1959). If there is a roughness element at the beginning of the surface, then no laminar zone will form, with the turbulent boundary layer being formed from the beginning shortening the distance required for full development of the boundary layer (Chow, 1959). Within the laminar region, the roughness of the surface has little effect on the thickness as the friction is transmitted through the fluid just by the shearing action that is occurring

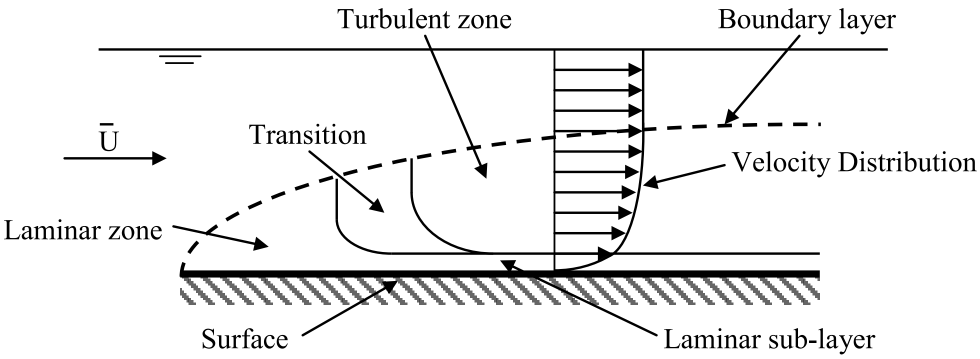

Figure 2.3. Structure of the Boundary Layer, adapted from Fig 3.9 Chadwick et al. (2004)

within it (Chadwick et al., 2004). However, in the turbulent area of a boundary layer, the effect that the surface roughness has is dependent on roughness height, k (Chow, 1959).

If the roughness height is within the laminar sub-layer, then the roughness elements will have no effect on the flow outside of the laminar sub-layer. In this situation the surface is referred to as hydraulically smooth. If the roughness elements do extend into the turbulent zone, then this increases the amount of eddy formation leading to greater energy loss, and increased apparent frictional shear (Chadwick et al., 2004); this surface is referred to as either transitional or rough (Schlichting and Gersten, 2000). Schlichting and Gersten (2000) defined boundaries to determine hydraulically smooth, transitional and rough surfaces using the roughness height;

$$\text{Hydraulically Smooth} \qquad 0 < \frac{U_* k}{\nu} < 5 \tag{2.4}$$

$$\text{Transition} \qquad 5 < \frac{U_* k}{\nu} < 70 \tag{2.5}$$

$$\text{Fully Rough} \qquad 70 < \frac{U_* k}{\nu} \tag{2.6}$$

where ν is the kinematic viscosity, and u_* is the shear velocity as defined by;

$$U_* = \sqrt{gRS}, \tag{2.7}$$

where g is gravity, R is the hydraulic radius and S is the bed slope. When the surface is rough so that roughness extends fully into the boundary layer, then the flow becomes independent of Reynolds number and the effect of viscosity is removed (Schlichting and Gersten, 2000). Within a stream bed, k can greatly vary both spatially within the stream, and also between streams. Low and mid-order streams most often exhibit hydraulically rough flows, where the roughness is greater than the laminar sublayer, leading to turbulence at the bed, which leads to high levels of mixing and diffusion, and the laminar sublayer is not present (Davis and Barmuta, 1989). The roughness of the bed will have an effect on the shear stress produced at the bed, and therefore might be an important factor to consider when describing the spatial distribution of the retention of leaves.

Velocity profiles (as seen in Figure 2.3) illustrate how the velocity changes with height from the bed, allowing the identification of the boundary layer, and are also useful in identifying fully developed flow. The velocity profile within the boundary layer can be described by the Prandtl von-Karman equation (Chow, 1959; Nezu and Nakagawa, 1993);

$$u = \frac{U_*}{\kappa} \ln \frac{z}{y_0} \tag{2.8}$$

Where κ is the von-Karman constant that has been determined by experiment to be 0.4 (Chow, 1959) and y_0 is the constant of integration. This relationship shows that within the boundary layer the velocity is a logarithmic function of the distance z (depth) (Chow, 1959). This law has been taken further with specific equations being developed for smooth and rough surfaces. When a surface is smooth then y_0 is completely dependent on the kinematic viscosity, ν, and the shear velocity, U_*, and therefore is approximated to $y_0 = m\nu/U_*$ where m has been found to equal 1/9, therefore giving the smooth law;

$$\text{Smooth Law} \qquad u = 2.5u_* \ln \frac{9zU_*}{\nu} \tag{2.9}$$

When the surface is rough, the constant y_0 is dependent on the roughness height k, and therefore y_0 is approximated to mk, where now m is a constant equal to 1/30, to give the rough law;

$$\text{Rough Law} \qquad u = 2.5u_* \ln \frac{30z}{k} \tag{2.10}$$

Within the turbulent zone the roughness height k is taken to be the equivalent sand grain roughness. Although these equations were derived from work carried out in pipes, they are now widely applied to open channel flow conditions (Nezu and Nakagawa, 1993). However, the equations can be used to calculate the bed shear stress, or the shear velocity, only if a logarithmic velocity profile is seen; if not then the relationship is not valid. Biron et al. (1998) and Rowinski et al. (2005) found the best results when the log distribution was only fitted to 20% of the depth above the bed. Velocity profiles are obtained by taking time-averaged point measurements of the velocity at regular intervals above the bed, which are then plotted against height. When the roughness elements are present, e.g. in the case of a gravel bed river, lower velocities are present within the roughness zone, with the fluid skimming over the top. This creates a distinct shear in the logarithmic profile which was seen to correspond to approximately the D_{50} of the bed material (Biron et al., 1998). This discontinuity of the velocity profile can be used to identify the roughness height within a stream.

2.4.3 Parameters of Open Channel Flow

Flow characteristics vary over a large spatial and temporal scale, so it is crucial within research to decide which scale is the most important to allow the proper understanding of the driving factors and the linkages between physical and ecological systems (Hart and Finelli, 1999). However, flume experiments provide the opportunity to control flow conditions, allowing linkages to be more clearly identified. A number of physical and hydraulic parameters, such as discharge, velocity, flow depth, substrate size, are used by engineers and ecologists to characterise conditions within streams (Davis and Barmuta, 1989), which can then be equated to leaf retention. The area mean velocity, $\bar{U}$, calculated by dividing the discharge, Q, by the cross-sectional area, A, describes the average velocity over the cross-section, but can not be used to evaluate local variations due to variations of the bed, and therefore may not be representative of the many different habitats that might exist across that area. To provide a more relevant measure, point velocity measurements can be taken over a very small sample volume, allowing comparisons between leaf retention and velocities at a local scale.

The shearing action in laminar flow can be characterised by the friction between the layers of water. Within turbulent flow, it is more difficult to characterise the flow, the individual particles in the fluid are 'jostling' with each other (Chadwick et al., 2004), and making the motion of these particles very complex. A point velocity, u, (for the x-direction), can be broken down into two components,

1. The time-averaged velocity of the flow at a point, $\bar{u}$,
2. The fluctuating component, u_i', the difference between the time-averaged velocity and the instantaneous velocity.

Therefore,

$$\begin{aligned} u_i &= \bar{u} + u_i' \\ v_i &= \bar{v} + v_i' \\ w_i &= \bar{w} + w_i' \end{aligned} \tag{2.11}$$

for the longitudinal (x), lateral (y) and vertical (z) directions respectively, and where time-averaged fluctuating components, $\bar{u'}$, are equal to zero. The time-averaged velocities

($\bar{u}$, $\bar{v}$ and $\bar{w}$ for the three directions: longitudinal, lateral and vertical respectively) can be used to describe the local time-averaged conditions. Different methods are used to describe the variation within the fluctuating components, and therefore the degree of turbulence present. The most commonly used method is the root-mean-square (RMS) of the fluctuating component, referred to as the turbulence intensity, for the x-direction;

$$u_{rms} = \sqrt{\overline{u_i'^2}} \tag{2.12}$$

The Mean Kinetic Energy (MKE) and Turbulent Kinetic Energy (TKE) can also be calculated from the fluctuating components of three-dimensional velocity measurements, using the following formulas:

$$MKE = (\overline{u^2} + \overline{v^2} + \overline{w^2})/2 \tag{2.13}$$

$$TKE = (\overline{u'^2} + \overline{v'^2} + \overline{w'^2})/2 \tag{2.14}$$

where u, v and w refer to the instantaneous velocity measurements and u', v' and w' refer to the fluctuating components of the velocity from the mean (as shown in Equation 2.11) in the longitudinal, lateral and vertical direction respectively.

As previously stated in Section 2.4.2, the bed shear stress is caused by the frictional force created at the bed due to the movement of water at the bed. The evaluation of the bed shear stress is particularly difficult in complex three-dimensional flow situations (Biron et al., 2004) such as rivers where there is a highly irregular roughness caused by the gravel bed (Rowinski et al., 2005). The cross-sectional average bed shear stress is given by;

$$\tau_0 = \rho g R S \tag{2.15}$$

where ρ is density, g is gravity, R is the hydraulic radius (which when the width is large can be approximated to the flow depth, z_0) and S is the slope. This can be related to the shear or frictional velocity, U_* (see Eq. 2.7), and is given by;

$$\tau_0 = \rho {U_*}^2 \tag{2.16}$$

Both of these parameters can be considered as 'global' or cross-sectionally averaged characteristics, as they are related to parameters such as the cross-sectional area, hydraulic radius and slope, and therefore give the bed shear stress over one cross-section of the reach under uniform flow conditions. As with the cross-sectionally averaged velocity parameter, calculated from the discharge and flow area, they do not take into account any changes that occur within the reach due to local variation in the velocity or bed substrate. Although these are useful parameters for descriptive purposes, their usefulness in describing leaf retention at a local spatial scale might be limited. Like with velocity, the bed shear stress can also be calculated at a local scale using three-dimensional velocity measurements taken near to the bed; however there is debate as to what height point velocity measurements should be taken to gain an accurate calculation of the bed shear stress. The estimation of the bed shear stress becomes more problematic when there is irregular roughnesses associated with gravel beds, at it is harder to identify where the near bed measurements should be carried out (Rowinski et al., 2005). Biron et al. (2004) suggest that the measurements should be made at a relative depth of 0.1, as this was where they observed the maximum value of bed shear stress.

A number of methods can be used to calculate the local bed shear stress using the fluctuating velocity components from three-dimensional velocity measurements. The first is the Reynolds stress method which uses the longitudinal and vertical components;

$$\tau = -\rho\overline{u'w'} \tag{2.17}$$

where ρ is the density of water. Near-bed measurements can be used with this method the estimate the shear stress near the bed, but to get a more accurate representation of the bed shear stress, a turbulence profile of the Reynolds stress needs to be taken which is then extrapolated to the bed. The second method used is based on the Turbulent Kinetic Energy, and considers the lateral fluctuations as well as the longitudinal and vertical:

$$\tau = C_1[0.5\rho(\overline{u'^2} + \overline{v'^2} + \overline{w'^2})] \tag{2.18}$$

where C_1 is a proportionality constant, which has been found to be ≈ 0.19 (Kim et al., 2000). This method has been widely used in oceanography, but does not appear to be widely used within fluvial hydraulics (Biron et al., 2004).

Both Biron et al. (2004) and Rowinski et al. (2005) carried out comparisons between different methods of calculating the bed shear stress; however not all the methods investigated have been discussed here. Biron et al. (2004) carried out laboratory experiments, investigating the bed shear stress with a simple boundary layer over plexiglass and sand, and then the spatial variation in a more complex flow situation, which involved a sand bed and the presence of flow deflectors. Whereas Rowinski et al. (2005) compared shear velocities calculated using different bed shear stress methods to the 'global' or cross-sectional average bed shear stress (Eq. (2.15)) over an armoured gravel bed in laboratory experiments.

The Reynolds stress method was found to be in the best agreement with the 'global' bed shear stress (Rowinski et al., 2005). The logarithmic method (Eq. 2.8) was found to over estimate the shear stress and produce a larger amount of variation (Biron et al., 2004;

Rowinski et al., 2005). The turbulent kinetic energy (TKE) model produced results with the same gradient as the 'global' method, however the values were consistently under estimated. Rowinski et al. (2005) therefore suggested that the Reynolds stress method was the best local analogue to the global value; however this method assumes two-dimensional flow, suggested it can not be used when strong secondary currents are present.

Under the simple boundary conditions the average bed shear stress from the Reynolds stress and TKE method showed good agreement over the sand bed, but the TKE method greatly over estimates over the much smoother boundary of the plexiglass (Biron et al., 2004). Direct comparison of these two methods at all heights and both the bed substrates, showed a consistent over estimation by the TKE method compared to the Reynolds stress method (Biron et al., 2004), in contrast to the results of Rowinski et al. (2005). The results of Biron et al. (2004) would be expected as the fluctuating velocity components in the TKE method are squared, and therefore only the magnitude of the fluctuations is considered and not the sign. In the Reynolds method, the sign is considered, which when the mean is calculated could reduce the value. When a more complex flow field was considered, the TKE method produced the best match to the bed topography, and expected regions of scour in the set up (Biron et al., 2004).

Biron et al. (2004) suggested that under a simple boundary layer the TKE method is not the most suitable, and that the Reynolds stress method should be used were three-dimensional velocity measurements are available, despite the similarity in results over the sand bed. However in complex flow fields, they suggested that the Reynolds stress model is no longer appropriate as it is sensitive to misalignment, and in that case the TKE is clearly the most appropriate (Biron et al., 2004). Rowinski et al. (2005) suggested that the Reynolds stress method should be used, when the flow is considered to be two-dimensional, however if the flow is three-dimensional it is suggested that the spatial variation needs to be taken into consideration through the use of spatial averaging terms within stresses.

2.5 Flow around Retentive Structures

The larger protrusions, such as cobbles, boulders, and pebble clusters, associated with the gravel beds found within streams have an important role in defining the spatial distribution of ecological ecosystems within a stream. Section 2.3 discussed their role in the retention of organic matter within streams, which is an essential input of energy. Near-bed flows are important factors in determining the spatial distribution of benthic macro-invertebrates (e.g Davis and Barmuta, 1989; Bouckaert and Davis, 1998), with the wake of a protrusion providing a favourable environment for invertebrates shown by a significantly greater abundance (Bouckaert and Davis, 1998). Also the wakes and lower velocities present within the lee of a protrusion provide cover, resting and feeding opportunities for fish (Shamloo et al., 2001). In the wake of an obstacle the mean kinetic energy is converted to turbulent kinetic energy (Nepf, 1999). The TKE in the wake of a pebble cluster has been found to be twice that found when the pebble cluster is not present, (Lacey and Roy, 2007). It is suggested that particular characteristics of the wake, such as the rate of turbulent energy dissipation, and the characteristic turbulence length scales have an effect on small-scale ecosystems, affecting nutrient mixing, and even predator prey reactions (Lacey and Nikora, 2008).

The investigation of the flow structure around and wake characteristics of large roughness elements (LRE), such as hemispheres and boulders, has been investigated in both flume experiments (e.g. Savory and Toy, 1986; Acarlar and Smith, 1987; Shamloo et al., 2001; Tavakol et al., 2010) and natural streams (e.g. Buffin-Bélanger and Roy, 1998; Lacey and Roy, 2007; Lacey and Nikora, 2008). The wake of such elements is highly complex and three-dimensional in structure (Acarlar and Smith, 1987). To understand the patterns and distributions of many ecological factors within a stream, accurate knowledge of how these structures affect the velocity and turbulence structure needs to be gained. Simple shaped objects are often investigated as they allow easier characterisation of the flow structures. However these obstacles are also analysed because of their analogues to natural and man-made structures. For example wooden dowels are investigated in the place of vegetation, ribs and bars investigated to look at larger structures such as wooden logs, and spheres and hemispheres are used in place of sediment, isolated boulders, and pebble clusters frequently seen in gravel-bed rivers.

2.5.1 Flow around a Cylinder

When a retentive structure, such as a boulder or pebble cluster, protrudes into flow it is subject to drag that is made up from two components; the surface friction, and form drag which is a result of pressure gradients (e.g. Douglas et al., 2001). The frictional drag occurs in the region adjacent to the surface of the body, and results in decreased velocities and the formation of a boundary layer. The magnitude of this drag force is therefore a function of the surface area of the object. The form drag is created by pressure differences that are created across the object, making it a function of the projected area. The total drag force (F_D) on an object within a fluid is given by;

$$F_D = \frac{1}{2} C_D \rho \bar{U}^2 A \tag{2.19}$$

where C_D is the drag coefficient, ρ is the density of the fluid, $\bar{U}$ is the free stream velocity and A is the area of the body perpendicular to the flow.

The presence of a single or an array of objects within the flow has an affect on the flow type, which, as previously mentioned, can be described by the Reynolds number. The calculation of the Reynolds number involves the use of a characteristic length, that refers to the turbulent length scale of interest. In open channel flow, the flow depth or hydraulic radius are used in as the characteristic length, however when there is an obstacle in the flow, the diameter of the object is used. For example, in the case of cylinders, the stem diameter is used to calculated the Reynolds number, which is then referred to as the Stem Reynolds number (Re_d) (Nepf et al., 1997; Poggi et al., 2004). For each object shape, there is a distinct relationship between the drag coefficient and the Reynolds number.

The flow round a isolated cylinder has been widely researched and is presented in fluid mechanics textbooks (e.g. Douglas et al., 2001). Figure 2.4 shows an illustration of the flow around a cylinder. This considers a circular cylinder, of infinite length placed transversely to the flow. In a frictionless fluid, for example outside of the boundary layer, as the flow moves from A to B the pressure is converted to kinetic energy resulting in acceleration of the flow, from B to C the kinetic energy is converted back to pressure, resulting in the fluid particles decreasing in velocity. Therefore, there is a pressure decrease from A to B, known as a favourable pressure gradient, accompanied by a decrease in boundary layer thickness and an increase in pressure from B to C, known as an adverse pressure gradient, accompanied by rapid thickening of the boundary layer. At C the particle is returned to the same velocity as before the cylinder, and there is no loss of energy. The flow upstream and downstream of the cylinder is symmetrical with two stagnation points present, one at the front and the other at the rear of the object. This is because the pressure at the rear stagnation point is the same as at the upstream stagnation point, so there is no resultant force.

However, when friction is considered, such as the fluid in the boundary layer, it means frictional drag is also present. The presence of the friction means that more energy is converted to kinetic energy between A and B, and therefore there is not enough left to convert back to pressure between B and C, leading to incomplete pressure recovery. The combined effect of the shear stress in the boundary layer, and the adverse pressure gradient, if sufficient, causes the flow to separate from the surface. The boundary layer separates from the body due to the deceleration of part of the velocity profile resulting in the boundary layer being pulled up away from the body. Separation leads to thickening of the boundary layer, due to the presence of reversed flow. A combination of pressure gradients and friction is responsible for the location of the separation point. The motion of the fluid particles is arrested, and the pressure forces the fluid to move in the opposite direction, leading to the formation of vortices in the wake (Schlichting and Gersten, 2000). The presence of eddies behind an object results in a significant increase in drag acting on the surface (Douglas et al., 2001). The shedding of these vortices also has an effect on the structure of the wake

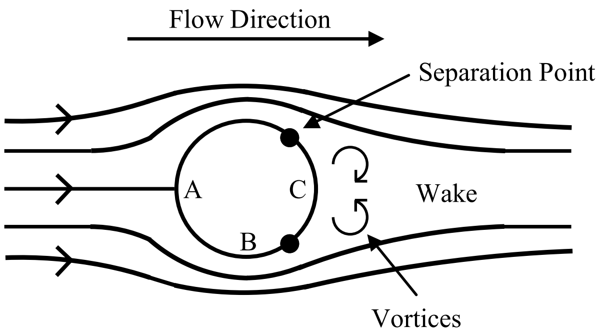

Figure 2.4. Illustration of the flow around a cylinder, taken from Douglas et al. (2001)

and the pressure gradient present. Upstream there is no separation at the stagnation point (A), despite the large pressure gradient, due to the lack of friction.

The wake of an object is characterised by the presence of decreased or negative velocities (Tavakol et al., 2010) due to the presence of large-scale eddies and increased turbulence (Lacey and Roy, 2007). Therefore there is a high rate of energy dissipation, resulting in decreased pressure in the wake (Douglas et al., 2001). The dissipation of energy consists of the transfer of kinetic energy from the mean kinetic energy described in Eq. 2.13 to turbulent kinetic energy (Eq. (2.14)) through the generation of eddies (Nepf, 1999). Lacey and Nikora (2008) suggest that the high values of turbulent energy dissipation seen in the wake will promote particle-particle interaction, and therefore from an ecological point of view, predator-prey interactions, that could not occur in unobstructed flows. The decrease in pressure in the wake means that the pressure acting on the stagnation point on the upstream face of the object is greater than the pressure acting at the rear of the object, and therefore a resultant force, referred to as the pressure drag, acts on the object in the direction of flow. The larger the pressure difference, or smaller the pressure recovery, the large the wake and the greater the pressure drag. However this is dependent on Reynolds number and is not true after 2×10^5, where the drag coefficient reduces, due to the boundary layer on the cylinder changing from a laminar boundary layer to a turbulent boundary layer (Douglas et al., 2001).

In a wake, the velocities are smaller because of the loss of momentum due to the drag force on the body (Schlichting and Gersten, 2000). With distance downstream from an isolated body, the lateral width of the wake increases and the difference between the velocities within the wake and the free stream decreases (Schlichting and Gersten, 2000). The expansion and size of the wake can be described using wake theory (Schlichting and Gersten, 2000) where;

$$\frac{u_1}{U_\infty} = \frac{U_\infty - u}{U_\infty} = \frac{\sqrt{10}}{18\beta}\left(\frac{x}{C_D d}\right)^{-1/2}\left\{1 - \frac{y^{3/2}}{b}\right\}^2 \tag{2.20}$$

where;

$$b = \sqrt{10}\beta(xC_D d)^{1/2} \tag{2.21}$$

and U_∞ is the free stream velocity, u_1 is the difference between the measured velocity and the free stream velocity, β is the proportionality constant of the mixing length, l and the wake width, b, x is the distance in the longitudinal direction behind the object, y is the lateral position relative to the centre of the object, C_D is the drag coefficient, and d is the object diameter. However this relationship is only valid for large x where $x/C_D d > 50$.

The development of the wake created by an isolated cylinder has been characterised in terms of the Stem Reynolds number (see Figure 2.5), where increases in the Re_d are associated with increase in the size and complexity of the wake up to a Stem Reynolds number of 2×10^5, when the size of the wake reduces. When considering real fluids, symmetrical flow with two stagnation points due to no resultant force only occurs at very low Reynolds numbers ($Re_d < 0.5$), and no wake is seen (Fig. 2.5 A). This is due to the inertial effects being negligible, and therefore at the low velocities associated with such low Reynolds number, the drag produced is due to the friction on the body. In this range of Reynolds numbers the relationship between drag coefficient and Re_d is linear, and therefore the velocity is directly proportional to the drag produced.

A slight increase in the Reynolds number ($2 < Re_d < 30$) leads to separation of the boundary layer from the cylinder, and the formation of two symmetrical counter rotating eddies behind the cylinder (Fig. 2.5 B). These vortices remain stationary with the flow closing behind them. The formation of the wake behind the cylinder means that the relationship between drag coefficient and Reynolds number is no longer linear. Increasing the Reynolds number further leads to elongation of the fixed eddies, until an Re_d of $\approx$90; however this threshold is dependent on the turbulence level in the free stream (Nepf et al., 1997). At this threshold the eddies break free of the cylinder (Fig. 2.5 C), shedding from alternative sides being carried away by the flow, creating turbulence in the wake (Nepf et al., 1997; Douglas et al., 2001). The exact Reynolds number for shedding is dependent on the flow conditions. Nepf et al. (1997) observed Re_d of less than 200 the turbulent diffusivity was the same as when no stems were present, illustrating that there is no turbulence contributed to the wake when the vortices are not shed. However when Re_d was greater than 200 the turbulent diffusivity was greater than when no stems were present, showing that the shedding of vortices increases turbulence and therefore diffusivity in the wake.

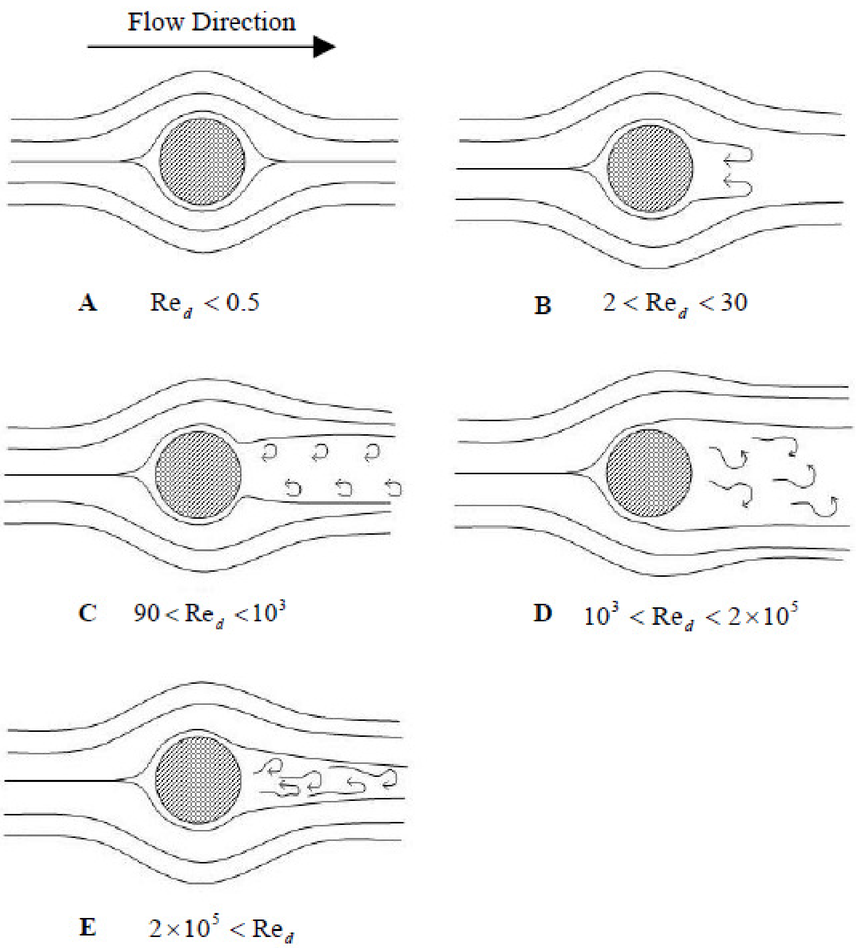

Figure 2.5. Illustration of the development of the wake of a cylinder in relation to increasing Stem Reynolds number, taken from Douglas et al. (2001)

Further increases in the Reynolds number up to a Re_d of 10^3 increases the frequency of shedding, leading to continuous alternative shedding of eddies in two distinct lines behind the cylinder. At this stage the pressure drag is three times the surface drag. This distinct pattern of vortex shedding is called von Karman street vortices. Once the Reynolds number reaches 10^3 (Fig. 2.5 D) the discrete vortices can no longer be seen, instead a highly turbulent wake is produced due to the high level of shear. At this stage the pressure drag is responsible for the majority of the drag. Up to a Re_d of 2×10^5 the boundary layer of the cylinder is laminar. But at this threshold (Fig. 2.5 E), again depending on the level of turbulence in the free stream, the boundary layer of the cylinder becomes turbulent before it separates from the body, moving the separation point on the cylinder further downstream, and creating a decrease in the drag coefficient. The flow around a emergent cylinder and its wake can be approximated to two-dimensional flow; however we are concerned with submerged boulders, where the flow and object wake will be of a more three-dimensional nature.

2.5.2 Flow around a Boulder

The characterisation of the flow structure has been investigated for both two-dimensional, (e.g. Engel, 1981; Douglas et al., 2001; Best, 2005; Stoesser et al., 2008) and three-dimensional (e.g. Savory and Toy, 1986; Acarlar and Smith, 1987; Nezu and Nakagawa, 1993; Shamloo et al., 2001) obstacles and bed forms, leading to the identification of a number of coherent structures. In particular, the flow regime around an isolated hemisphere has been studied in both air (e.g. Savory and Toy, 1986; Tavakol et al., 2010) and water (e.g. Acarlar and Smith, 1987; Shamloo et al., 2001), due to its analogue as a retentive structure. Coherent structures identified in rivers are classified into two categories; bursting phenomena, semi-cyclic patterns of sweeping and ejection motions, and large-scale vortical motion, such as 'rollers', secondary currents and boils (Nezu and Nakagawa, 1993).

Different methods have been used to visualise the presence of coherent structures, such as dye and hydrogen-bubble-wire visualisation techniques (e.g. Acarlar and Smith, 1987), detailed velocity measurements (e.g. Savory and Toy, 1986; McLean et al., 1994; Shamloo et al., 2001; Lacey and Roy, 2007; Kanani et al., 2010) and large-eddy simulations (e.g. Stoesser et al., 2008). Two studies of particular interest that examine the wake of a submerged hemisphere are those of Savory and Toy (1986) and Acarlar and Smith (1987). Savory and Toy (1986) investigated the near-wake, defined at 2D (a distance of two diameters) downstream of the object, of a hemisphere (190mm diameter) in both smooth and rough boundary layers using a three-dimensional grid of velocity profiles. Whereas Acarlar and Smith (1987) used dye and hydrogen-bubble-wire visualisation techniques to identify the flow around different sized hemispheres (6 to 36mm in diameter) in a laminar boundary layer and velocities ranging from 3 to 30 m/s.

Immediately upstream of an obstacle within the flow, a standing vortex or 'horseshoe' vortex forms due to the retardation and rolling up of the boundary layer vortex sheets that are moving towards to obstacle (Savory and Toy, 1986; Acarlar and Smith, 1987; Nezu and Nakagawa, 1993). This vortex bends around the obstacle (Acarlar and Smith, 1987), creating trailing vortices in the wake that rejoin at a downstream point (Savory and Toy, 1986). The strength of the horseshoe vortex, and the contribution it makes to the wake, is affected by the initial boundary layer conditions (Savory and Toy, 1986). The presence of the horseshoe vortex results in the production of high bed shear stresses immediately upstream of the obstacle (Shamloo et al., 2001) and the formation of a stagnation point on the upstream face of the obstacle (Douglas et al., 2001). Acarlar and Smith (1987) found the height of this standing vortex to be $0.4h$ (where h is the height of the boulder). Whereas, Shamloo et al. (2001) identified a horseshoe vortex about $0.2h$ in size, half the size seen by Acarlar and Smith (1987) whilst investigating the flow around an isolated hemisphere of diameters 74 and 130mm, for a number of relative submergences.

As discussed in the previous section in relation to a cylinder, a wake is formed downstream of an obstacle or bed form characterised by decreased streamwise velocities (Nepf et al., 1997; Tavakol et al., 2010) and increase turbulence (Lacey and Roy, 2007). The wake can be divided into two regions, a recirculation zone immediately downstream of the obstacle, consisting of negative streamwise velocities, and a region of reduced velocities that extends outwards downstream of the obstacle, (Zavistoski, 1994). The degree of negative velocities found in the recirculation zone have been found to be greater in a smooth boundary layer compared to a rough boundary layer (Savory and Toy, 1986), suggesting that the increase in turbulence in the free flow decreases the scale of the negative velocities produced in the recirculation zone. The structure and development of the wake can be characterised by Reynolds number (Douglas et al., 2001). As well as a longitudinal profile, the wake of an obstacle also has a distinct lateral profile of reduced velocities with the greatest velocity deficit present at the centre of the obstacle (Savory and Toy, 1986), and where the lateral edges of the wake are indicated by peaks in the streamwise turbulence intensity U_{rms} (Tavakol et al., 2010).

Acarlar and Smith (1987) found that a velocity deficit was present $2D$ downstream of the a single submerged hemisphere, however this had disappeared by a distance of $5D$ downstream (Re_r=30-3400, where the characteristic length is the radius of the hemisphere) and Tavakol et al. (2010) observed the wake to be approximately $1D$ in width, however the peaks in U_{rms} move inwards as the wake moves downstream. Lower peak values of turbulence intensity were seen for the thick boundary layer compared to the thin boundary layer (Tavakol et al., 2010). The region of velocity deficit observed by Shamloo et al. (2001) was seen to increase with decreasing boulder submergence, for a relative flow depth (y/h) of 4.12 the wake was $2D$ in length, but this increased to $3D$ for a relative flow depth of 1.85, and at flow depths lower than this recovery of the velocities was not seen.

When considering submerged obstacles and bed forms, such as dunes and boulders, the boundary layer separates from the body near the crest, generating a free shear layer and separation vortices due to Kelvin Helmholtz instabilities, (Nezu and Nakagawa, 1993; Best, 2005). For hemispheres these separation vortices are arch shaped and are anchored in the trailing legs of the horseshoe vortex, (Savory and Toy, 1986; Shamloo et al., 2001). The vortices grow and join together as they rotate down towards the reattachment point

(Best, 2005), surrounding the recirculation zone and separating it from the free flow (Nezu and Nakagawa, 1993). The reattachment point, defined by Savory and Toy (1986) as the point downstream of the obstacle where the velocity immediately above the bed is zero, defines the size of the recirculation zone, and varies between two-dimensional and three-dimensional structures.

For a backwards step, the instantaneous reattachment length has been seen to vary between 3-9h (where h is the height of the step) (Nezu and Nakagawa, 1993), and for steep two-dimensional dunes (l/h ratio of dunes greater than 0.05) it was found to be $4h$, and did not vary with flow depth (Engel, 1981). For a single three-dimensional hemisphere the reattachment length was found to be much shorter, with Savory and Toy (1986) observing reattachment lengths of $1.25D$ in a smooth boundary layer and $1.1D$ for a rough boundary layer, however Tavakol et al. (2010) observed reattachment lengths of approximately half these, $0.6D$ and $0.65D$ respectively. Savory and Toy (1986) suggest that the reattachment length is affected by the scale and intensity of turbulence, so that in the rough boundary layer the increased turbulence leads to quicker thickening of the boundary layer, leading to a greater curvature of the shear layer, shortening the reattachment length. The greatest values of turbulent kinetic energy in the wake were seen at a distance of 1.4D from the downstream side of a pebble cluster in the study by Lacey and Nikora (2008), with this distance corresponding to the greatest rate of turbulent energy dissipation. This distance would put this point in the near-wake, but outside of the recirculation zones documented by Savory and Toy (1986) and Tavakol et al. (2010), suggesting there is greater turbulence associated with reattachment of the boundary layer and possibly the development and shedding of hairpin vortices. However, measurements were only taken at two elevations within the flow, one at 70% of the boulder height and one above the boulder, so the three-dimensional nature of the wake is not characterised.

The separation vortices are periodically shed from the reattachment point (Savory and Toy, 1986), moving towards the surface as they are convected downstream by the mean flow, and creating boils when they interact with the free water surface, (Nezu and Nakagawa, 1993; Best, 2005). After being shed these vortices deform, forming a 'hairpin' shape and therefore can be referred to as hairpin vortices (Acarlar and Smith, 1987). When considering two-dimensional dunes, the 'roller' (cross-streamwise) vortices created at separation are thought to be deformed by secondary instabilities into the hairpin shape (Stoesser et al., 2008) before being elongated and transported towards the surface forming boils (Nezu and Nakagawa, 1993), which consist of an upwelling region due to the head of the hairpin, and two vortex tubes, due to the counter-rotating legs (Best, 2005). The discussed flow structure around a hemisphere is summarised in Figure 2.6.

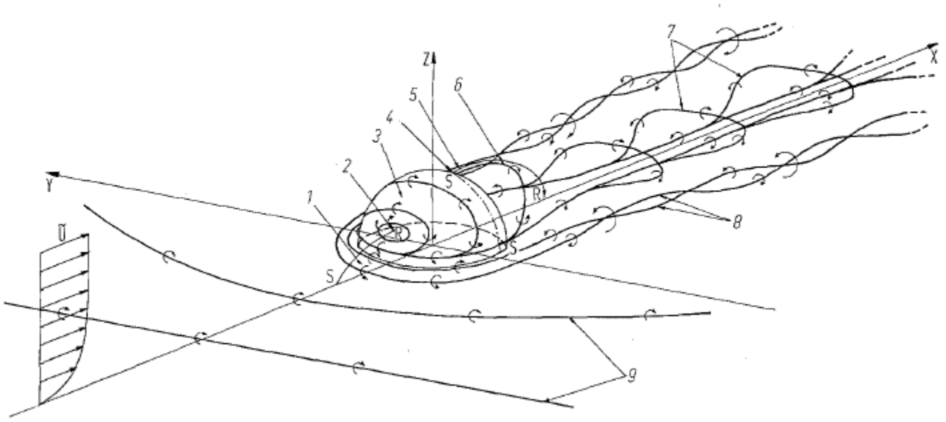

Figure 2.6. Illustration of the vortices formed by the flow around a hemisphere, 1) horseshoe vorticity, 2) stagnation point, 3) generation of vorticity, 4) separation line, 5) dividing streamline, 6) shear layer vorticity, 7) vortex loops, 8) trailing vortices, 9) boundary layer vorticity, S refers to separation and R refers to reattachment. Figure taken from Savory and Toy (1986) (Figure 6)

Acarlar and Smith (1987) described the formation of hairpin vortices generated by a single submerged hemisphere (6 to 36mm in diameter) in greater detail, shown in Figure 2.7. They observed that after separation from the hemisphere the boundary layer moves downstream dragging fluid with it. The outer flow rotates inwards towards the bed. This creates a pressure gradient and centrifugal force that concentrates the vortex, forming the hairpin vortex. The formed vortex consists of a head region and a pair of counter rotating legs. After formation, the vortex is shed and the formation of the next begins leading to the vortices being nested inside of each other, with the legs of the downstream vortex sitting in the head of the newly formed vortex. Once it has been shed, the vortex moves away from the bed at a 45° angle. The passing of the legs through the boundary layers leads to their stretching and the formation of a kink. When the vortex is in the shear layer, the flow in the shear layer causes it to rotate towards the bed; however velocities that are induced create lift, forcing the vortex further away from the bed. The formation of the hairpin vortex was seen to be independent of the horseshoe vortex, as its elimination through the use of a half-teardrop bluff body did not affect the formation or structure of the hairpin vortex (Acarlar and Smith, 1987).

Acarlar and Smith (1987) observed two peaks within the turbulence intensity profile $2D$ downstream of the hemisphere at the relative heights of $z/r = 0.5$ and $z/r = 1$, which it is suggested illustrate the presence of the legs and head of the hairpin vortex respectively. Further downstream at 5D, the upper peak has moved upwards to $z/r = 1.5$, which supports the suggested model of the vortex move upwards away from the wall, with distance downstream. Acarlar and Smith (1987) use the formation of the hairpin vortices to di-

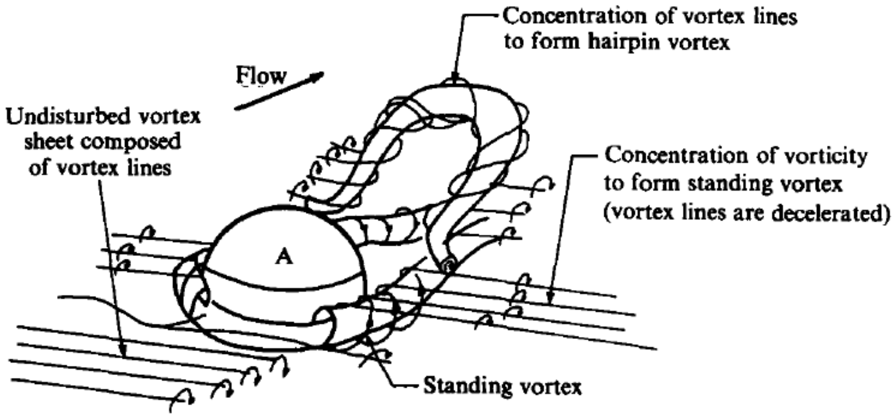

Figure 2.7. Illustration of the formation of a hairpin vortex in the wake of a hemisphere, taken from Acarlar and Smith (1987)

vide the wake of the hemisphere into three regions; a near-wake $(0 - 1.5D)$ immediately downstream of the hemisphere where the hairpin vortices are formed, a growth region $(1.5 - 7.5D)$ where the hairpin vortices grow and evolve, and the far-wake $(7.5 - 40D)$ region where secondary structures are present due to the hairpin vortices. However it is not suggested how these regions compare to the generally defined regions of the recirculation zone and velocity deficit region (Zavistoski, 1994).

The effects of obstacles on the flow has also been investigated in natural streams, by examining the flow structure around pebble clusters (Buffin-Bélanger and Roy, 1998; Lacey and Roy, 2007; Lacey and Nikora, 2008). The near-wake of the pebble cluster was indicated by a region of marked increase in the standard deviation of the longitudinal and lateral velocities, u and v, and an increase in the Reynolds stress (Buffin-Bélanger and Roy, 1998). TKE was shown to be increased due to the presence of the pebble cluster, with a magnitude in the wake of twice of when the pebble cluster was not present (Lacey and Roy, 2007). Buffin-Bélanger and Roy (1998) identified a number of regions within the flow around an isolated pebble cluster, with a relative submergence (y/h) of approximately two.. The flow is accelerated over the top of pebble cluster; this flow separates from the cluster travelling back on itself to form the recirculation zone directly behind the protrusion, and causing regions of high turbulence and stress in the near-wake. Behind the recirculation zone, reattachment of the boundary layer occurs. This progresses into a region where upward sweeps of fluid are present before the flow returns to the upstream profile. Above the recirculation zone, a region of vortex shedding is observed, again associated with high levels of turbulence intensities and shear stresses. A large region downstream was seen to be affected by the presence of the pebble cluster. However velocity measurements were only taken in a single longitudinal plane down the centre of the protrusion, and therefore the three-dimensional nature of the wake could not be defined. The regions identified here are very similar to the model of flow described by Best (2005) for two-dimensional dunes.

2.5.3 Relative Submergence

Buffin-Bélanger and Roy (1998) suggest that the relative submergence (flow depth relative to the height) of the protrusion is important in controlling the vertical expansion of the wake and turbulence. Shamloo et al. (2001) examined the effect of relative submergence (varying it from 0.6 to 4.3) on the expansion of the wake of a hemisphere considering both emerged and submerged conditions. The major observation was that when the flow depth was greater than the hemisphere height ($y/h > 1$), the flow over the top of the boulder consisted of two layers; the lower layer was affected by the shear layer and mixed with the wake, whereas the upper layer, dependent on the flow depth, was not seen to interact with the recirculation zone. This is similar to the observations of Stoesser et al. (2008) examining the flow over two-dimensional dunes, where a free surface layer was identified above the shear and wake layers, and was characterised by lower turbulence.

Shamloo et al. (2001) identified four different flow regimes in relation to the relative submergence. In regime one, where the flow depth is greater than $4h$, the hemisphere was not seen to have an effect on the water surface, and in this situation the upper layer of flow did not interact with the wake. In regime two, where the relative flow depth is between $1.3h$ and $4h$, the upper layer of flow was still seen to not interact with the wake, but the effect of the hemisphere was seen at the water surface by the creation of waves. In regime three, for relative flow depths of $1.1h$ to $1.3h$, the upper layer of flow does interact with the wake, as the boundary layer causes mixing throughout the whole depth, leading to negative velocities being present at the water surface. The last regime, four, describes the emergent case where the relative flow depth is less than h. Here there is strong backflow behind the hemisphere and the upper layer of flow is not present. These changes in flow regimes with relative flow depth result in a change in the size and shape of the wake, with the wake decreasing in length and increasing in width, with decrease in relative flow depth (Shamloo et al., 2001). This shows that the suggestions of Buffin-Bélanger and Roy (1998), were correct and that greater vertical expansion of the wake occurs at lower flow depths, but that this is relative to the boulder height.

2.5.4 Roughness Arrays

In the natural environment of a gravel bed river, although isolated protrusions will be present, it is more likely that multiple protrusions will be present in the same location in a stream, for example in a riffle section. Therefore, although it is important to understand how an individual protrusion, such as a boulder or pebble cluster, affects the flow,

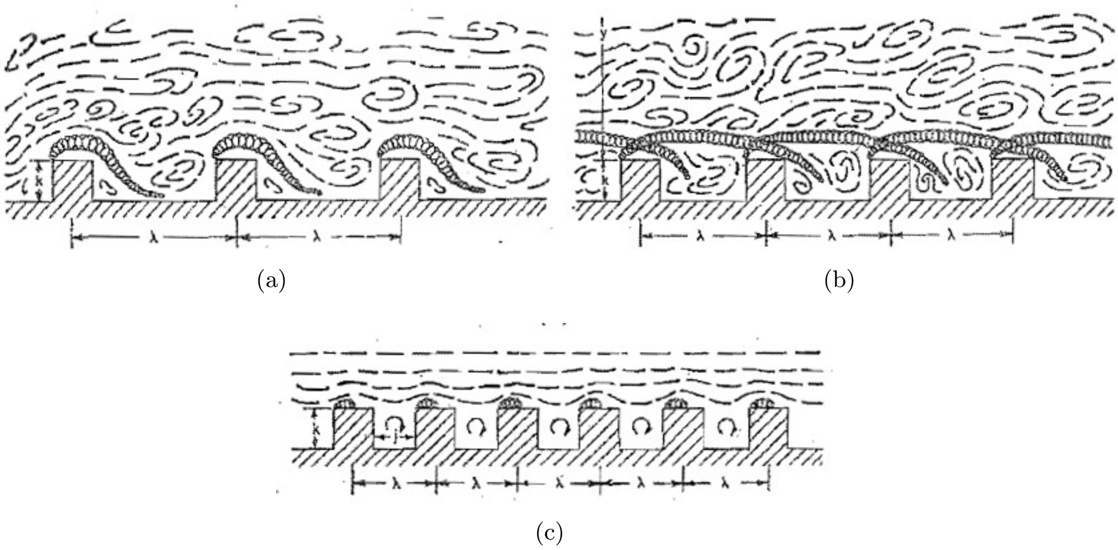

Figure 2.8. Illustrations of the three types of rough-surface flow, (a) Isolated roughness flow, (b) Wake interference flow and (c) Quasi-smooth flow, taken from Chow (1959) (Figure 8-4).

it is also important to understand how these protrusions might interact and the combined effect they might exhibit. The predominant factor that drives their combined effect will therefore be their density and arrangement.

When considering more than one obstacle it becomes more complicated to define the flow structure. Depending on the proximity of the obstacles, the wake of an upstream obstacle may affect the flow structure of the downstream obstacle. The wake structure within an array, whether it is laminar of turbulent, affects the wake contribution to the turbulent kinetic energy and diffusivity (Nepf, 1999). Within a sparse array the obstacles are placed at a distance from each other so that the wake of one obstacle does not affect the next obstacle within the array, and therefore the force exerted by the array on the flow will be equal to the sum of the force exerted by each individual cylinder. However, in a dense array the spacing is such that there is interaction between the wake of an obstacle and the next downstream obstacle. The wake of the upstream obstacle reduces the oncoming velocity of the downstream obstacle, and subjects it to increased turbulence due to the characteristics of the wake. This in turn will affect the separation point on the obstacle, pressure gradient and therefore drag on the downstream obstacle, with a reduction in drag and drag coefficient present (Nepf, 1999). This is referred to as the 'sheltering effect' (Raupach, 1992), which in arrays can combine to produce a significant reduction in the drag of the array compared to if the obstacles were placed individually within the flow (Li and Shen, 1973; Nepf, 1999). The degree of sheltering effect within a parallel array is more sensitive to the longitudinal spacing than a staggered array, which appears to be unaffected for a given lateral spacing (Li and Shen, 1973).

In hydraulically rough flow, three flow types, shown in Figure 2.8, have been identified dependent on the density of roughness elements (Chow, 1959); 1) isolated roughness flow, where the spacing of the elements is greater than the length, resulting in the elements acting in isolation, and therefore the wake of one element has dissipated before reaching the next element; 2) wake interference flow, the spacing of the elements is similar to the wake length, and therefore the wake of one element interacts with the wake of the next, causing high local velocities; and 3) quasi-smooth flow, where closely packed elements allow the flow to skim over the top, while slow flowing stable eddies are present between the elements.

When considering a single object the wake can be measured and defined by detailed velocity measurements, however when an object is in an array then the collective effect of the objects needs to be defined. The combined sheltering effects of cylinders within a uniform array has been widely researched due to its analogue to vegetation, and the effects it has on the quantification of the drag coefficient of vegetation within streams and rivers. Li and Shen (1973) compared methods of determining the effect of a cylinder on the downstream velocity, and therefore a downstream cylinder, in order to predict any change in the drag coefficient due to the presence of the array. In particular Li and Shen (1973) examined the model proposed by Petryk (1969), suggesting that the effect on the downstream velocity of multiple obstacles in the flow could be described by the linear superposition of the velocity deficits seen in the wakes of the obstacles. This in turn can then be used to calculate the effect on the drag coefficient of the the array. However, Raupach (1992) suggested that the combined sheltering effects of a uniformly or randomly distributed array can be calculated by random superposition of the individual sheltering volume.

More recently research has focused on measuring the area or volume of wake relative to the total area or volume of flow (Nepf et al., 1997; Canovaro and Francalanci, 2008; Huthoff, 2009). Canovaro and Francalanci (2008) compared the wakes produced by a row of macro-roughness elements, to the wake created by a single object. Canovaro and Francalanci (2008) defined the wake as the volume of negative velocities which is in contrast to the definition used by Zavistoski (1994) and Nepf (1999), where a region of reduce streamwise turbulence intensity in the was considered. Canovaro and Francalanci (2008) found the wake of the multiple elements to be greatly reduced from what would be expected from the wake of a single element, due to interaction between the macro-roughness elements. They related the wake volume as a ratio of the volume of water between elements to the surface density (the area of the element as a ratio of the area between elements), identifying a semi-linear relationship where the wake volume ratio increased with surface density. However a discontinuity was seen in this relationship at a surface density of $\approx$0.4. It is suggested that this discontinuity represents the transition from the elements acting in isolation, to the wakes of the elements interfering (Canovaro and Francalanci, 2008), and that this is related to the density of maximum flow resistance (Canovaro et al., 2007). Huthoff (2009) suggests that the wake filling factor (the volume of wake to the volume of water) can be used to generate an equivalent roughness length for the flow over a roughness of an array of obstructing obstacles, quantifying the resistance to the flow.

Arrays of dowels have been used to model the effects of vegetations within streams (e.g. Li and Shen, 1973; Nepf et al., 1997; Nepf, 1999). Nepf et al. (1997) suggests that the lateral diffusion of particles within a stem array is affected by the volume of wake that is present. The lateral movement of a particle in a random walk model can be described by the length of the time step and the local turbulence, described by root-mean-square (RMS) of the velocity (Nepf et al., 1997). In a homogeneous turbulence field, the lateral motion will be the same at every time step. But in an array, such as stream vegetation, the level of turbulence present at a location will be affected by whether the particle is in the wake of a stem or not, as turbulence is greater within the wakes of protrusions. Therefore, to model the lateral diffusion it is necessary to know the probability of a particle being in the wake or not. This probability can be described by the Wake Fraction (WF), which is the unit area occupied by the wake. Nepf et al. (1997) state that the WF of an array can be extrapolated from the wake of a single stem, which can be defined by a dimensionless ratio, M, which is the ratio of wake area to stem area.

Zavistoski (1994) defines the wake of a cylinder from the inwake turbulence, where the edge is defined as where the level of turbulence is within 10% of the free-stream value, leading to a wake of $20D$ in length and $2D$ in width, therefore giving an M of 40 (Nepf, 1999). Wake area fractions can then be generated from the stem density, P and M for multiple arrays. It is suggested that where P is small, then the WF will increase linearly as there are no interactions between the wakes, but as P gets larger the wakes will begin to overlap and WF will increase less with each increase in P until the WF equals 1, and the entire volume consists of wake. Nepf et al. (1997) tested this model, using randomly placed stems, and different wake sizes (M), comparing the results to experimental lateral diffusivities. The model compared well to WF calculated from the measured diffusivities, but this was dependent on shedding being present (Nepf et al., 1997), suggesting that when shedding was not present, the diffusivity was better described by the bed generated turbulence and not the turbulence produced by the stems. Both of these studies have shown that the presence of shedding has an effect on the relationship between the wake size within an array and the size of the elements creating the wake. As the WF has been shown to affect lateral diffusion within a flow due to the presence of turbulence from the protrusion, it is therefore possible that the WF will also affect the diffusion or movement of leaves and therefore their retention with a stream.

2.6 Summary

Temperate low-order stream ecosystems gain the majority of their energy from terrestrial sources of organic matter. This organic matter has two possible fates; it is either retained within the system, or it is exported out of the system. Therefore for the stream ecosystem to gain the benefit of this input, it is essential that the material is retained. Retention of the material allows biological processing to occur, releasing the energy and nutrients, allowing growth of macroconsumers and supporting the rest of the food web that is present within a stream. As the rate of processing is due to microbial and macro-invertebrate metabolism, it is affected by physical characteristics of the stream such as dissolved oxygen, light availability and temperature.

The retention of leaves has been seen to be negatively related to an increase in discharge, with spates resulting in increased transport of retained material. A negative relationship is also seen with flow depth, as the organic matter is less likely to contact the protrusions when the flow depth is greater, and retention has been seen to increase with increased complexity of the bed. It is suggested that flexibility of the leaves helps them to be retained, as it gives them the ability to 'wrap' themselves around protrusions. Different retentive structures have been identified, such as boulders, pebble clusters, woody-debris and backwaters. The effectiveness of these structures has been seen to vary between streams and has also seen to be dependent on the presence or absence of other structures. The transport of organic matter in streams can be fitted to a negative exponential model, where the slope, k_R, known as the retention coefficient, describes the ability of the stream reach to retain matter, and provides a useful comparison between streams and experiments.

Streams are governed by the principles of open channel flow, the parameters of which can be used to define the flow conditions at both the 'global' cross-sectional scale and the local scale. As well as the use of time-averaged velocities, the fluctuating components of the instantaneous velocity measurements can be used to describe the turbulence present using different methods. A number of methods of calculating the bed shear stress have been presented, and a comparison of the different methods suggested that different methods should be used depending on the complexity of the flow.

The protrusion of an object into the flow is subject to two types of drag from the presence of friction and pressure gradients. The wake of an object is characterised by decreased velocities and increased turbulence, due to the presence of large-scale eddies, and has a distinct longitudinal and lateral profile. The flow around a emergent cylinder has been well characterised and documented. The development and structure of the wake has been shown to be related to the Stem Reynolds number. Detailed visualisation of the wake of a hemisphere has shown the presence of two vortices: a horseshoe vortex immediately upstream of the hemisphere and a hairpin vortex, which forms after separation from the crest and is then shed from the reattachment point. The size of the wake has been shown to vary depending on the level of upstream turbulence. In natural environments, although isolated protrusions do occur, it is more likely that protrusions will occur in a random array. The spacing or density of the protrusion will affect how they affect the flow, and whether the wake of one element will interact with the wake of the next. The size of the wake relative to the volume of water can be measured, and used to quantify the effect of the array on parameters of the flow.

3

EQUIPMENT, METHODS AND MEASUREMENTS

This chapter describes the methods and equipment used to investigate the physical and hydraulic factors which influence the retention of leaves within streams. It will discuss each item of equipment to be used, and where necessary the methods and results of any calibration carried out. Methods that are consistent across all experiments will be described here, however the more detailed procedures involved in each of the experiments will be presented in the later Chapters.

3.1 Flume

The experiments presented in this thesis were carried out in the NERC flume, School of Engineering, Cardiff University. It is a bi-directional recirculating tilting flume, 17m in length, 1.2m in width and 1m in depth. The walls and base of the flume consist of smooth glass creating very little flow disturbance and allowing all round visibility. The flow at the inlet is straightened using a 0.2m thickness of honeycomb, and a net is fitted at the outlet (length of 17m) to prevent debris entering the impeller. A weir was added to the flume at a distance of 15.35m in the downstream direction (see Figure 3.1) in order to control the surface water profile along the flume, which will be discussed in Section 3.1.3. The addition of the weir to the flume decreased the working length of the flume from the full 17m to a 15.35m length.

The flume is fitted with a bi-directional impeller pump. The discharge of the flume is controlled by altering the power provided to the pump via the control box. A Controlotron 1020 Clamp-on Transit-time Flowmeter measures the instantaneous and cumulative discharge of the flume. The measurement of discharge and calibration of the flowmeter will be discussed in Section 3.3. Rails mounted on the top of the flume carry a motorised instrument carriage which is both a means of gaining access to the flume and also holds instrumentation such as the Nortek Vectrino ADV for taking velocity measurements, the use of which will be described in Section 3.2.

3.1.1 Bed Slope

The flume can be set at slopes varying from a positive slope (uphill) of 1 in 1000 to a negative slope (downhill) of 1 in 300. For the experiments in this thesis it was necessary to implement slopes (downhill) of 1 in 300 and 1 in 1000. These slopes where set up using standard surveying techniques, by comparing staff heights at lengths of 0 and 15m, and varying the slope until the required slopes of 1/300 and 1/1000 were reached. Measurements were taken at these locations and not over the full length due to the reduced working area.

3.1.2 Flow Depth

In order to measure the flow depth within the flume throughout the experiments a series of rulers (measuring to a precision of 1mm) were placed at intervals, ranging from 0.5m to 1.5m, on the side wall of the flume. The placement of the rulers relative to the flume bed could not be done exactly and therefore to ensure accurate measurements of flow depth the height of each of the rulers were calibrated using standard surveying techniques. The staff was placed on the flume bed next to each ruler in turn and the heights on the two

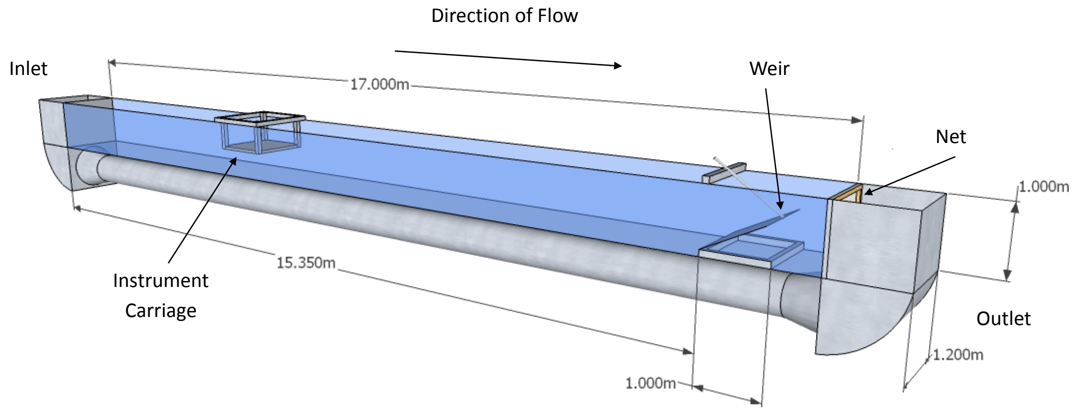

Figure 3.1. To scale illustration of the NERC flume

compared using the level. The difference between the two provided a calibration that could be applied to all measurements taken using the ruler.

3.1.3 Uniform and Gradually Varied Flow

In order to obtain uniform flow a rectangular weir was fitted within the flume at 15.35m downstream from the inlet (see Figure 3.1). The weir was hinged at the base and could be raised and lower by small increments. Uniform flow was investigated using standard methods, a discharge was obtained, and the water surface profile was measured, to the nearest millimetre, using the rulers described in Section 3.1.2. The weir was raised in order to change the water surface profile, however this resulted in a change in discharge. Once this was corrected, by the addition of extra water, the water surface profile was measured again. When compared it was discovered the there was no change in the slope of the water surface for constant discharge and varying weir heights. A number of combinations of water depth and discharge were investigated, however the slope of the water surface profile remained constant and could not be changed with the equipment available.

The experiments were therefore carried out under gradually varied flow conditions. For each experiment a discharge and flow depth at the mid-flume length were chosen and the water surface profile was recorded, by measuring the water depth along the flume using the rulers described in Section 3.1.2. For each experimental set up the water surface profile was plotted, evaluated and is presented. A linear regression relationship was fitted to each profile, which is presented along with the 95% confidence interval. The water surface profile for the flat bed experiments presented in Chapter 4 is given in Figure 3.2. The profiles for each combination of boulder density (see Section 3.5.3) and flow depth

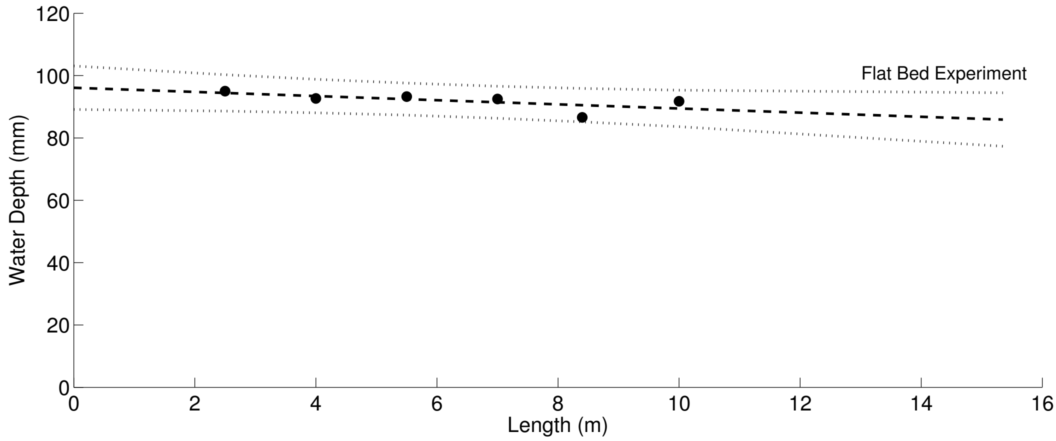

Figure 3.2. Water surface profiles for Flat Bed experiments presented in Chapter 3. The dashed lines represent the lines of best fit.

for the experiments presented in Chapters 5 and 6 are given in Figures 3.3 and 3.4. The water surface profile for the experiments presented in Chapter 4 were not significantly different from zero, and therefore for these experiments conditions were considered to be pseudo-uniform flow. However, for all other experiments the flow was subcritical and all the slopes were classified as M1 slopes (Chow, 1959).

3.2 Velocity Measurements

3.2.1 Velocimeter

Velocity measurements were taken using an Acoustic Doppler Velocimeter (ADV). ADVs calculate the velocity of the water using the Doppler effect (Jewett and Serway, 2008), by means of the assumption that particles present in the water are moving at the same velocity as the water itself. This therefore often requires the water to be seeded, to create a sufficient signal-to-noise ratio (SNR) to allow accurate measurements. The frequency of the reflected signals measured at the receivers are shifted due the movement of the particles, the magnitude of the shift can then be used to calculate the velocities in each direction. Further information on the working principles of an ADV can be found in Lohrmann et al. (1994).

A downwards-looking Nortek Vectrino Velocimeter was used for the flume experiments presented in this thesis. This consists of a central transmitter, 6mm in diameter, which is surrounded by four equally spaced receivers, allowing three-dimensional velocities to be measured. The four receivers produce two vertical (denoted as $w1$ and $w2$) measurements alongside the streamwise (u) and cross-streamwise (v) measurements. The sampling vol-

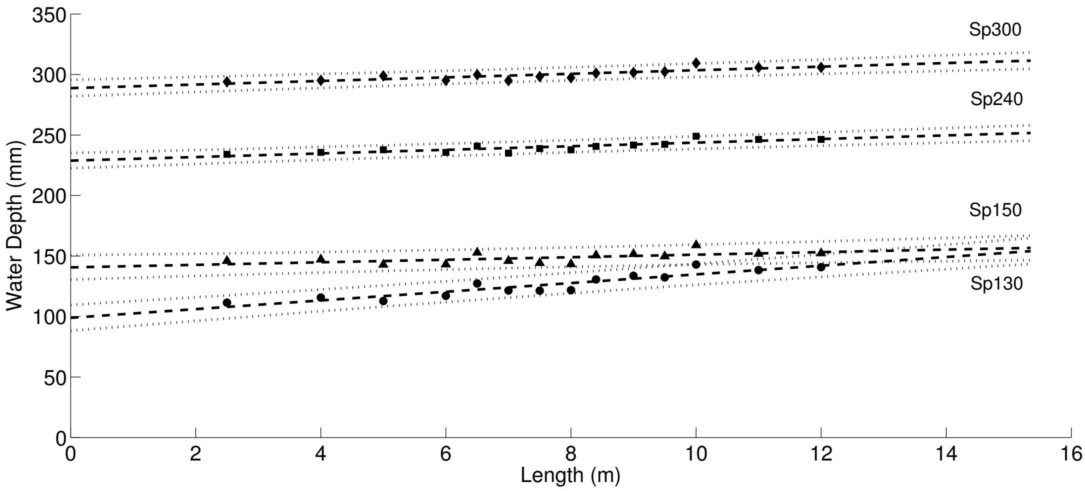

(a)

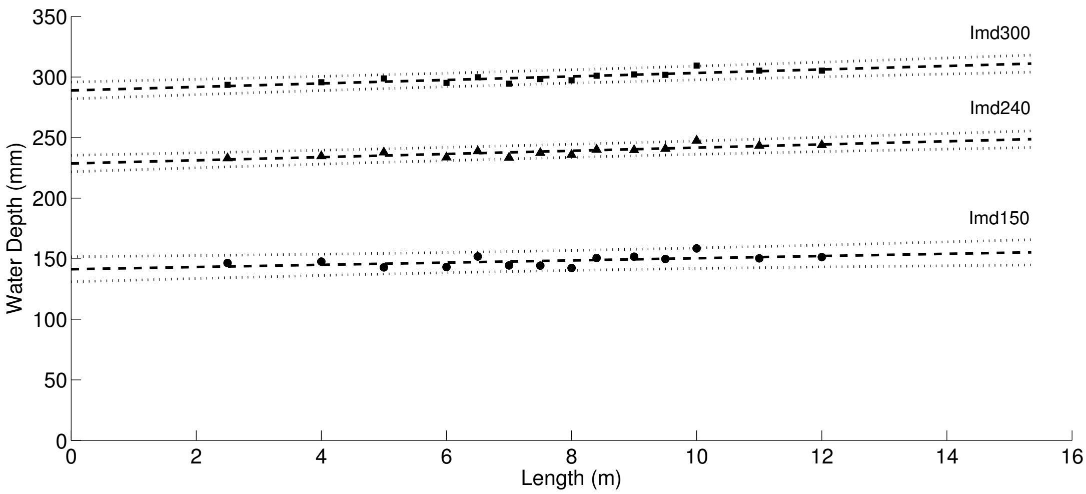

(b)

Figure 3.3. Water surface profiles for each of the flow depths for the (a) Sparse (Sp) and (b) Intermediate (Imd) densities for the different flow depths (130, 150, 240 and 300mm). The dashed lines represent the lines of best fit.

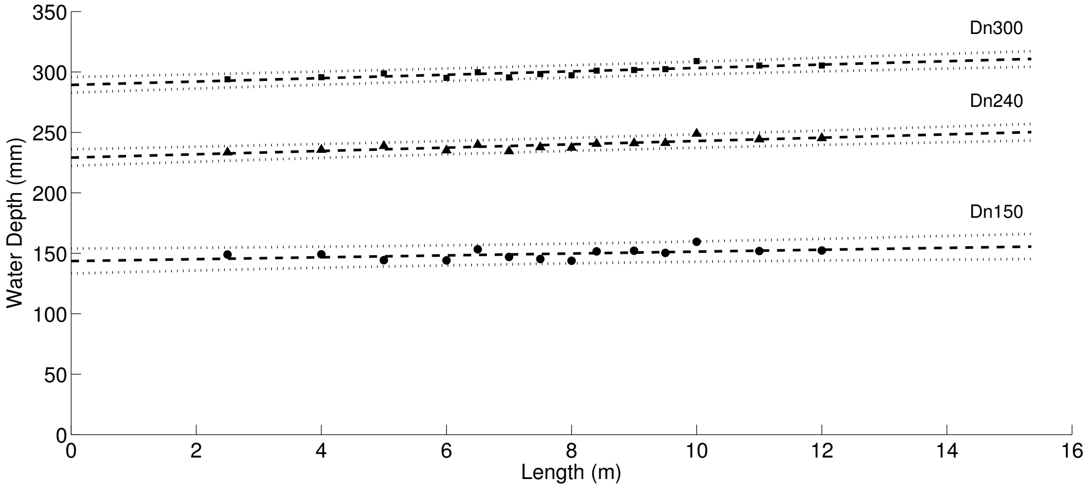

(a)

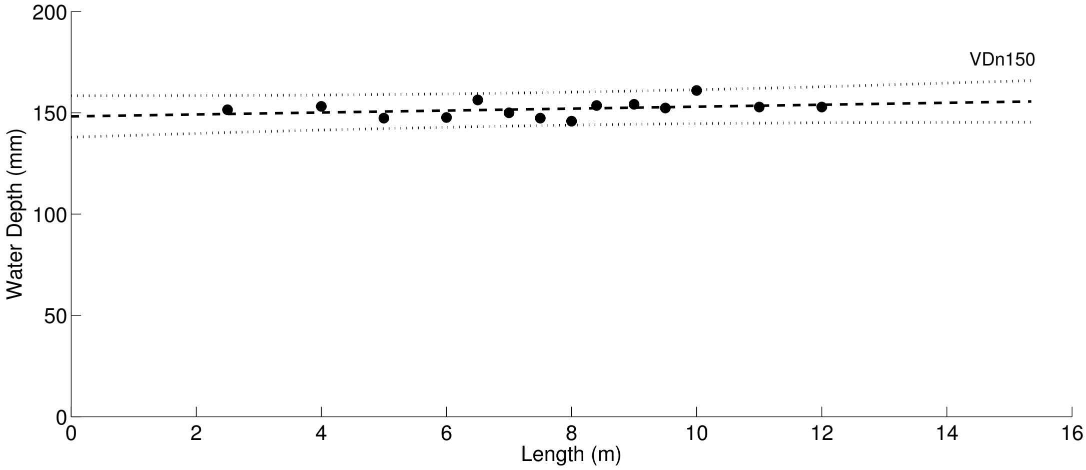

(b)

Figure 3.4. Water surface profiles for each of the flow depths for the (a) Dense (Dn) and (b) Very Dense (VDn) densities for the different flow depths (150, 240 and 300mm). The dashed lines represent the lines of best fit.

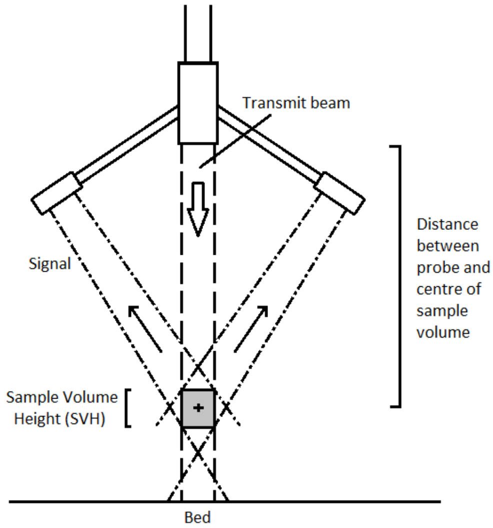

Figure 3.5. Illustration of an ADV probe, the intersection of beams, and location of sample volume, after Precht et al. (2006))

ume is located at the intersection of the transmitted and received beams, shown in Figure 3.5, centred approximately 50mm from the transmitter, with each individual probe being separately calibrated. The sampling volume is defined as the region of high signal-to-noise ratio, (SNR), showing that the acoustic signal is strong relative to the background noise (Sontek, 1997; Finelli et al., 1999).

The sampling volume height (SVH) can be configured by means of the software and ranges from 1 to 9.1mm dependent on the transmit length, where smaller transmit lengths allow smaller sample volumes. Measurements can be taken at sampling rates from 1 to 200Hz (with Vectrino+ firmware), and with a range of different nominal velocity ranges, from ±0.03m/s to ±4m/s. The Vectrino can also be used to measure the distance between the transmitter and a surface below it, such as the bed, to the resolution of 1mm and temperature, to a resolution of 0.1°C, and an accuracy of 1°C.

To use the Vectrino correctly there must be accurate knowledge of the exact location and height of the sample volume. Previous research on three-probe ADVs has shown the sampling volumes to be much larger than specified and the centre location of the sample volume to be different to that stated by the manufacturers (Finelli et al., 1999; Precht et al., 2006). As stated the sample volume centre for a Nortek Vectrino ADV is located approximately 50 mm from the transmitter, and there is a minimum sampling volume of 1mm, allowing measurements to be taken on a very small scale (Nortek, 2004).

If either of these two parameters are not as specified then this could lead to significant errors in the velocity measurements. For example, if the sample volume is lower than expected or is larger than expected, near-bed measurements (e.g. 1mm or 2mm from the bed) could result in part of the sample volume intersecting with the bed, leading to underestimations of the water velocity (Sontek, 1997; Finelli et al., 1999) due to the reflection from the stationary bed. It was therefore deemed necessary before use of the ADV that calibration was carried out to test both the spatial positioning of the vertical centre of the sampling volume relative to the probe transmitter and the actual size of the sample volume relative to the stated size.

Finelli et al. (1999) showed that a stationary acoustic target can be used to locate the sample volume placement and size, as this will allow the acoustic signal to be reflected, indicated by an increased SNR. One would expect, therefore, there to be a steep increase in the SNR as the acoustic target enters the sample volume, and a steep decrease as it leaves, with a peak SNR value at the vertical centre of the sample volume.

3.2.2 Velocimeter Calibration

The following method is based on the method of Finelli et al. (1999) which determines the SVH using an acoustic target in still water. The manufacturers specify that the vertical centre of the sample volume for this probe is approximately 50mm from the probe transmitter, with no tolerance stated (Nortek, 2004). An acoustic target was created using two pieces of monofilament 0.16mm fishing line crossed at 90° to each other in a cylindrical plastic bucket. The bucket had a diameter of 219mm at the bottom, changing to 267mm at the top, and was 257mm in height. The filament was stretched across the width of the container so that the cross was located at the centre of the container at a height of 146mm from the base. The container was filled with tap water, which was left for 24 hours to de-gas and to allow any particles to settle. The ADV was mounted on a vertical scale centred over the acoustic target. The receivers were placed at a 45° offset to the filaments.

SNR (dB) measurements were collected for one minute at 200Hz at a variety of elevations, to ensure the sample volume moved through the acoustic target. SNR measurements were taken at distances of 25 to 70mm between the probe and acoustic target. The probe was moved at 5mm increments in the outer distances, and then 1 mm increments were used between the distances of 35 and 55mm, for accurate definition of the sample volume. Nominal SVH of 2.5mm, 4mm and 7mm, with a transmit length of 1.8mm, and SVHs of 1mm, 2.5mm and 4mm, with a transmit length of 0.3mm were tested. The use of two different transmit lengths allows a greater range of sample volumes to be tested, and duplication of two nominal SVH.

Separate SNR data is produced for each of the four receivers, ($u, v, w1$ and $w2$). For each height above the acoustic target, time-averaged SNRs were calculated for each receiver, from which a grand mean was determined. This approach is valid due to the spatial overlap of the receivers and has been used by other researchers (Finelli et al., 1999). The raw SNR produced here is a logarithmic value of the ratio of signal amplitude to noise amplitude, it is therefore possible to linearise it to allow for further analysis. Therefore two approaches were used to analyse the SNR data to determine the size and placement of the sample volume. The first uses the grand mean of raw SNR values, whereby the grand mean was plotted against the distance between the acoustic target and the probe for each of the tested nominal SVH, and transmit lengths. For the second approach linearisation was carried out on the raw SNR, prior to a mean being calculated, using the following formula (Nortek, 2004):

$$\text{Linear SNR} = 10^{(\text{raw SNR}/20)} \tag{3.1}$$

A time-averaged mean was then calculated for each receiver, from which a grand mean of the four receivers was calculated for each probe height. This linear grand mean was then also plotted against the distance between the probe and acoustic target.

In order to identify the SVH, an increase in SNR needs to be distinguished from any background level present. Therefore, for both the raw SNR and the linear SNR a background level was calculated by spatially averaging the SNR values in the height regions of 55 to 70mm and 25 to 35mm, as SNR values at these heights did not feature in any of the sample volumes. Figure 3.6 shows the results for a transmit length of 0.3mm, while for the transmit length of 1.8mm the results are shown in Figure 3.7. On both figures the background raw SNR levels have been shown along with the vertical centre and the limits of the sample volume. The boundaries of the sample volume were defined by the SNR value exceeding the background SNR level, and these were verified by evaluating the gradient of the SNR distance curves.

These results show a very distinct sample volume. The background SNR level was extremely small, comparable to those seen by Precht et al. (2006) and does not vary significantly between the different tests. Finelli et al. (1999) and Precht et al. (2006) found that the linear SNR data indicated smaller SVH than the raw (or logarithmic) SNR, and were more closely related to the nominal SVH. Finelli et al. (1999) showed that the raw SNR data is a better indicator of actual SVH. However in this experiment there is good agreement between the raw SNR data and the linearised SNR data, with both indicating the same SVH. A summary of the results is presented in Table 3.1.

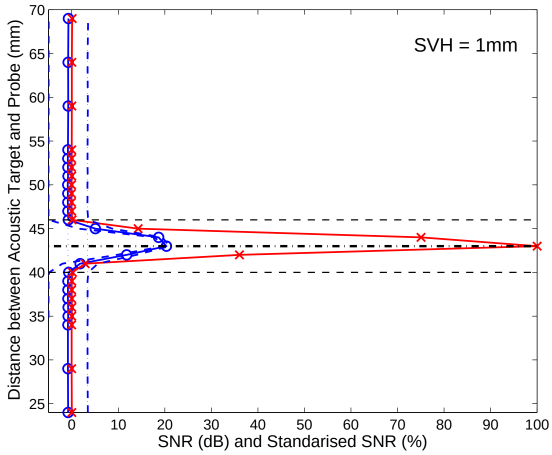

(a)

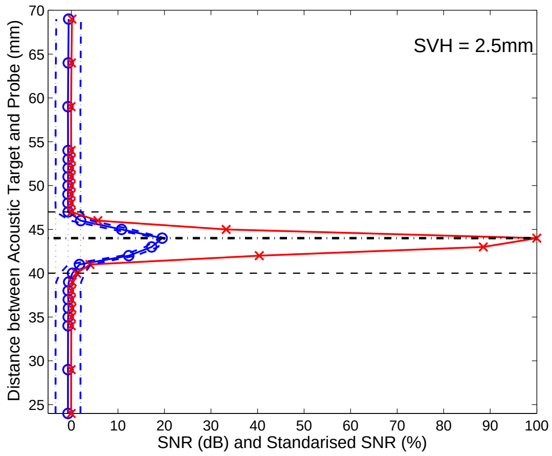

(b)

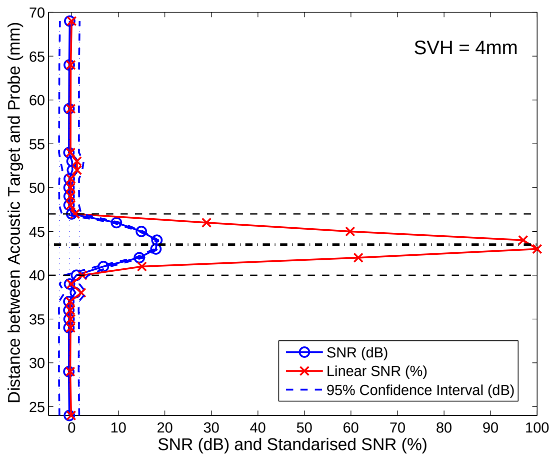

(c)

Figure 3.6. Results of the sample volume mapping with a constant transmit length of 0.3mm, for the nominal SVH of (a) 1mm, (b) 2.5mm and (c) 4mm. Each graph shows the raw SNR (dB) data with 95% confidence intervals and the Linear SNR data (adjusted for the background Linear SNR level and normalised to the maximum). The vertical dotted lines represents the background SNR level for raw SNR and 95% confidence intervals. The dash-dot line shows the centre point of the sample volume, and the two dashed lines show the limits of the sample volume.

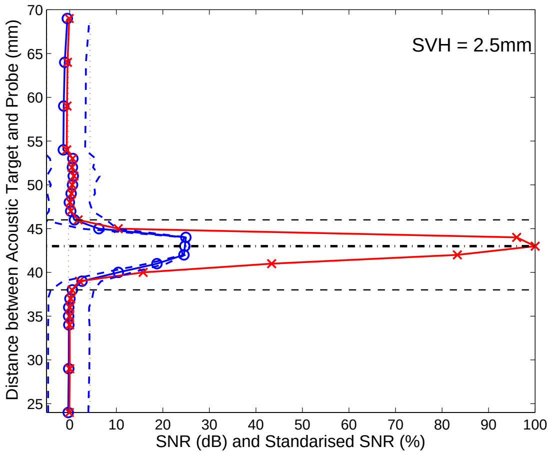

(a)

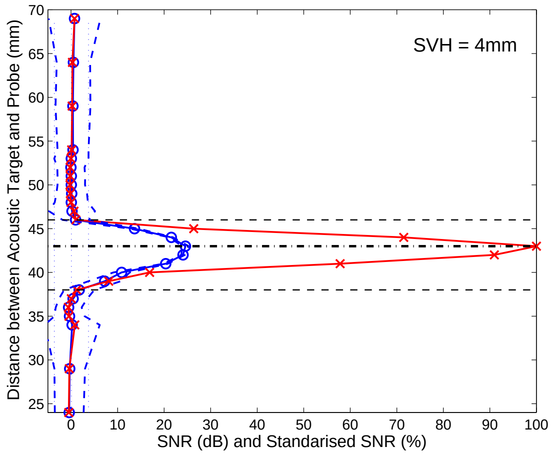

(b)

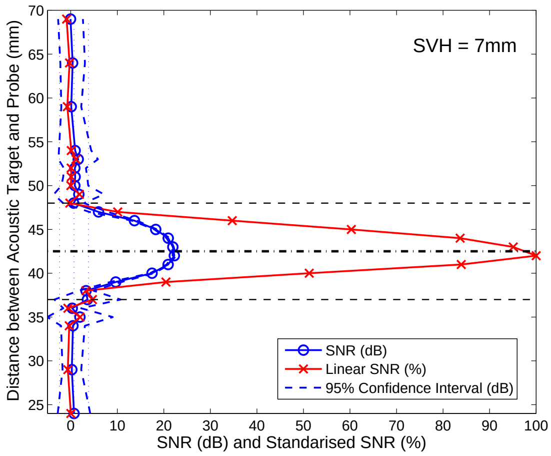

(c)

Figure 3.7. Results of the sample volume mapping with a constant transmit length of 1.8mm, for the nominal SVH of (a) 2.5 mm, (b) 4 mm and (c) 7 mm. Each graph shows the raw SNR (dB) data with 95% confidence intervals and the Linear SNR data (adjusted for the background Linear SNR level and normalised to the maximum). The vertical dotted lines represents the background SNR level for raw SNR and 95% confidence intervals. The dash-dot line shows the centre point of the sample volume, and the two dashed lines show the limits of the sample volume.

Transmit Length (mm)	Nominal SVH (mm)	Actual SVH (mm)	% Error	SVH Range (mm)	Vertical centre (mm)	Max SNR (dB)	Max St Dev (dB)	Min St Dev (dB)
0.3	1	6	600	3-7	43	20.36	3.50	0.12
	2.5	7	280	4-8	43.5	19.50	3.02	0.19
	4	7	175	6-8	43.5	18.30	3.62	0.10
1.8	2.5	8	320	5-9	42	24.95	2.17	0.32
	4	8	200	7-9	42	24.58	1.37	0.29
	7	11	157	9-12	42.5	22.26	1.31	1.31

Table 3.1. Sample volume calibration results including comparison of nominal SVH to actual SVH, vertical centre and error analysis.

These results show that the maximum SNR levels for a transmit length of 0.3mm are lower than those seen for a transmit length of 1.8mm even for comparable nominal SVH, suggesting it may be harder to obtain high SNR levels for smaller transmit lengths. For both transmit lengths, a decrease of 10.77% and 10.08%, respectively, in the maximum SNR values can be seen as the sample volume size increases. The error in the actual SVH compared to the nominal SVH decreases with increasing nominal SVH (Table 3.1). Despite the range of nominal SVH tested there appears to be little variation within the actual SVH over this range, with a smallest obtainable SVH of 6mm, which gives a closest measurement to the bed of 3mm. The same error was seen by both Finelli et al. (1999) and Precht et al. (2006). Precht et al. (2006) tested the Nortek Vector, a field ADV similar to the Vectrino, although it has three probes not four. The error observed here for the Vectrino is comparable to that observed for the Vector. However the error observed for the SonTek ADVfield observed by Finelli et al. (1999) and for the Nortek NDVfield observed by Precht et al. (2006) was considerably greater. A comparison of this data can be seen in Figure 3.8.

An error analysis was carried out to identify whether the differences seen between the two transmit lengths were significant, (see Table 3.1). The standard deviation was calculated for the mean SNR at each height. The 95% confidence interval, shown on Figures 3.6 and 3.7, illustrates the variation in the standard deviation over height. The largest variation is seen in the regions used to calculated the background SNR levels, and little variation is seen round the peak of the SV. Minimum and maximum background SNR levels were used to evaluate the variation in SVH.

These results show that there is greater uncertainty in the SVH for the smaller nominal SVH and that the variation is skewed towards a smaller rather than larger SV. Comparing the actual results for the SVH there appears to be a difference between the results for the

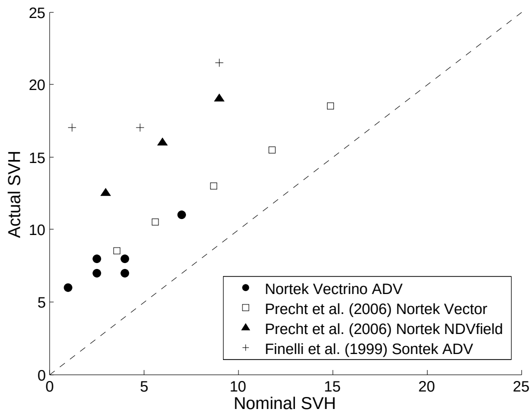

Figure 3.8. Comparison of the sample volume data found in this experiment to that of Finelli et al. (1999) and Precht et al. (2006). The dashed line is a line of equality, where nominal SVH equals actual SVH

two transmit results, however there is considerable overlap between the ranges for comparable nominal SVH's, and when tested they were found not to be significantly different. The difference in the actual results could be due to calculation of the background SNR level, as the maximum standard deviation in this region is much greater for the smaller transmit length of 0.3mm, giving more uncertainty in its calculation. The data suggests that it might be possible to achieve a smaller actual SVH for a given nominal SVH for the smaller transmit length but that this might be outweighed by the reduction in data quality (Lohrmann et al., 1994), illustrated by the lower maximum SNR.

The vertical centre point of the SV varied between the nominal SVH's examined. The mean vertical centre from the six tests was found to be 42.75mm (s = 0.69mm) from the probe transmitter, approximately 7mm closer to the probe than the approximate distance of 50mm stated by the manufacturers (Nortek, 2004). Each probe is calibrated by the manufacturers, where the distance for a specific probe can be retrieved from the configuration file. In the case of our probe, the value for the vertical centre of the sample volume was 46.77mm from the probe transmitter. Although this is closer to our calculated mean, there is still a large error of 4.02mm. With the sample volume being centred much closer to the probe than would be expected this will result in significant errors when taking velocity measurements. Measurements that we would expect to be 1–2mm above the bed would in fact would be closer to 10mm above the bed, and therefore would be sampling a higher section of the velocity profile than expected. Instead of under estimating the velocities present, as Finelli et al. (1999) suggested based on their work, due to intersection with the bed, we would expect the contrary, overestimating the velocities and underestimating the thickness of the boundary layer.

3.2.3 Velocity Measurements

The placement and SVH of all measurements presented in this thesis were be based on the data presented in the previous Section. It was assumed that the actual vertical centre of the sample volume is located 43mm from the probe. For all velocity measurements a transmit length of 1.8mm was used to yield higher quality data. A nominal SVH of 2.5mm was used, yielding an actual sample volume size of 8mm. All measurements were taken at 200Hz, and the length of sample will be stated in each experiment. Seeding material was added to the water to provide acoustic targets and ensure higher quality data.

3.2.4 Processing Velocity Data

The data was initially converted to a usable format (.dat) using the Nortek Vectrino software. These files were processed and analysed using Matlab. As stated the Vectrino records instantaneous velocity measurements at a rate of 200Hz, for a set period of time. The quality of the recorded data is shown by the SNR, as discussed, and the correlation. All velocity samples were filtered using Matlab to remove poor quality data; for this minimum thresholds of 8dB SNR and 70% correlation (Rusello et al., 2006), where both criteria was met. Data that did not meet this criteria was removed and was not included in any analysis. The data was then be used to calculate time-averaged velocities and turbulence statistics, which will be discussed in the results sections of later chapters.

3.3 Discharge

The discharge, Q, of the flume was measured using a Controlotron 1020 Clamp-on flowmeter which measures the instantaneous and cumulative discharge in L/s and KL respectively. It was necessary to calibrate the flowmeter to allow quick and accurate measurements of the flume discharge to be taken throughout the experiments. A velocity-area method was used to determine the flowrate, using BS ISO 748:2000 for guidance. This resulted in an equation (given in Section 3.3.2) that easily allows the flowmeter discharge reading to be converted into a discharge (L/s). This calibration only applies to the flowmeter when set to a water temperature of 13°C, (Controlon, 2005), and between 28 and 215 L/s.

3.3.1 Flowmeter Calibration

Calibration was carried out with bed material in place, this material is further described in Section 3.5. The bed consisted of two longitudinal strips of material, a sand (D_{50} = 1.3mm) and a coarse gravel (D_{50} = 30mm), each 600mm in width and extending the full length of the flume to the weir at 15.35m. A cross-section approximately midway along the flume, (8m from the inlet), was used for the calibration of the flowmeter, (see Figure 3.9). As the height of the bed varied over the width due to the variation in the material, it was

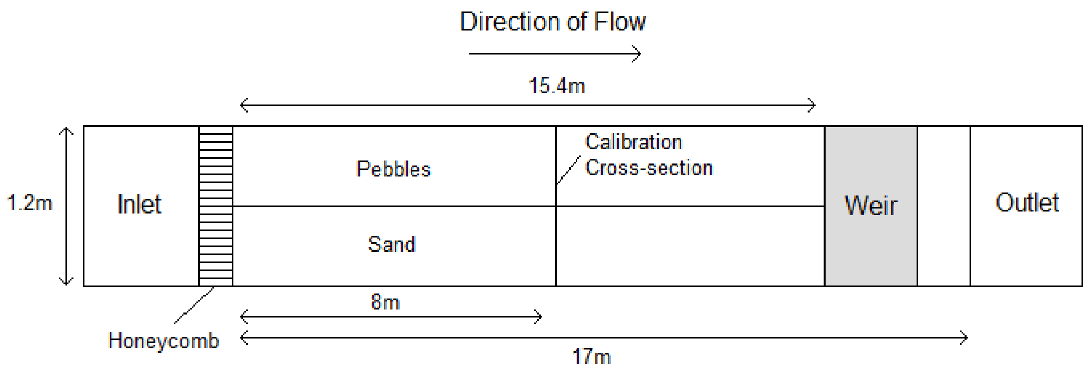

Figure 3.9. Plan view of the NERC flume

necessary to define an intermediate datum that could be used. The datum was calculated by taking depth measurements every 1cm across the width of the flume using a Nortek Vectrino ADV at a fixed height. The depth was subtracted from the fixed height to give the depth of the bed material at that point. The average of these depths was calculated. The mean depth was 43.93mm and therefore the datum was set to 44mm. The error in this measurement will be discussed later. The profile of the bed and the linear datum can be seen in Figure 3.10.

A water elevation of 435mm at the sample location (8m from the inlet) was maintained for all discharges, giving an average flow depth of 391mm at the sample location. The discharge was evaluated using a velocity area method, where the velocity is integrated over the area to give the discharge.

$$Q = \sum_{i=1}^{n} u_i . a_i \tag{3.2}$$

where, Q is the total discharge, n is the number of cells, u_i is the cell velocity and a_i is the cell area. The cross sectional area was divided into a number of smaller cells, with greater weighting (i.e. smaller cells, in the areas where there are steepest velocity gradients). Velocity measurements were taken in the centre of each of these cells. To gain an accurate discharge nine verticals were used, with six velocity measurements being taken in each vertical, giving a total of 54 cells, ranging from 0.004515 m^2 to 0.01944m^2 in size. The distribution of velocity measurements is presented also in Figure 3.10.

The slope of the flume was maintained at 1/1000. The flow was gradually varied flow, (see Section 3.1.3), with the positive water surface slope of 0.0012. The weir height was varied to maintain a constant cross-sectional flow area for different discharges. The measured dis-

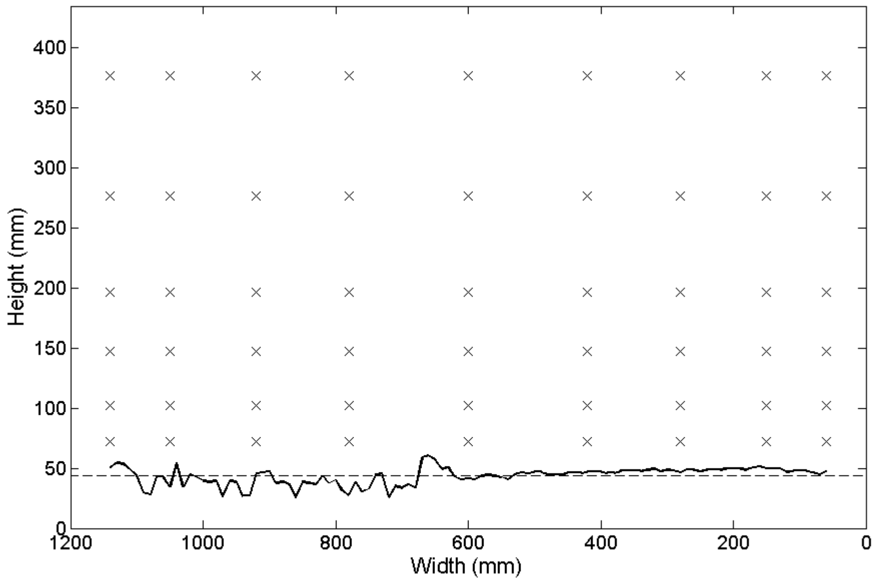

Figure 3.10. Bed profile and velocity measurement grid for discharge calibration. The solid line represents the bed profile, dashed line represents the average datum, and crosses represent the velocity measurement locations.

charge, Q_M, was obtained from the Controlotron 1020 Clamp-on Flowmeter. Cumulative discharge readings were taking over a period of 5 minutes, from which an time-averaged measured discharge was calculated. The actual discharge was calculated from three dimensional velocity measurements taken using a Nortek Vectrino ADV (see Section 3.2) at 200Hz for three minutes to ensure an accurate mean could be calculated. Poor quality velocity data, i.e. with a SNR less than 8 and Correlation less than 70% (Rusello et al., 2006), was removed before a mean velocity was calculated. A constant nominal Sample Volume Height (SVH) of 7mm was used resulting in an actual sample volume size of 4mm, with the velocity range being set to an appropriate value.

For each velocity point a time-averaged longitudinal velocity, ($\bar{u}$), was found, which was integrated over the cell area to calculate the discharge. The cell discharges were summed to calculated the calibrated discharge, Q_C. All discharges were recorded in litres per second. The method was carried out for a number of different measured discharges ranging from 28.73 to 215.23 L/s, the upper limit being constrained by movement of the bed material. In order to test the flowmeter calibration and ensure it was not an artefact of the water depth or another factor in the flume, two additional sets of measurements were taken for different flow conditions, using average water depths of 291mm and 441mm and different discharges within the stated range.

3.3.2 *Calibration Results*

Linear regression was carried out to find a relationship between the measured discharge and calibrated discharge, for the constant flow depth. A highly significant relationship was identified, (p-value < 0.005, R-sq 99.6%), giving the following calibration equation;

$$Q_C = 0.97365 Q_M + 3.583 \tag{3.3}$$

This relationship is shown in Figure 3.11. A Paired t-test comparing the calibrated discharges to those calculated from Q_M using Eq. 3.3, showed the mean of the difference not to be significantly different ($p = 0.548$). A General Linear Model was used to test the effect of flow depth on this relationship. Again, measured discharge was found to be a highly significant ($p < 0.005$) predictor of the calibrated discharge. However, flow depth was not significant at the 95% confidence limit, ($p = 0.350$), showing that the relationship is not an artefact of the constant cross sectional area. This effect was tested further by comparing discharges calculated using Eq. 1, to those calculated from a linear regression equation generated using all data points, ($Q_C = 0.97891 Q_M + 3.478$). A Two-Sample t-test compared the means of the two data sets showing them not to be significantly different ($p = 0.978$).

3.3.3 *Error*

The height placement of the Vectrino for the velocity measures is subject to a $+/-0.5$mm tolerance due to the accuracy of the scale. This error would not affect the calculation of the discharge for each cell as the measurements were taken at the centre of each cell, and therefore it will not affect the total discharge. This could affect the calculation of the average datum, resulted in a maximum mean bed height of 44.43mm, and a minimum of 43.43mm; although the first would have rounded to the selected datum, the second would have given a datum of 43mm. This change in the datum of 1mm represents an 0.256% increased in area. However this will not produce a linear increase in the discharge as this increase in area is at the boundary layer, where velocities are predominately at their lowest, and therefore will not produce a significant change in the calculated discharges. In rounding of the mean bed height from 43.93mm to the datum of 44mm error was introduced into the total cross-section area. There is an approximate 75 mm^2 underestimation of the area, which represents 0.016% of the total cross-sectional area, and represents a 0.022% error in the highest discharge.

3.3.4 *Discharge Measurements*

Discharge measurements for all experiments were taken using the Controlotron 1020 Clamp-on Flowmeter. Cumulative measurements were taken over 5 minutes from which

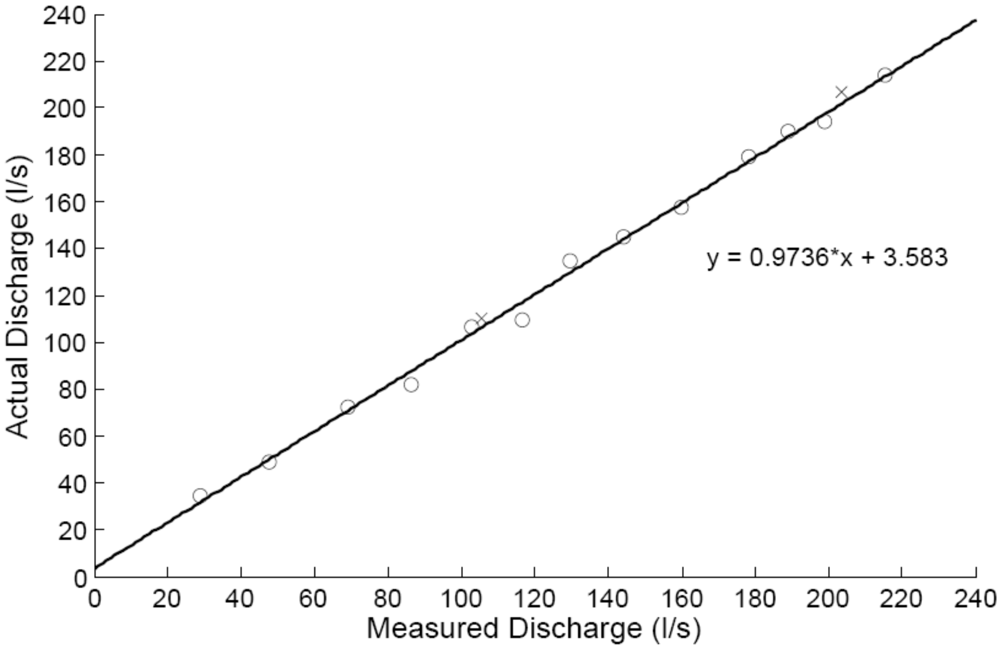

Figure 3.11. Calibration relationship between flowmeter readings and calibrated discharge. Circles represent measurements taken at the constant water depth, and squares represent measurements carried out at different water depths.

a time-averaged discharge was calculated in L/s. Discharges for all experiments were recorded and throughout experiments the discharge was checked at regular intervals. All measured discharges were converted to calibrated discharges using Equation 3.3.

3.4 Leaves

The leaves used in this experiment were collected from various locations within the Cardiff area. A variety of different leaves from deciduous trees were used, however the samples consisted predominately of Oak and Beech leaves. No effort was made to standardise the size of the leaves, to reflect the variety seen in nature. All the leaves were collected in Autumn, from the floor so that they had dropped naturally. This means that leaves are all dead and would be in the same state of decomposition as when they enter the stream. The presented experiments investigate the movement and retention of leaves present within the water column, not the movement of leaves as they enter the stream from a windfall event. Leaves travelling within the water column will be saturated with water and at some stage of decay. To replicate this within the experiments the leaves were soaked in cold water for a period of time prior to being used. It was therefore necessary to investigate the length of time needed for the leaves to become saturated.

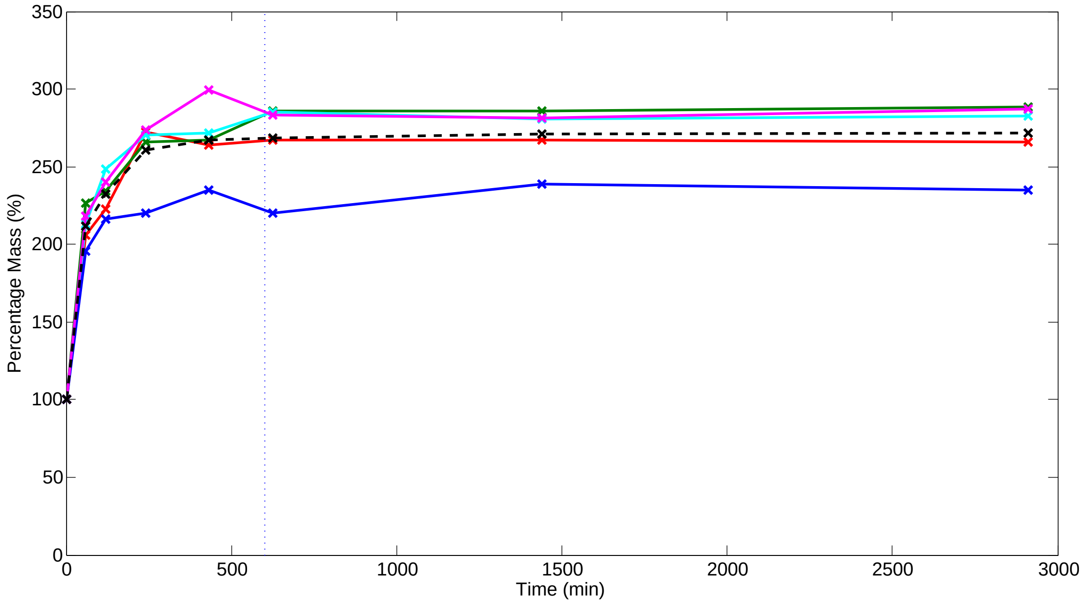

Figure 3.12. Change in leaf mass over time during saturation process. The coloured lines represent the five batches, the black dashed line represents the mean values and vertical dashed line indicates 600 minute threshold.

A hundred leaves were chosen at random, and divided into five batches of 20. Each batch was weighed to give an initial mass, and then placed in a 1 litre glass beaker containing 750ml of cold tap water. At given time periods, in turn, each batch of leaves was removed from the water. To gain an accurate weight of just the leaves, excess water was removed from the outside of the leaves and then they were weighed and the mass recorded. While the leaves were out of the water the timer was stopped. The leaves were returned to the water and the process repeated after the next time period. As each batch of leaves had different starting masses, the masses were converted to a percentage mass to provide easier comparison of results, where 100% was the starting mass.

The results can be seen in Figure 3.12. This shows that each leaf more than doubles its mass when it is saturated with water, and for some of the batches their mass nearly triples. The variation seen in the increase in mass will be due to the variation in the leaves used, the different species and sizes. Although there is variation in the increase in mass, all of the batches of leaves have the same saturation point, seen by the flattening of the curve. At 600 minutes, shown by a vertical dashed line on the graph, all except one of the batches have reached saturation point. The batch that appears to have lost mass at this point, also seems to have reached saturation when considering the earlier and later points. Therefore, for leaves to be used in these experiments they should be soaked in cold water for a minimum of 600 minutes, or 10 hours.

3.4.1 Use of Leaves

For use in all experiments presented in this thesis leaves were chosen at random and divided into batches of 200. Only complete predominately undamaged leaves were used to ensure that they all behaved in a similar manner. Each batch was placed in a bucket and soaked in cold tap water for a minimum of 24 hours. This time period is much longer than suggested by the previous section but allowed for any variation in the leaves and their starting conditions, ensuring they reach saturation point. Although soaking the leaves for longer than 24 hours will not affect their saturation, periods longer than two days will be avoided as this could lead to the start of decomposition and therefore change the properties of the leaves. When the leaves have been removed from the experiment, they were allowed to dry and any damaged leaves were removed. Due to a limited number of leaves to carry out all experiments, leaves were reused. However they were returned to the population and re-chosen at random.

3.5 Bed Materials

The experiments presented in Chapters 4, 5 and 6 used three different bed materials. The properties of these bed materials, and any set arrangements used in the experiments are described in the following sections.

3.5.1 Sand

A 1-2mm Silica sand was used in the experiments presented in Chapter 4. A sieving method, in accordance with the BS 1377-2:1990 (*Methods Of Test For Soils For Civil Engineering Purposes Part 2: Classification Tests BS1377-2*, 1990), was used to obtain a Particle Size Distribution (PSD) (shown in Figure 3.13) and classification for the soil. A sample of approximately 100g as stated was randomly obtained from a large sample, this was then dry sieved using the methods stated in BS 1377-2:1990. The sand is classified as a coarse sand with a D_{50} of 1.3mm. The sand is uniformly graded which is shown by the PSD and the coefficient of uniformity which is 1.56 (less than 4). This is also shown by the sand predominately being retained on the 1.18mm and 600μm sieves.

3.5.2 Pebbles

The Pebbles used within the experiments presented in Chapter 4 were specified as having a diameter between 20 and 40mm. Again a sieving method was carried out in accordance with the British Standard (BS 1377-2:1990) to obtain the grading and PSD (shown in Figure 3.13) . Due to the larger particle size it was necessary to use a larger sample of approximately 15kg which again was obtained randomly from a much larger sample. This material has a D_{50} of 28mm, and is classified as a coarse gravel. It is again uniformly

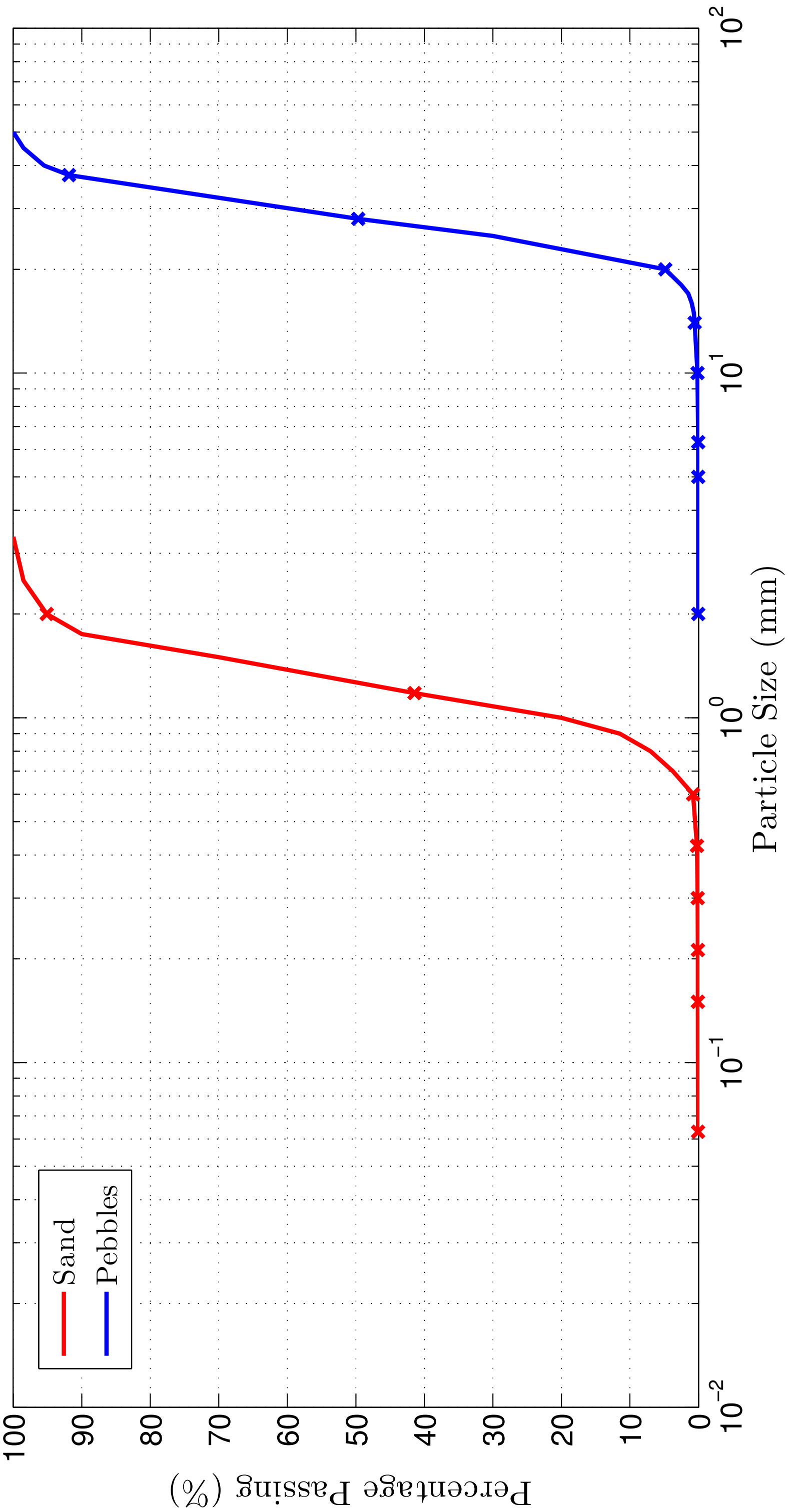

Figure 3.13. Particle size distribution of the Sand and Pebbles used in the experiments presented in Chapter 4.

graded shown by a uniformly coefficient of 1.35. Over 99% of the particles are retained on sieves between 20 and 40mm as stated by the manufacturers.

3.5.3 Boulders

The boulders discussed here are used in the experiments presented in Chapters 5 and 6. It was necessary for these experiments to create idealised obstacles which will be referred to throughout this thesis as boulders. Therefore, china bowls were used as the moulds for casting the concrete in order to create regular hemispheres. It was necessary to line these bowls with cling film which then had to be removed from the surface of the boulders when they were demoulded, which led to an uneven surface. However any dents in the surface were small in comparison to the size of the boulders and therefore it was thought that they would not affect the roughness properties of the boulders. The boulders were cast in concrete, consisting of one part cement, two parts sand and one part aggregate, where the water added varied. The mixture was vibrated to remove air bubbles. After demoulding the boulders were left in water to cure.

The boulders were 155mm in diameter, and nearly hemispherical, although the height varied between boulders. To gain an average height for the boulders a random sample of 12 boulders (10% of total) were choosen and their height measured, giving an average of 76mm ($s = 0.818$mm). Another random sample of 12 boulders were choosen and weighed to gain an average weight of 2184.9g ($s = 36.2$g). From this and the average height, an average density of 2285.5 Kg/m^3 was calculated.

For the experiments presented in Chapters 5 and 6 the boulders were placed directly on the glass flume bed, in a staggered array with a specified longitudinal and lateral spacing, illustrated in Figure 3.14. The longitudinal spacing (S_x) and lateral spacing (S_y) were varied to allow for differing boulder densities. The staggered arrays were centred along the lateral middle of the flume (width = 600mm), and only whole boulders were used within the arrays. The first line of the array was started at a length of 100mm and the array continued for the length of the flume to the weir at 15.35m. A Boulder Area Fraction was calculated for each arrangement of boulders to quantify the plan area of the flume occupied by the boulders. As only whole boulders were used within the arrangement, the Boulder Area Fractions were calculated over the whole are of the flume and not just over the control volume, using the following formula;

$$BAF = \frac{\pi r^2 n}{xy} \tag{3.4}$$

where r is the boulder radius, n is the number of boulders present, and xy represents the plan area of the flume (the working length up to 15.35m), where x is the length of flume,

	S_x (mm)	S_y (mm)	Boulder Area Fraction	No. of boulders
Sparse	500	360	0.047	46
Intermediate	400	220	0.097	95
Dense	300	180	0.130	127
Very Dense	250	150	0.218	213 (129)

Table 3.2. Definition of boulder densities used in experiments

and y is the width. These densities along with the spacing of each arrangement, and the number of boulders used is presented in Table 3.2.

Due to the limitation on the number of boulders manufactured, it was not possible to create a full length array for the Very Dense arrangement and therefore for this situation the boulders were only placed in a 9m working section from 5.1m to, and including, 14.1m. Therefore, for the Very Dense density, two boulder numbers are presented in Table 3.2. The first is the number of boulders required at this density to cover the full working length of the flume, while the number in brackets is the number of boulders used to cover the 9m section. Throughout this thesis the boulder density will be referred to by the names presented in this table. A visual representation of each of the densities is presented in Figure 3.15.

3.6 Summary

This chapter has presented the equipment that was used to carry out the experiments presented in later chapters. The calibration method of this equipment, where necessary, has been discussed and the results have been presented. The necessity of calibration of the Vectrino was highlighted by the large error was seen in both the vertical location and size of the sampling volume which would have significantly effected the results that will be presented. The use of the equipment, and the method used to take measurements has also been described.

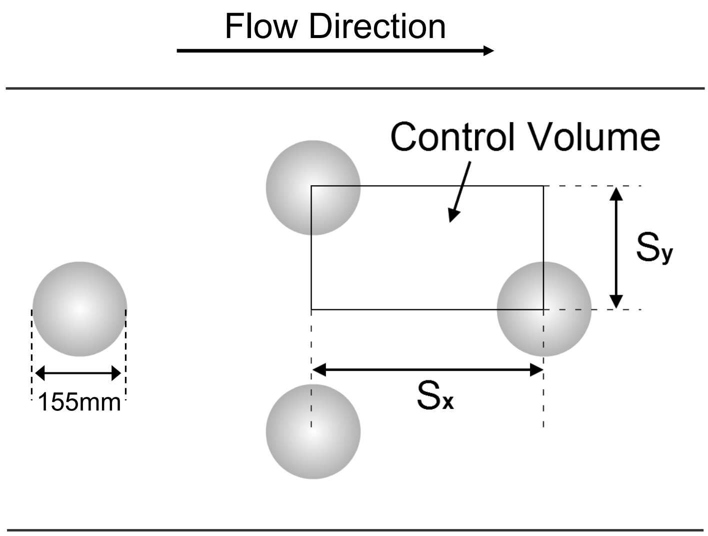

Figure 3.14. Diagram illustrating the arrangement of the boulders and how the spacing of each arrangement will be defined. The control volume is the area where velocity measurements will be taken.

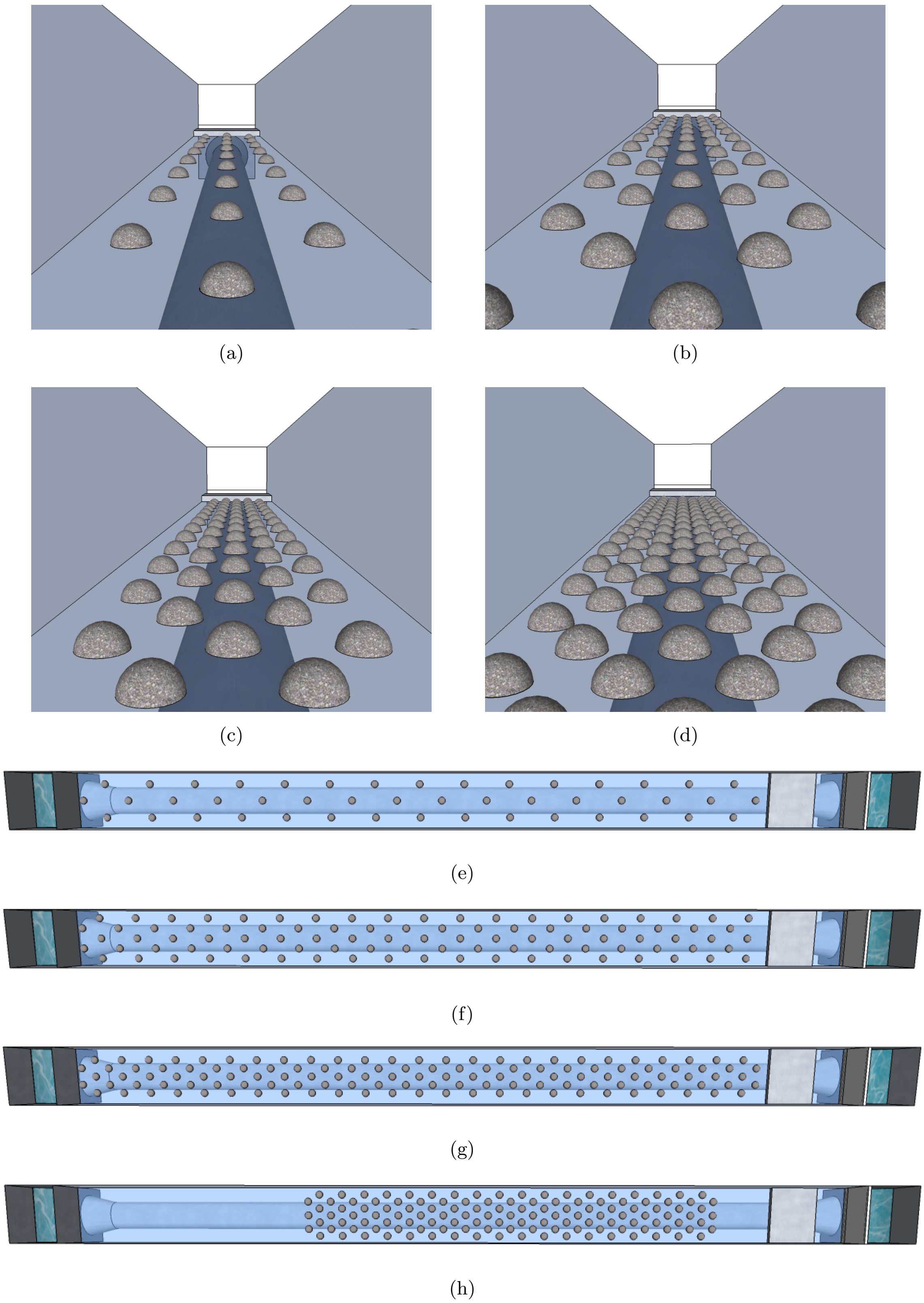

(a) (b) (c) (d) (e) (f) (g) (h)

Figure 3.15. Perspective (a-d) and plan (e-h) diagrams depicting the four boulder densities (a,e) Sparse, (b,f) Intermediate, (c,g) Dense, (d,h) Very Dense. All diagrams are drawn to scale.

4

EFFECTS OF BED HETEROGENEITY

This chapter presents flume experiments that aims to identify the role of physical and hydraulic conditions on leaf retention within a stream ecosystem. An idealised setup was created where the retention of two physical different substrates could be directly compared under the same global conditions. The substrates used were a sand ($D_{50} = 0.93$mm) and pebbles ($D_{50} = 28$mm). All leaf settlement locations and number of leaves retained were recorded, along with the bed morphology and hydraulic conditions at four locations of high retention. A significant difference in leaf retention was seen between the two bed substrates, with much higher retention seen on the pebbles, suggesting retention is a factor of either substrate size or bed heterogeneity. Leaves were retained in physical locations where protrusions in the bed were present and hydraulic conditions were stable.

4.1 Introduction

Leaves from riparian trees are an important source of energy within a stream ecosystem, and provide a major source of additional nutrients. Leaf matter within a stream is broken down by fungal and bacterial action (Gessner and Chauvet, 1994). The formation of leaf packs within a stream ecosystem not only provides a region of high nutrient input, but also provides a new niche for macroinvertebrates within the stream. In order to get these benefits the stream is dependent on physical mechanisms of retention, such as rocks, woody debris, pools and backwaters, and vegetation. However the retention and movement of leaves is also affected by the size and density of the leaf, depth of the stream, and discharge (Webster et al., 1994, 1999). It is suggested by Webster et al. (1994) that leaf retention is not only a passive process, but is also dependent on the probability of contact with a protrusion, and this probability decreases with increased flow depth.

Hoover et al. (2006) concluded that leaves were retained in either shallow, high flow riffles, where they were obstructed by large protrusions, or they passively settled in the slower moving, deeper pools, in their comparison of the retention of alder leaves between riffles and pools within the Spring Creek, British Columbia. Protrusions are distinct roughness elements, such as single pebbles or pebble clusters, that visibly differ in height from the surrounding bed material. Ehrman and Lambert (1992) suggested that the presence of woody debris was important for retention of organic matter (leaves and wood) in low gradient streams with small particle substrate (e.g. sand), as it provides the necessary spatial variation in bed height that would otherwise not be present. It follows that as bed particle size increases, so would the heterogeneity of the bed height, and therefore the ecosystem would be less reliant on the presence of woody debris for leaf retention. This illustrates the importance of bed protrusions and bed particle size in leaf retention. The presence of debris dams did not just affect the bed heterogeneity, but also effected the local hydraulic conditions slowing the flow, and increasing hydraulic retention (Ehrman and Lambert, 1992).

The downstream movement of leaves within a stream is not a continuous process, but instead is a series of steps, involving short periods of transport in the water column, followed by longer periods of retainment on the bed, after which there is further downstream movement (Webster et al., 1999). Transport length, T_x, defined as the average transport distance of the material before it is retained on the bed (Webster et al., 1999), was seen to be closely related to flow depth, with an increase in flow depth resulting in an increase in the transport length of artificial leaves in three differing streams (Webster et al., 1994).

Leaf pack formation is thought to occur at locations where the interaction between the physical and hydraulic conditions leads to specific turbulent artefacts. The physical and hydraulic attributes of a stream are inherently linked as the bed roughness has an important impact on the velocity profile and degree of bed generated turbulence (Chow, 1959; Vermass et al., 2008). The median particle size, D_{50}, of bed substrate relates to the roughness height, k, which in turn affects the velocity distributions and boundary layer thickness. This relationship is shown in the velocity distribution law for rough surfaces (Chow, 1959, Chapter 8). Protrusions formed within the bed substrate are an important mechanism of leaf retention. Detailed analysis of the spatial variation in velocities over protrusion elements has been carried out, in both the laboratory experiments (e.g. Acarlar and Smith, 1987; Pokrajac et al., 2003; Canovaro and Francalanci, 2008) and natural streams (Buffin-Bélanger and Roy, 1998). The latter, examining a pebble cluster with a relative submergence (ratio of the flow depth to obstacle height) of approximately two, showed acceleration over the pebble cluster, with a recirculating zone present behind the cluster creating a dead zone. Canovaro and Francalanci (2008) examined protrusion elements (rectangular blocks) at a lower relative submergence of 1.6 within a laboratory experiment. The velocities over the element were not presented, but presentation of the velocities in the region between the elements showed a region of negative and zero streamwise velocity present immediately behind the block.

Although there has been research examining the importance of leaf packs within stream ecosystems, and the retention of leaves on obstacles within the flow, there is little investigating the combined hydraulic and physical conditions that cause leaves to be retained. The effects of climate change will result in increased discharges and flow depths, changing the hydraulic conditions within a stream. Therefore, by knowing the mechanics for leaf retention and leaf pack formation, the effect of climate change on nutrient input and niche creation within stream ecosystems can be predicted. This chapter presents flume experiments examining the retention of leaves and formation of leaf packs on two physically different substrates. It examines the contributions of hydraulic and physical characteristics on the settlement of leaves at four specific leaf pack locations, using detailed bed profiles and velocity measurements.

4.2 Method

The experiments were carried out in a glass-walled recirculating flume 17m in length, 1.2m wide and 1m in depth as described in section 3.1. An idealised river bed was created using two physically different materials. Two longitudinal strips of substrate, (described in Section 3.5) were placed on the glass flume bed; sand (D_{50} = 1.3mm) covered the flume width from 0-600mm and pebbles (D_{50} = 28mm) covered the flume width from 600-1200mm.

The use of two longitudinal strips of differing bed substrate allowed the retention of two bed types to be investigated simultaneously under the same bulk hydraulic conditions, such as discharge, flow depth and water surface profile. However it is acknowledged that a shear layer might be generate between the two substrate type, due to the difference in roughness of the two bed materials.

Although every effort was carried out to create a level bed, due to the differing size of the substrate used, the depth of the bed was not uniform throughout the length of the flume. An average bed elevation was calculated from cross-stream bed profiles taken at 17 longitudinal locations between 2.5 and 12m from the inlet. The Vectrino ADV distance function was used to measure the depth of the bed from a fixed height. Measurements were taken every 5cm along the width of the flume over the sand and every 2.5cm over the pebbles, the resolution of bed elevation sampling was changed between bed materials to reflect the greater variation seen within the coarse substrate. A area-weighted mean bed profile was calculated for each of the profiles from which a grand mean was calculated giving a mean bed depth of 50mm ($s = 4.6mm$).

The water surface elevation was measured to the nearest millimetre, using rulers attached to the flume's side wall, as described and presented in Section 3.1.3. This showed that uniform flow conditions could not be obtained, but that the slope of the water profile is not significantly different from the bed slope, and therefore the conditions will be considered to be pseudo-uniform flow. A constant surface water profile was maintained for the experiments described in this section, with an average flow depth of 89mm. The longitudinal bed slope was fixed at 1 in 1000. The discharge was measured using the flowmeter, described in Section 3.3, and the experiments were carried out with a mean calibrated discharge of 33.2L/s ($s = 0.09$L/s).

Leaves used in the experiment, described in Section 3.4, were divided into batches of 200 and soaked for a minimum of 24 hours before use. For each experiment 200 leaves were released by hand at a longitudinal length of 1m from the inlet, evenly across the width of the flume. Leaves not retained on the bed were removed from the net at the downstream end, before a second batch of 200 leaves were released. A total of 400 leaves (two batches of 200 leaves) were released in each experiment. The central coordinates (length/width) of all leaves retained on the bed and the number of leaves present at each location were recorded. This experiment was repeated until a correlation could be seen in the leaf settlement locations.

Hydraulic analysis was carried out at four locations of high retention, each location centring around a particular leaf pack. At these locations an investigation of both hydraulic and physical characteristics was carried out. Firstly an $x-y$ measurement grid of velocity profiles, centred around the leaf pack location, was taken. The longitudinal and lateral spacing of the velocity profiles within the grid varied from 5mm to 20mm, with a higher resolution nearer the centre of the grid. The velocity measurements were taken using a Nortek Vectrino ADV (Section 3.2), at 200Hz, with a sampling period of 90 seconds. A nominal sample volume of 2.5mm was used, which was shown in Section 3.2.2 to give an actual sample volume of 8mm, centred 43mm from the Vectrino head.

Velocity measurements were taken at constant heights above the bed for all profiles, but due to variation in the bed the absolute heights of the measurements varied between profiles. At each profile location, the bed height was measured using the Vectrino ADV allowing the measurement heights within the profile to be calculated. It was not possible to take measurements over the whole profile at some locations due to the bed interfering with the receiving of the reflected beams, indicated by a significant decrease in SNR and correlation values. The velocity data was processed using Matlab, with poor quality data being removed as specified in Section 3.2.4.

Secondly, a complete bed profile of the velocity grids was taken using the depth function of the Vectrino ADV, with depth readings being taken every 5mm over the $x-y$ grid area. This was carried out in still water as this gave a more stable readings. From this a number of physical bed parameters were defined for each of the four locations of high retention. The grid roughness height, k, is defined as the difference between the maximum and minimum bed heights within the grid location. The protrusion height, or stone roughness height refers to the height of the major protrusion that is found within the measurement grid. Relative protrusion, as defined by Hoover et al. (2006), describes the degree to which the substrate protrudes into the flow, and is the ratio of the protrusion height to the flow depth (average grid flow depths were used).

4.3 Results and Discussion

To obtain good correlation of leaf settlement locations, 13 experiments in total were carried out, giving a total release of 5200 leaves of which only 417 (8.02%) were retained on the bed as either single leaves or leaf packs. Figure 4.1(a) shows the locations of the retained leaves, where the size relates to the number of leaves. The largest leaf pack formed consisted of six leaves, with the majority of leaves being retained as single leaves. The greater retention of single leaves could be due to the method of release of the leaves, with effort being made to release them individually. A significant difference was seen in leaf retention rates between the pebble and sand bed material, with 3.4 times more leaves being retained on the pebble bed (322 compared to 95). A comparison of leaf pack formation on the two

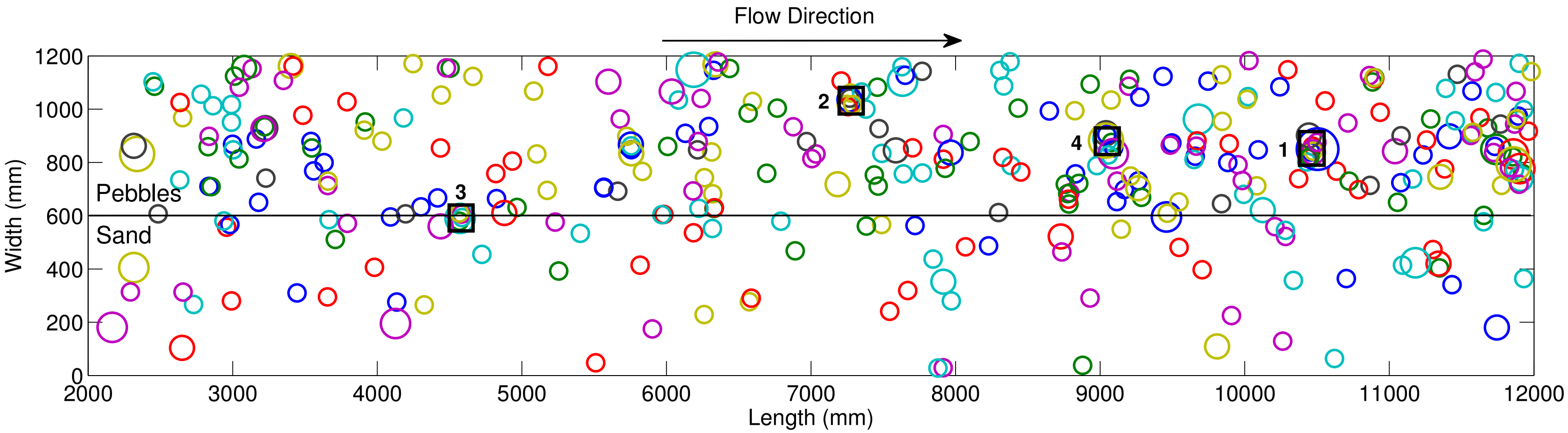

(a)

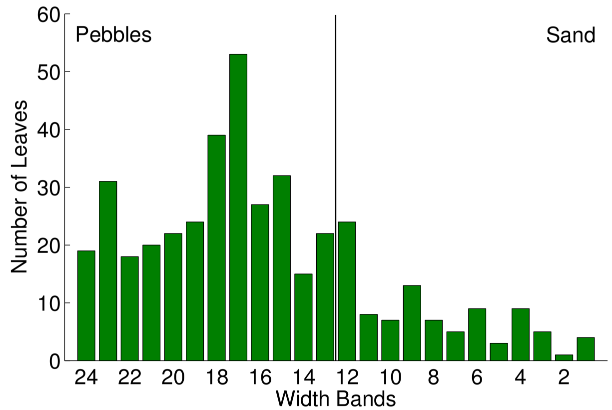

(b)

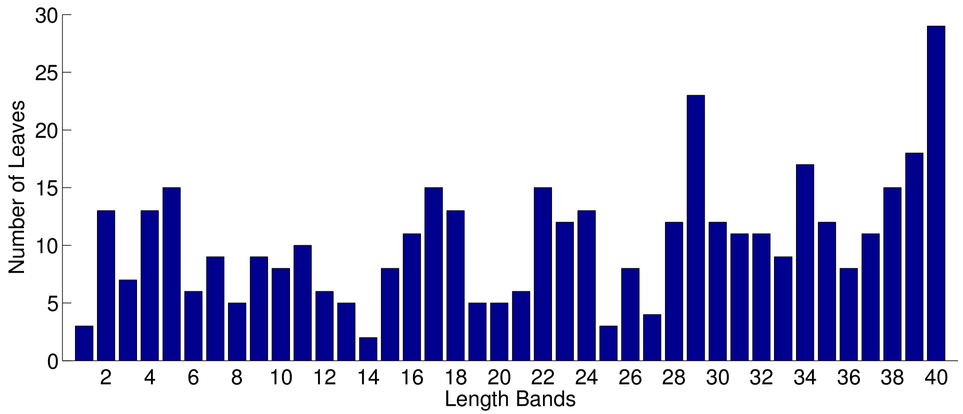

(c)

Figure 4.1. (a) Location of leaves retained on the bed. The size of the circle relates to the number of leaves retained at that point (smallest circle represents a single leaf, greatest represents seven leaves) and colours indicate the different experiments, the boxes show the locations of the velocity measurements. (b) The number of leaves retained in each width band. (c) The number of leaves retained in each length band.

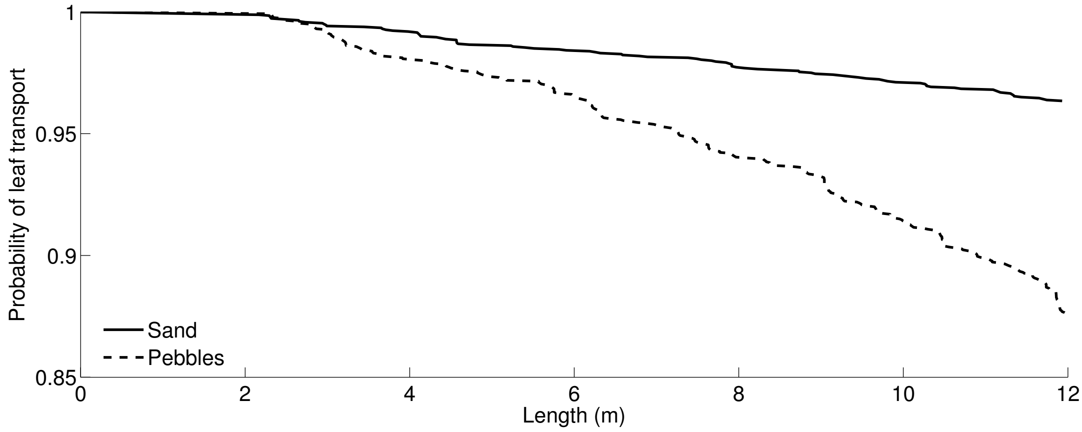

Figure 4.2. Comparison of the probability of leaf transport against length between the sand and pebbles.

differing bed materials showed a similar result, with 36 leaf packs formed on the pebble bed compared to only 13 on the sand bed. This suggests that leaf retention is a function of substrate size, and therefore affected by bed heterogeneity and hence boundary layer thichness.

The difference in the longitudinal distribution of retention between the sand and pebbles was further examined by comparing the probability of leaf transport (P_T) for each substrate, using the assumption that exactly half of the inputted leaves were transported on each substrate. The probability of leaf transport is the inverse of the cumulative probability of leaf retention at a given length and is therefore given by;

$$P_T(x) = 1 - \sum_{i=0}^{x} \frac{L(i)}{L_0} \tag{4.1}$$

where $L(i)$ is the number of leaves retained at a length i, and L_0 is the total number of leaves. The probability of leaf transport against length for each substrate is shown in Figure 4.2. Although the two substrates appear to behave in a similar manner for the first two metres, there is then a distinct difference between their retentive abilities. This similarity could be due to the release of the leaves at 1m causing disturbance within the flow therefore preventing retention within the first few metres of the flume. The more rapid decrease seen for the coarse substrate further illustrates its increased ability to retain leaves. The negative exponential model (e.g. Webster et al., 1987; Hoover et al., 2010) was applied;

$$L(x) = L_o e^{-k_R x} \tag{4.2}$$

where, k_R is the retention coefficient (m^{-1}) (Webster et al., 1987; Hoover et al., 2010) or the instantaneous rate of leaf removal from the water column (Ehrman and Lambert, 1992). This model was found to be a good fit, giving retention coefficients of 0.00285 (R-sq 95.7%) and 0.00872 m^{-1} (R-sq 87.0%) for the sand and pebbles respectively. The difference between these coefficients illustrates the greater retentive ability of the pebbles, further suggesting that the increased heterogeneity of the bed increases the retention either directly or due to its effect on the velocity profile. The retentive coefficient seen on the pebbles is comparable to that seen by Ehrman and Lambert (1992) in reaches containing a moderate presence of woody debris. Whereas the retention coefficient of the sand is very low and is only just within the range of values reported by Young et al. (1978).

To further investigate the distribution of retention the width of the flume was divided into 24 equal strips, each 50mm in thickness, where the number of leaves retained in each strip were counted. The results of this are shown in Figure 4.1(b), which further illustrates the significant difference (two-sample t-test $p < 0.005$) in retention seen between the two substrates. The greatest leaf retention can be seen at width band 17 which corresponds to a width of 801–850mm. This greater retention on the pebbles could be attributed to the greater roughness height, and bed heterogeneity associated with the larger substrate, which in turn affects the boundary layer thickness and velocity structures.

If retention was unaffected by spatial variation within the bed profile then we would expect to see an even distribution of retention across the width of the flume, due to even release of leaves, and therefore a binomial distribution with a probability of 1/24. The retention pattern seen on the sand is closely related to a binomial distribution, when considering the sand retention independent of pebbles. For this distribution (n=95, p=0.083), 7 or 8 leaves would be expected to be retained in each width band. All the data, except for Band 12, falls within the 95% confidence interval (3-14) for this distribution. This suggests that retention on the sand follows a binomial distribution, from which it is inferred that the bed and hydraulic conditions are steady and constant, as they do not affect retention locations. However the pebbles, and including band 12, does not appear to follow this distribution suggesting here there is sufficient variation in the bed morphology and therefore hydraulic conditions to influence the settlement location.

The length of the flume (between longitudinal distances of 2000 and 12000 mm) was also divided into a number of bands, each 250mm in thickness. The leaf retention rates in each length band can be seen in Figure 4.1(c). There appears to be an initial settlement region, followed by a series of peaks and troughs, resulting in 5 regions of higher settlement. These regions are at length bands of 17, 22–24, 29, 34 and 40. These regions are separated by an average distance of 1.5m, except the region between bands 29 and 34 which is only 1.25m.

Grid No.	Grid Area (cm^2)	n	k (mm)	Leaf Pack area (cm^2)	$< \bar{z_0} >$ (mm)	D (mm)	Relative Protusion	$\bar{U}_{bed}$ (m/s)
1	48	66	55	20.83	101	-	-	0.065
2	100	72	65	47.36	101	-	-	0.071
3	67.5	42	47	63.12	96	25	0.260	0.102
4	67.5	42	65	81.85	100	35	0.350	0.042

Table 4.1. Velocity grid parameters. n= no. of velocity profiles measured, k= roughness height, D= major protrusion height, $< \bar{z_0} >$= spatially-averaged flow depth, $\bar{U}_{bed}$ = mean near-bed velocity where near-bed is defined as within 10mm of the bed.

This distance of 1.5m is very similar to the average transport length of 1.56m observed by Webster et al. (1994) for a similar flow depth. It is known that the movement of leaves downstream is a stepwise motion, involving entrainment, transport and settlement. This motion was observed throughout these experiments; the leaves were seen to 'tumble' over the bed, and when contacting the bed would either be retained or re-entrained into the water column.

The locations of each of the measurement grids are illustrated in Figure 4.1(a). A summary of grid, hydraulic and leaf pack parameters can be seen in Table 4.1. The area-mean velocity ($\bar{U}$) for the experiment was 31.1 cm/s. In all four cases the flow depth was greater than the average flume flow depth of 89mm (see Table 4.1). Although the longitudinal and lateral coordinates of the leaf packs were recorded, their height relative to the bed could not be measured, however it is assumed that the leaf is resting on the bed. Therefore, an estimate of the leaf pack height has been calculated from the bed profile, leaf pack size and position. These estimated locations are shown in later figures (4.4 and 4.5). A similar characteristic was seen by Hoover et al. (2006) where flow depths at leaf settlement locations were seen to be significantly greater than those at reference locations. A mean near-bed velocity ($\bar{U}_{bed}$) was calculated from the velocities within 10mm of the bed for each of the grids. These were seen to be similar for Grids 1 and 2, with the highest near-bed velocities being observed in Grid 3 at the interface between the two bed substrates. This would be expected as this grid covers both the bed materials, and velocities would be higher on the sand due to the lower roughness. The lowest mean near-bed velocity was seen in Grid 4, which corresponds with the formation of the largest leaf pack, so this could be due to the lower near-bed velocities present. However, for the other grids there is not a correlation between near-bed velocities and leaf pack size suggesting it is affected by more than near-bed velocities alone.

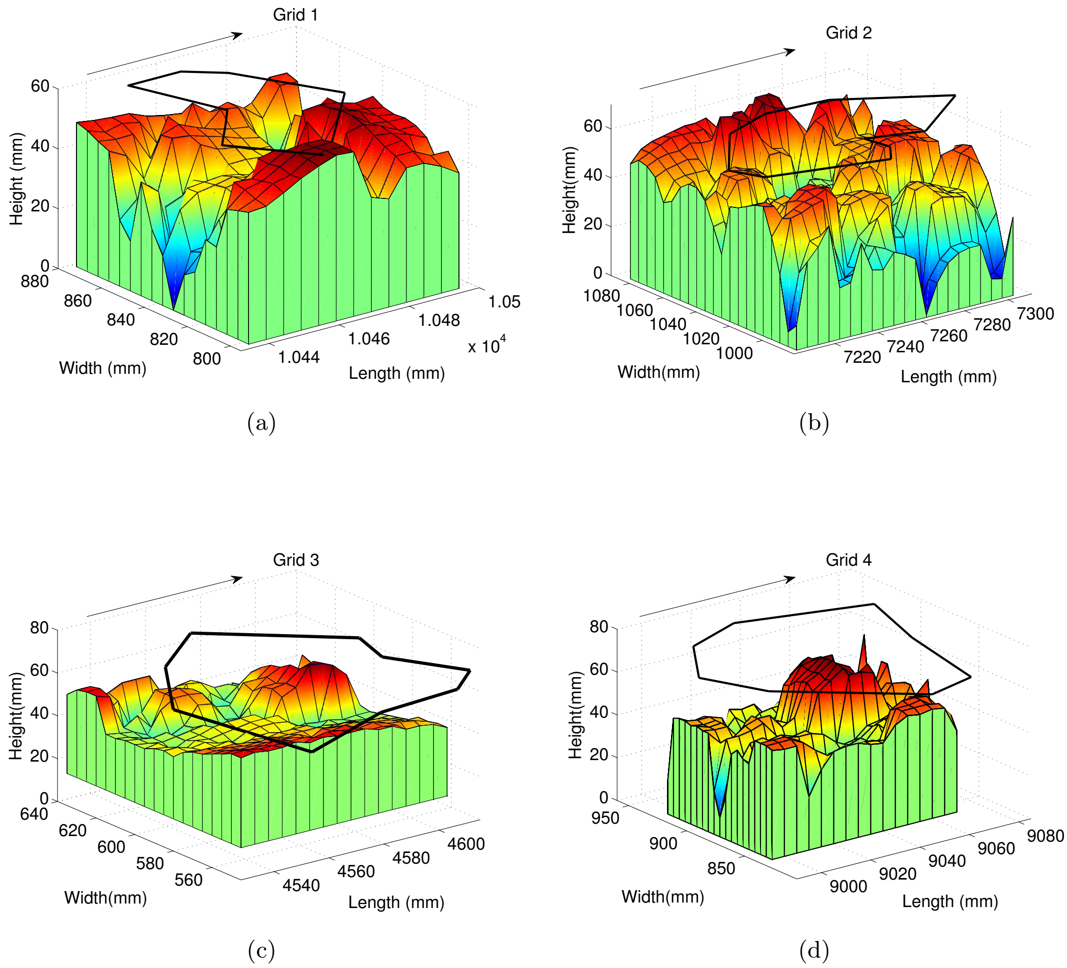

Figure 4.3. Three-dimensional bed profiles for (a) Grid 1, (b) Grid 2, (c) Grid 3 and (d) Grid 4. Solid black lines represents approximate leaf pack location, the arrows depict the direction of flow.

The roughness height, k, differs between the four grids, being lowest in Grid 3, as would be expected as this grid covers both the sand and pebbles. Figure 4.3 shows three-dimensional bed profiles for each of the grid locations, with a representation of the leaf pack location. From this figure the lower heterogeneity in Grid 3 can be seen, illustrated by the lower roughness height, k. Any protrusions into the flow that might aid leaf retention are only due to random variations in the bed and are therefore relatively small. Examining Figure 4.3 shows that distinct protrusions are only visible in Grids 3 and 4, with Grids 1 and 2 only having large variation within the bed. Grids 3 and 4 are seen to support the largest leaf packs, suggesting that the presence of protrusions could be important in leaf retention. The relative protrusions seen in this experiment are comparable to those seen in pools by Hoover et al. (2006), where a mean relative protrusion of 0.28 was observed in reference locations, and who noted that much greater leaf retention rates were observed in pools compared to riffles, where the flow depth was approximately twice that of the riffles, (mean values of 9.52cm compared to 20.96cm).

Time-averaged values were calculated for each velocity component u (streamwise), v (cross-streamwise), w (vertical), at each point within the measurement grid. Due to the variation in absolute height of the measurements, it was necessary to mesh the data onto a regularly spaced grid to allow interpolation and visualisation. This was carried out using Matlab with three-dimensional linear interpolation being used to fill in the missing data. All graphs presented are of planes that contain real data. For each of the grid locations two graphs have been presented. Figure 4.4 presents the velocity vector and contour plots for Grids 1 and 2, with Grids 3 and 4 are shown in Figure 4.5. The first is a contour plot showing a longitudinal plane of the streamwise velocities (u). This shows the variation in longitudinal velocity over height and length for a given width, vectors composed of the longitudinal and vertical velocity components are imposed over the contours, along with a representation of the leaf pack location. The second graph presents a plan view of the $u - v$ vector velocities at a specific height. Again a representation of the leaf position is given. It can be seen from these estimates of leaf pack locations, that part of the leaf pack will be above and below the roughness height in each case, due to each leaf pack resting on a high region of the bed.

In each of the contour plots an elevated region of the bed is clearly visible at the leading edge of the leaf pack, however comparing these to the bed profiles shows that only those seen in Grids 3 and 4 actually protrude into the flow, and can therefore be considered as protrusions, whereas those seen in Grids 1 and 2 are due to variation of the bed. In each case due to the size of the leaf pack it is necessary for it to rest on top of the protrusion, and therefore it appears that the flow is pushing the leaf pack onto the protrusion allowing the leaf pack to form and remain stable. The stronger velocities seen in Grid 3 (Fig 4.5(a))

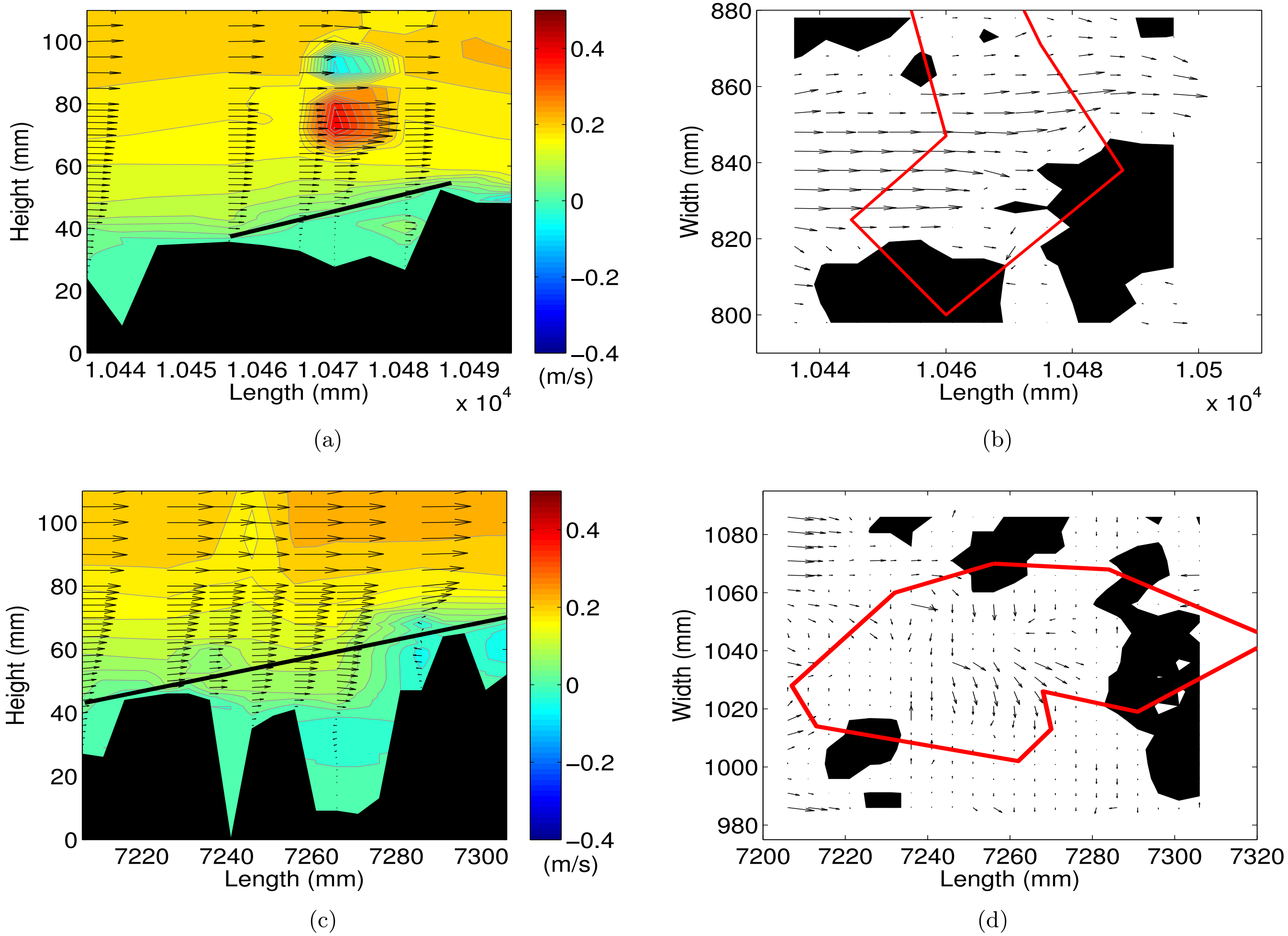

Figure 4.4. (a) Contour plot of streamwise velocities with $u - w$ vectors of Grid 1 at a width of 843mm, (b) $u - v$ Vector plot of Grid 1 at a height of 45mm, (c) Contour plot of streamwise velocities with $u - w$ vectors of Grid 2 at a width of 1036mm, (d) $u - v$ Vector plot of Grid 2 at a height of 50mm. Solid black/red lines represent approximate leaf pack locations, and solid black areas represent the bed, flow is from left to right.

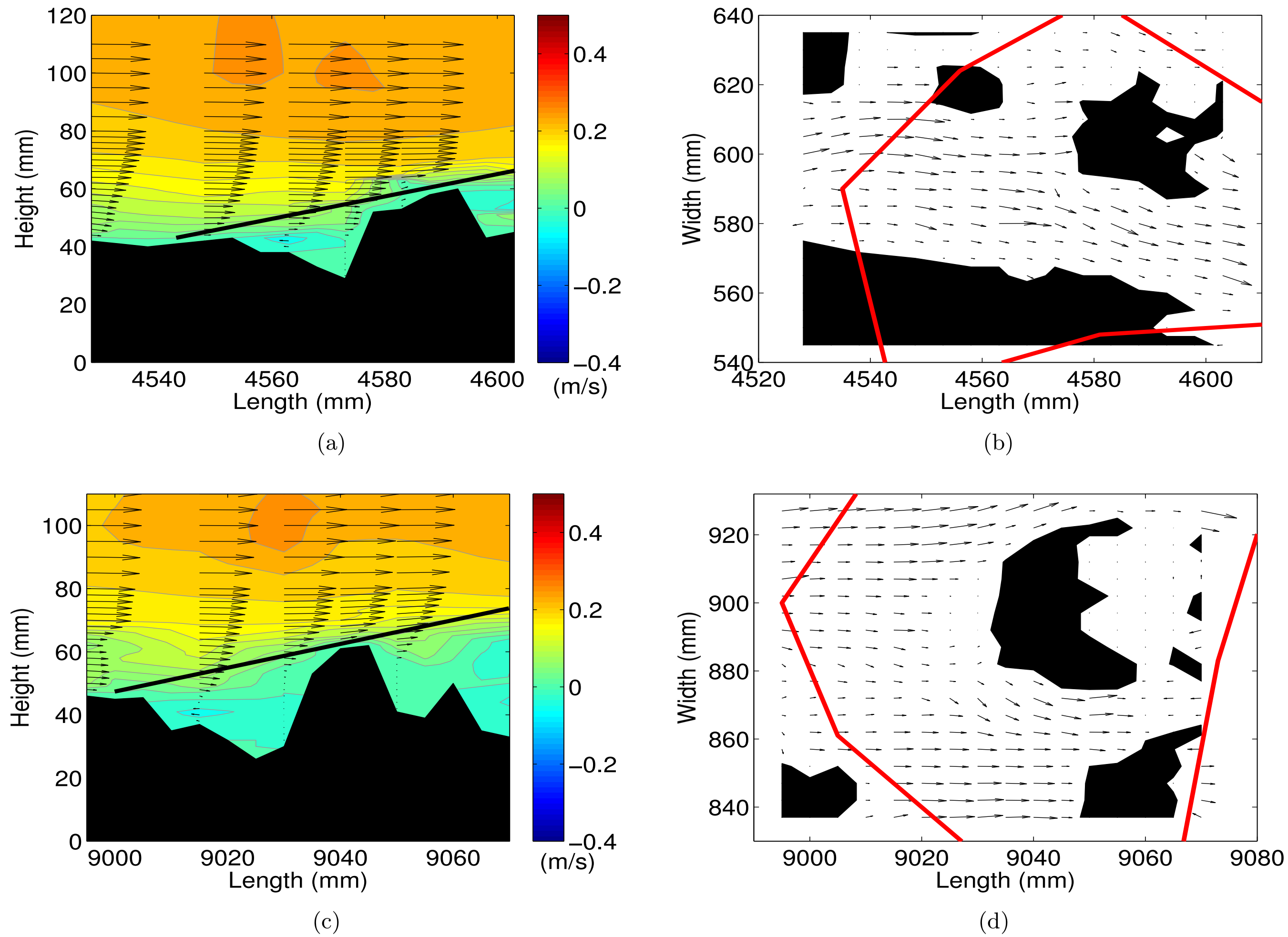

Figure 4.5. (a) Contour plot of streamwise velocities with $u-w$ vectors of Grid 3 at a width of 600mm, (b) $u-v$ Vector plot of Grid 3 at a height of 48mm, (c) Contour plot of streamwise velocities with $u-w$ vectors of Grid 4 at a width of 907mm, (d) $u-v$ Vector plot of Grid 4 at a height of 50mm. Solid black/red lines represent approximate leaf pack locations, and solid black areas represent the bed.

and Grid 4 (Fig 4.5(c)) flowing over the top of the leaf pack could explain the largest leaf packs (see Table 4.1) forming in these locations as a greater force will be generated to hold the leaf pack in place.

In Grids 1 and 4 there are large areas of zero or low near-bed streamwise velocities, which could be referred to as a dead zone, in front of the protrusions under the estimated leaf pack location. This is clearly shown in the vector plot for Grid 4 (Figure 4.5(d)) where there is a dead zone both in front and behind the protrusion, and the vectors show that the flow is being forced around the protrusion at this height. As the leaf pack is much wider than the protrusion, the flow that is being forced around it might be helping to keep the leaf pack in place by 'wrapping' it around the protrusion. Although there is also a dead zone present in Grid 3, it is much less pronounced. Figure 4.5(b) shows the outline of the leaf pack compared to the grid location. At this height (50mm) a channel has been formed by the physical properties of the bed that forces the flow around the protruding bed material. This further suggests that the flow is responsible for the formation of the leaf pack, producing a downward force onto the protrusion and the adjacent sand bed. A similar 'channel' effect can also be seen in Grid 1 (Figure 4.4(b)) and in Grid 4 (Figure 4.5(d)), where the water is forced around the protrusion.

Although there are dead zones present below the leaf pack in grid 2, these are formed for different reasons. Grid 2 exhibits the greatest variation in bed height (see Figure 4.4(c)) and the dead zones present here seem to result from the effects of the previous protrusion, as seen by Buffin-Bélanger and Roy (1998) and Canovaro and Francalanci (2008). The leaf pack has formed in the same manner as the other leaf packs, resting on the major protrusion with the water flow pushing it up against the protrusion. However, in this situation there are established velocity profiles below the estimated leaf pack location, instead of the dead-zones seen in the other grids. As the velocity measurements were taken when the leaf packs had been removed it is possible that once the leaf pack had formed, it would have created a dead zone below it where the water flow being forced over the top and therefore creating a downward force onto the leaf pack. Figure 4.4(d) shows a plan view at a height of 50mm, here it can be seen that the flow is very different to the other three grids. Here there are zero and negative longitudinal velocities present along with significant cross-streamwise velocities, showing that there are secondary cell circulations in the lateral plane. This is likely to be due to the great variation and variability seen in the bed at this grid location, creating greater fluctuations in the velocities as the water is forced between the multiple bed protrusions.

It appears that Grids 2, 3 and 4 all exhibit stable hydraulic conditions that have allowed the leaf packs to form, with fully developed velocity profiles. In Grid 1 at a height of 65-80mm

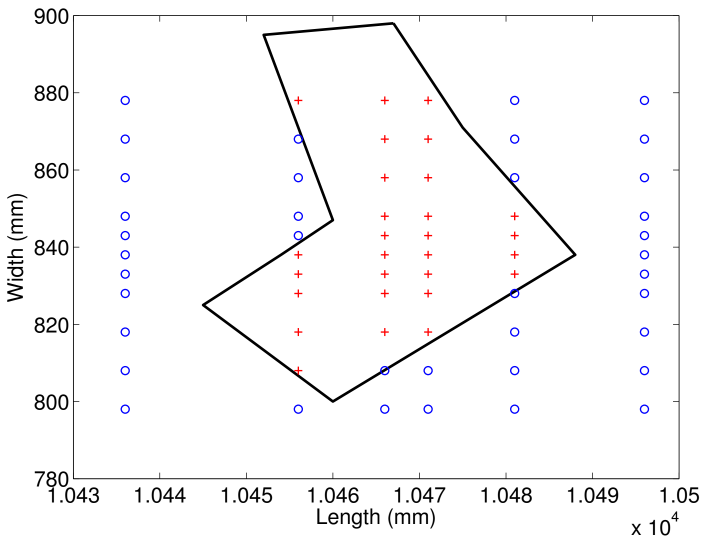

Figure 4.6. Illustration of the points that were included in the calculation of the spatially-averaged streamwise velocities for the leaf pack footprint (crosses) and grid (circles), shown here for Grid 1.

(see Figure 4.4(a)) there is a region of higher streamwise velocities (positive region), above which there is a region of reduced and negative longitudinal velocities (negative region). Further investigation of the data shows that the negative region actually starts alongside the positive region at the same height, extending up and over. These two regions are not isolated, with another positive/negative pair present at a width of 868mm and a height of 80-100mm. In this case the region of increased streamwise velocities sits above and in front of the negative region. In both of these locations the streamwise velocities are dominant, with little or no vertical or lateral movement of the water flow. The reason for the creation of these eddies is unknown, and would need further investigation. It is possible that the presence of these increased and reduced streamwise regions are artefacts of both the ADV weak spot that might be present at this height and the interpolation. However, evidence of these weak spots are not present in the other grids. We would also expect to see the formation of eddies in grid 3 due to the intersection of the two differing bed materials; however the velocity and turbulence statistics do not show their presence.

Hoover et al. (2006) have suggested that leaf pack formation in riffles occurs in regions that have lower velocities compared to the average velocity which was determined by measuring parameters at a number of reference locations throughout the stream. To investigate this theory two spatially-averaged streamwise (u) velocity profiles were produced for each of the grid locations, using only measured data. The first was produced from the velocity profiles present within the footprint of the leaf pack, and the second using the velocity profiles that were found outside the leaf pack footprint; this is illustrated in Figure 4.6. These two regions were then compared, to see if the average velocities are lower in the leaf pack region. Figure 4.7 shows the results of this comparison for each of the grids. There appears to be little variation between the two profiles, except for Grid 1 where there is variation below the maximum bed height and artefacts present in the leaf pack profile above the maximum bed height.

The variation between the profiles was tested using a paired t-test, the difference was not significant for Grids 1, 3 and 4 ($p = 0.1168, 0.4111$ and 0.5091 respectively), but the velocities within the leaf pack footprint for Grid 2 were significantly lower ($p < 0.005$) than those outside the leaf pack footprint. As the paired t-test assesses the difference between paired measurements in two samples, it will only be significant if the difference is skewed towards the positive or negative. Grid 1 appears to show a difference between the profiles, but the profiles appear to oppose to each other, and therefore the result was not significant. The spatially-averaged velocities from the leaf pack footprint appear to be more variable below the maximum bed height for each of the grids. For grid 1, above a height 80mm, the presence of the vortices mentioned previously can be seen within the leaf pack footprint, showing that these would be present above the formed leaf pack. However, as previously discussed the negative velocities at this high could be due to the weak spot of the ADV. Also at this height the number of velocity measurements at each height due to the resolution of the profile is reduced, and therefore these outlying points could have skewed the mean.

4.4 Summary

Webster et al. (1994, 1999) suggested that the retention of leaves within a stream is due to physical attributes of the stream bed, for example the presence of protrusions or pools, as well as being affected by the flow depth and discharge of the stream. The experiment presented in this chapter has aimed to identify the role of both hydraulic and physical characteristics within a stream on leaf retention and the formation of leaf packs. This was achieved by comparing two physically different substrate materials under the same mean-area velocity conditions. Soaked leaves were released into the flume and the locations of those retained on the bed were noted, this was repeated to obtain a correlation. Four $x-y$ grids of velocity profiles were taken at locations of high retention, along with bed profiles of each of the grids' locations.

The results clearly show that differences in retention characteristics of the two bed materials, with a significantly greater retention seen on larger substrate material along with the formation of more and larger leaf packs and a much high retention coefficient. This

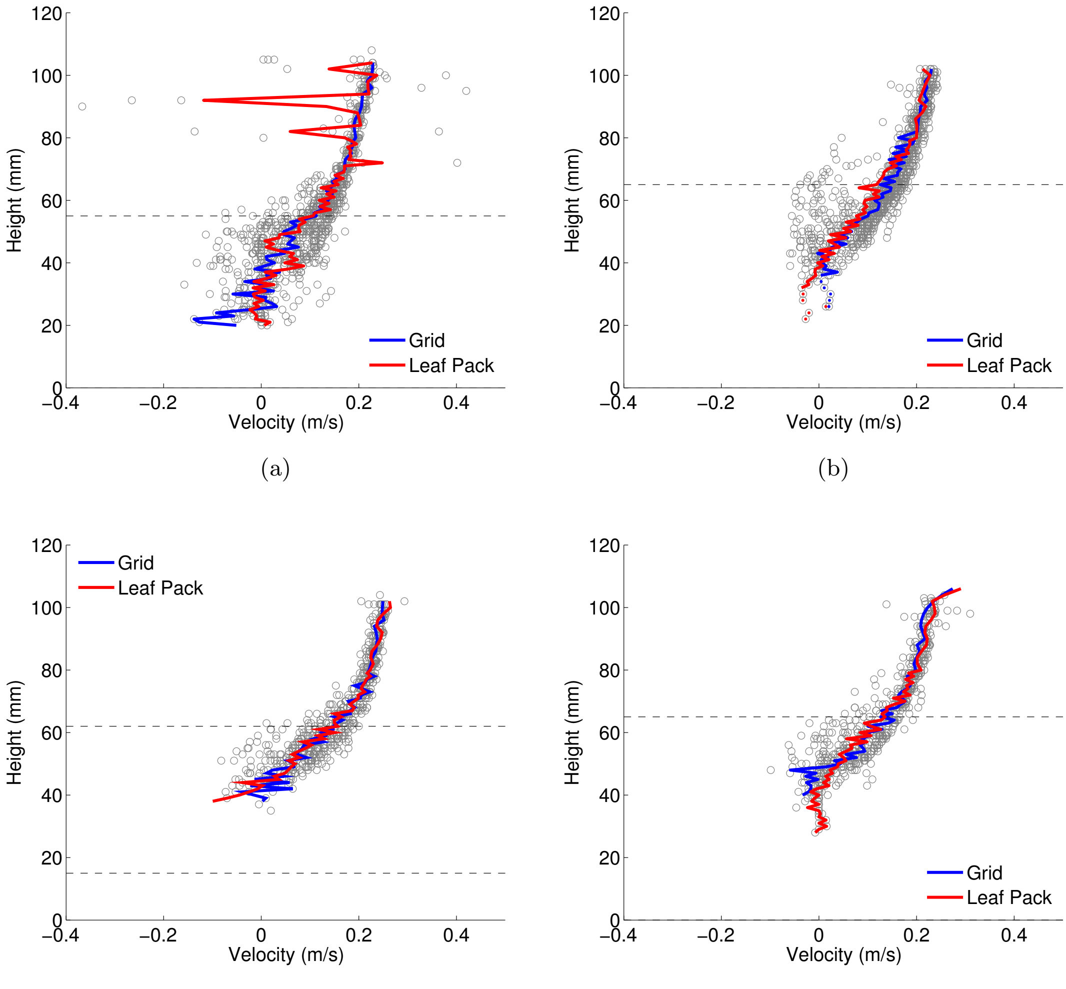

(a) (b) (c) (d)

Figure 4.7. Plot of streamwise velocities against height, showing the grid spatially-averaged profile (blue) and the leaf pack spatially-averaged profile (red) for (a) Grid 1, (b) Grid 2, (c) Grid 3 and (d) Grid 4. Dashed lines represent the maximum and minimum bed height, where only one is present the minimum bed height is zero.

shows that there is a link between bed substrate and the retention of leaves within a system, which could be due to the direct effect of increased bed heterogeneity that the larger substrate creates, or the associated effect the greater roughness has on the velocity profile, such as the boundary layer thickness. The importance of variation in the bed is also illustrated by larger protrusions into the flow allowing the formation of larger leaf packs and therefore increasing leaf retention. However, the data also shows that small spatial variations in the bed are sufficient in low flow depths to promote the retention of leaves.

The retention at the four locations investigated can be summarised in terms of physical and hydraulic properties within the grid. Grid 1 did not exhibit stable hydraulic conditions, with the presence of eddies above the leaf pack location. There was variation within the bed without the presence of an isolated protrusion, however there was a dead zone present below the leaf pack location. The leaf pack retention location of Grid 2 was found to have significantly lower velocities throughout the profile than the rest of the grid, as well as the largest variation within the bed height that lead to larger variation in the longitudinal velocities below the maximum bed height. The retention in Grids 3 and 4 can be attributed to the presence of an isolated protrusion, over which there were stronger velocities compared to Grids 1 and 2, creating a downward force onto the protrusion that allowed the formation of larger leaf packs.

The presented plots show that in each case the flow of water, appears to push the leaf pack onto the bed allowing it to remain stable. This would be expected as the flow of the water over a leaf would create a downward force, holding the leaf in place. The complicated bed structure of this experiment means that it is difficult to identify the exact mechanism of leaf retention. The importance of physical characteristics on leaf retention could be seen, but it was hard to isolate any hydraulic conditions that aided leaf retention.

5

RETENTION OF LEAVES ON BOULDERS

The annual input of deciduous leaves into temperate headwater streams represents a major flux of carbon and energy of considerable ecological importance. However, the exact hydraulic factors that determine how leaves are retained and trapped into leaf packs have never been quantified fully. A series of flume experiments were used to investigate how boulder submergence and density affected leaf retention. An idealised situation was created using uniform concrete hemispheres in a regular staggered array in which the flow depth and array density were varied systematically for a constant discharge. Saturated leaves were then added and percentage retention was recorded. Boulder density significantly affected both retention efficiency and retention per boulder, but the effects of flow depth were significant only when combined with the Boulder Volume Fraction (the volume of boulders relative to the volume of water in the flume). The absolute number of boulders affected retention, but the interacting effect of boulder density was found to be more significant. There appeared to be an optimum density of boulders that maximised leaf retention, which could relate to the velocity and turbulence fields generated by the presences of the boulders within the water flow. While further investigation is required, this data suggests that leaf retention is linked to the presence of retentive structures, but that the interacting effects of these structures can have both a positive and negative effect.

5.1 Introduction

The contribution made by allochthonous litter to the energetics, carbon dynamics and secondary production in temperate headwater streams has been well recognised for over four decades (Cummins, 1974; Young et al., 1978; Webster et al., 1987; Tank et al., 2010). A wide range of heterotrophs are dependent directly on leaf litter as a food source, while their actions in processing this material into finer fragments also release energy and nutrients that become important to other organisms and processes downstream (Vannote et al., 1980). The effects are so large that whole seasonal cycles in rivers are determined by litter inputs, and there is continued interest in examining litter processing as major indicators of whole stream function (Hladyz et al., 2011). It is particularly surprising therefore, that the exact hydraulic factors that determine how leaves are retained and trapped into leaf packs have never been quantified fully.

Organic matter entering streams can be divided into categories based on size; large wood (diameter > 4cm), sticks (diameter < 4cm), coarse particulate organic matter (CPOM) e.g. leaves, and fine particulate organic matter (FPOM) (0.45μm - 1cm diameter) (Webster et al., 1999). The largest input is usually in the form of coarse particulate organic matter or leaves (Webster et al., 1999). Once the leaves become waterlogged and sink (Hoover et al., 2006), they have two fates; either being retained and broken down or transported further downstream (Webster et al., 1999). This balance between transport and retention has major consequences on the availability of nutrients and energy for local and more downstream processes (Webster et al., 1999). This, in turn, is governed by interactions between the character of the leaves (e.g. Webster et al., 1987; Hoover et al., 2010), physical aspects of the stream (e.g. Webster et al., 1994; Larrañaga et al., 2003), discharge patterns (e.g. Young et al., 1978; Webster et al., 1999; Larrañaga et al., 2003), and local mechanisms of retention provided by features such as rocks, woody-debris, pools and backwaters, and instream or bank vegetation (e.g. Webster et al., 1987, 1994; Ehrman and Lambert, 1992; Hoover et al., 2010). However, it is also suggested that retention is merely defined by the probability of contacting a 'retentive structure' and the ability of the particles to be retained and not dislodged from the obstacle.

Many leaves only travel short distances before they are retained and processed (Young et al., 1978; Webster et al., 1987; Ehrman and Lambert, 1992; Webster et al., 1994), with the probability of retention affected by reach attributes, such as depth (e.g. Webster et al., 1994), gradient (e.g. Larrañaga et al., 2003) and the presence of retentive structures (e.g. Webster et al., 1987; Ehrman and Lambert, 1992). There is debate about whether different methods of retention exist between riffles and pools (Hoover et al., 2006), with specific obstacles or 'retention structures' being involved in riffles (Ehrman and Lambert, 1992;

Cordova et al., 2008), or whether the number of structures is important (Webster et al., 1987; Ehrman and Lambert, 1992; Hoover et al., 2010).

Discharge has a negative effect on retention (Webster et al., 1994; Larrañaga et al., 2003; Cordova et al., 2008; Hoover et al., 2006), with leaf travel distances thought to be related to the peak discharge during storm events (Webster et al., 1987). Seasonal variations in retention also occurs, with greater retention in summer and autumn, linked in turn to the seasonal patterns of discharge and flow depth (Webster et al., 1994). Hoover et al. (2006) suggest that the strong relationship between discharge and leaf retention simply indicates a more direct relationship with one or more of the many variables that vary in relation to changes in discharge, such as flow depth, velocity and channel width. Increased flow depth reduces retention (e.g. Webster et al., 1994) suggesting that retention is not a passive process, but that it is dependent on the probability of leaves encountering retentive structures, with this probability decreasing with increased water depth (Webster et al., 1994).

While retention in streams has been investigated using a variety of materials from FPOM (Webster et al., 1987, 1999), CPOM, such as leaves (Young et al., 1978; Webster et al., 1987; Ehrman and Lambert, 1992; Webster et al., 1994, 1999; Larrañaga et al., 2003; Hoover et al., 2006; Cordova et al., 2008; Hoover et al., 2010) up to woody-debris of varying sizes (Ehrman and Lambert, 1992; Webster et al., 1994; Cordova et al., 2008), scales of investigation have also varied. Field experiments have examined the parameters affecting leaf retention using both artificial (e.g. Webster et al., 1994; Larrañaga et al., 2003; Cordova et al., 2008) and real leaves (e.g. Young et al., 1978; Webster et al., 1987; Ehrman and Lambert, 1992; Hoover et al., 2006; Cordova et al., 2008). However, only a few experiments have been carried out in the controlled setting of a flume (e.g. Webster et al., 1987; Hoover et al., 2006). This is surprising as the the controlled and highly calibrated environment a flume provides could aid in the quantification of leaf retention processes.

The experiments discussed in Chapter 4 showed the need for leaf retention mechanisms to be examined in a more simplified situation. This chapter presents a series of flume experiments where the effect of boulder density and flow depth were examined by varying them in isolation. These experiments allow the investigation of whether retention is dependent on the probability of contact with an obstacle, a factor that is affected by the number of boulders and boulder submergence, or whether it is due to the interaction of adjacent boulders within an array and the effect they have on the velocity and turbulence fields.

5.2 Method

These experiments were carried out in parallel to those presented in Chapter 6 using the NERC glass walled recirculating flume, the setup and calibration of which is described in Section 3.1. This included calibration of the bed slope, the attachment and calibration of rulers to the flume wall to measure the flow depth, and the identification of the flow type and water surface profiles. Flow conditions and retentive structure density in the flume were then varied systematically to create conditions under which the retention of leaves was examined.

5.2.1 Retentive structures

Idealised concrete boulders (see Section 3.5.3) were used to provide uniform protrusions at known locations, to allow the examination of leaf retention. The boulders were placed in a staggered array directly on the glass bed. The longitudinal and lateral spacing of the boulders was varied to give a variety of densities. The leaf retention experiments were only carried out at three of the four densities discussed in Section 3.5.3: Sparse (Sx = 500mm, Sy = 360mm), Intermediate (Sx = 400mm, Sy = 220mm) and Dense (Sx = 300mm, Sy = 180mm). Four flow depths; 130, 150, 240 and 300mm were used to test retention, selected to vary the submergence ratio of the boulders (ratio of the flow depth to boulder height): 1.71, 1.97, 3.16 and 3.95, however only the latter three were used for all densities.

The discharge was measured and calibrated as outlined in Section 3.3 using Controlotron 1020 clamp-on flowmeter. The discharge was kept constant for all combinations of boulder density and flow depth to allow easier comparison and to remove the effect of discharge on leaf retention. Due to the nature of the flume it was not possible to obtain a constant single discharge, and instead the calibrated discharge was maintained within the range of 45.74–45.84 L/s; it was deemed that ± 0.05 L/s was within the accuracy of the flume. The average discharge of 45.79 L/s was used to calculate all parameters.

These experiments were carried out under gradually varied flow conditions, discussed in Section 3.1.3. The water surface profiles for each flow depth and boulder density combination were measured with the use of calibrated rulers fixed to the flume wall, recorded and presented in Section 3.1.3, (Figures 3.3 and 3.4). Each experiment conformed to M1 profile (Chow, 1959), where the flow depth increased with distance downstream. A best-fit water surface profile was calculated for each situation from which a mean flow depth could be calculated over the working length of the flume (15.35m). Although every effort was made to carry out the experiments at exactly the same flow depths, (130mm, 150mm, 240mm, and 300mm), increased boulder density affected the flow depth by 1-2 mm, although these effects were small enough to be ignored.

	Mean Water Depth (m)	Boulder Submergence	Slope	$\bar{U}$ (m/s)	$\bar{U}_{Blockage}$ (m/s)	ϕ_{xyz}
Sparse	0.127	1.671	1:300	0.300	0.306	0.019
	0.149	1.961	1:1000	0.256	0.260	0.016
	0.240	3.158	1:1000	0.159	0.160	0.010
	0.300	3.947	1:1000	0.127	0.128	0.008
Intermediate	0.148	1.947	1:1000	0.256	0.267	0.033
	0.239	3.145	1:1000	0.159	0.163	0.021
	0.300	3.947	1:1000	0.127	0.129	0.016
Dense	0.150	1.974	1:1000	0.256	0.266	0.044
	0.241	3.171	1:1000	0.159	0.163	0.028
	0.300	3.947	1:1000	0.127	0.130	0.022

Table 5.1. Description of the conditions for each experimental setup

Overall, ten combinations of density and depth were used to investigate leaf retention, conditions of which are shown in Table 5.1. It was intended to carry out all experiments at a slope of 1/1000, but it was necessary to change this to a steeper slope (1/300) to obtain the shallower depth of ≈0.130m. Due to the different slope required this flow depth was only used with the Sparse density to remove the possible effect of gradient.

For each permutation, two area mean velocities were calculated using the mean flow depth and mean discharge; the first ($\bar{U}$) ignores any cross-sectional area reduction due to the presence of the boulders and is therefore unaffected by density. The second ($\bar{U}_{Blockage}$) reduces the cross-sectional area to take into account the presence of the boulders before the velocity is calculated, and therefore this varies with both boulder density and depth. Calculating a solid volume fraction, relating the volume of boulders to the volume of water, allowed the creation of a parameter that can be used to consider the effects of both the boulder density and flow depth at the same time. This is referred to as the Boulder Volume Fraction (ϕ), and it was calculated in the following manner:

$$\phi_{xyz} = \frac{2/3\pi r^2 hn}{xyz} \tag{5.1}$$

where r is the boulder radius, h is boulder height, and n is the number of boulders present, xyz represents the volume of water, where x is the length of flume, y the width and z is water depth. All measurements are in metres.

5.2.2 Leaf Additions

The leaves used to examine retention were described in Section 3.4. Fallen deciduous leaves were collected from various locations consisting predominantly of oak leaves. These

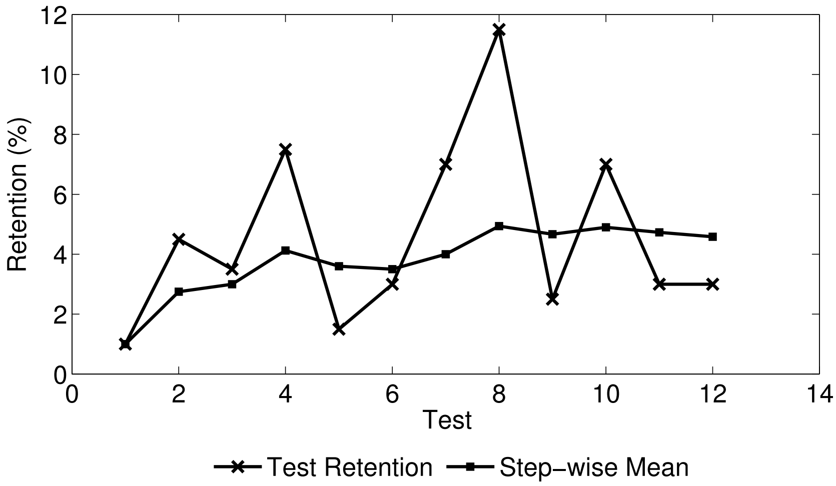

Figure 5.1. Comparison of the test retention efficiency to the step-wise mean retention efficiency for the Sparse density and a flow depth of 240mm.

experiments consider the retention of conditioned leaves that have already being entrained into the water column, and are therefore saturated. The leaves were divided into batches of 200 and soaked in cold water for a minimum of 24 hours, as described in Section 3.4. Batches of leaves were released by hand at a length of 5m, to ensure developed flow conditions, evenly across the width of the flume near the bed. Leaves that were not retained on the boulders were caught on a net at the end of the flume and were removed. It was ensured that conditions were stable and all retained leaves were stable before results were recorded. Leaves retained on each boulder were then counted and recorded ignoring any that were retained on the sides and base of the flume.

5.2.3 Data analysis and calculation of retention

For each input of leaves a retention efficiency (E_R), the number leaves retained divided by number added, was calculated (Webster et al., 1987). Due to the variability in the E_R, the experiment was repeated with a mean retention efficiency ($\bar{E}_R$) being calculated after each repeat. The experiment was repeated until consistency was seen in the mean; usually 10-14 repeats (Figure 5.1; Table 5.2). A standard deviation was calculated for each $\bar{E}_R$, allowing the variation to be quantified. ANOVA and general linear models (GLM) were used to examine the effect of the different varied and calculated parameters on the retention. All statistical tests were performed in Minitab.

To evaluate the distribution of leaves retained down the flume, a probability of retention was calculated at each length where boulders were present ($P_R(x)$) for each of the experimental setups to allow comparison between the different depths and densities. This was the calculated as the ratio of retained leaves at a length ($L(x)$), to the total number of leaves added (L_0), taking into consideration the number of boulders present at that length ($n(x)$);

$$P_R(x) = \frac{L(x)}{n(x)L_0} \tag{5.2}$$

From this a probability of leaf transport can be calculated as the number of leaves that travelled a distance (x), divided by the total number of leaves;

$$P_T(x) = 1 - \sum_{i=0}^{x} P_R(i) \tag{5.3}$$

This equation differs to the one presented in Chapter 4 (Eq. (4.1)), as the number of protrusions here is known and therefore accounted for by including n. The relationship of probability of transport could be fitted to an negative exponential distribution (e.g. Young et al. (1978); Webster et al. (1987); Ehrman and Lambert (1992); Hoover et al. (2010)) shown here;

$$L(x) = L_o e^{-k_R x} \tag{5.4}$$

where, k_R is the retention coefficient (m^{-1}) (Webster et al., 1987; Hoover et al., 2010) or the instantaneous rate of leaf removal from the water column (Ehrman and Lambert, 1992). This describes the ability or effectiveness of the stream to retain leaves, and therefore is a useful parameter to compare between experiments. The inverse of the retention coefficient gives the mean transport distance (T_m); where,

$$T_m = \frac{1}{k_R} \tag{5.5}$$

This is the distance at which 63.2% of leaf input is expected to have been retained by the stream (Webster et al., 1987). The retention coefficient can also be calculated from the calculated retention efficiency (Webster et al., 1987);

$$k_R = \frac{\ln 100 - \ln(100 - E_R)}{x} \tag{5.6}$$

where x is the length over which the E_R was calculated. Equation 5.6 was used to calculate the distance total retention distance (T_T), using k_R from equation 5.4 and setting the E_R to 99% (Young et al., 1978).

	Mean Depth (m)	$\bar{E}_R$ (%)	St Dev (%)	$\bar{E}_R$ per Boulder (%)
Sparse	0.127	4.708	2.158	0.1519
	0.149	3.750	2.031	0.1210
	0.240	4.583	3.066	0.1478
	0.300	3.536	2.179	0.1141
Intermediate	0.148	12.042	4.314	0.1911
	0.239	20.250	4.991	0.3214
	0.300	23.000	5.768	0.3651
Dense	0.150	10.667	2.863	0.1226
	0.241	18.636	4.075	0.2142
	0.300	17.833	4.634	0.2050

Table 5.2. Leaf retention results for each experiment setup

5.3 Results and Discussion

Over all the experiments, leaf retention efficiencies varied from 0.5% to 32%. Between 10 and 14 tests were carried out for each experimental set-up, giving mean retention efficiencies that varied between 4.708% and 23% (see Table 5.2). These are much lower than the retentions seen in the experiments of Webster et al. (1987), however the range for all their experiments did vary from 1.3–99%. Our much lower retentions could be due to the much higher discharges used in our experiments, 45.79 L/s compared to just 2 L/s.

The maximum retentions are comparable to the retention attributed to boulders by Larrañaga et al. (2003) and the retentions seen at the lowest density are comparable to the retention due to boulders seen by Ehrman and Lambert (1992). The highest retentions and highest mean retention was present at the intermediate density and a flow depth of 300mm. The mean retention rates have been plotted to allow for the identification of the effect of boulder density and flow depth. Figure 5.2(a) compares the variation in retention rates with density using the Boulder Area Fraction and Figure 5.2(b) compared the variation between flow depths.

Retention efficiency did not exhibit a linear relationship with density (Figure 5.2(a)). A similar pattern was seen for the different flow depths, with the retention efficiency peaking at the intermediate density (0.0973), indicating an optimum density for retention. An increase in retention with Boulder Area Fraction supports the idea that retention is affected by the probability of a leaf coming into contact with an obstacle; the greater the number of obstacles the greater the probability (Ehrman and Lambert, 1992; Hoover et al., 2010). Reaching a maximum could indicate that at this point, further increase in the number of boulders has no more effect as another associated factor starts to have an equal or

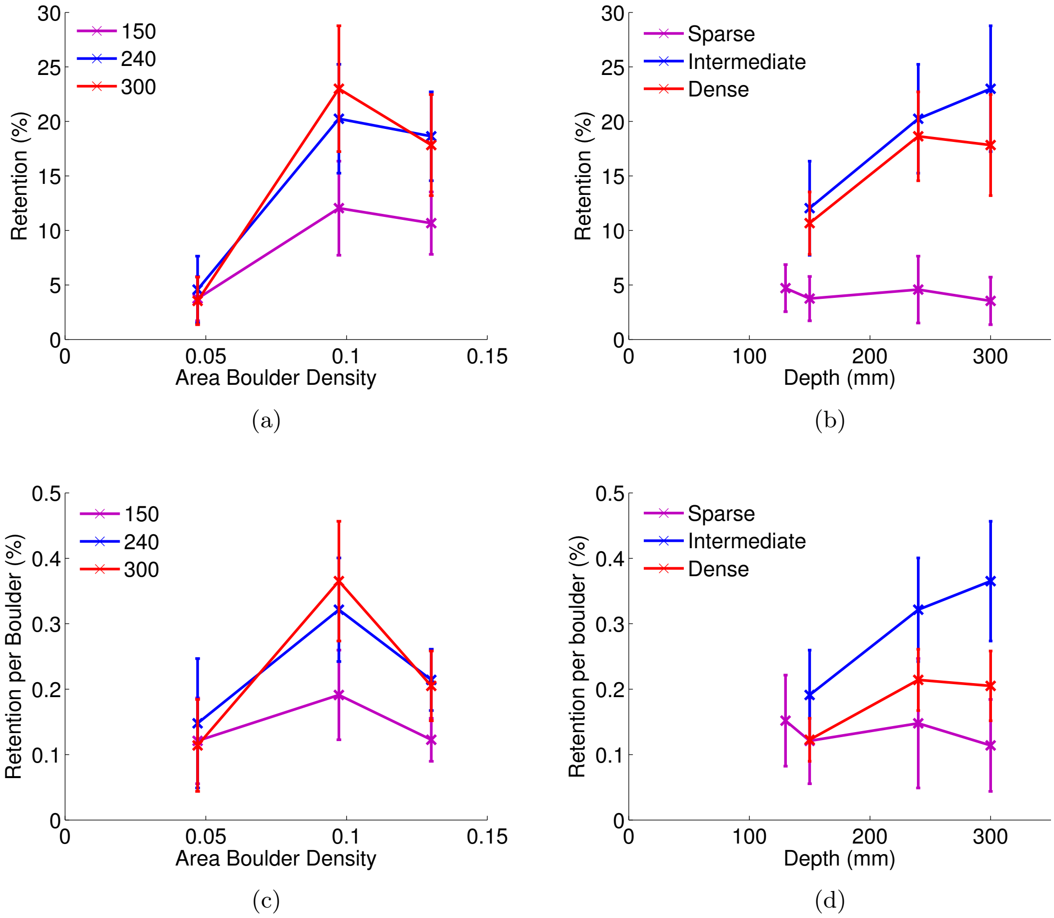

Figure 5.2. Variation in retention efficiency and retention efficiency per boulder with (a,c) boulder density for each flow depth and (b,d) for flow depth with each boulder density

outweighing negative effect. At the lowest density there is no variation in the retention efficiency for all flow depths, but as the density increases a difference between the flow depths emerges. For the higher two densities (intermediate and dense) retention rates for a flow depth of 150m, compared to those at the flow depths of 240 and 300mm were found to be significant different (Two-sample t-test between points, all $p < 0.005$). However there is not a significant difference (Two-sample t-test $p = 0.932$) between the flow depths of 240mm and 300mm, suggesting that increasing the flow depth from 240mm to 300mm has little effect on retention.

The nature of the relationship between flow depth and retention efficiency varied between the different densities (Figure 5.2(b)). Retention rates for the sparse density do not change significantly with flow depth (ANOVA, $p = 0.543$), showing that this range of flow depths does not affect retention at this density. At the higher two densities, the retention efficiency increased with flow depth, reaching a limit at the dense configuration, similar to the carrying capacity that is seen in ecosystems. The highest retention efficiency for all flow depths is present at the intermediate density, however it was not significantly different from the dense density for the flow depths of 150 and 240mm, (Two-sampled t-test, $p = 0.369$ and $p = 0.432$ respectively). This suggests that up to this flow depth, the increase in flow depth had the same effect on retention for both densities.

A possible explanation of this relationship suggests that retention increases with flow depth until a maximum is reached at which further increases in flow depth have no impact on retention. This relationship appears to be affected by density suggesting that the maximum is reached at different flow depths for different densities. The sparse density has reached its maximum, the retention at the intermediate density is still increasing, and a maximum was reached at a flow depth of approximately 240mm for the dense density leading to no increase with further increase in flow depth (Figure 5.2(b)). The rate of increase in retention efficiency with flow depth is the same for the two higher densities, however the dense density reaches the maximum earlier than the intermediate density.

The observed increase in retention with flow depth is the reverse to that seen by Webster et al. (1994) where travel distance increased significantly with flow depth. These experiments were carried out in real streams and therefore increases in flow depth would have been related to increases in discharge, and area mean velocity. Due to a constant discharge the increase in flow depth reported here represents a decrease in area mean velocity. Although this factor has not been isolated in the literature, a consistent negative relationship been retention and discharge has been identified (e.g. Webster et al., 1987, 1999; Larrañaga et al., 2003) suggesting that reducing velocity would increase retention. This observation of increased retention with increased flow depth, and therefore boulder submergence, also suggests that retention is not reliant on probability of contact which decreases with increased boulder submergence.

Previous research has shown that leaves are actively retained on ‘retentive structures’, such as boulders and woody-debris (e.g. Hoover et al., 2006; Cordova et al., 2008). It has been suggested that the number of obstacles present affects the degree of retention observed (Ehrman and Lambert, 1992; Hoover et al., 2010), due to an increased probability of contact. Chapter 4 suggested that there was a relationship between retention rates and bed substrate, implying that bed morphology and therefore the presence of protrusions was important. Therefore it is necessary within this data to isolate any effect on retention rates that comes from the different number of protrusions present at the different densities. This will have two purposes; firstly it allows the effect of the number of protrusions to be identified, and secondly, identifies if interactions between the obstacles have any effect on retention. Therefore, a retention efficiency per boulder (E_{RB}) was calculated for each experiment, where the $\bar{E}_R$ was divided by the number of boulders present at that density. As the leaves entered the flume at a length of 5m, only the number of boulders contained within the section from 5-15.35m was used. The retention per boulder for each set up is shown in Table 5.2 and presented graphically in Figures 5.2(c) and 5.2(d).

Comparing Figures 5.2(a) and 5.2(b) to 5.2(c) and 5.2(d), illustrates the difference between the absolute retention efficiency, and the per boulder retention efficiencies. There is a change in the relationship for both cases when considering the retention efficiency per boulder, however there is still variation present between the different densities. This suggests that although the number of boulders present has an effect on retention, the degree of retention is not just reliant on the probability of hitting a protrusion, but that it is also affected by interaction between the boulders or the effects that the boulders have on the hydraulic conditions. The density of roughness elements influences whether there is interactions of the wake, which in turn might influence the retention of leaves. The number of boulders present being important, is in contrast to the research of Webster et al. (1987), who found just their presence to be important.

Figure 5.2(c) shows that once the number of protrusions has been taken into account, there is an optimum density for retention, with lower and higher densities retaining less organic material, with the same pattern visible at each of the compared flow depths. By allowing for the number of protrusions, the retention rates for the dense set up have been greatly reduced compared to the other two densities where the pattern has not visibly changed. This is particularly true for a flow depth of 150mm, where the retention efficiency per boulder at the sparse and dense densities are very similar (Table 5.2) but when considering just retention the highest Boulder Area Fraction retained more than double that of the lowest Boulder Area Fraction (3.75% compared to 10.67%). Less variation is present in retention rates per boulder between the three flow depths; with no variation with flow depth for the sparse density (ANOVA, $p = 0.543$), but there is significant variation with flow depth at the higher two density, (ANOVA, $p < 0.005$).

The shape of the relationship between flow depth and retention efficiency (Figure 5.2(d)), has not changed due to comparing within boulder densities, and therefore every line is divided by the same number. However it does highlight the difference in retention between the three densities. At each flow depth the retention does vary significantly with density, (ANOVA, all $p < 0.01$). Retention is clearly greater for the intermediate density, at all flow depths (Two-sample t-test, all $p < 0.05$). The dense density is now more closely related to the sparse density rather than the intermediate.

A two-way ANOVA was carried out to investigate the effects of both flow depth and density on both the retention efficiency and the retention efficiency per boulder. For both measures of retention, flow depth was found to be not significant ($p = 0.121$ and $p = 0.142$), but density was found to significantly explain the variation seen, ($p = 0.009$ and $p = 0.027$) with no interacting effect between the two variables being suggested. This reduction in the p-values once the number of boulders involved in each density is taken into consideration suggests that some of the variation was explained by the number of boulders. The density of obstacle have been evaluated in literature, although it is the density of woody-debris available that is often considered. The presence of obstacles, or woody-debris, was seen to increase retention (e.g. Webster et al., 1987; Ehrman and Lambert, 1992) and in particular Cordova et al. (2008) found the increases in volume and density of wood present to significantly increase leaf and artificial leaf retention.

Two parameters, the area-mean velocity and the Boulder Volume Fraction, were calculated to allow for comparison of the joint effect of both the boulder density and flow depth. As discussed the number of boulders has an effect on the retention of a system (Figure 5.2), but other relationships are also present therefore only the retention efficiency per boulder will be considered from this stage on. The $\bar{U}_{Blockage}$ is more closely related to flow depth, but the consideration of the blockage effect due to the boulders means that it also varies slightly with density. The calculation of a Boulder Volume Fraction varies with both the density at which an experiment was carried out and the flow depth. The variation of retention per boulder, with $\bar{U}_{Blockage}$ and Boulder Volume Fraction are presented in Figures 5.3(a) and 5.3(b) respectively.

The relationships in Figure 5.3(a) are, as expected, very similar to those seen when comparing the change in retention with flow depth for the different densities, (Figure 5.2(d)). As the relationship between the flow depth and velocity are inverse, e.g. for a constant discharge an increase in flow depth results in a decrease in area mean velocity, the graph is reversed. The area mean velocity increases as the retention per boulder decreases, except for the sparse density that remains relatively constant. A linear relationship is present at the intermediate density, with a sparse point also fitting this relationship. This could suggest that there is an absolute limit of retention, shown by this linear relationship. This limit could be a function of the boulder size, or related to the degree of interaction between boulders. The possible presence of a maximum retention efficiency was suggested in Figure 5.2. As this possible maximum is not located at the maximum density, it suggests that as the obstacles get closer to each other, their interaction affects velocity structures which in turn affect the retention.

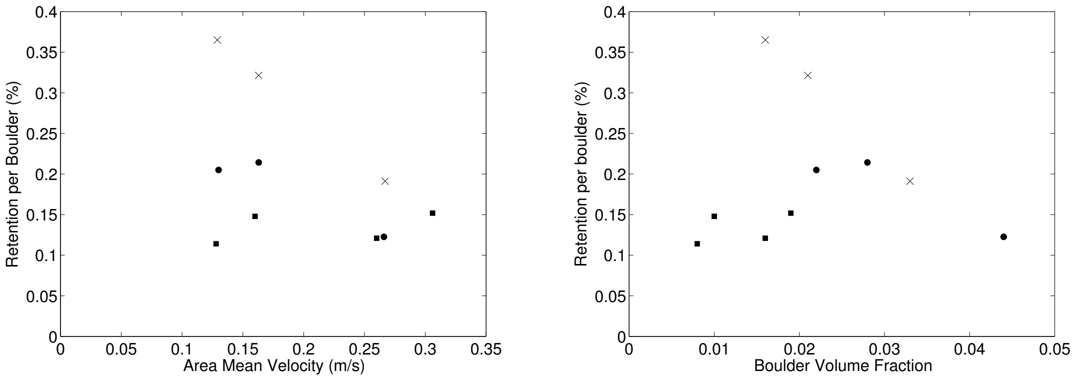

(a) (b)

Figure 5.3. Variation of retention efficiency per boulder with (a) area mean velocity and (b) Boulder Volume Fraction. Squares represent the sparse, crosses the intermediate and circles the dense densities.

Figure 5.3(b) illustrates the combined relationship of flow depth and boulder density clearer, as this parameter provides a better synthesis of the flow depth and density parameters. A linear relationship is present at the intermediate density between the Boulder Volume Fraction and the retention efficiency per boulder, with the retention decreasing as the Boulder Volume Fraction increases. Points for the denser setup also appear to fit with the idea of a maximum linear relationship, before the retention remains constant at approximately 0.2%. Again the Sparse density remains relatively constant, despite an increase in Boulder Volume Fraction.

These relationships could be investigated further by considering what would be expected to happen at the extremes of the relationship. When the velocity tends towards zero, a large increase in retention would be expected. We might expect 100% retention at a very low or zero velocity, but this would be a passive process whereas we are actually considering retention per boulder. The results presented ignored retention on any structure other than the boulders, and therefore this passive retention would not be included in our measure. Also the maximum retention per boulder seen, even if 100% of leaves were retained, would be dependent on and vary greatly with the number of boulders present. At the other extreme, there will always be a chance of retention, so we would expect retention to tend towards zero as velocity increases but that zero would not be reached. Although this appears to be a linear relationship locally, when considering the expected behaviour at the extremes this suggests that an negative exponential model might be better suited.

Considering the extremes of the Boulder Volume Fraction (BVF) is more complicated. The actual extremes of zero and one can not be considered because at both the retention will be zero, as when BVF equals zero there are no boulders, and BVF can not equal one as there would be no water for the leaves to be retained in. However as the BVF tends towards zero, either the flow depth is very large or there are very few boulders present, or a combination of both. Both of the factors used to calculate BVF have an effect on retention, and therefore the greater availability in combinations might result in greater variation in the retention per boulder. However the relationship we are considering is maximum possible retention, and therefore it is possible to get high values of retention per boulder at low BVF, as even if retention is very low you will be dividing by small numbers of boulders, e.g. if mean retention efficiency was just 1% but there are only 2 boulders present, retention per boulder would be 0.5%. The other extreme, tending towards one, suggests that there will be a larger number of boulders, and smaller volumes of water, and although this might lead to higher absolute retentions, larger numbers of boulders present will lead to very small retentions per boulder. So again it might be better to consider this as an exponential relationship instead of a linear relationship, particularly in the region we have examined.

The exponential model was compared to each of the maximum retention relationships, each of these were calculated using just the points that run along this possible maximum line and were found to have an $R^2 > 98\%$. The relationships are as follows:

$$E_{RB_{max}} = 0.6954e^{-4.91\bar{U}_{Blockage}} \tag{5.7}$$

$$E_{RB_{max}} = 0.7003e^{-39.92BVF} \tag{5.8}$$

where $E_{RB_{max}}$ refers to the maximum retention efficiency per boulder, $\bar{U}_{Blockage}$ is the area mean velocity taking into account the blockage effect of the boulders, and BVF refers to the Boulder Volume Fraction. There is high degree of similarity between the two relationship, each has the same constant of approximately 0.7, and the gradient is approximately a factor of 10 different, due to the BVF and $\bar{U}_{Blockage}$ varying by approximately the same amount. From these relationships it could be suggested that if we assume the 63 boulders present at the intermediate density, the density at which the highest retention was present, then a maximum retention of approximately 44% would be possible for our size of boulders or experimental setup, e.g. discharge. It is not possible to suggest why this relationship might exist, with these parameters, however this should be investigated further by carrying out a greater combination of experiments looking at a much larger ranges of BVF and $\bar{U}_{Blockage}$.

GLM analysis showed that neither $\bar{U}_{Blockage}$ or BVF are significant predictors of the retention efficiency per boulder, ($p = 0.229$ and $p = 0.876$ respectively) even when both are considered, ($p = 0.178$ and $p = 0.435$ respectively). However in earlier analysis density proved to be significant in explaining retention. When density and $\bar{U}_{Blockage}$ are considered together, then both are significant, ($p = 0.011$ and $p = 0.037$ respectively), with velocity having a negative effect on retention, and density having a varying effect. This suggests that $\bar{U}_{Blockage}$ can be used to predict the retention efficiency per boulder, when the additional information of varying density is added, further illustrating that there is a significant difference between the different densities.

Probability distributions were produced firstly to compare like flow depths for the differing densities, (Figure 5.4), and to compare like boulder densities for the different flow depths, (Figure 5.5). In calculating the probability of retention, the upstream retention of leaves was not considered, and therefore L_0 was not reduced with increase in longitudinal distance. However, taking this factor into consideration did not produce significantly different distributions. These figures show that the distribution of retention seen for each of the experimental set ups does differ in places, with more variation being seen at some locations than others. Comparing between the three flow depths, 150, 240 and 300mm, (Figure 5.4) shows that the probability of retention increases with flow depth, with larger peaks being seen at the greater depths. The greatest variation between the densities is present at the 240mm flow depth.

The distributions of retention changes as the flow depth increases. At a flow depth of 150mm there is only a single region of higher retention, within 3m of leaf input. But for the flow depths of 240mm and 300mm, the distributions become multimodal, with more than one location of high retention. This change in distribution is most obvious for the sparse density, where at the 150mm flow depth a high retention region is present within the first 3-4m (Figure 5.4(a)), with very little probability of retention over the rest of the length. At the increased flow depth of 240mm, two peaks are present, the greatest at 0-2m, and a second smaller peak at 4m (Figure 5.4(b)). At each flow depth the greatest peaks are observed at a different density, the sparse for 150mm, the dense for 240mm, and the intermediate for 300mm flow depths. Despite the largest peaks being present at the dense set up at 240mm flow depth, we know from Table 5.2 that overall retention is actually greater at the intermediate density at this flow depth.

At the lower two flow depths there is a degree of commonality between the different densities, but at the highest flow depth (300mm), the distribution of sparse is different to that of the higher densities. The intermediate and dense configurations have high probabilities of retention near the input, 1–2.5m, but for sparse density greatly reduced probability is present within this region, instead peaking later at 3m (Figure 5.4(c)). For all the flow depths only the intermediate density has reduced probability of retention after 6m in

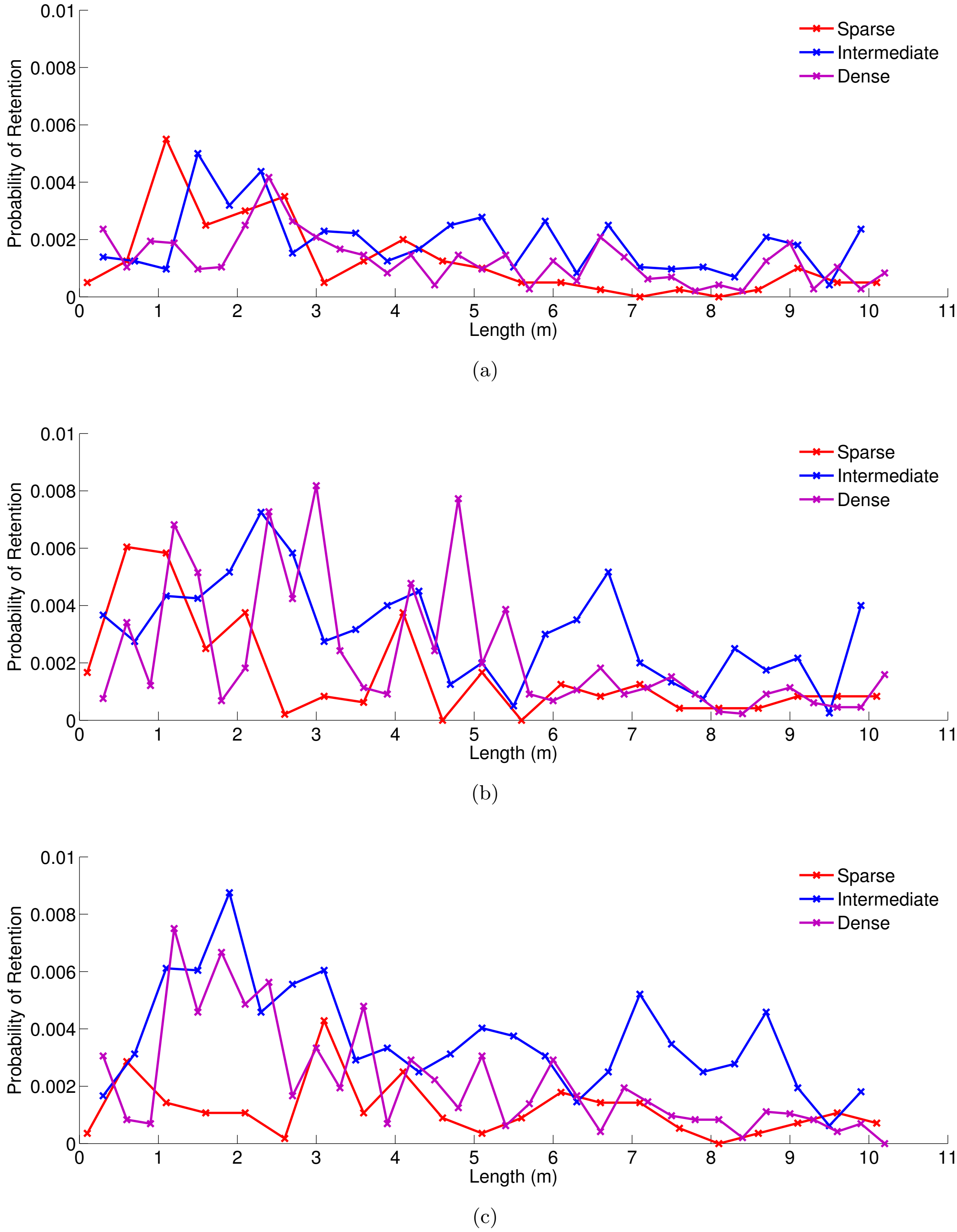

Figure 5.4. Probability of leaf retention for a given length for each boulder density at each flow depth (a) 150mm (b) 240mm and (c) 300mm.

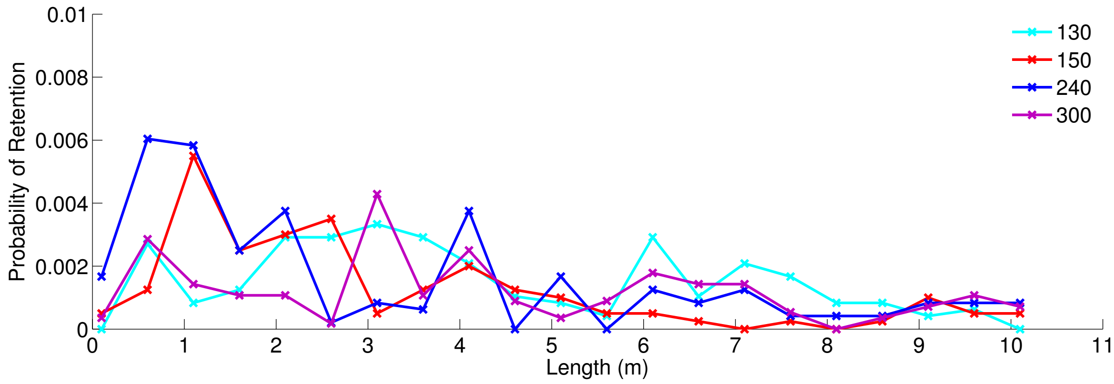

(a)

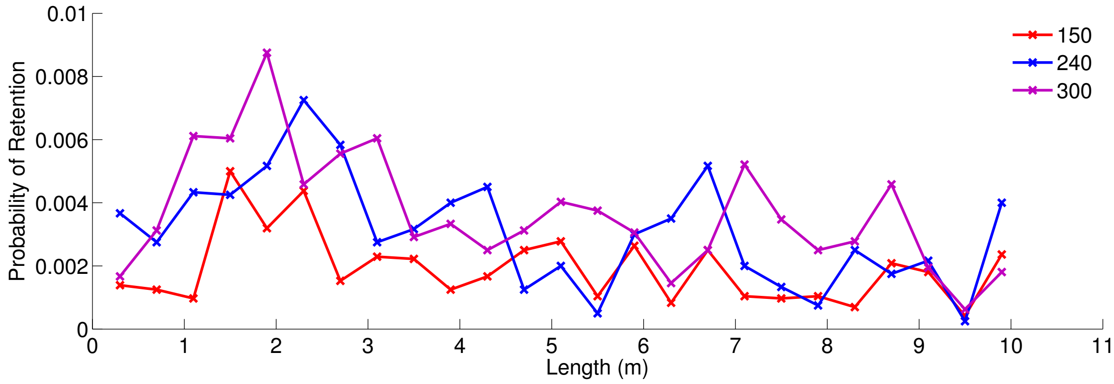

(b)

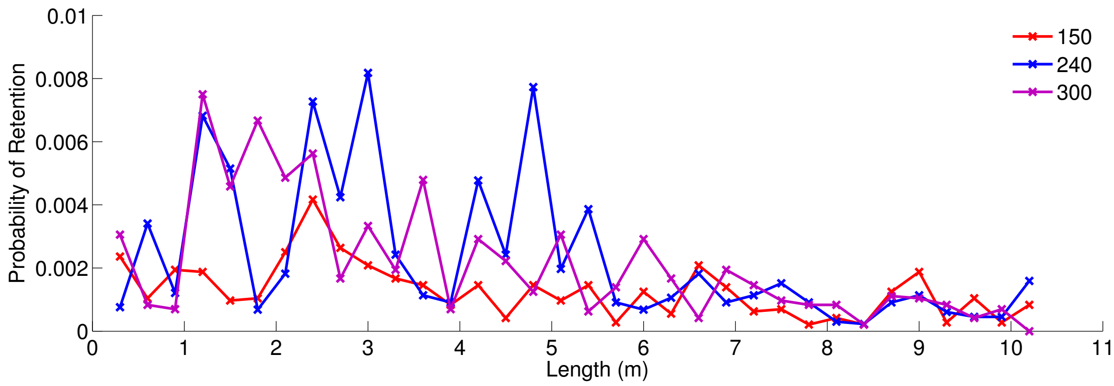

(c)

Figure 5.5. Probability of leaf retention for a given length for each flow depth at each boulder density (a) Sparse (b) Intermediate and (c) Dense.

length. This suggests that for the intermediate density there is a more consistence chance of a leaf being retained down the length of the channel, however for the other two densities, it is more likely that a leaf will be retained earlier in the channel. It might be possible to fit bi- or multi-modal distributions to each of these histograms; however to be sure of an actual relationship it would be necessary to have a larger sample of leaves, which would allow the distribution to be more distinctly visible.

Figure 5.5 compares the probability of retention distributions for each of the flow depths between densities. The lowest retention is seen at the sparse density, and the highest overall retention is at the intermediate density, with the greatest variation between the flow depths present at the dense density. As was shown in Figure 5.4 for all flow depths, the distribution of retention is different for the intermediate density than for the sparse and dense densities. At the intermediate density the probability of zero retention does not occur once, with a more uniform chance of a leaf being retained over the length. At the other two densities, very low retention is observed after 6m, showing that a leaf is more likely to be retained up to this distance than after it. Due to the spacing at the sparse density, channels of straight flowing water were present between the longitudinal rows of boulders. An observation was made, that if the leaves entered these channels then there were more likely to be carried directly to the end of the flume.

At the lowest density the distributions for the 150 and 240mm flow depths are initially very similar up to about 4m, with high retention zones seen near the input. However after around 6m, it is the flow depths of 240 and 300mm that have similar retention patterns. The distribution of the flow depth of 130mm, is much more rounded, than the others densities. This difference could be due to the different slope that this set up was carried out at. At the highest two densities the retention for the 150mm flow depth is lower that the other flow depths, which would be expected as an increase in flow depth was shown to increase retention, due to the decrease in velocity.

Hoover et al. (2010) also examined the probability of retention over the length of their experimental reaches. The distributions exhibited for the retention of leaves were much wider than those seen for stiffer material (Hoover et al., 2010). Within pools the distribution was much smoother than the distributions presented in Figures 5.4 and 5.5. This variability, especially in the intermediate and dense densities, is much more comparable to the retention patterns that Hoover et al. (2010) found in riffles, where a number of peaks in retention were seen. They only examined the distribution over 4m, but there are similarities between their 4m and the retention seen within the first 4m of our pattern.

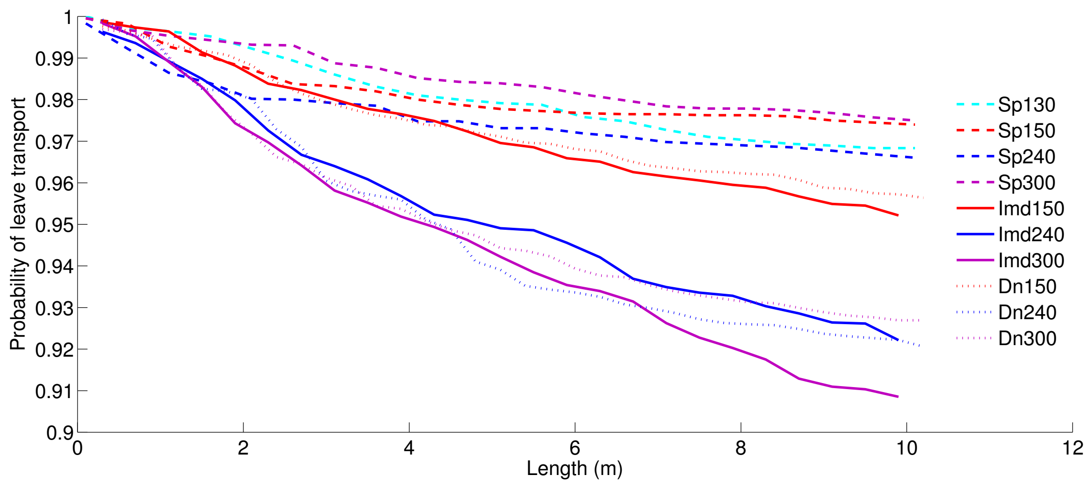

Figure 5.6. Probability of leaf transport against length for each combination of flow depth and boulder density. (Sp, Imd and Dn represent the Sparse, Intermediate and Dense density respectively, and 130, 150, 240 and 300 referred to the four flow depths)

The probability of a leaf travelling a particular distance was calculated to allow for easier comparison of the patterns of retention between the ten different combinations of flow depth and boulder density. The results are presented in Figure 5.6. Firstly this illustrates that the highest probability of retention over 10m is 9%, at the intermediate density for a flow depth of 300mm. This illustrates the effect of increasing the flow depth, and therefore reducing velocity and that the intermediate flow depth is the most retentive. There are definite groupings in the pattern of leaf transport with length, and therefore the way leaves are retained. The profiles of the sparse densities follow the same shape, apart from the flow depth of 240mm, where the first 1.5m has a greater gradient than the other flow depths. The next grouping consists of the flow depths of 150mm for the intermediate and dense configuration, which follow exactly the same profile shape. The last group consists of the 240 and 300mm flow depths for the densities of intermediate and dense.

The results of fitting the negative exponential model (Eq 5.6) are shown in Table 5.3, along with the goodness of fit shown by the R^2 value, the calculated mean transport distances, and total transport distances. The retention coefficients varied from 0.00284 to 0.01070 m^{-1}. These k values are comparable to those presented in Chapter 4 for the sand and pebbles. The retention characteristics of the sand is comparable to that of the sparse density, with the same value of retention coefficient seen at this density and a water depth of 300mm. However the retention of the pebbles was more comparable to the intermediate and dense densities at the 240 and 300mm water depths. Chapter 4 that suggested that larger size of the particles lead to greater heterogeneity of the bed, and therefore higher

	Mean Depth (m)	-k (m^{-1})	Rsq (%)	T_x (m)	T_T (m)
Sparse	0.127	0.00370	95.4	270.42	1245.21
	0.149	0.00330	59.6	303.12	1395.93
	0.240	0.00422	45.4	236.74	1090.24
	0.300	0.00284	93.8	351.99	1620.97
Intermediate	0.148	0.00537	96.6	186.25	857.73
	0.239	0.00911	93.8	109.78	505.56
	0.300	0.01070	96.7	93.47	430.43
Dense	0.150	0.00499	91.8	200.56	923.62
	0.241	0.00977	88.9	102.38	471.45
	0.300	0.00912	84.2	109.63	504.84

Table 5.3. Results of fitting the negative exponential model of leaf transport to the results presented in Figure 5.6 for each combination of flow depth and boulder density.

retention due to a greater number of retention locations present. This is supported by the difference in the comparison of the k values. The retention coefficients presented in Table 5.3 are directly in line with those seen for wet and dry beech, oak and maple leaves by Young et al. (1978). Ehrman and Lambert (1992) compared the retention among three reaches of varying presence of woody-debris. The higher values of retention coefficient are comparable to those observed in reaches with high wood density; however the lowest values are lower than the range reported by Ehrman and Lambert (1992) even in non-woody reaches. However, the k_R values reported here are two to three orders of magnitude smaller than those reported by Hoover et al. (2006, 2010), suggesting that their streams were much more highly retentive than our experiments.

The mean transport length was calculated to provided an easier comparison of retention ability as these are more reported in the literature. Cordova et al. (2008) provides a comprehensive summary of reported experiments and mean transport distances for leaves. Generally most transport distances are much shorter than the ones presented here, however they are comparable to those of Young et al. (1978) and Ehrman and Lambert (1992). Both these experiments are batch release experiments so are directly comparable. It would not be expected to get results comparable to experiments that released leaves individually, as it would expected that this would lead to higher retention rates due to the lack of interference between leaves. This is confirmed by comparing the results presented in Cordova et al. (2008), where individually released leaf experiments have reported much shorter mean transport distances. However this paper does not state which values are calculated from the retention coefficient and which are from observation, which could lead to discrepancies. The results observed here suggest that we would require a minimum of 430m to see total retention in the case of the intermediate density for a flow depth of

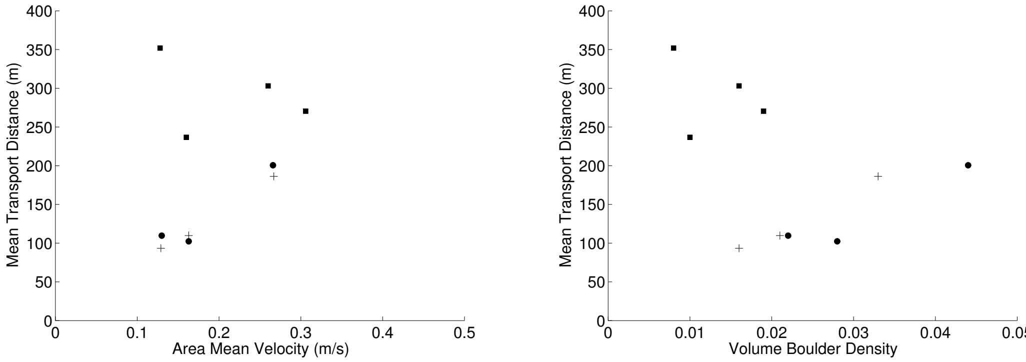

(a) (b)

Figure 5.7. Variation of mean transport length with (a) area mean velocity and (b) Volume Boulder Fraction. Squares represent the sparse, crosses the intermediate and circles the dense densities)

300mm, but the worse case scenario would require approximate 3 times this distance for the same retention, a range that is similar to Young et al. (1978).

Figure 5.7 illustrates how the mean transport distance varies with $\bar{U}_{Blockage}$ and Boulder Volume Fraction. Due to the inverse nature between mean transport distance, and retention efficiency the relationship is the reverse of that seen in Figure 5.3. Therefore, in this situation we would expect to see a minimum transport distance. Figures (5.7(a) and 5.7(b)) show that a relationship can be seen involving the data for both the intermediate and dense densities where the minimum transport distance increases with increase in $\bar{U}_{Blockage}$ and Boulder Volume Fraction, with the sparse data sitting at much longer distances.

A two-way ANOVA found flow depth to be non-significant, and boulder density to be significantly related to k_R, and mean transport distance. A GLM analysis showed the area mean velocity to be significantly ($p = 0.032$) related to k_R when considered with BVF, but BVF itself was was not significant ($p = 0.068$). The reverse is true when relating them to mean transport distance, although $\bar{U}_{Blockage}$ was only just not significant ($p = 0.055$). When considering the retention coefficient and mean transport distance, the addition of flow depth makes the other factors non-significant. This suggests that neither of these parameters are effective predictors of retention.

5.4 Summary

Temperate stream ecosystems are dependent on the input of terrestrial organic matter to provide carbon and energy to the system (Cummins, 1974). Leaves are either retained or transported, with the balance between these two mechanisms having major consequences on the availability of nutrients and energy at both the local scale, and further downstream. The retention of leaves is thought to differ between riffles and pools (Hoover et al., 2006) and is dependent on the interaction between characteristics of the leaves, physical aspects of the stream and the presence of retentive structures. Despite important of this material, the exact hydraulic factors determining the retention of leaves has not been fully quantified. The results of the experiments in Chapter 4 suggested the important of retentive structures, such as protrusions, but also showed the need to investigate different factors that might affect retention in the the controlled environment of a flume. A series of flume experiments were carried out to investigate how the number of boulders, the density of boulders and boulder submergence affect the retention efficiency. Uniformly sized concrete boulders were placed in regular array, where the spacing was varied systematically along with the flow depth, and the retention of leaves was examined. A constant discharge was used, allowing the effect of flow depth to isolated from an increase in discharge, the effect of which is well documented within the literature.

The retentive efficiencies seen in this series of experiments are generally lower than other reported experiments. The number of boulders was found to lead to an increase in retention, however when the number of boulders was taken into account variation with both flow depth and boulder density was still seen. Therefore retention increases as the number of boulders increases due to the increased probability of contact, but an effect due the interaction between adjacent boulders is also present. The density of roughness elements affects the wake structure, with interaction of wakes occurring at higher densities. At the sparse density the boulders are independent of each other, however at the higher densities interactions might occur that either hinder or aid retention. Although variation within retention was seen with both boulder submergence and density, only density was found to be significantly related to both measures of retention, with an optimum density for retention suggested. This suggests that flow depth itself does not effect retention; but that the joint effect of both flow depth and velocity that is seen in discharge does. Density was also found to be significantly related to the retention coefficient and the mean transport distance.

Area mean velocity and the Boulder Volume Fraction were used to examine the joint effects of flow depth and density. Neither of these factors individually were seen to significantly explain the variation seen in the retention efficiency per boulder, however boulder density and area mean velocity together were both significant with the area mean velocity having a negative effect on retention and boulder density having a variable effect. It was suggested that a maximum retention relationship might exist, but the clarification and confirmation of this relationship would require lot more experiments to be carried out over a wider range of area mean velocities and boulder volume densities.

The experiments have shown that retention does vary with flow depth and boulder density, but that the variation with flow depth is better described by the reduction in velocity rather than the boulder submergence. An increase in flow depth, and therefore boulder submergence was not seen to harm retention, despite the suggest that it reduces the probability of contact with an obstacle. The presence of an optimal density for retention at the intermediate density, suggests that as the boulder spacing decreases, at a certain threshold the velocity and turbulence field that is produced has a negative effect on retention that outweighs the increase in the number of boulders. The links between retention and the velocity and turbulence field present within the different boulder arrays will be discussed in Chapter 6.4.

6

FLOW AROUND BOULDERS

Large protrusions found in gravel bed rivers are important in defining the spatial variability of a number of ecological factors, through their effect on the velocity and turbulence fields. A series of flume experiments was carried out to investigate how the flow structure around an array of boulders changed with boulder submergence and boulder density. Detailed three-dimensional velocity measurements at four flow depths for a constant boulder density, and four boulder densities for a constant flow depth. Global, spatial and depth-averaged parameters were used to compare between the different setups. A number of previously defined structures within the flow were identified. The similarity between the different flow depths illustrated the repeatability of the results and indicated that the flow structure does not change with boulder submergence. Increases in boulder density were associated with larger wakes, increased TKE within the boulder layer, and stronger lateral and vertical velocities. Wake volume was seen to increase with both flow depth and boulder density. For increasing boulder density the flow structure changed from an isolated and non-interacting wake structure to a wake-interaction, where the wakes of adjacent boulders were observed to 'overlap'. Linking the hdyraulic results to the ecological results suggested that retention occurs when the shear stress immediately upstream of the boulder neared zero.

6.1 Introduction

Characteristics of the flow around both two-dimensional (e.g. Engel, 1981; Douglas et al., 2001; Best, 2005; Stoesser et al., 2008) and three-dimensional obstacles (e.g. Savory and Toy, 1986; Acarlar and Smith, 1987; Nezu and Nakagawa, 1993; Shamloo et al., 2001) have been investigated over a long time period, with the identification of the presence of a number of structures. The investigation of flow structure around and wake characteristics of isolated large roughness elements (LRE), such as hemispheres, boulders and pebble clusters, has been investigated in laboratory experiments in both air (e.g. Savory and Toy, 1986; Tavakol et al., 2010) and water (e.g. Acarlar and Smith, 1987; Shamloo et al., 2001) and in natural streams (e.g. Buffin-Bélanger and Roy, 1998; Lacey and Roy, 2007; Lacey and Nikora, 2008).

Two structures are found to be common to all obstacles present within the flow; the presences of a standing or 'horseshoe' vortex and stagnation point upstream of the obstacle and the creation of a wake downstream of the obstacle (Savory and Toy, 1986; Acarlar and Smith, 1987; Shamloo et al., 2001). The wake of an obstacle is characterised by decreased streamwise velocities (Tavakol et al., 2010), and higher turbulent kinetic energy (Lacey and Roy, 2007) and shear stresses (Bouckaert and Davis, 1998). A distinct lateral profile of the wake is produced, with greatest velocity deficit seen at the centre of the obstacle (Savory and Toy, 1986) and the lateral edges of the wake are indicated by peaks in the root-mean square of the streamwise velocity, U_{rms}, with the peaks in U_{rms} moving inwards as the wake moves downstream (Tavakol et al., 2010). The vertical expansion of the wake has been linked to the submergence of obstacle (Buffin-Bélanger and Roy, 1998), with an increase in submergence leading to reduced expansion, (Shamloo et al., 2001).

More detailed analysis of two-dimensional (e.g. cylinders and dunes) and three-dimensional (e.g. hemispheres) obstacles using different visualisation techniques, such as dye and hydrogen-bubble-wire visualisation techniques (Acarlar and Smith, 1987) and detailed velocity measurements (Savory and Toy, 1986; Shamloo et al., 2001; Stoesser et al., 2008), has identified the generation of coherent turbulence structures due to the presence of the obstacles. For submerged obstacles separation of object boundary layer occurs near the crest creating separation, or 'arch' vortices and shear layer, due to the Kelvin Helmholtz instabilities, that surround the recirculation zone (Savory and Toy, 1986; Nezu and Nakagawa, 1993; Best, 2005). Deformation of the 'arch' vortices created at the separation point leads to the formation of 'hairpin' vortices which are shed from the reattachment point downstream of the boulder (Acarlar and Smith, 1987; Nezu and Nakagawa, 1993; Stoesser et al., 2008). They are then convected downstream by the mean flow travelling towards the surface creating boils when it is reached (Best, 2005).

Large protrusions, such as cobbles, boulders, and pebble clusters, associated with gravel beds found in streams have an important role in defining the spatial distribution of a number of ecological factors (e.g. Bouckaert and Davis, 1998; Shamloo et al., 2001; Lacey and Nikora, 2008). Boulders, or rock clusters are important habitat features for fish, as the wakes and lower velocities that are created downstream provide cover, resting and feeding opportunities (Shamloo et al., 2001). Particular characteristics of the wake of an obstacle, such as decreased velocities and increased rate of turbulent energy dissipation (Lacey and Roy, 2007; Lacey and Nikora, 2008), have an effect on the exchange of material between organisms and the ecosystem (Hart et al., 1996). High values of turbulent energy dissipation promote particle-particle interaction, increasing nutrient dispersal and predator-prey interactions (Lacey and Nikora, 2008). The wake region also provides a significantly more favourable environment for invertebrates when compared to the region upstream of a boulder, despite no difference in the near-bed velocities at the two locations (Bouckaert and Davis, 1998). However, although isolated boulders or pebble clusters occur in riffle areas they are more likely to be arrays of protrusions from the bed.

The size and intensity of the wake regions is affected by the proximity of protrusions (Buffin-Bélanger and Roy, 1998). Three hydraulically rough situations have been identified: 1) isolated roughness flow, 2) wake-interference flow, and 3) quasi-smooth flow (Chow, 1959). Different methods have been used to describe the wake size created by multiple protrusions, for example Nepf et al. (1997) defined the Wake Fraction (WF), the unit area that is occupied by the wake, whereas Huthoff (2009) defined a wake filling factor f which was the ratio of wake volume to total flow volume. As the density of protrusions increases, then the wakes of adjacent protrusions begin to 'overlap', and therefore interact, (Nepf, 1999; Canovaro and Francalanci, 2008). Nepf (1999) identified a non-linear relationship between increase in Wake Fraction and increase in density. However, Canovaro and Francalanci (2008) identified a semi-linear relationship linking wake volume ratio to surface density, that had a distinct discontinuity at a surface density of about 0.4, corresponding to the maximum flow resistance (Canovaro et al., 2007), and that this is the transition from isolated element behaviour to interfering wakes (Canovaro and Francalanci, 2008).

Previous chapters have shown a variation in the retention of leaves with bed heterogeneity, boulder submergence and boulder density. This chapter presents a series of flume experiments that investigate the effect of the boulders on the velocity and turbulence fields, at four flow depths for the same boulder density and four boulder densities for the same flow depth, using detailed velocity measurements taken over a control volume. The density of the boulders was varied from the boulders acting in isolation to the boulder wakes interacting at higher densities. These experiments identify how the flow structure and wake size changes with both boulder submergence and density.

6.2 Method

These equipments were carried out using the NERC glass walled recirculating flume, the set up and calibration of which was described in Section 3.1, in parallel to those presented in Chapter 5. Idealised concrete boulders placed in a staggered array allowed the characterisation of the velocity and turbulence field within the array at four boulder densities (Sparse, Intermediate, Dense and Very Dense) at a single flow depth and four flow depths (130, 150, 240, and 300mm) at a single density.

6.2.1 Experimental parameters

Idealised concrete boulders (see Section 3.5.3) were created and placed in a staggered configuration directly on the glass bed to mimic boulders within streams. The lateral and longitudinal spacing of the boulders was varied to create four densities; Sparse, Intermediate, Dense and Very Dense, the spacing and arrangement of which is described in Section 3.5.3. The discharge was measured using Controlotron 1020 clamp-on flowmeter, the calibration of which was stated in Section 3.3. The discharge was kept constant for all combinations, a single discharge could not be maintained, instead the discharge was kept within the range of 45.74–45.84 l/s, giving an average discharge of 45.79 l/s which was used to calculate all parameters.

As described in Section 3.1.3, these experiments were carried out under gradually varied flow conditions. The water surface profiles for each flow depth and boulder density combination were measured and presented in Section 3.1.3, (Figures 3.3 and 3.4), with each profile conforming to the M1 profile (Chow, 1959). A best fit line allowed the calculation of a mean depth for each situation. Every effort was made to carry out the experiments at the same flow depths (130mm, 150mm, 240mm, and 300mm), there was variation between the different configurations ($\leq 2.3\%$), but they were compared as if identifical. All experiments, except the flow depth of 130mm (which required a steeper slope 1/300), were carried out with a slope of 1/1000.

Table 6.1 shows the experimental combinations where velocity structures within the boulder array were investigated. As with Chapter 5, for each experiment a number of parameters are presented. The mean flow depth presented is calculated over the working length of the flume (15.35m) for the best fit water surface profile. Two area mean velocities have been calculated using the mean flow depth and the average discharge; the first ($\bar{U}$) ignores any reduction in mean cross-sectional area due to the boulders, the second ($\bar{U}_{Blockage}$) takes into account the presence of the boulders reducing the cross-sectional area. For the Very Dense set up, two $\bar{U}_{Blockage}$ have been calculated, this is due to there only being a section of boulders at this density. The first refers to if the flume was full at this density,

	Mean Flow Depth (m)	Boulder submergence (z_0/h)	Bed Slope	$\bar{U}$ (m/s)	$\bar{U}_{Blockage}$ (m/s)	Boulder Volume Fraction	Re_d
Sparse	0.127	1.671	1:300	0.300	0.306	0.019	47430
	0.149	1.961	1:1000	0.256	0.260	0.016	40300
	0.240	3.158	1:1000	0.159	0.160	0.010	24800
	0.300	3.947	1:1000	0.127	0.128	0.008	19840
Intermediate	0.148	1.947	1:1000	0.256	0.267	0.033	41385
Dense	0.150	1.974	1:1000	0.256	0.266	0.044	41230
Very Dense	0.152	2.000	1:1000	0.256	0.271	0.073	42005
					(0.251)		38905

Table 6.1. Description of the conditions for each experimental setup

the value in brackets is a more realistic value as this allows for just the section of boulders at that density. The Reynolds number (Re_d) has been calculated for each set up using $\bar{U}_{Blockage}$ and the diameter of the boulder as the characteristic length.

6.2.2 Velocity Measurements

In Section 3.5.3 a control volume was defined as the region between two diagonally adjacent boulders, (Figure 3.14). The control volume allows all aspects of the flow around the boulders to be assessed. It includes half of the wake of one boulder, the flow approaching another boulder, and how these two regions interact. Using a control volume therefore allows us to minimise the area over which there is a need to take velocity measures without compromising on characterisation of the velocity structure present. It is assumed that the control volume is typical of the set-up and that the flow is symmetrical. For this to be true the location of the control volume must be within the fully developed boulder flow field.

For each boulder density a control volume was chosen at approximately the same downstream location within the flume, over which an $x-y$ grid of velocity profiles was taken. The relative size and location of the four control volumes for each of the boulder densities are shown in Figure 6.1. For easy comparison the boulder locations within each control volume were kept constant, i.e. 'top-left' referred to as the upstream boulder and 'bottom-right' referred to as the downstream boulder. The longitudinal location of the initial control volume (sparse density) was determined by analysis of velocity profiles over the length of the flume, allowing the region of developed flow to be identified. The exact location of the control volumes for the other densities was affected by boulder arrangement, but kept as near to the original as possible, ensuring a consistent comparison at a location where the flow is fully developed. Each of the control volumes is located along the centreline of the flume (width=600mm), and extends towards the far wall of the flume

	Boulder Area Density	Location x (mm)	Location y (mm)	Control Volume Area (m^2)	No. of Velocity Profiles
Sparse	0.047	8600–9100	600–960	0.180	43
Intermediate	0.097	8900–9300	600–820	0.088	44
Dense	0.130	8600–8900	600–780	0.054	44
Very Dense	0.218	8850–9100	600–750	0.0375	36

Table 6.2. Size and location of the control volumes for each density and the number of velocity profiles taken at each density.

(designated width of 1200mm). The longitudinal and lateral size of the control volume was equal to longitudinal and lateral spacing of the tested density. The properties of each control volume can be seen in Table 6.2.

The velocity measurements were taken using a downward looking Nortek ADV Vectrino. All measurements were taken at 200Hz for 90 seconds using a transmit length of 1.8mm and a nominal SVH of 2.5mm resulting in an actual SVH of 8mm, giving a minimum measurement height of 4mm above a boundary. The use and calibration of this ADV has been discussed in Section 3.2. The vertical resolution of measurements varied between 2 and 10mm. Measurements were concentrated in the region of greatest velocity gradients, such as near the bed and the region surrounding the top of the boulders. The same velocity profiles were used for all control volumes, however the top measurement point varied with flow depth. For the flow depths of 240 and 300, measurements were not made above a height of 154mm as after this point the velocity profile remained constant with change in height. For each density the distance sensor on the Vectrino was used to gain a zero distance for the measurements. The velocity data was processed using Matlab as stated in Section 3.2.4. Time-averaged velocities in all three dimensions (u,v and w) were calculated at each of the measurement locations within the control volume.

To test for developed flow conditions to locate the initial control volume, four velocity profiles were taken, each 1m apart, starting at a length of 6850mm, and ending at a length of 9850mm, at the midline of the flume, (width=600mm). These locations represent the centre point between four adjacent boulders. The comparison of these profiles allowed the control volume to chosen and confirmed that that flow at this control volume was typical of the set up. For the Very Dense boulder density it was again necessary to check where there was developed flow due to there only being a section of boulders. For this single point velocity measurements were taken at a height of 120mm along the lateral centre of the flume every 500mm in length from 4850mm to 12350mm. These measurements were taken at 200Hz for a 2 minute sampling period, and for each length a time-average streamwise velocity ($\bar{u}$) was calculated and compared. The consistency in these measurements confirmed that developed flow was present at the location of the measurement grid.

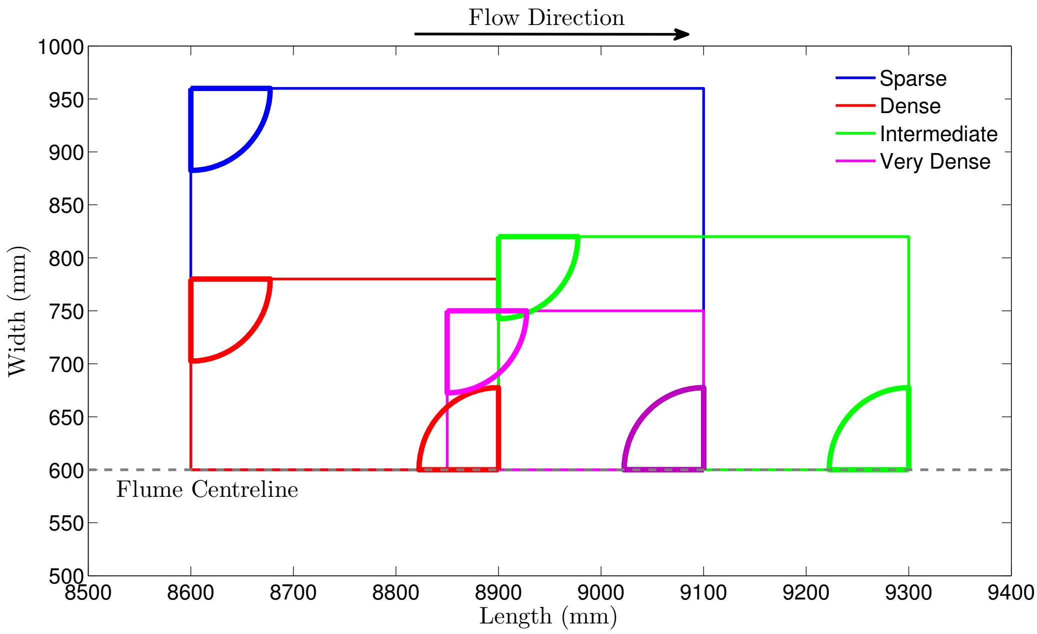

Figure 6.1. Diagram showing the relative size and location of the control volumes for the four different boulder densities. Quarter circles represent size and location of boulders for each control volume. Note that the full width of the flume is 1200mm

The experiment was designed to examine a range of boulder densities, varying from a density whereby each boulder wake acted in isolation from its neighbour to boulder densities where the boulder wake structures interact and overlap with the wakes of neighbouring boulders. It was therefore necessary to ensure that for the sparse density the boulders were acting in isolation and independently. To test this, all the boulders upstream of the control volume were removed, leaving the boulder involved in the control volume. The downstream boulders were left in place (see Figure 6.2). The $x-y$ grid of velocity profiles was repeated as before so that the results could be directly compared. This was carried out at the minimum flow depth of 130mm and the maximum flow depth of 300mm.

6.2.3 Data Analysis

A number of parameters were calculated to allow direct comparison between the experiments carried out at the different flow depths and boulder densities. Depth-averaged (denoted by a z subscript e.g. $\bar{U}_z$) and spatially-averaged (denoted by angled brackets e.g. $<\bar{U}>$) parameters were calculated by applying a weighting to each measurement, therefore creating a mean value over either the depth or horizontal plane of measurements:

$$\bar{u} = \sum_{i=1}^{n} w_i u_i \tag{6.1}$$

where the weightings are normalised so that they sum to one. The standard deviation for these measurements were calculated in the following manner:

$$\bar{s}_{weighted} = \sqrt{\sum_{i=1}^{n} w_i(u_i - \bar{u})^2} \tag{6.2}$$

again the weightings were normalised so that they summed to one. The weightings for both depth and the horizontal plane were created by assuming the boundaries of the areas to be halfway between two adjacent points, resulting in the measurement points being located approximately at the centre of the area they represent, e.g.

$$w_i = \frac{0.5(x_{i+1} - x_{i-1})}{x_n} \tag{6.3}$$

For the creation of all spatially averaged parameters, only real data was used to minimise any error in the measurement created through interpolation. As well as the calculation of depth and spatially averaged variables, global-averaged variables were also calculated, denoted by the subscript xyz e.g. $\bar{U}_{xyz}$. This was done by applying both the vertical and spatial weighting to the parameter, and summing, as the weightings were normalised. Calculating the standard deviation of each of these spatially averaged mean will allow the variation in the mean over the control volume to be quantified, and therefore gives an indication of the form-induced stress.

Two turbulence parameters were used to quantify the formation and development of turbulence within the control volume, and in particular in the downstream wake of each boulder. These included the root-mean-square of the velocity components, which are referred to as turbulence intensities, for the longitudinal direction, defined as;

$$U_{rms} = \sqrt{\overline{u'^2}} \tag{6.4}$$

and the turbulent kinetic energy (TKE) defined as;

$$TKE = (\overline{u'^2} + \overline{v'^2} + \overline{w'^2})/2 \tag{6.5}$$

where u', v' and w' refer to the fluctuating components of the velocity in the longitudinal, lateral and vertical direction respectively (as shown in Equation 2.11).

The turbulence characteristics near the bed were also used to evaluate the flow structure around the boulders. Two methods were used to calculate point specific values (Biron et al., 2004) of the shear stress using the velocity measurements taken at 4mm from the bed. The first method assumes that the viscous stresses are negligible compared to the turbulent stresses in fully developed flow and therefore the Reynolds stress in the near-bed

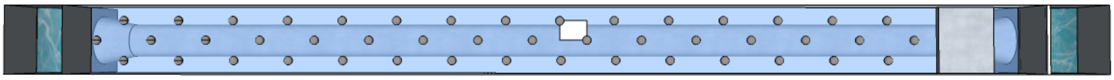

(a)

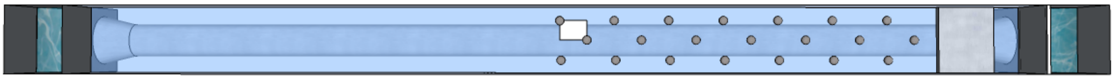

(b)

Figure 6.2. Perspective diagram illustrating the removal of upstream boulders to test for interaction, (a) with upstream boulders in place and (b) upstream boulders removed.

region can be used to estimate the bed shear stress;

$$\tau = -\rho \overline{u'w'} \tag{6.6}$$

where ρ is the density of water. The second method used is based on the turbulent kinetic energy, so therefore considers the lateral fluctuations in the time-averaged velocities as well as the longitudinal and vertical (Biron et al., 2004), where:

$$\tau = C_1[0.5\rho(\overline{u'^2} + \overline{v'^2} + \overline{w'^2})] \tag{6.7}$$

where C_1 is a proportionality constant, which has been found to be 0.19 (Kim et al., 2000).

The irregular nature of the velocity profile locations required interpolation to be carried out in order to produce contour plots from the three dimensional measurement grid. The measured data was placed into a evenly spaced grid and a two-dimensional thin-plate spline interpolation was applied in the $x - y$ plane, at each height. A coarsely spaced regular grid was used to minimise the presence of interpolated data within the contour plots. The location of real data points are marked on all contour plots to minimise any errors being generated in the reading of the plots. Also care was taken to minimise the presence of artefacts from the interpolation within the presented data.

6.3 Results and Discussion

6.3.1 Flow structures around boulders

In order to describe how the flow structures around boulders change with both boulder submergence and boulder density, first the general structures and patterns observed in the flow must be described. As discussed in the Introduction (Section 6.1), a number of common coherent structures have been reported by researchers in this field, and this section will aim to identify these structures from the patterns present within the velocity profiles. This will then allow differences and changes to these structures as functions of boulder submergence and boulder density to be identified.

It is assumed at present that the boulders at the sparse density are acting independently, however this assumption will be tested and discussed in Section 6.3.2. Therefore this density will be treated as the null hypothesis, with all other densities being compared to it. The experiments for the four boulder densities were all carried out at a flow depth of 150mm, and so this flow depth will be used along with the sparse density for comparisons. Therefore, this section will examine the flow structures present at the sparse density with a flow depth of 150mm.

Figure 6.3(a) shows a longitudinal slice of velocities, at the cross-streamwise centreline of the boulder. This figure has been created by joining two planes within the control volume, first the longitudinal $(x - z)$ plane at $y/D = 0$, where the flow approaching the downstream boulder was characterised, and the longitudinal $(x - z)$ plane at $y/D = 2.32$, where the flow behind the upstream boulder is characterised. Joining these two planes creates duplicated data at the longitudinal centreline of the boulder; the mean of the values from the two planes at each height was used. The velocities have been normalised to the globally-averaged streamwise velocity, U_{xyz}, for the sparse density and flow depth of 150mm. The use of the globally-averaged velocity, and not the area mean velocity, is discussed in Section 6.3.3. Vectors composed of the streamwise (u) and vertical (w) velocities were generated to help illustrate the movement of the water over the boulder.

A number of regions within Figure 6.3(a) can be identified; (1) a boundary layer and reduced streamwise velocity region immediately upstream of the boulder, (2) a region of negative velocities immediately downstream of the boulder, (3) a region of reduced streamwise velocities extending downstream from the boulder within the boulder flow layer, (4) a region of reduced streamwise velocities extending from the crest of the boulder, and (5) two regions, one upstream and one downstream of the boulder, of negative and reduced streamwise velocities at the top of the control volume.

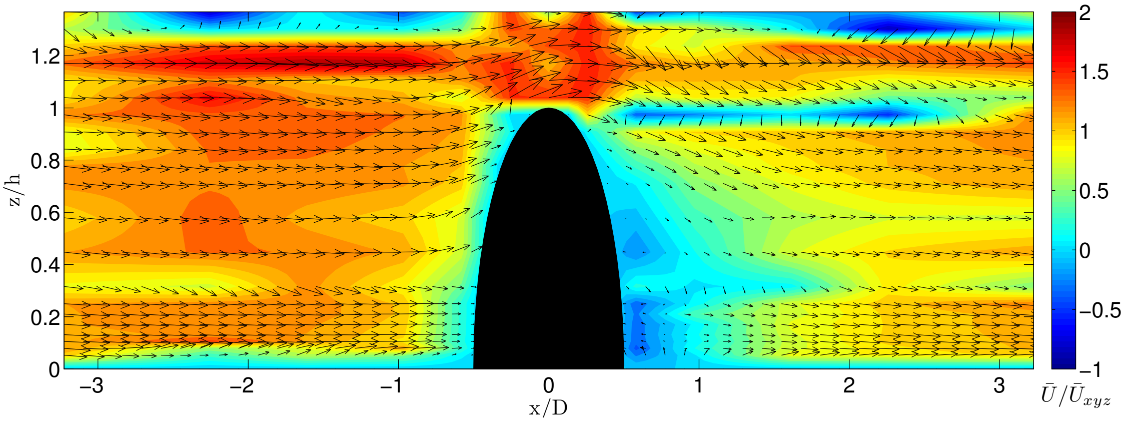

(a)

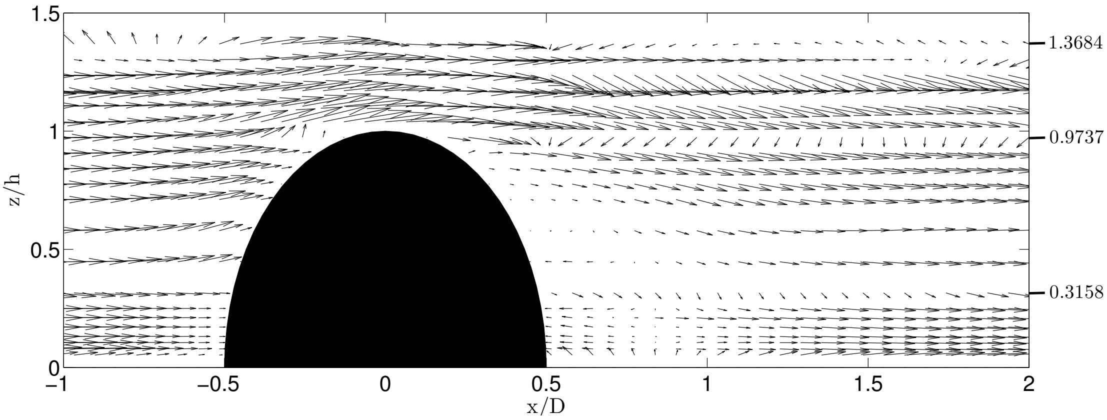

(b)

Figure 6.3. Longitudinal $(x - z)$ plots at the sparse density for a flow depth of 150mm. (a) Contour plot of streamwise velocities (u) with $u - w$ vectors overlayed, and (b) $u - w$ vector plot showing the recirculation zone in more detail. Streamwise velocities are normalised to the globally-averaged streamwise velocity for the sparse density at 150mm flow depth. Vectors represent relative not absolute velocities.

The boundary layer upstream of the boulder can be clearly seen in the velocity contours, covering a relative height of less than 0.1. The presence of vertical velocities within this boundary indicates the presence of the rolling boundary layer vortices, the concentration of which form the standing or horseshoe vortex that has been found to be immediately upstream of an obstacle in the flow (Acarlar and Smith, 1987; Savory and Toy, 1986; Nezu and Nakagawa, 1993). The horseshoe vortex is not visible from the velocity vectors. However, there is a region of reduced velocities immediately upstream of the boulder, which will be referred to as the dead-zone. It is proposed that this region might be important in describing the retention of leaves discussed in Chapter 5. The dead-zone extends the full height of the boulder, however it is more pronounced below the relative height of 0.4

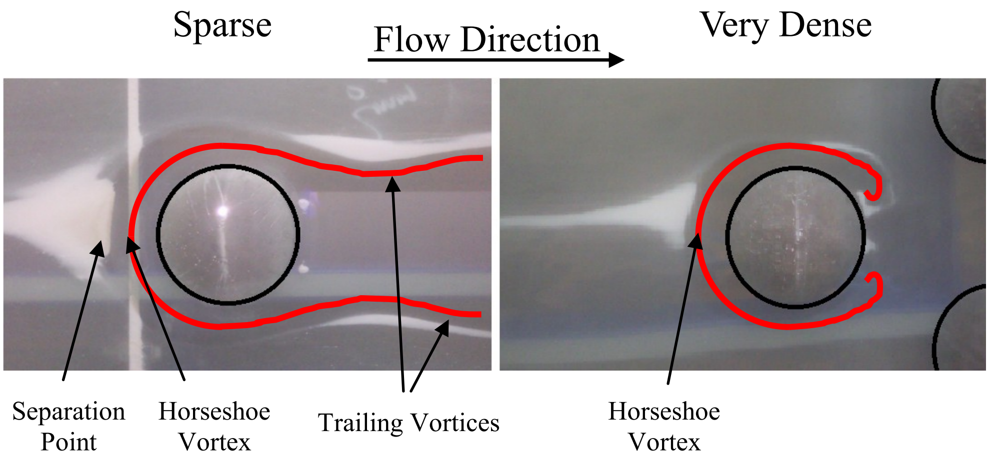

Figure 6.4. Photographs showing the deposition patterns of seeding material around a boulder on the flume bed at the sparse and very dense density arrangements. The footprints of the boulders are indicated.

where it extends further upstream (x/D=0.75). This region may represent the presence of the horseshoe vortex.

Throughout the experiments photographs were taken of interesting patterns that were observed. It was possible to use the spherical seeding material as a visualisation method, where the pattern of settling of this material on the bed allowed visualisation of characteristics of the flow. Figure 6.4 shows the pattern of seeding material deposition for the sparse and very dense density, shown by the white material on the grey flume bed. A clear ring where no deposition has occurred is clearly visible surrounding the boulder in both cases. At the sparse density there is a much larger deposition area in front of the separation point, and lines can be seen downstream of the boulder. These lines may indicate the presence of the trailing vortices that occur due to the curving of the horseshoe vortex around the front of the boulder. These are not present at the very dense density, however there is greater deposition at two locations directly behind the boulder suggesting at this density the trailing vortices are not present but instead the greater density of boulders forces the flow in behind the boulder, creating greater recirculation.

The pattern observed in Figure 6.4, in particular at the sparse density, very closely resembles the dye visualisation observed by Shamloo et al. (2001)(Fig. 1(b)) that indicated the presence of a horseshoe vortex, and therefore it will be assumed that a horseshoe vortex is present immediately upstream of the boulder. The high shear stress that is created by the horseshoe vortex on the bed creates the clear region of dye as seen in Figure 6.4 and by Shamloo et al. (2001)(Fig. 1(b)). However the clear region is often greater in size than the size of the horseshoe vortex due to the oscillation of the vortex (Shamloo et al., 2001). The width of the clear region in Figure 6.4 coincides with the width of the reduced velocity area in Figure 6.3(a). The height of this region being associated with the horseshoe vortex (z/h=0.4) again coincides with the measured height of the standing vortex by other researchers (Acarlar and Smith, 1987).

The upper portion of the dead-zone will correspond to the stagnation point that is located on the upstream side of boulders. This occurs due to the flow being forced up and over the boulder, as is shown in Figures 6.3(a) and 6.3(b). A boundary layer forms on the upstream face of the boulder, with significantly reduced velocities present adjacent to the boulder. The presence of this dead-zone could aid the retention of leaves on to the upstream face of the boulders, with the size of the region affecting the number of leaves that could be retained. This will be investigated in Chapter 6.4.

The region of reduced velocities downstream of the boulder is referred to as the wake. Different definitions of the wake region have been used in the literature; Zavistoski (1994) and Nepf et al. (1997) defined the edge of the wake as where the level of turbulence, described by the turbulence intensity (U_{rms}), was within 10% of the free stream value. Here we are considering the time-averaged velocities, not the turbulent fluctuations from the time-averaged value, and therefore will adjust this definition to apply to the velocities, defining the wake region as the region where streamwise velocities are equal to or less than 90% of the free stream velocity. The wake appears to extend $1.5D$ downstream of the boulder, however at a relative height (z/h) of 0.6 the wake extends much further downstream (Figure 6.3(a)). A detached region of wake is also present at a relative height of 0.3. This may indicate the presence of vortex shedding from the wake, as the Reynolds number (see Table 6.1) is above the threshold for vortex shedding that was observed for cylinders (Douglas et al., 2001).

Within the wake is the recirculation zone characterised by negative velocities. For this set-up, this zone is divided into two recirculation regions, a lower ($0 \approx 0.3z/h$) and upper ($0.4 \approx 0.7z/h$) region (Figure 6.3(a)). The sizes of these regions are small, with a reattachment length of approximately $0.4D$, in comparison to the observations of other researchers, for example Engel (1981) who reported a reattachment length of $4h$ for two-dimensional dunes. Analysis of a more detailed plot of the vectors in this region (Figure 6.3(b)), suggests that both vortices are rotating clockwise, circulating towards the boulder.

The region of negative and reduced streamwise velocities downstream of the crest of the boulder could be caused by a number of mechanisms; the separation of the shear layer with vortices being shed from the top of the boulder (Best, 2005), the rotation of the

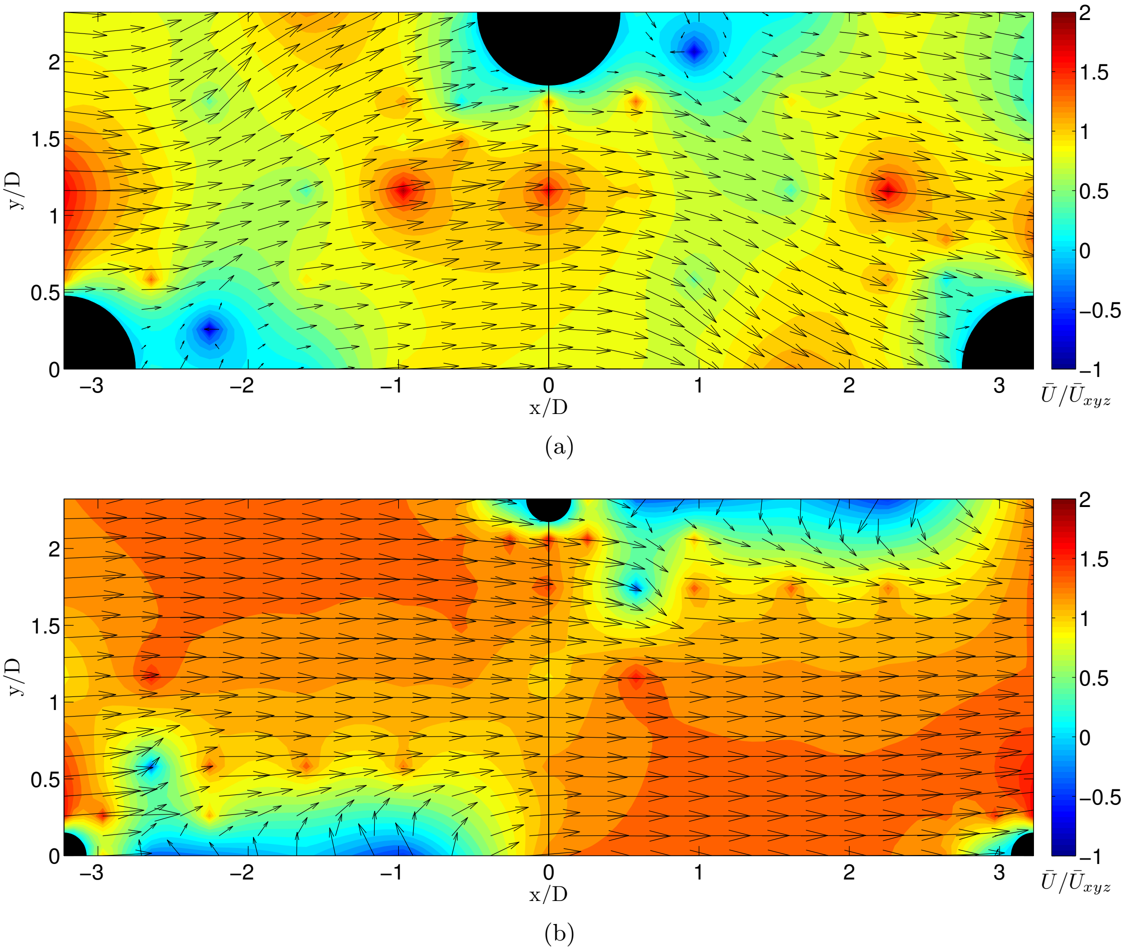

Figure 6.5. Plan view $(x-y)$ contour plots of the streamwise velocities and $u-v$ vectors at the relative heights (z/h) of (a) 0.3158 and (b) 0.9737 for the sparse density at the flow depth of 150mm. Note the boulders are different sizes due to the different heights of the plots.

arch vortex towards the bed (Savory and Toy, 1986), or the head of a hairpin vortex, as illustrated by Acarlar and Smith (1987, Fig. 7). Figure 6.5(b) shows a plan view $(x-y)$, using mirrored data, of the streamwise velocities and $u-v$ vectors at a relative height of 0.9737 within the control volume. Comparing this to Figure 6.5(a), which shows a plan view at the relative height of 0.3158 where the wake plan area is greatest, illustrates that the free shear layer at the top of the boulder is much greater in area than the wake. Figure 6.5(b) confirms that this region is associated with the crest of the boulder, as the region does not extend laterally into the flow between the boulders. As with the recirculation zone, this region consists of two vortices, rather than one large eddy. The location of this region suggests that it is a free shear layer, consisting of separation vortices formed from the crest of the boulder due to Kelvin-Helmholtz instabilities along the shear layer (Best, 2005; Stoesser et al., 2008).

The last area of interest identified within the flow was the presence of two negative and reduced streamwise velocity regions focused around a relative height of 1.3 (Figure 6.3(a)). These two regions, one upstream of the boulder and the other downstream of the boulder are separated from one another due to the high streamwise velocities found over the crest of the boulder. Figure 6.6 shows three plan views ($x - y$) of the streamwise velocities and the $u - v$ vectors at the relative heights of 1.2368, 1.3026 and 1.3684, the heights at which this region is present (Figure 6.3(a)). Unlike with the free shear layer, Figures 6.6(b) and 6.6(c) illustrate the dominance of these flow mechanisms, with low velocities extending over the majority of the control volume only with the exception of the areas directly over the boulders, where high velocity fluid is present.

At a relative height of 1.2368 the streamwise velocities are dominant, however there are cross-streamwise velocities present, with the flow meandering between the boulder, even though the boulders are not creating blockages at this height. The cross-streamwise velocities are in the same order of magnitude as the streamwise velocities at some locations. The region of interest is shown clearly in Figures 6.6(b) and 6.6(c). The vectors show that the streamwise velocities are small in comparison to the cross-streamwise velocities in the areas between longitudinally adjacent boulders, but the streamwise velocities are dominant in the regions between laterally adjacent boulders. However, the flow at a relative height of 1.3026 is flowing in the opposite cross-streamwise direction to the flow at a relative height of 1.3684. This suggests that vortices are present between these heights, as these regions are also associated with both positive and negative vertical velocities as was shown in Figure 6.3(a).

Figure 6.7 shows the TKE for an $x - z$ plane corresponding to that presenting the streamwise velocities in Figure 6.3(a). Increased TKE is associated with the upstream boundary layer, the downstream wake and the free-shear layer. However, the greatest TKE is associated with the vortices downstream of the boulder at the relative height (z/h) of 1.2-1.3. In this region there are both high and low streamwise velocities, implying steep velocity gradients and therefore high values of TKE (Figure 6.3(a)). This effect is not seen in relation to the region upstream of the boulder, with turbulence here in the same order as that seen in the wake (z/h = 0.3). This difference could be due to negative vertical velocities present in the downstream region that are not present in the upstream region.

The strong cross-streamwise velocities and their counter-rotating nature suggest that the eddys shown in Figures 6.3(a) and 6.6 are secondary currents present within the surface flow layer. However, reported values of cross-streamwise velocities within these structures are in the region of 2-3% of the maximum streamwise velocity (Nezu and Nakagawa, 1993), whereas maximum cross-streamwise velocities presented here are in the same order

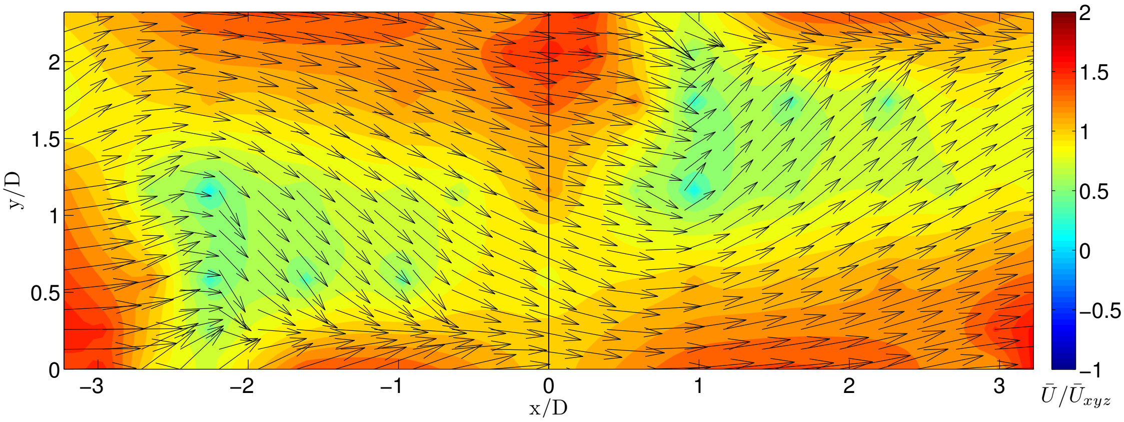

(a)

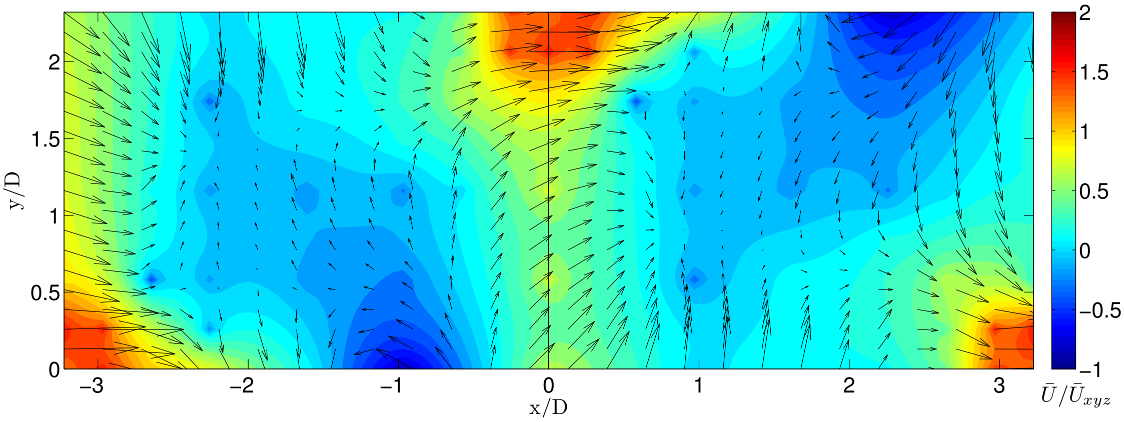

(b)

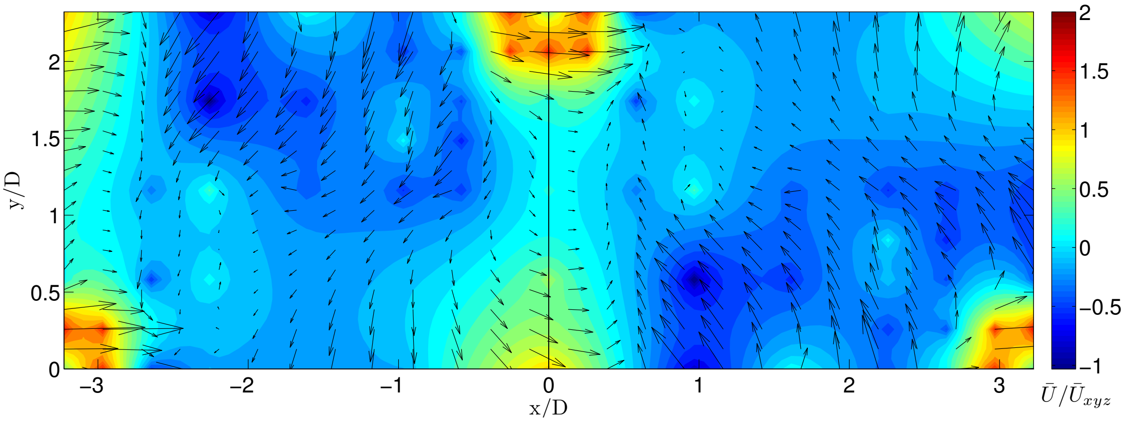

(c)

Figure 6.6. Plan view $(x-y)$ contour plots of the streamwise velocities and $u-v$ vectors at the relative heights (z/h) of (a) 1.2368 (b) 1.3026 and (c) 1.3684 for the sparse density at the flow depth of 150mm

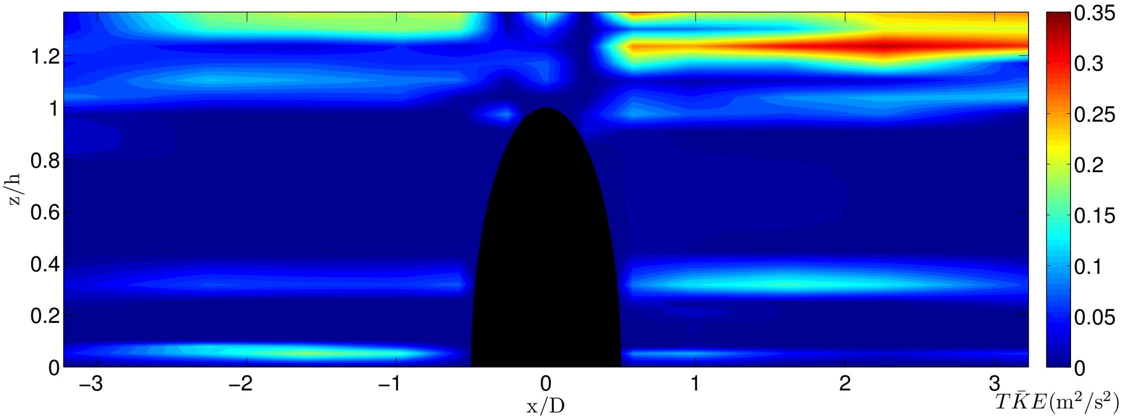

Figure 6.7. Longitudinal ($x - z$) contour plot of Turbulent Kinetic Energy (TKE) at the sparse density for a flow depth of 150mm.

as maximum streamwise velocities in this region, with the mean cross-stream velocities being approximately 20% of the streamwise. In straight channels, secondary currents are seen to extend in the longitudinal direction, creating longitudinal ridges in a mobile bed (Nezu and Nakagawa, 1993). However as the boulders are placed in a staggered array, it could be suggested that the presence of the next downstream boulder diagonally could create a discontinuity within the secondary current, leading to the creation of a new secondary cell, rotating in the opposite direction due to the location of the next boulder. The survey by Best (2005) found that secondary currents were associated with the crest line of three-dimensional dunes, and that these coherent structures are responsible for the majority of momentum flux within the system. This supports these results where the greatest TKE is associated with these secondary currents, and therefore the greatest energy dissipation. Figure 6.8 suggests a schematic model of these structures and their location within the flow depth.

This section has aimed to identify the structures within the flow around an array of boulders, at the sparse density for a flow depth of 150mm, and this set-up will be used as the comparison for the other flow depths and boulder densities within later sections of this chapter. The structures that have been identified has been summarised in Figure 6.9. This figure has been divided into three velocity regions; recirculation zones where $\bar{U}/\bar{U}_{xyz} < 0$, wake regions where $0 < \bar{U}/\bar{U}_{xyz} < 0.9$, and free flow regions where $\bar{U}/\bar{U}_{xyz} > 0.9$. Confirmation of these identified structures would require more detailed flow visualisation in future experiments. However, the definitions used to identify these regions, and the structures defined will be used throughout the chapter to help describe how the flow patterns change with both boulder submergence and density.

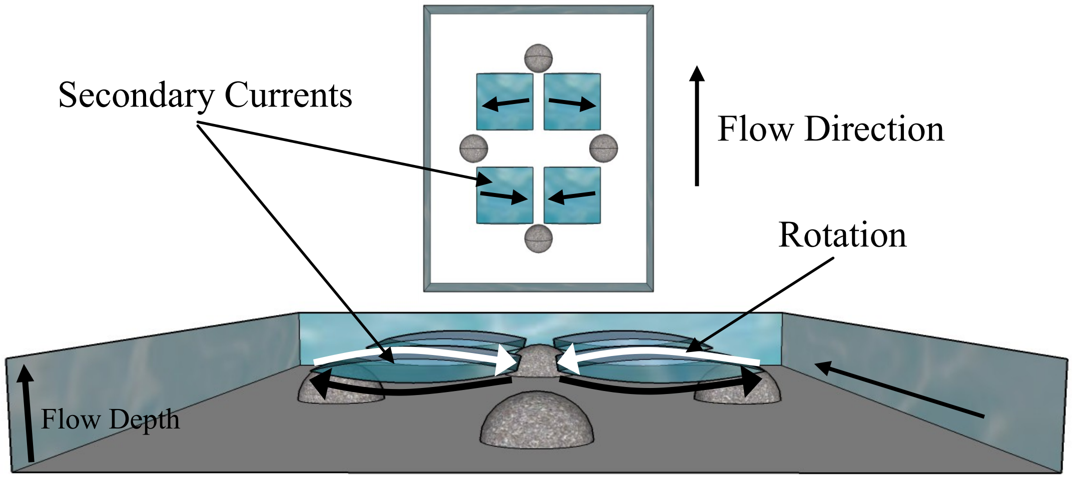

Figure 6.8. Schematic of the suggested location of secondary currents within the surface flow layer.

6.3.2 Boulder Flow Interaction

Evaluation of whether the boulders were acting independently in the sparse density was achieved by comparing the velocity measurements from the sparse density to velocity measurements when the boulders immediately upstream of the control volume were removed (referred to as Int in Tables). The comparison was carried out using three approaches: comparing globally-averaged parameters (denoted by the subscript xyz), spatially-averaged profiles (denoted by $<>$) and depth-averaged profiles (denoted by the subscript z), calculated from the 43 velocity profiles that were taken over the measurement grid.

Table 6.3 shows the globally-averaged mean streamwise velocity, turbulent kinetic energy (TKE) and the streamwise turbulence intensity. A comparison was carried out at the minimum and maximum flow depths used within these experiments, 130mm and 300mm respectively. Small differences were seen between the presence and absence of upstream boulders in the volume-average streamwise velocities, +3.6% and -7.3% with the presence of upstream boulders for the flow depths of 130mm and 300mm respectively. Both these differences are small in comparison to the standard deviation, which represents the spatial variation over the control volume, and are well within the 95% confidence interval. The standard deviation of the streamwise velocity in the presence of upstream boulders was ≈25% greater for a flow depth of 300mm, suggesting the presence of the upstream boulders creates more variation in the velocities over the control volume than was seen in the absence of the upstream boulders, but this effect was not observed at the 130mm flow depth.

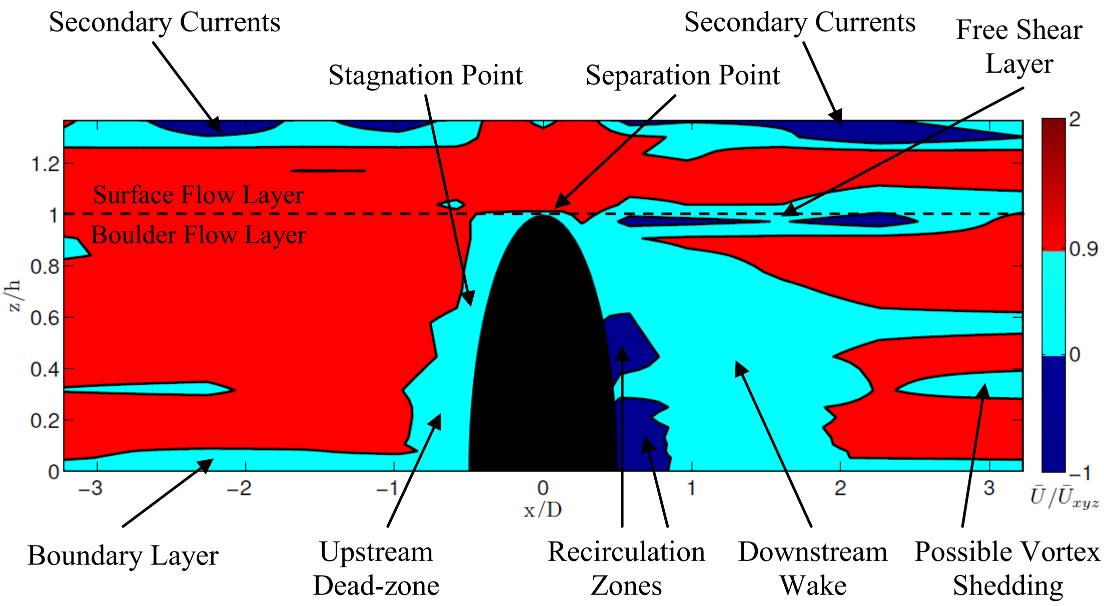

Figure 6.9. Schematic longitudinal $(x - z)$ plane contour plot illustrating the presence of the different identified regions within the flow.

The globally-averaged TKE measurements showed increases in the TKE with the presence of the upstream boulders, +8.9% and 12.5% for the flow depth of 130mm and 300mm respectively. The presence of the upstream boulders allows full development of the turbulent boundary layer, which might have been affected by the removal of the upstream boulders, therefore reducing the globally-averaged TKE in the absence of the upstream boulders. This increase in turbulence associated with the presence of the upstream boulders is also illustrated by the higher values of $\bar{U}rms$ seen in the sparse density, 8.9% and 11.8% respectively. These show good agreement with the TKE increases in the presence of upstream boulder.

Figure 6.10 shows a comparison for each flow depth of the spatially-averaged streamwise velocity against height, and the spatially averaged TKE against height, with error bars showing the 95% confidence interval. For the spatially-averaged streamwise velocities there is better agreement between the velocity measurements associated with the presence and absence of upstream boulders at a flow depth of 300mm compared to 130mm. For a flow depth of 130mm, the presence of the upstream boulders leads to increased velocities over the relative height range of 0.1 to 0.9, which could be due to the blockage effect of the extra boulders, however this is not seen at a flow depth of 300mm as there is a greater depth over which to spread the effect of the blockage. For a flow depth of 300mm, there is variation in the profile above the boulder height (z/h=1), until a constant velocity is reached at a relative height of 1.5. The variation in the two profiles is associated with a positive peak at about z/h=1.3 and a negative peak at about z/h=1.4. At both of these

	Upstream Boulders	$\bar{U}_{xyz}$ (m/s)	TKE_{xyz} (m^2/s^2)	$\bar{U}rms_{xyz}$ (m/s)
Int130	No	0.2289 (0.0477)	0.0153 (0.0188)	0.1045 (0.0721)
Sp130	Yes	0.2374 (0.0494)	0.0168 (0.0183)	0.1148 (0.0743)
Int300	No	0.0783 (0.0497)	0.0349 (0.0596)	0.1130 (0.1207)
Sp300	Yes	0.0730 (0.0634)	0.0399 (0.0657)	0.1281 (0.1322)

Table 6.3. Globally-averaged parameters comparing the presence (Sp) and absence (Int) of upstream boulders for two flow depths. Brackets indicate the standard deviation of the spatial variation of the point measurements within the control volume.

locations the presence of upstream boulders seems to have increased the peak values. This could be due to the increased turbulence that was indicated by the increased volume averaged turbulence intensity ($\bar{U}rms$) and the TKE.

At a flow depth of 130mm the size of the confidence intervals are fairly constant over the profile with little variation between the presence and absence of upstream boulders. At the flow depth of 300mm the standard deviation was smaller below the boulder height than above, showing there is greater spatial variation above the boulder height. Again there was consistency in the size of the confidence intervals with the presence and absence of upstream boulders. Much better agreement can be seen in the TKE profiles for both flow depths. At 130mm there is deviation at the very top of the profile ($z/h \approx$1.1) with higher turbulence associated with the absence of the upstream boulders. The standard deviation, indicated by the error bars, varies throughout the profile, increasing in size with increased TKE, but is comparable in magnitude between the two conditions. The significance of the artefacts seen within the profiles will be discussed later in this section. There is good of similarity between the TKE profiles at 130 and 300mm up to the relative height of 1.1.

Figure 6.11 shows plan view ($x - y$) contour plots of the depth-averaged streamwise velocities comparing between the presence of the upstream boulders, and the absence of the upstream boulders, again for both flow depths. As the discharge was kept constant for all flow depths and boulder densities, the velocities for the 300mm flow depth are much lower than for the shallower depth. There is good agreement in the spatial distribution of velocities for a flow depth of 130mm, with the main difference being the reduced size of the lower velocity region on the stoss side of the boulder, in the presence of upstream boulders. For the flow depth of 300mm, there is a visual difference between the two contour plots. The presence of upstream boulders increased the wake size downstream, as well as resulting in the wake travelling laterally towards the downstream boulder. This is not present in the absence of the upstream boulders, instead with an area of increased velocities present to the side of the downstream boulder. The predominant streamwise velocity u is approximately 12% lower in the presence of the upstream boulders, however

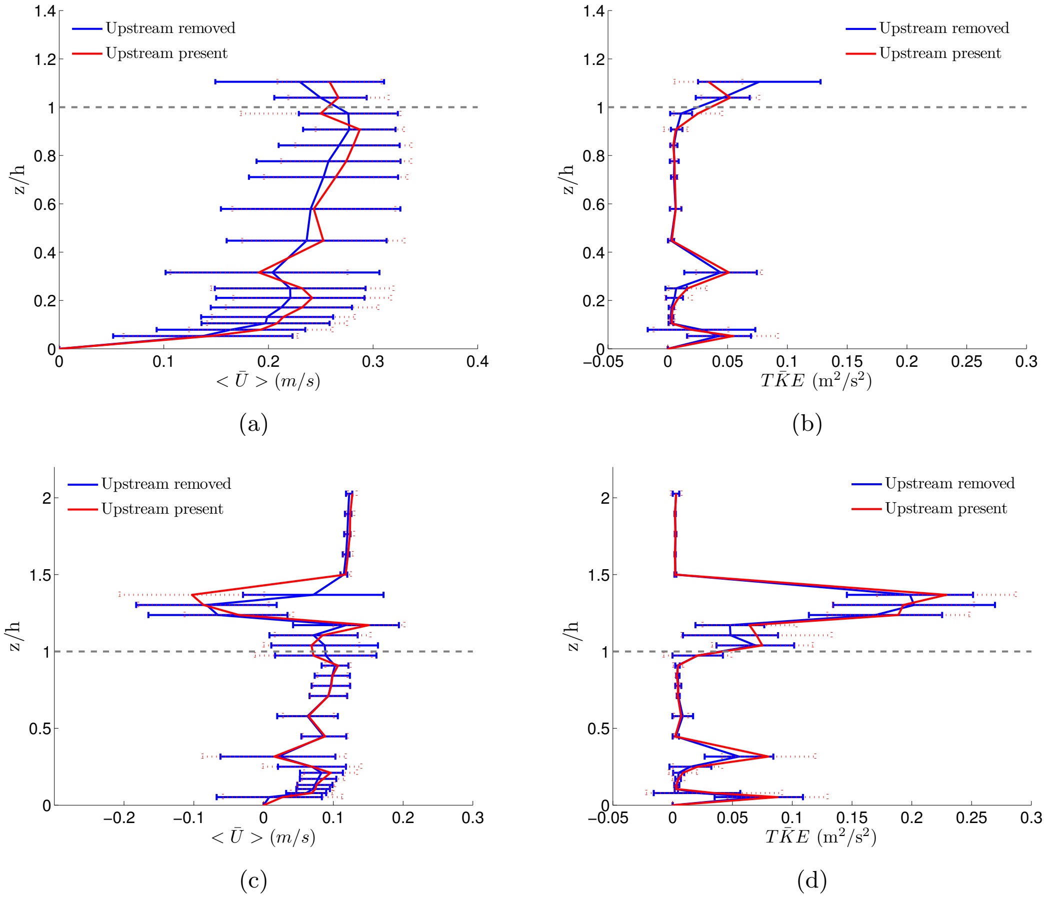

Figure 6.10. Comparison of the spatially-averaged streamwise velocity and TKE with height in the presence of upstream boulders and absence, at the sparse density for flow depths of (a,b) 130 and (c,d) 300mm. The errors bars indicate the 95% confidence interval, solid blue where upstream boulders are removed and dotted red where upstream boulders are present.

the volume-average streamwise velocity suggested a difference of 7.3%.

Three measures (volume, depth and spatially averaged velocities) have been used to evaluate the effect of removing the upstream boulders and therefore establish whether the boulders within the sparse density are acting independently and that no wake inference is occurring. Although a difference was seen in the structure of the depth-averaged velocities for the flow depth of 300mm, at 130mm there was very little difference, and there was good agreement between the spatially averaged profiles and the globally-averaged variables for both flow depths. No visual interaction between the wake and the downstream boulder was observed. Therefore it can be assumed that at the sparse density the boulders are acting independently as an array of isolated boulders.

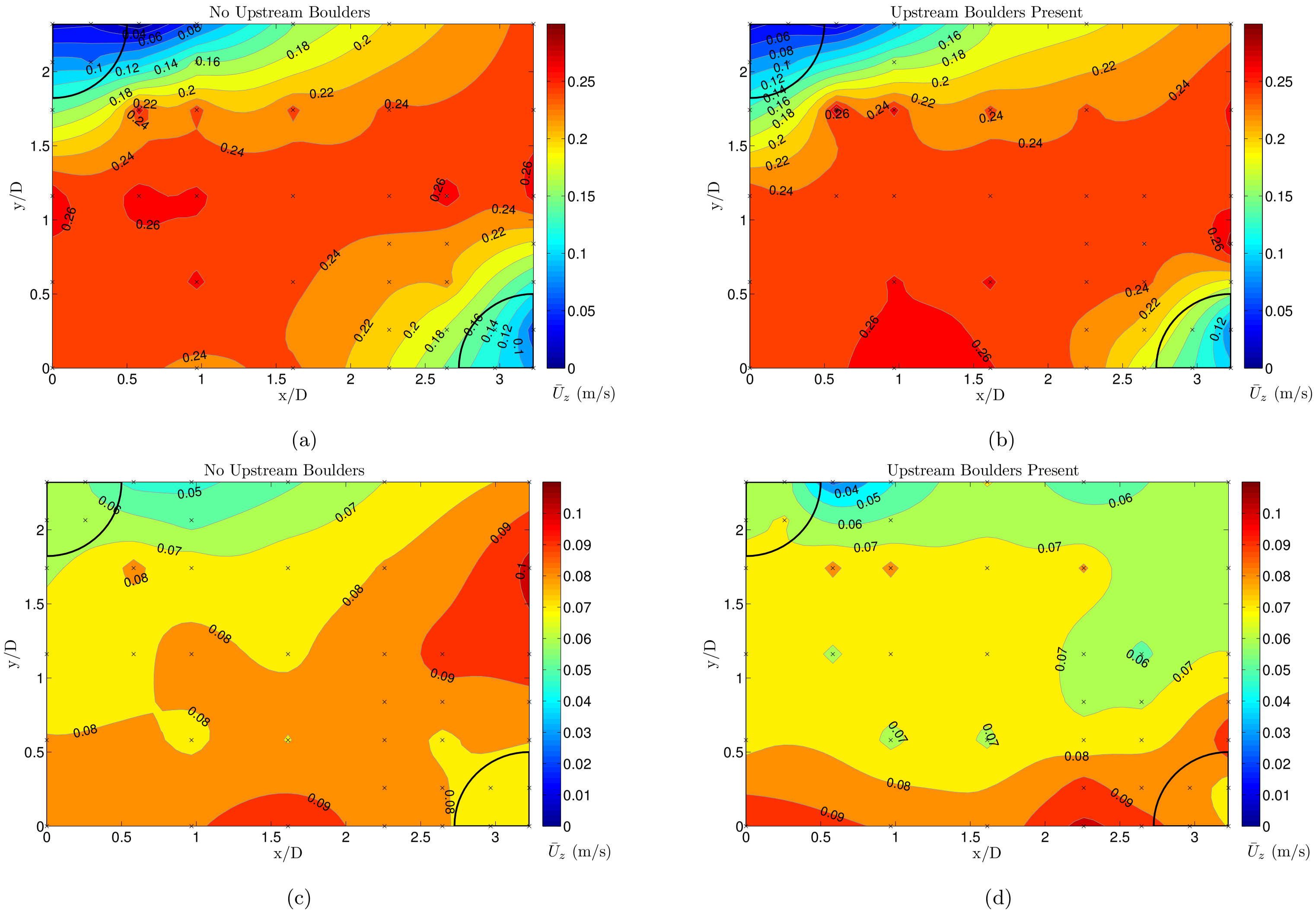

Figure 6.11. Plan view $(x - y)$ contour plot of depth-averaged streamwise velocities for sparse density at the flow depths of (a,b) 130 and (c,d) 300mm. The presence and absence of upstream boulders is indicated on each plot.(Flow is from left to right)

Flow Depth (mm)	y/h	$\bar{U}_{xyz}$ (m/s)	$\bar{U}_{BL}$ (m/s)	TKE_{xyz} (m^2/s^2)
130	1.711	0.2374 (0.0494)	0.2347 (0.0512)	0.0168 (0.0183)
150	1.974	0.1912 (0.0627)	0.1997 (0.0446)	0.0455 (0.0532)
240	3.158	0.1181 (0.0514)	0.1092 (0.0341)	0.0312 (0.0541)
300	3.947	0.0730 (0.0634)	0.0730 (0.0286)	0.0399 (0.0657)

Flow Depth (mm)	$\bar{U}rms_{xyz}$ (m/s)	$\bar{V}rms_{xyz}$ (m/s)	$\bar{W}rms_{xyz}$ (m/s)
130	0.1148 (0.0743)	0.0840 (0.0446)	0.0293 (0.0087)
150	0.1776 (0.1207)	0.1404 (0.1118)	0.0386 (0.0229)
240	0.1202 (0.1166)	0.1158 (0.1145)	0.0271 (0.0203)
300	0.1281 (0.1322)	0.1376 (0.1388)	0.0301 (0.0282)

Table 6.4. Globally-averaged parameters for each flow depth at the sparse density, with standard deviations in brackets.

6.3.3 Effects of Boulder Submergence

The effect of boulder submergence (flow depth divided by the boulder height) on the flow structure around a regularly spaced array of boulders was analysed at four flow depths for the sparse density. Table 6.4 compares the globally-averaged parameters at the different flow depths for the sparse density. Two globally-averaged streamwise velocities were calculated, one over the whole profile height, denoted by the subscript xyz, and a second that is globally-averaged over the boulder height ($z/h \leq 1$) and not the over the whole profile, denoted by the subscript BL. It should be noted that due to the use of a downward looking probe velocity measurements were take to maximum heights of 84, 104, 154 and 154mm for the flow depths 130, 150, 240 and 300mm respectively.

As the discharge remained constant for all experiments, the globally-averaged streamwise velocities decreased as the flow depth increased, however the standard deviation associated with each of the parameters remains similar, indicating a similar spatial variability over the control volume. Comparing the globally-averaged velocities to the calculated area-mean velocities (see Table 6.1), shows the measured globally-averaged velocities are approximately 75% of the area-mean velocity derived from the measured discharge when taking into consideration the blockage effect, $U_{Blockage}$. Calculation of the 95% confidence interval of the globally-averaged velocities, show them to be significantly different with the area-mean velocities three of the four flow depths. It is suggested that this difference is due to the velocity measurments not being able to be take over the full flow depth. Therefore, the globally-averaged velocities were used in place of the area-mean velocities as the free stream velocity.

Comparing the boulder layer globally-averaged streamwise velocity to the values calculated over the full profile height, shows little variation between the two measurements (all $\leq 7.5\%$). As with $\bar{U}_{xyz}$, the boulder layer velocities decrease with increase in flow depth due to the constant discharge. At the flow depth of 150mm the value calculated in the boulder layer is slightly greater than when considering the whole profile, suggesting that the average velocity above the boulder layer is less than within the boulder layer. For the flow depths of 130 and 240mm, the velocities within the boulder layer are lower than when considering the whole profile. At the flow depth of 300mm the two values were found to be the same but the standard deviation of the measurements differs, showing that the spatial variation over the control volume is much lower within the boulder layer. The standard deviation of the boulder-volume means decreases as the flow depth increases, suggesting that there is less spatial variation within the boulder flow layer as the surface flow layer increases. For the flow depth of 130mm the standard deviation of the boulder-averaged streamwise velocity is in the same region as for the globally-averaged values, however at this flow depth only two velocity measurements at each profile location where taken above the boulder height allowing for little variation between the globally-averaged and boulder layer parameters. As the standard deviation of the spatially-averaged mean is an indicator of the form-induced stress, the decrease in the standard decrease within the boulder layer also shows that the form-induced stress decreases with increased submergence. However, when considering the full flow depth there is no pattern with increased submergence, which is supported by Aberle et al. (2007) who found that the form-induced stresses were independent of discharge.

The turbulence intensities were evaluated by examining the root-mean-square of the three velocity components, u, v and w. There is similarity between flow depths for each of the three turbulence intensities ($\bar{U}rms_{xyz}$, $\bar{V}rms_{xyz}$ and $\bar{W}rms_{xyz}$). The cross-streamwise fluctuations are in the same order of magnitude as the streamwise fluctuations showing that there is significant variation in the cross-streamwise direction. However, the vertical fluctuations are an order of magnitude lower showing that these velocities are less significant. The turbulence intensity, for all three components, is comparable for the flow depths of 130, 240 and 300mm, but is greater for the flow depth of 150mm, indicating higher turbulence at this flow depth compared to the others. Higher turbulence intensities would be expected with higher time-averaged velocities present at the lower flow depths. For the flow depths of 150, 240 and 300mm the standard deviations of all the turbulence intensities are in the same order as the globally-averaged values and each other, implying similar spatial variation over the control volume. However for the flow depth of 130mm, the standard deviation is much lower, showing that there is far less spatial variation at this flow depth.

The presence of turbulence is also shown by the globally-averaged TKE (Eq. 6.5). Less than half the TKE seen at the flow depths of 150 to 300mm is seen at 130mm, showing less turbulence is present at this flow depth. The highest turbulence is seen at a flow depth of 150mm, as was suggested by the turbulence intensities. Section 6.3.1 identified the presence of secondary currents located at a relative height of approximately 1.3 that was associated with dominant values of TKE, for the sparse density and flow depth of 150mm. The significantly lower turbulence associated with the flow depth 130mm could be due to the absence of these coherent structures at this flow depth, as the highest measurements were made at a relative height of 1.1052. Which, in turn might explain the much lower value of cross-streamwise turbulence intensity at this flow depth, as these structures are associated with the presence of cross-streamwise velocities.

Spatially-averaged profiles of the streamwise velocity and TKE for each of the flow depths examined at the sparse density, are presented in Figure 6.12. There is good agreement in the shape of the profiles between the four flow depths. The presence of the same flow structures at each boulder submergence illustrates the repeatability of the results as there is consistency in the artefacts observed. We identified the presence of the boundary layer in the profile approaching the boulders in Section 6.3.1, and this was seen to have a thickness of $z/h \leq 0.1$. For the higher boulder submergences, flow depths of 240 and 300mm, a uniform velocity profile can be observed above the boulder at a relative height of greater than 1.5. However, a uniform velocity profile is not reached for the lower boulder submergences, flow depths of 130 and 150mm, and thus a free stream velocity can not be obtained for these flow depths. This suggests that this density of boulders generates a boundary layer thickness of z/h=1.5, and that based on the two flow depths examined the thickness of the boundary layer is not affected by the submergence ratio of the boulder.

Most of the previous work in the literature reports the impact of a single hemisphere on the boundary layer. Shamloo et al. (2001) observed a similar sized boundary layer (relative height of approximately 1.4), for a single hemisphere 130mm in diameter at relative submergences of 4.12 and 1.85. Acarlar and Smith (1987) examined much smaller single hemispheres in laminar flow, when the hemisphere had a diameter of 8.4mm; downstream at a distance of $4D$ the boundary layer had a relative thickness of approximately 1.7, however this increased to $\approx$2.3 at $10D$ downstream, $\approx$2.9 at $40D$ and $\approx$4 at $80D$ downstream. Whereas in a wind experiment by Savory and Toy (1986) a hemisphere with diameter of 190mm generated a boundary layer thickness of z/h=1.34 in a smooth boundary layer, and z/h=1.93 in a rough boundary layer. As we have an array of isolated boulders, they will have a greater combined effect on the boundary layer; however the thickness of our boundary layer falls between the two values reported by Savory and Toy (1986).

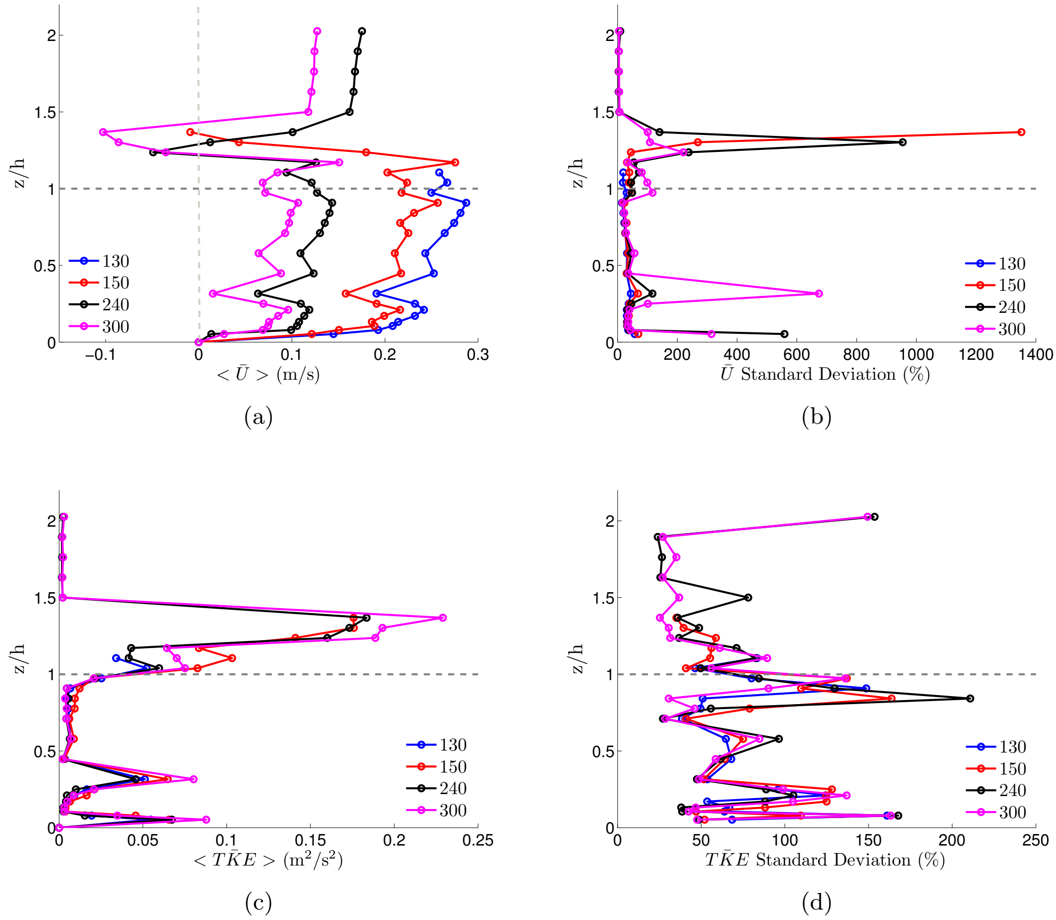

Figure 6.12. Comparison of spatially-averaged (a) streamwise velocity and (b) its associated standard deviation and (c) TKE and (d) associated standard deviation against height for each flow depth at the sparse density.

Section 6.3.1 identified the presence of a number of structures in the flow surrounding a boulder, the signatures of which can be seen in the spatially-averaged velocity profiles. The standard deviation of spatially-averaged velocity, and therefore the form-induced stress, is generally low at each height within the control volume. However, there are three distinct peaks that are associated with particular artefacts in the velocity profiles. At a relative flow depth of less than 0.1 the large standard deviation present is associated with the steep velocity gradient that is observed adjacent to the boundary. A reduction in velocity is present for all flow depths at a relative height of approximately 0.3, which illustrates the position of greatest influence of the boulder wake. The presence of this structure in the spatially-averaged profile shows that the wake is dominant within the control volume at this height. A consistent reduction in velocity (approximately 0.05m/s) is seen for each of the boulder submergences suggesting that the wake has a greater effect at the higher flow depths as the reduction in velocity is greater in proportion to the mean velocity. The standard deviation associated with this velocity deficit (Figure 6.12(b)) increases with increase in flow depth, showing greater spatial variation in the streamwise velocity within the control volume. Therefore it is suggested that the extent of the wake and magnitude of reduced velocities associated with it and the recirculation zone, increase with flow depth, and therefore boulder submergence. This is illustrated in Figure 6.13, which shows the $x-y$ planes of the streamwise velocities and $u-v$ vectors for each of the boulder submergences at a relative flow depth of 0.3158.

At the crest of the boulder ($z/h = 1$) a smaller reduction in velocity relative to that seen for the wake is present. This represents the free shear layer and associated vortices that was identified in Section 6.3.1. Above the boulder height, peaking at approximately z/h=1.4, a much larger velocity deficit is present (Figure 6.12(a)). This is not present at the 130mm flow depth as the profile depth was not high enough, as discussed previously. At the other flow depths the reduction in velocity is so pronounced that it results in negative velocities. The magnitude of the velocity deficit decreased only slightly with increasing flow depth, but the standard deviation shows that the spatial variation in the streamwise velocities, and therefore form-induced stress, at this height decreased significantly with increased boulder submergence. The cause of this large reduction in velocity was identified in Section 6.3.1, Figures 6.6 and 6.9, where secondary currents were identified at the relative height of 1.3684. These were indicated by strong cross-streamwise velocities and reduced or negative streamwise velocities, with the only exception being directly over the boulder locations where increased streamwise velocities were seen. The spatially-averaged profiles show that these secondary currents are the dominant structure within the control volume at each flow depth.

There is good agreement in the spatially-averaged TKE profiles between the different flow depths. Three peaks are exhibited which coincide with the locations of the artefacts, discussed above, in the spatially-averaged velocity profiles and the associated increases in standard deviation. This would be expected as greater fluctuation in the spatial variation in velocity implies greater velocity gradients, hence greater magnitude of turbulence as confirmed in the TKE profile. As discussed, the increased turbulence near the boundary is due to the steep gradient in velocity associated with the laminar sublayer within the boundary layer, and at a relative height of approximately 0.3 there is higher turbulence associated with the wake, and recirculation zone present downstream of the boulder. Above the wake region there are very small and consistent values of TKE up to the boulder height where the TKE increases over height to a peak value at a relative height of about 1.4, which is associated with the large velocity deficit seen in the velocity profiles (Figure 6.12(a)).

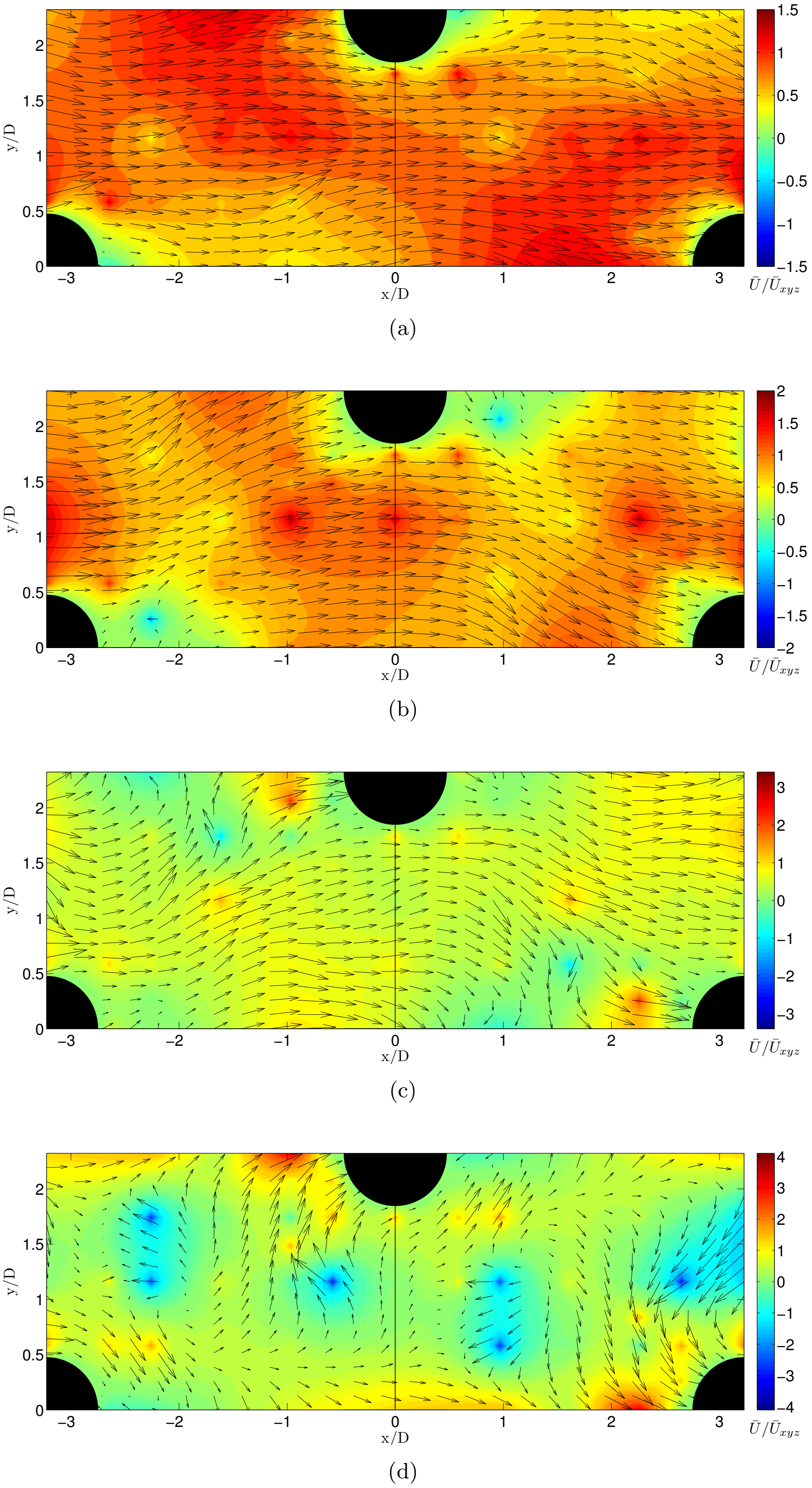

Figure 6.13. Plan view $(x - y)$ contour plot of streamwise velocities with $u - v$ vectors for each of the flow depths (a) 130, (b) 150, (c) 240 and (d) 300mm at a relative flow depth of 0.3158.

The lower section of the peak is associated with the free shear layer that was identified downstream of the boulder crest. In Figure 6.5 this region was shown to be more pronounced than the wake, however its presence is less pronounced in the spatially-averaged profile. The upper section of the peak is due to the dominant secondary currents present at this height (Figure 6.6(c)) discussed in relation to the velocity profile. The greatest magnitude of turbulence is associated with these secondary currents. Best (2005) reported that a large percentage of momentum flux in three-dimensional dunes (in a similar staggered configuration) was due to the presence of secondary currents above the dune crests. At all heights there is a significant level of standard deviation, however there is an overall trend of reduction in the standard deviation with height indicating that there is greater consistency in the spatial distribution of TKE in the surface flow layer above the boulder.

Depth-averaged profiles were calculated for the boulder layer (where $z/h \leq 1$) and over the whole profile depth. It was discussed previously that a free stream velocity was not reached for the boulder submergences relating to the 130 and 150mm flow depths (see Figure 6.12(a)) hence the depth-averages for all flow depths were not averaged to the water surface but to the last measurements point within the profile, i.e. 84, 104, 154 and 154mm for the flow depths 130, 150, 240 and 300mm respectively. Figure 6.14 shows a plan view $(x - y)$ of the boulder layer depth-averaged streamwise velocities for the four flow depths. The velocities are normalised to the boulder layer globally-averaged velocities calculated for each flow depth, $\bar{U}_{BL}$ (presented in Table 6.4).

Examining all four of the contour plots shows that there is a high degree of similarity between the different flow depths. A definition of the wake region was given in Section 6.3.1, where it was defined as the area where the velocity is less than 90% of the free stream velocity. As discussed a free stream velocity is not reached for the flow depths of 130 and 150mm, and the globally-averaged velocities were found to be significantly lower than the calculated area-mean velocities when the blockage effect of the boulders is considered. Therefore the globally-averaged streamwise and boulder-layer averaged streamwise velocities was used in place of the free-stream velocity for all analysis. At a flow depth of 130mm the wake has a length of approximately $2.2D$ from the downstream edge of the boulder. As the flow depth increases the wake length shortens up to the flow depth of 240mm, after which the wake extends again; for example it is $2.1D$ at 150mm, $1.5D$ at 240mm, but $2D$ at 300mm. This shortening of the wake length is accompanied by a slight widening of the wake immediately downstream of the boulder.

The lateral width of the wake at the 130mm flow depth is at its greatest immediately adjacent to the boulder at the longitudinal centre, where it has a width of 2D. However, immediately downstream of the boulder the wake width is only 1D. The change in wake

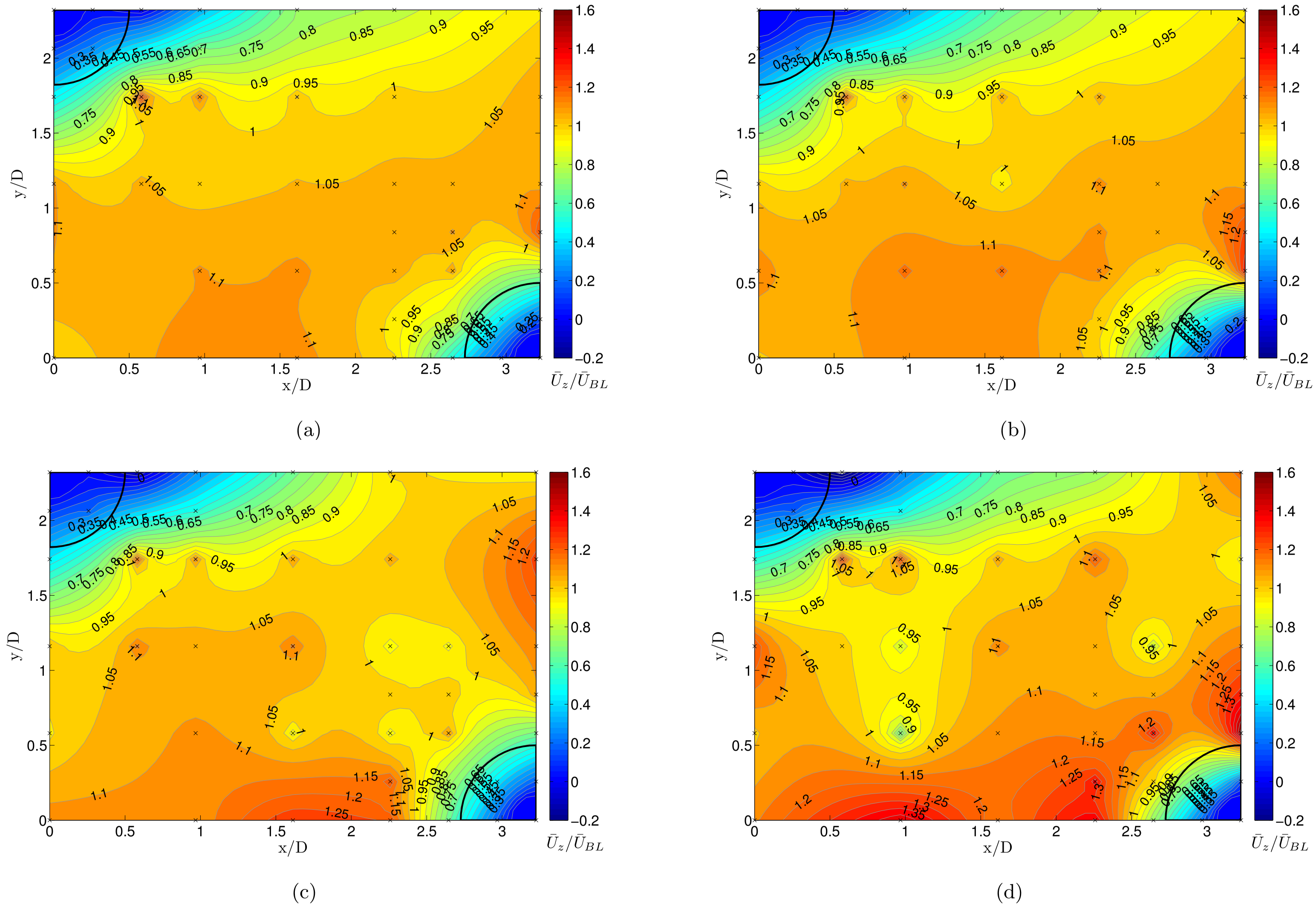

Figure 6.14. Plan view $(x - y)$ contour plot of depth-averaged streamwise velocities for the boulder layer $(z/h < 1)$ at the sparse density for the flow depths (a) 130, (b) 150, (c) 240 and (d) 300. Velocities are normalised to the boulder layer globally-averaged streamwise velocity for each flow depth.

width over flow depth is 1.3-2.3, 1.4-2.2 and 1.3-1.9 for the flow depths 150, 240 and 300 respectively. The lateral widening of the wake follows the same pattern as the wake length, with the wake narrowing again at the highest flow depth. Nepf et al. (1997) defined a dimensionless ratio of the wake area to obstacle area, M, which calculated for these results at a flow depth of 150mm would give values between 2.73 and 4.83, which is much smaller than the M of 40 measured for a single cylinder by Nepf et al. (1997).

An area of reduced velocities, referred to as the dead-zone, is seen in front of the downstream boulder and extends around the edge of the boulder. This area becomes smaller as the flow depth increases, which appears to be due to the increase in the magnitude of the upstream velocity region. This region becomes larger as the flow depth increases, resulting in the formation of two high velocity regions upstream of the boulder at the flow depth of 300mm. As the flow depth increases, a high velocity region also develops along side the upstream boulder at the longitudinal midpoint, with the velocities becoming stronger with increasing flow depth.

Figure 6.15 shows the depth-averaged streamwise velocities for the whole vertical profile. As the flow depth increases the similarity between the depth-averaged velocities within the boulder layer and the whole profile decreases due to the increased thickness of the surface flow layer, reducing the dominance of the boulder layer within the depth averaged profile. The wake length remains the same for flow depths of 130 and 150mm and then reduces to 1.5D and 1D for the flow depths 240 and 300mm respectively. At 300mm, however, a second velocity deficit region has developed further downstream. This could be part of the same wake or it could indicate the presence of vortex shedding from the boulder, the presence of which was suggested in Section 6.3.1. Furthermore as the flow depth increases the low velocity region associated with the presence of the boulders disappears due to an increasing portion of the fluid being part of the surface flow layer balancing out the zero velocities associated with the boulders. At the flow depth of 300mm, the dead-zone immediately upstream of the boulder is no longer present in the depth-averaged profile. The high velocity regions that were present upstream of the boulder in Figure 6.14 at the 240 and 300mm flow depths develop at lower flow depths when the whole velocity profile is considered, suggesting that these features are accentuated by the surface flow layer.

The depth-averaged TKE were also normalised to the globally-averaged values for each flow depth. The depth-averaged TKE, calculated over the full profile height, for each flow depth are presented in Figure 6.16. For all flow depths the predominant TKE for the control volume was between 0.9 and 1.1 of the globally-averaged value. As was seen in the depth-averaged velocity profile, reduced TKE is present in the region of both the boulders. However, unlike with the depth-averaged velocities, this effect does not disappear as the

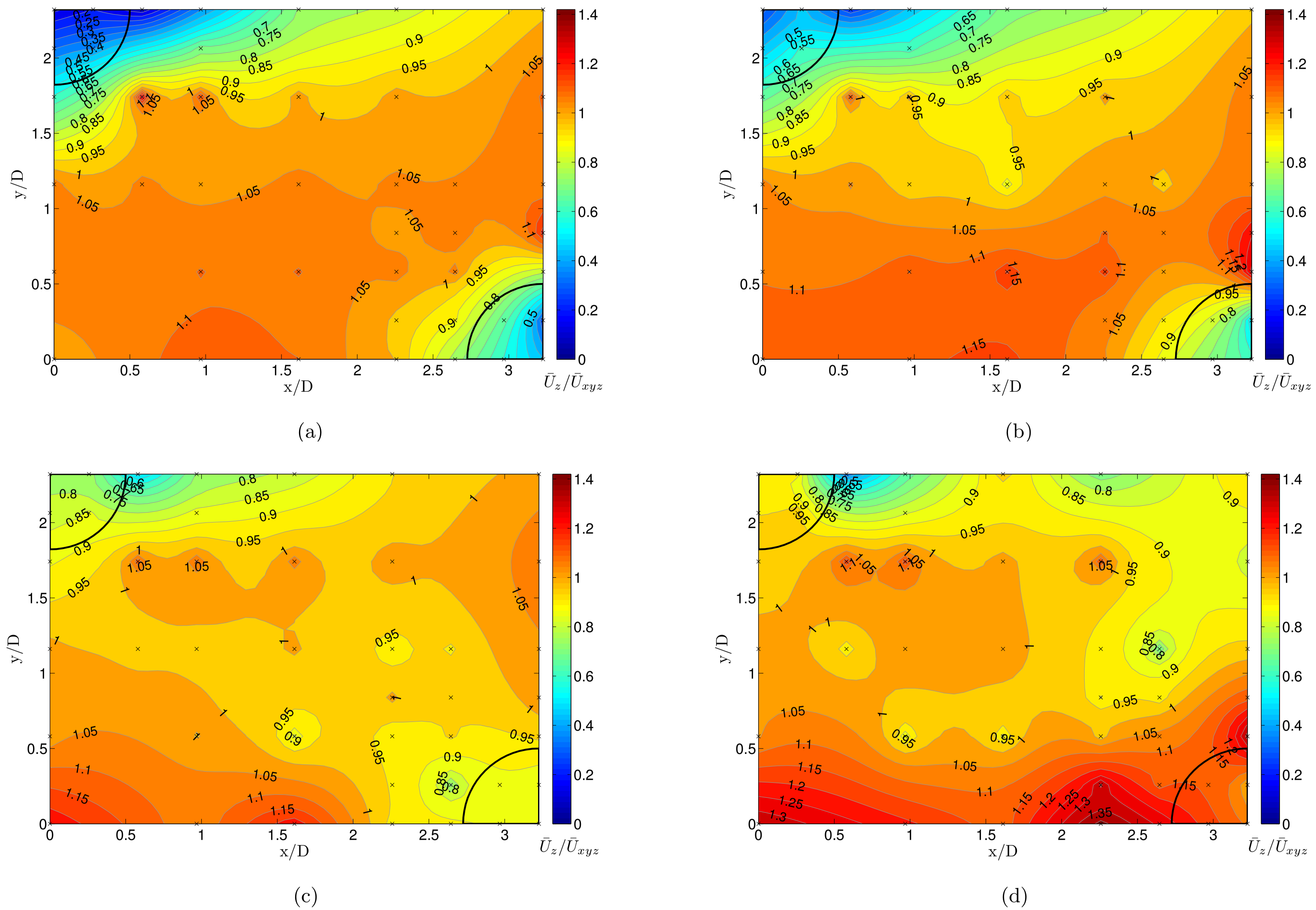

Figure 6.15. Plan view $(x - y)$ contour plot of depth-averaged streamwise velocities at the sparse density for the flow depths (a) 130, (b) 150, (c) 240 and (d) 300. Velocities are normalised to the globally-averaged streamwise velocity for each flow depth

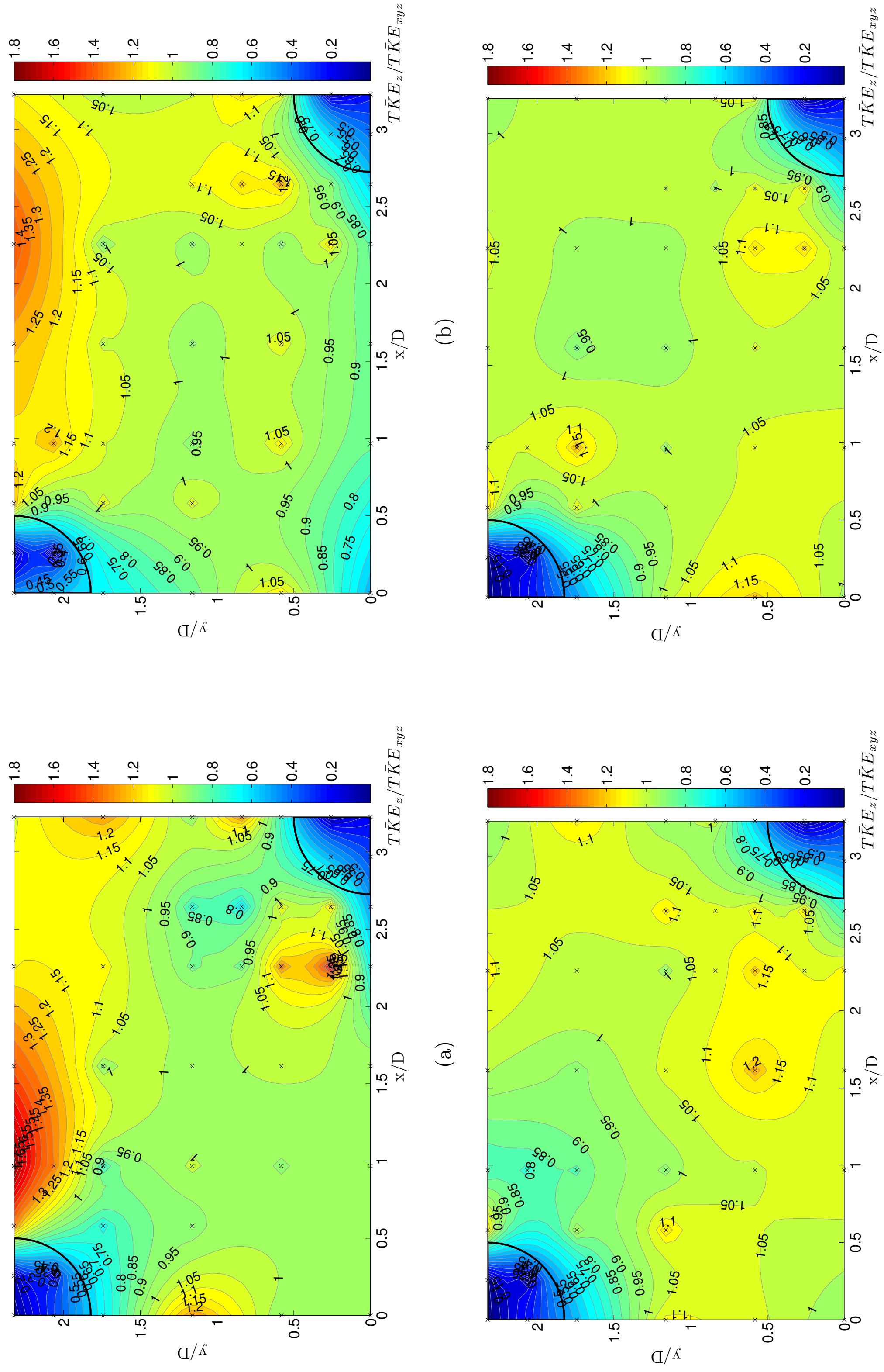

Figure 6.16. Plan view $(x - y)$ contour plot of depth-averaged TKE at the sparse density for the flow depths (a) 130, (b) 150, (c) 240 and (d) 300. TKE is normalised to the globally-averaged TKE for each flow depth

flow depth increases, therefore suggesting that the TKE over the boulders is also low. This was shown in Section 6.3.1, where high streamwise velocities were present over the top of the boulder, and were associated with low TKE (see Figure 6.7). At a flow depth of 130 there is high TKE associated with the wake of the boulder, with the maximum value located about $0.5D$ behind the boulder, and the region extending laterally as it moved downstream. At the flow depth of 150mm, the TKE has reduced magnitude and the region of increased TKE has moved downstream, with the maximum value located $1.75D$ downstream of the boulder. Lacey and Nikora (2008) observed a peak level of TKE at a distance of $1.4D$ behind a pebble cluster, at a relative height of 0.7. This observation falls between our two values, however we are examining the depth-averaged profile. At the flow depths of 240 and 300mm, no increased TKE is seen in the wake; the effect of the wake on the depth-averaged velocities was also highly diminished at these heights, suggesting the surface-layer flow at these flow depths cancels out the effect of the wake.

This section has investigated how changing the relative flow depth affects the flow structure around a regular array of boulders at a given density. Consistency, and therefore repeatability, was seen in the spatially-averaged profiles for the different flow depths, with the velocities reducing with increases in flow depth due to the constant discharge for each condition. A number of structures were identified in the spatially-averaged profile, indicating the boundary layer, the wake and possible vortex shedding from the top of the boulder. Analysis of the depth-averaged velocities showed a shortening and widening of the wake with increased boulder submergence however this pattern did not extend to the highest flow depth of 300mm, where the wake was seen to lengthen and narrow. High TKE was seen in the wake at the lowest flow depth but this effect was not seen at the other flow depths due to the larger surface flow layers.

6.3.4 Effects of Boulder Density

The effect of varying the longitudinal and lateral spacing of the boulders was compared, for a single flow depth of 150mm, at the four boulder densities described in Section 3.5.3. Table 6.5 presents the globally-averaged parameters for each of the densities. Again two globally-averaged streamwise velocities have been calculated, one that covers the full depth of the measurement volume, denoted by xyz, and another where only the boulder depth is considered, denoted by BL. For three of the four densities the globally-averaged streamwise velocities are similar, reducing slightly as the density increases due to the increased blockage effect created as the number of boulders present increases. However the dense density does not fit with this pattern with a much lower (17.9%) globally-averaged u velocity when compared to the sparse density. Further investigation within this section will aim to identify the reason for this reduction in velocity.

	$\bar{U}_{xyz}$ (m/s)	$\bar{U}_{BL}$ (m/s)	TKE_{xyz} (m^2/s^2)
Sparse	0.1912 (0.0627)	0.1997 (0.0446)	0.0455 (0.0532)
Intermediate	0.1840 (0.0657)	0.1964 (0.0583)	0.0477 (0.0569)
Dense	0.1569 (0.0599)	0.1487 (0.0585)	0.0437 (0.0494)
Very Dense	0.1803 (0.0724)	0.1583 (0.0609)	0.0282 (0.0310)
	$\bar{U}rms_{xyz}$ (m/s)	$\bar{V}rms_{xyz}$ (m/s)	$\bar{W}rms_{xyz}$ (m/s)
Sparse	0.1776 (0.1207)	0.1404 (0.1118)	0.0386 (0.0299)
Intermediate	0.1854 (0.1286)	0.1346 (0.1127)	0.0408 (0.0189)
Dense	0.1660 (0.1157)	0.1341 (0.1016)	0.0383 (0.0169)
Very Dense	0.1388 (0.0904)	0.1022 (0.0727)	0.0364 (0.0119)
	$\bar{U}rms_{BL}$ (m/s)	$\bar{V}rms_{BL}$ (m/s)	$\bar{W}rms_{BL}$ (m/s)
Sparse	0.1151 (0.0701)	0.0849 (0.0483)	0.0274 (0.0090)
Intermediate	0.1263 (0.0857)	0.0780 (0.0465)	0.0317 (0.0097)
Dense	0.1204 (0.0957)	0.1001 (0.0847)	0.0318 (0.0131)
Very Dense	0.0959 (0.0573)	0.0658 (0.0276)	0.0309 (0.0076)

Table 6.5. Globally-averaged parameters for each boulder density at a flow depth of 150mm. Standard deviations for each mean are given in brackets

Comparing the boulder layer averaged velocities to the full measurement volume shows that for the two lower densities (sparse and intermediate) the velocities are greater when only considering the boulder layer. The presence of secondary currents within the surface flow layer at the sparse density in Section 6.3.1, would have the effect of reducing the globally-averaged velocity. However the effect is minimal at the sparse density but is more pronounced within the intermediate density, where the boulder layer averaged streamwise velocity was 6.7% higher. At the two higher densities (dense and very dense) the boulder layer averaged streamwise velocities are lower than those for the full measurement volume. The fluid velocities in the surface flow layer at these densities must be higher, resulting in a greater globally-averaged velocity, suggesting a reduction in the dominance of the secondary currents that were identified in the surface flow layer. The standard deviations for both the boundary layer averaged u velocity and the full measurement volume averaged u velocity increase as the density increases, indicating a general increase in the spatial variation of the streamwise velocity, and therefore form-induced stress, within the control volume. The only exception to this is the dense set-up where the spatial variation in the streamwise velocity over the whole profile depth is the lowest of all the densities.

The TKE (Eq. 6.5) magnitude for the first three densities is relatively similar, however it is much lower (-38% compared to sparse) at the highest density. A possible reason for this could be due to the region of boulders at this density not covering the whole length of the flume resulting in the formation of a smaller turbulent boundary layer. The globally-averaged and boulder layer averaged turbulence intensities ($\bar{U}rms_{xyz}, \bar{V}rms_{xyz}, \bar{W}rms_{xyz}$) were also calculated to examine the variation between the densities. There is a general decrease in the volume-avergaged turbulence intensities with increase in density, although the intermediate density does not always conform to this trend. The streamwise and cross-streamwise turbulence intensities at the very dense density are greatly reduced compared to the sparse density, which would be expected due to the small globally-averaged TKE at this density. The cross-streamwise turbulence intensities are in the same order of magnitude as the streamwise turbulence intensities showing that there are significant fluctuations in the cross-streamwise velocities. The spatial variation within the control volume, shown by the standard deviation, of each of the three turbulence intensities decrease with increasing boulder density, again with the intermediate density as the exception.

Comparing the globally-averaged turbulence intensities to those averaged over the boulder layer, shows that the turbulence in all three directions is greatly reduced within the boulder layer. This reduction shows that the turbulence intensities are greater in the surface flow layer therefore increasing the globally-averaged. This is due to the presence of the secondary currents that were identified in the surface flow layer, which were dominant over the control area. This is further confirmed by the cross-streamwise turbulence intensities; strong cross-streamwise velocities are associated with the secondary currents, therefore the cross-streamwise turbulence intensities in the boulder layer are greatly reduced as these structures are not included. The standard deviation of the boulder layer averaged parameters is variable, with the greatest spatial variation associated with the dense set up and the lowest seen for the very dense density.

Both spatially-averaged and depth-averaged parameters were calculated to allow for comparison between the densities. Figure 6.17 shows the spatially-averaged streamwise velocities and TKE, with the standard deviation for each mean, for each of the densities at a flow depth of 150mm. Within the boulder layer ($z/h < 1$) there is a reasonable degree of similarity between the profiles of the different densities. The retardation of the flow due to the increased blockage effect as the number of boulders increased can be seen, and the increase in velocity in the surface-layer that was suggested by the globally-averaged velocity for the very dense configuration is evident. However, the expected pattern of highest velocities at the sparse density and lowest at the very dense density, is not conformed to at all heights.

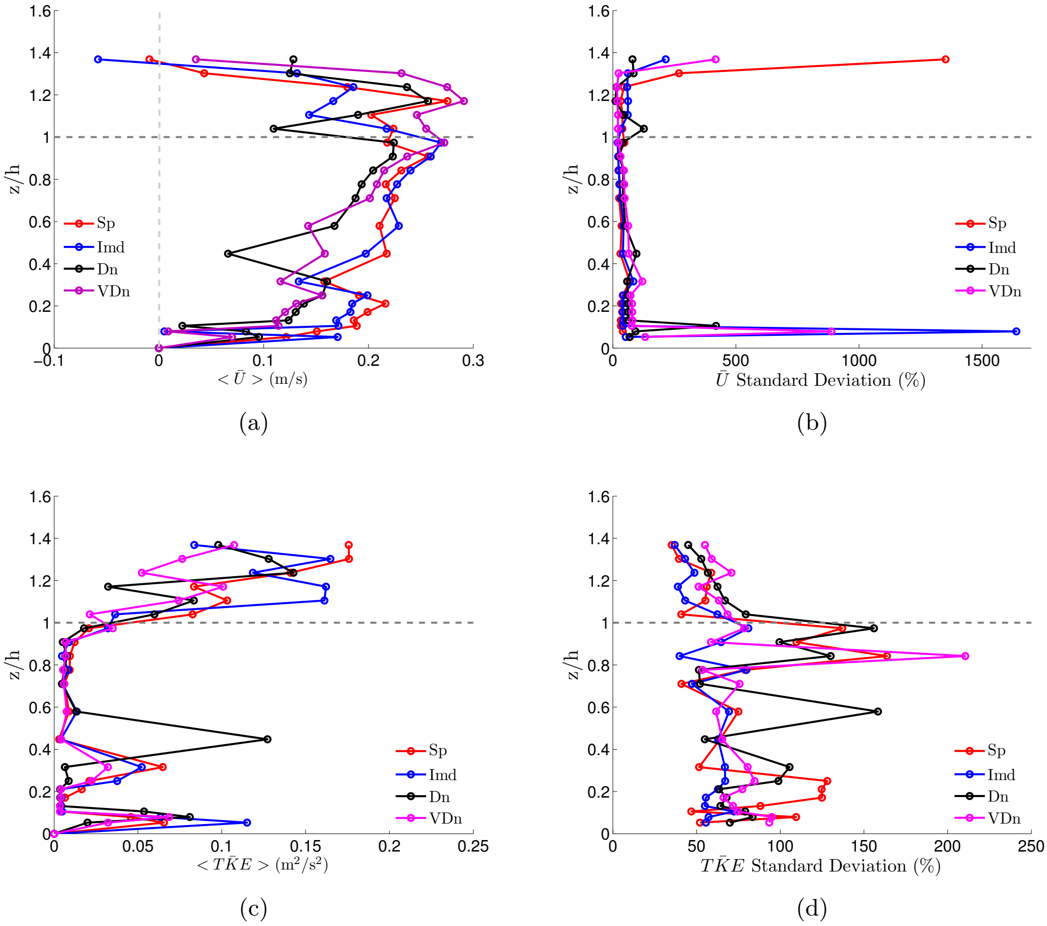

Figure 6.17. Vertical profiles of the spatially-averaged (a) streamwise velocities and (b) associated standard deviation and (c) TKE and (d) associated standard deviation against height for each boulder density at a flow depth of 150mm.

At the sparse density the boundary layer upstream of the boulder was found to be $0.1h$ in thickness, which is shown by the steep velocity gradient in the sparse profile (Figure 6.17(a)). However at this relative height the three other densities exhibit velocity deficits, which must be created by the presence of negative and reduced velocity regions. Figure 6.18 presents a longitudinal $(x - z)$ plane contour plot with $u - v$ vectors of the flow approaching and behind a boulder. This shows the presence of these regions upstream of the boulder at the intermediate and dense densities, and the increased dominance of the downstream wake and recirculation zone with increased density due to the reducing size of the control volume. The large standard deviations associated with these velocity deficits for the three densities, show that there is significant spatial variation in streamwise velocity over the control volume. As the standard deviation of the spatially averaged mean is also an indicator of the form-induced stress, it also indicates that this is large in this region. Aberle et al. (2007) found the form-induced stress to be greatest within the roughness layer, which is true for all densities except the sparse density.

At a relative height of 0.3 evidence of the boulder wake and recirculation zone, shown as a reduction in velocity, is evident in the spatially-averaged profiles for each of the densities. However at the dense density the velocity deficit is located higher, at approximately $z/h = 0.45$, suggesting that the largest proportion of the wake, or recirculation zone, is located much higher for this boulder density than for the other densities. Figure 6.18(c) shows that at this height the wake region extends much further downstream at this density compared to the others, to the extent that it is also present upstream of the next boulder. This region is associated with lower velocities in the dense configuration than seen at this height for the other densities. Section 6.3.1 suggested that vortex shedding might be occurring downstream of the boulder wake, as a distinct reduced velocity region was identified downstream of the wake in the sparse density. The low velocity region at the dense density is less distinct at the lower densities, and located at a lower relative height; however, it can be seen to develop with increasing density, before becoming absent at the highest density. The presence of the velocity deficit in the profile shows the dominance of the wake within the control volume.

Above the boulder flow layer the highest velocities are present at the very dense density, whereas below the boulder height ($z/h < 1$) this density is predominantly associated with the lowest velocities (Figure 6.17(a)). Above the boulder flow layer two reductions in velocity are present for each of the densities. The first velocity deficit is located immediately above the boulder height for the dense configuration, and slightly higher ($z/h \approx 1.1$) for the other densities. For the sparse density a free shear layer was identified immediately downstream of the boulder crest, which could be the reason for the velocity deficit; however Figure 6.18(a) shows that for the sparse density this region is too low to be responsible for velocity deficit. For the intermediate and dense configurations reduced velocities regions are visible at the correct height. Examining Figure 6.18 at the relative height of 1.1 for each density shows that relative velocity across the control volumes are in the region of 1 or less, which represents an absolute velocity of 0.1912m/s or less, with the exception of directly over the boulders. This region over the boulders is much greater in the highest density and therefore explains why this density has the smallest velocity reduction, with velocities not less than 0.2m/s.

The second velocity reduction in the spatially-averaged profile in the surface flow layer is present at the top of the measurement profile. The greatest reduction is seen at the intermediate density, and the smallest at the dense density. The very large standard deviations associated with these measurements indicate the large spatial variation associated with the averaged velocities at this height. This region of reduced velocity and its dominance within the control volume was shown in Section 6.3.1, Figure 6.5, for the sparse density, where secondary currents were identified by the strong cross-streamwise velocities. The

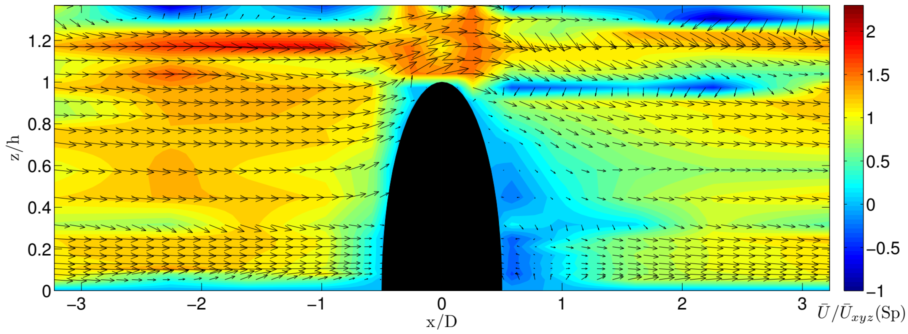

(a)

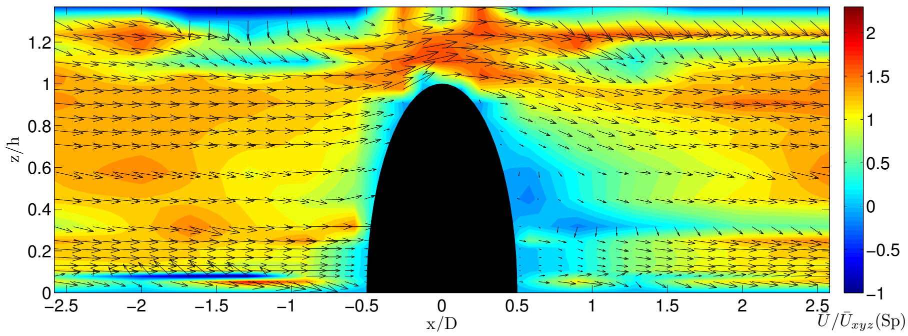

(b)

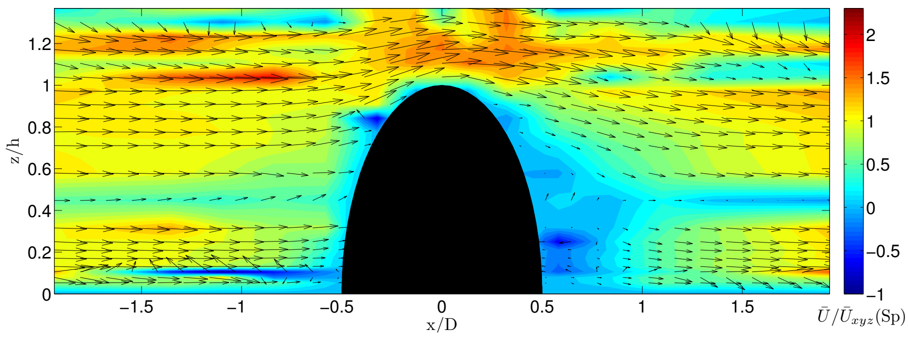

(c)

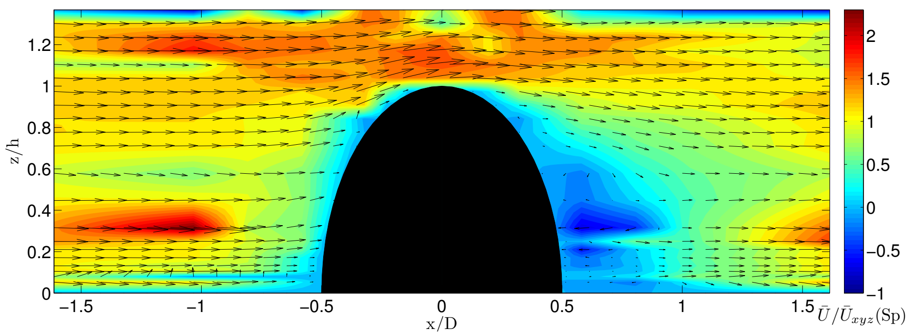

(d)

Figure 6.18. Longitudinal $(x - z)$ contour plots of streamwise velocities with $u - v$ vectors at a flow depth of 150mm for the boulder densities (a) Sparse, (b) Intermediate, (c) Dense and (d) Very dense. Streamwise velocities are normalised to the globally-averaged streamwise velocity at sparse density $(\bar{U}_{xyz}(Sp))$ for 150mm flow depth. Note that the x-axis scale changes to show the whole control volume. The flow direction is from left to right.

presence of these secondary currents at each of the densities is shown in Figure 6.18. Figure 6.19 shows the plan view $(x-y)$ contour plots, with $u-v$ velocity vectors, at the relative height of 1.3684, the height associated with these velocity deficit and secondary currents. The dominance of these secondary currents is clearly visible, with the presence of reduced streamwise velocities and strong cross-streamwise velocities throughout the control volume with the exception of directly above the boulders. The differences between the densities are the same as those illustrated in the spatially-averaged profiles (Figure 6.17), with the greatest velocity reduction at the intermediate density and lowest reduction at the dense density.

The spatially-averaged TKE profile (Figure 6.17(c)) coincides with the velocity profiles (Figure 6.17(a)), with regions of high TKE associated with the regions of reduced velocities seen in the velocity profile. Increases in TKE are associated with turbulent momentum exchange and hence the boundary layer, the boulder wake, and the secondary currents located in the surface flow layer. As with the velocity profile, the peak associated with the boulder wake at the dense density is located higher than at the other densities (Figure 6.17(c)). Throughout the rest of the boulder layer, the magnitude of TKE is negligible; however in the surface flow layer the TKE increases with height. In the surface flow layer the greatest TKE associated with the lower of the two velocity deficits is seen at the intermediate density, but the greatest TKE associated with the higher velocity deficit is seen at the sparse density.

Figure 6.20 compares the TKE for the four densities for the flow approaching the boulder and the flow downstream of the boulder, at the same longitudinal $(x-z)$ plane corresponding to Figure 6.18. Comparing these two figures shows that the higher TKE regions are associated with the high velocity regions below the identified secondary currents, due to the presence of strong velocity gradients in the region. The TKE observed at the very dense density is lower than that for the other densities, as is expected from the spatially-averaged profile. Although the TKE in the boulder flow layer was negligible, apart from the two previously mentioned features, the standard deviation below the boulder height is higher than in the surface flow layer. The two identified structures in the boulder flow layer are isolated features within the control volume, and therefore they represent a greater deviation from the mean, shown by a greater spatial variation. However, in the surface flow layer, there are higher velocities, and therefore a higher relative degree of turbulence, but greater uniformity in TKE distribution across the control volume due to the dominant nature of the identified structures.

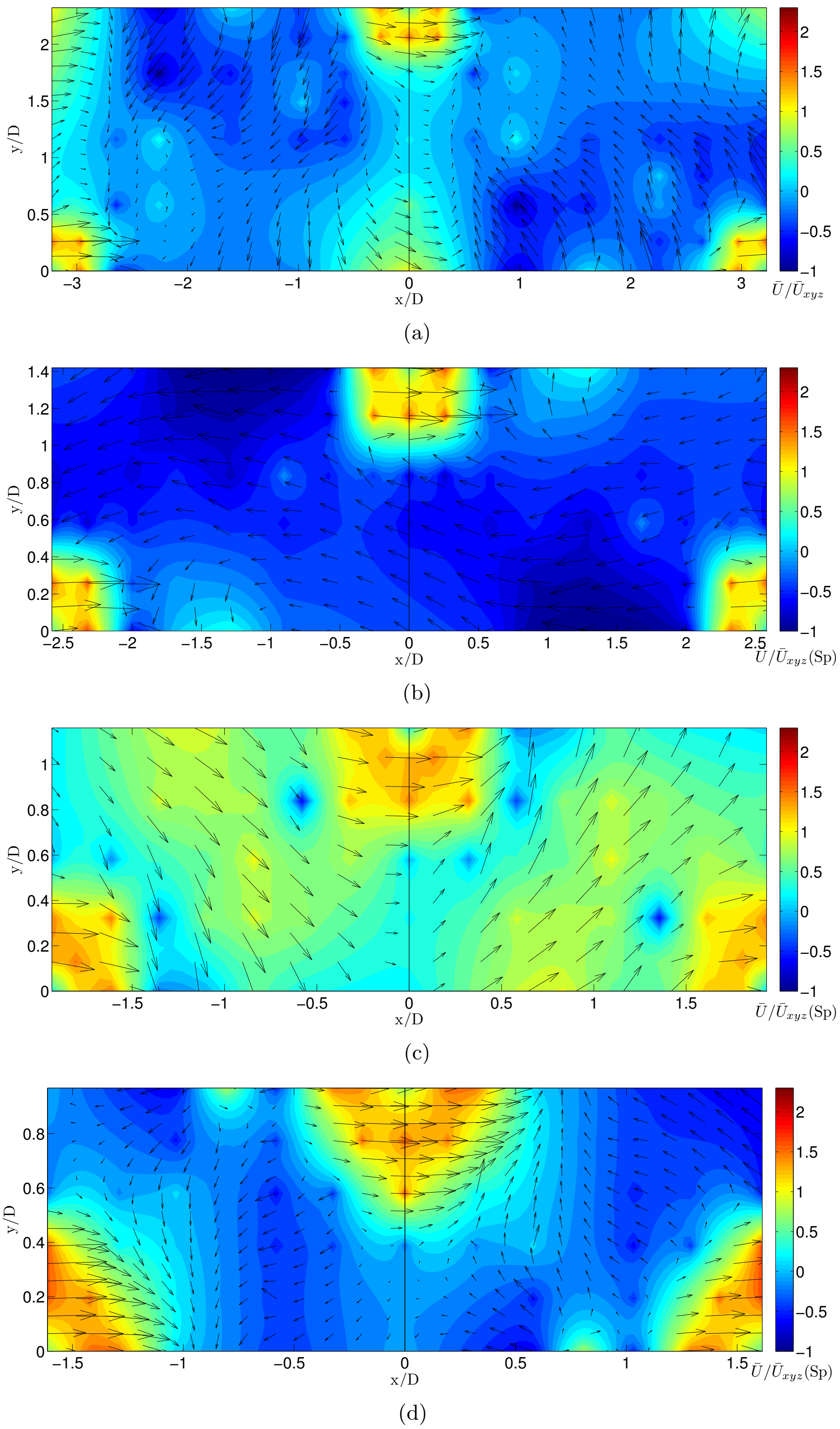

Figure 6.19. Plan view $(x-y)$ contour plot of streamwise velocities with $u-v$ vectors at a relative height of 1.3684 for the boulder densities (a) Sparse, (b) Intermediate, (c) Dense and (d) Very dense. Streamwise velocities are normalised to the globally-averaged streamwise velocity for the 150mm at sparse density.

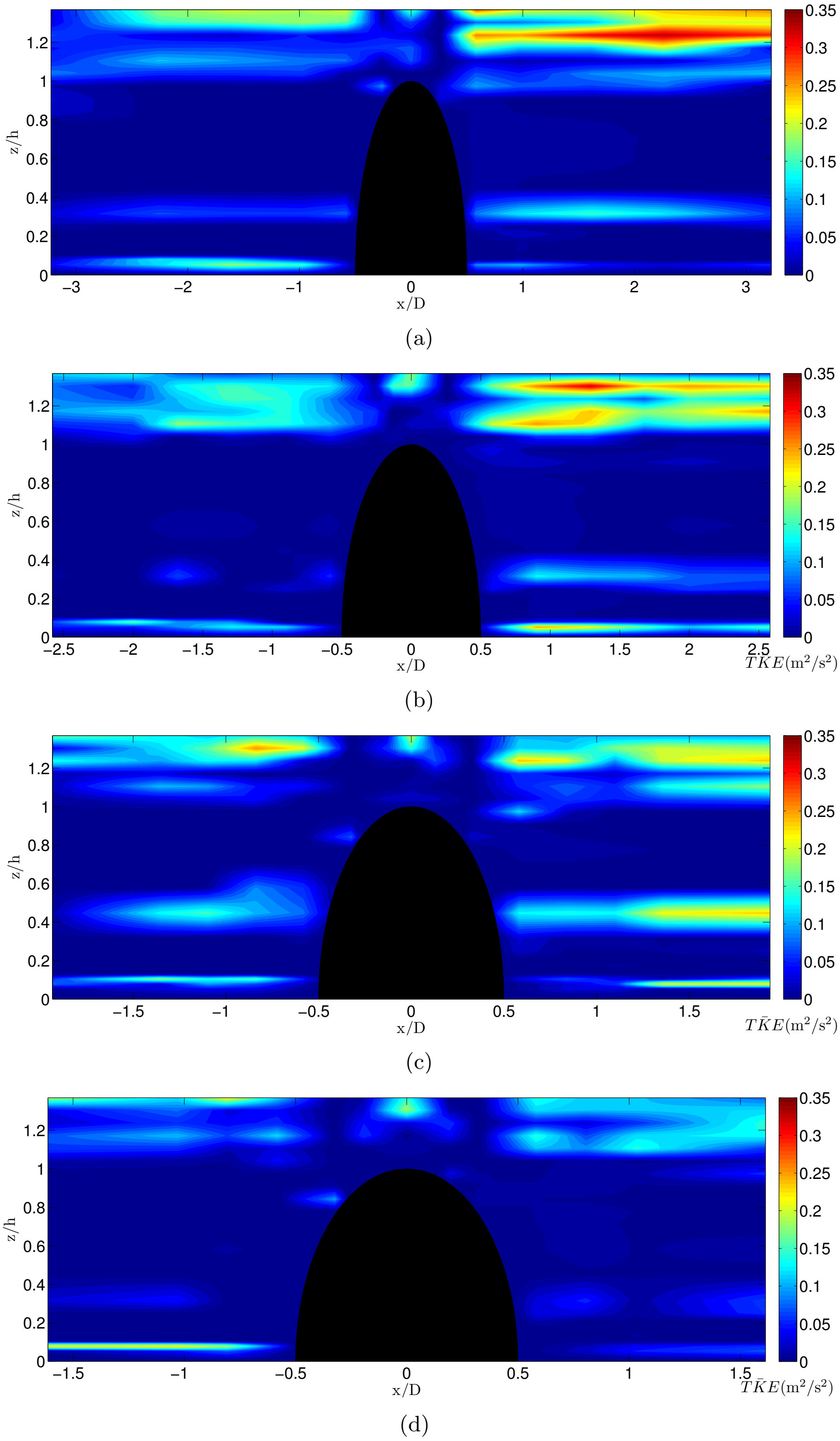

Figure 6.20. Longitudinal $(x - z)$ contour plots of TKE at a flow depth of 150mm for the boulder densities (a) Sparse, (b) Intermediate, (c) Dense and (d) Very dense. Note that the x-axis scale changes to show the whole control volume. The flow direction is from left to right.

To compare the velocity structures between densities, the depth-averaged velocities for each velocity component were normalised to the globally-averaged and boulder layer averaged streamwise velocity for a flow depth of 150mm at the sparse density ($\bar{U}_{xyz}(Sp)$). The boulder layer depth-averaged streamwise velocities are presented in Figure 6.21, with the full depth-averaged streamwise velocities presented in Figure 6.22. Within the boulder flow layer, the wake of each boulder is easily visible. As the density increases the downstream extent of the wake decreases; initially at the sparse density the wake extends approximately $2.2D$ downstream of the boulder, however at the very dense density it extends only approximately $0.85D$. The increased blockage effect at higher density leads to higher velocities passing over the top of the boulder then down towards the bed, which could lead to the shortening of the downstream wake.

Although the wake length shortens as the density increases, the total volume of wake within the control volume increases with boulder density as it extends laterally and joins up with the dead zone present upstream of the boulder. The greatest wake area as a proportion of the control volume area is seen at the dense density. Nepf et al. (1997) suggested theory on obstacle interaction states that as the density increases then more overlap is seen between the wakes until the entire volume is occupied by wake; therefore the rate of increase in the wake area fraction decreases with increase in density due to the overlapping of the wakes. It would be expected that the highest density would exhibit the greatest wake area fraction, however this is not seen in the data with the greatest wake present at the dense configuration.

Similar patterns are seen when examining the full measurement volume depth averaged velocities (Figure 6.22). However, contrary to the just considering the boulder layer, the downstream wake does not join with the upstream dead-zone at the very dense density. Again the greatest wake area is seen at the dense density. The shortening of the wake length with increased density is visible, as is the extension of the wake laterally. At the sparse density the wake length is $2.3D$ behind the boulder, resulting in it being slightly longer when considering the full measurement depth. The wake length is seen to reduce in length with increasing density to 0.8D at the very dense density, which is shorter than when considering only the boulder layer.

This difference between the boulder wake when considering the boulder flow layer and the full measurement height illustrates the effect of the surface flow layer, and the dominant structures identified within, on the depth-averaged profile. Figure 6.23 presents the streamwise velocities averaged over the surface layer ($z/h > 1$), normalised to the boulder layer globally-averaged streamwise velocity for the sparse densities at the flow depth of 150mm, to allow direct comparison to Figure 6.21. The dominance of the reduced and

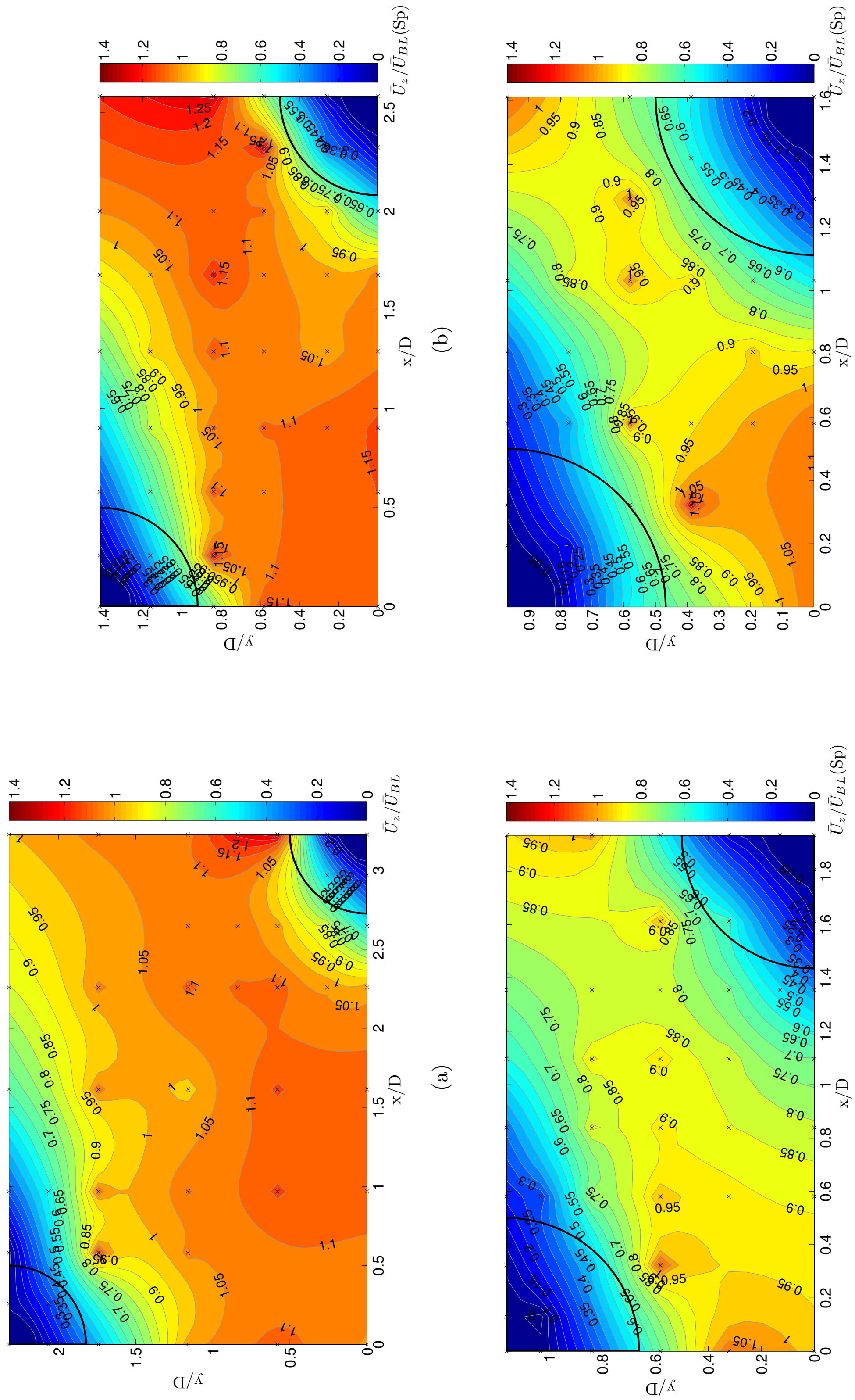

Figure 6.21. Plan view $(x-y)$ contour plot of depth-averaged streamwise velocities for the boulder layer $(z/h < 1)$ at a flow depth of 150mm for the boulder densities (a) Sparse, (b) Intermediate, (c) Dense and (d) Very dense. Velocities are normalised to the boulder layer average streamwise velocity for sparse density, $\bar{U}_{BL}(Sp)$, at a flow depth of 150mm.

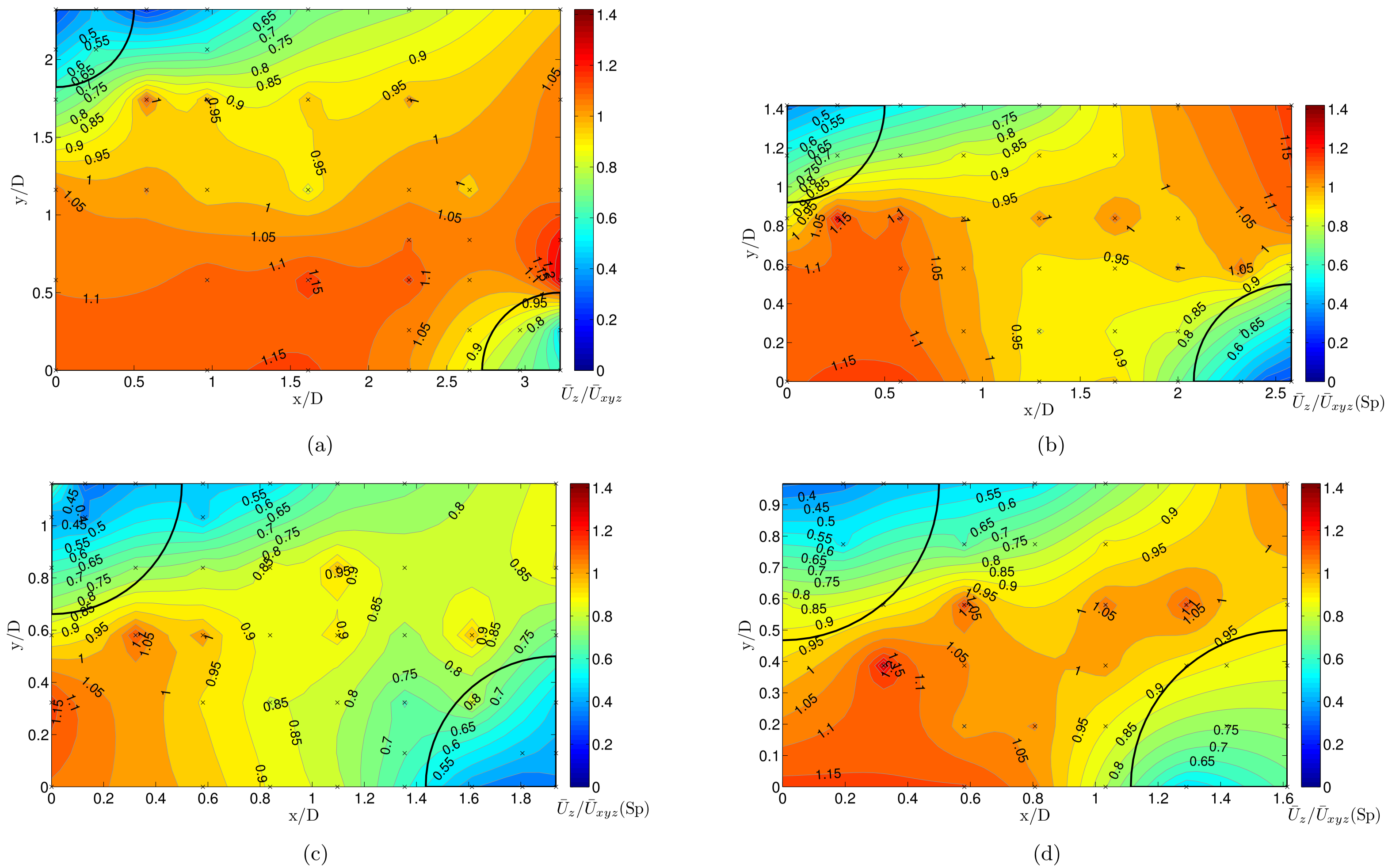

Figure 6.22. Plan view $(x-y)$ contour plot of depth-averaged streamwise velocities at a flow depth of 150mm for the boulder densities (a) Sparse, (b) Intermediate, (c) Dense and (d) Very dense. Velocities are normalised to the globally-averaged streamwise velocity for sparse density, $\bar{U}_{xyz}(Sp)$, at a flow depth of 150mm.

negative velocities associated with the secondary currents, which were shown in Figure 6.19, is evident, along with the increased streamwise velocities that were observed above the boulders. However these reduced velocities are not present in the surface layer averaged profile at the very dense density. The free shear layer was seen not to be present at the very density configuration, and the secondary currents occupy a smaller relative height than at other densities (Figure 6.18), therefore leading to higher averaged velocities in the surface flow layer. The presence of higher velocities at this boulder density compared to the others, means that, when the full measurement volume is considered, rather than the evidence of wake being enhanced, it is diminished.

The depth-averaged cross-streamwise v and vertical w velocities are shown in Figures 6.24 and 6.25 respectively. At the sparse density, there are elevated cross-streamwise velocities where the flow is forced around the upstream and downstream boulder. The highest depth-averaged cross-streamwise velocities were 20% of the streamwise velocity. The vertical velocities also follow the expected pattern, with downward movement of fluid in the wake of the boulder, as mentioned previously in Section 6.3.1. The greatest downward velocities are seen immediately downstream of the boulder and upward velocities are located immediately upstream of the boulder where the water is forced up and over the boulder.

As the density increases, the strength and presence of lateral velocities increases, as the corridor between the boulders reduces in size forcing the water diagonally between the two boulders. This is very apparent for the very dense density where the whole central region between the two boulders has high cross-streamwise velocities, a maximum of 25% of the streamwise velocities. The patterns exhibited at each density do not strictly follow this pattern due to the presence of strong cross-streamwise velocities located in the surface flow layer. The intermediate density does not fit this pattern, with a region of negative cross-streamwise velocities present upstream of the downstream boulder. At this density strong secondary currents are present in the surface flow layer (Figure 6.18), characterised by negative streamwise velocities, strong negative cross-streamwise velocities, and strong downwards velocities. The strength of the velocities in these regions, and their dominance within the control volume, has resulted in these structures being visible in both the spatially-averaged and depth-averaged profiles. These structures have been shown to be present at the other densities, but their influence is not shown explicitly in the corresponding depth-averaged profile. In section 6.3.1, Figure 6.6 showed that the cross-streamwise flow at the two successive relative heights were in oppositing directions, therefore in the depth-averaging the presence of these regions would cancel each other out. However, this is not the case for the intermediate density.

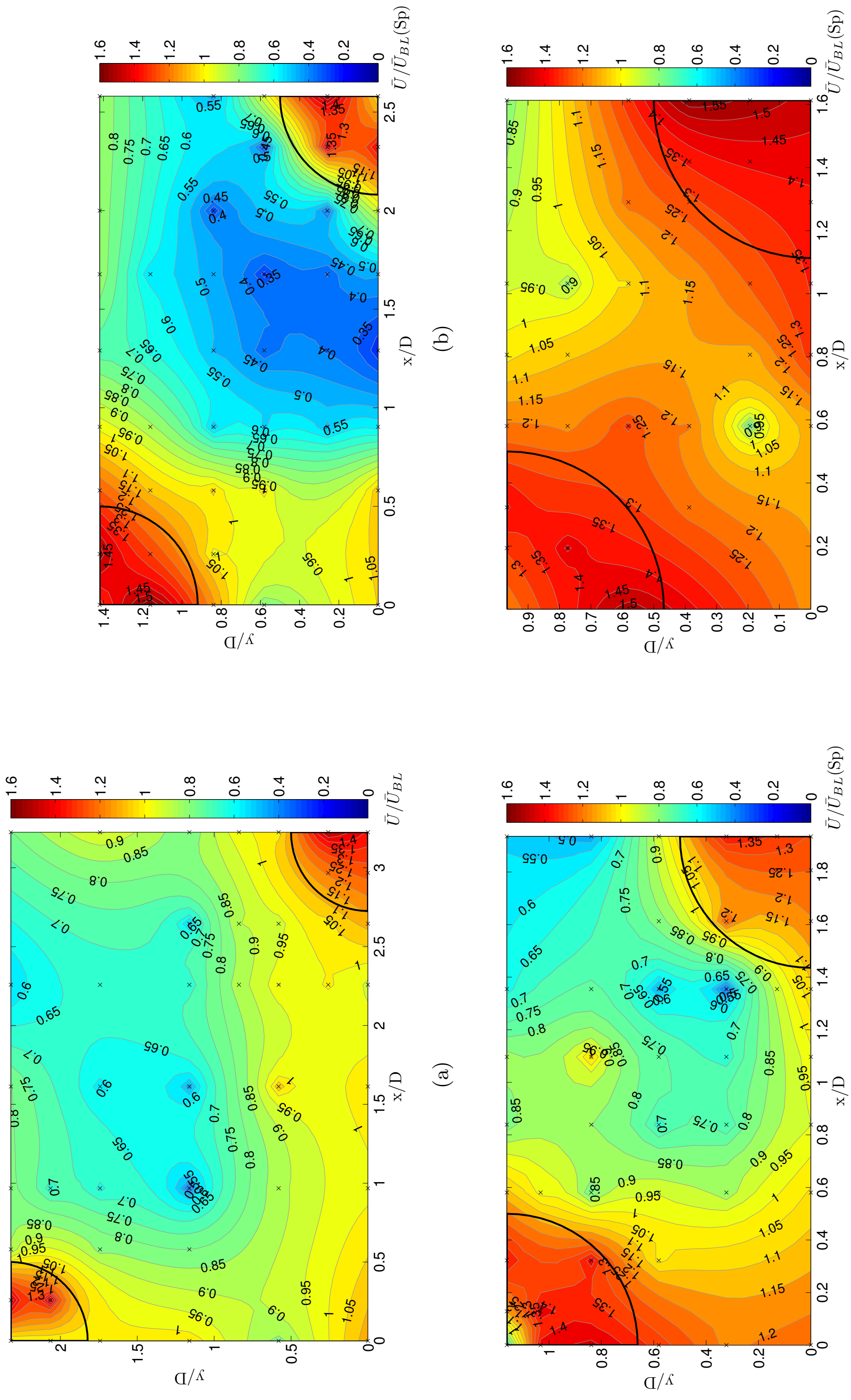

Figure 6.23. Plan view $(x-y)$ contour plot of depth-averaged streamwise velocities for the surface flow layer $(z/h>1)$ at a flow depth of 150mm for the boulder densities (a) Sparse, (b) Intermediate, (c) Dense and (d) Very dense. Velocities are normalised to the boulder layer average streamwise velocity for sparse density, $\bar{U}_{BL}(Sp)$, at a flow depth of 150mm

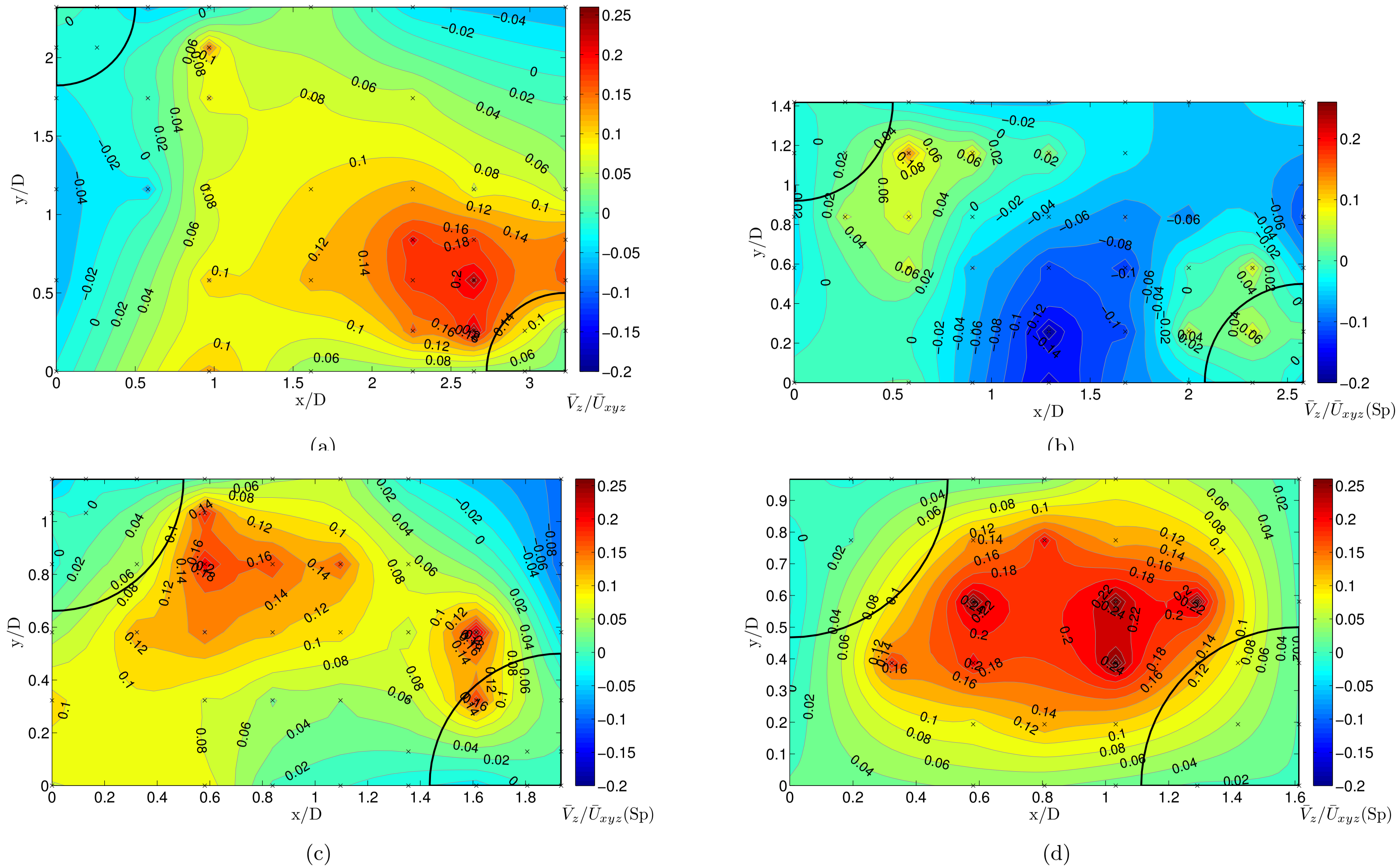

(a) (b) (c) (d)

Figure 6.24. Plan view $(x-y)$ contour plot of depth-averaged lateral (v) velocities at a flow depth of 150mm for the boulder densities (a) Sparse, (b) Intermediate, (c) Dense and (d) Very dense. Velocities are normalised to the globally-averaged streamwise velocity for sparse density, $\bar{U}_{xyz}(Sp)$, at a flow depth of 150mm. Direction of velocities follows the legend, with positive velocities indicating from bottom to top, and negative from top to bottom.

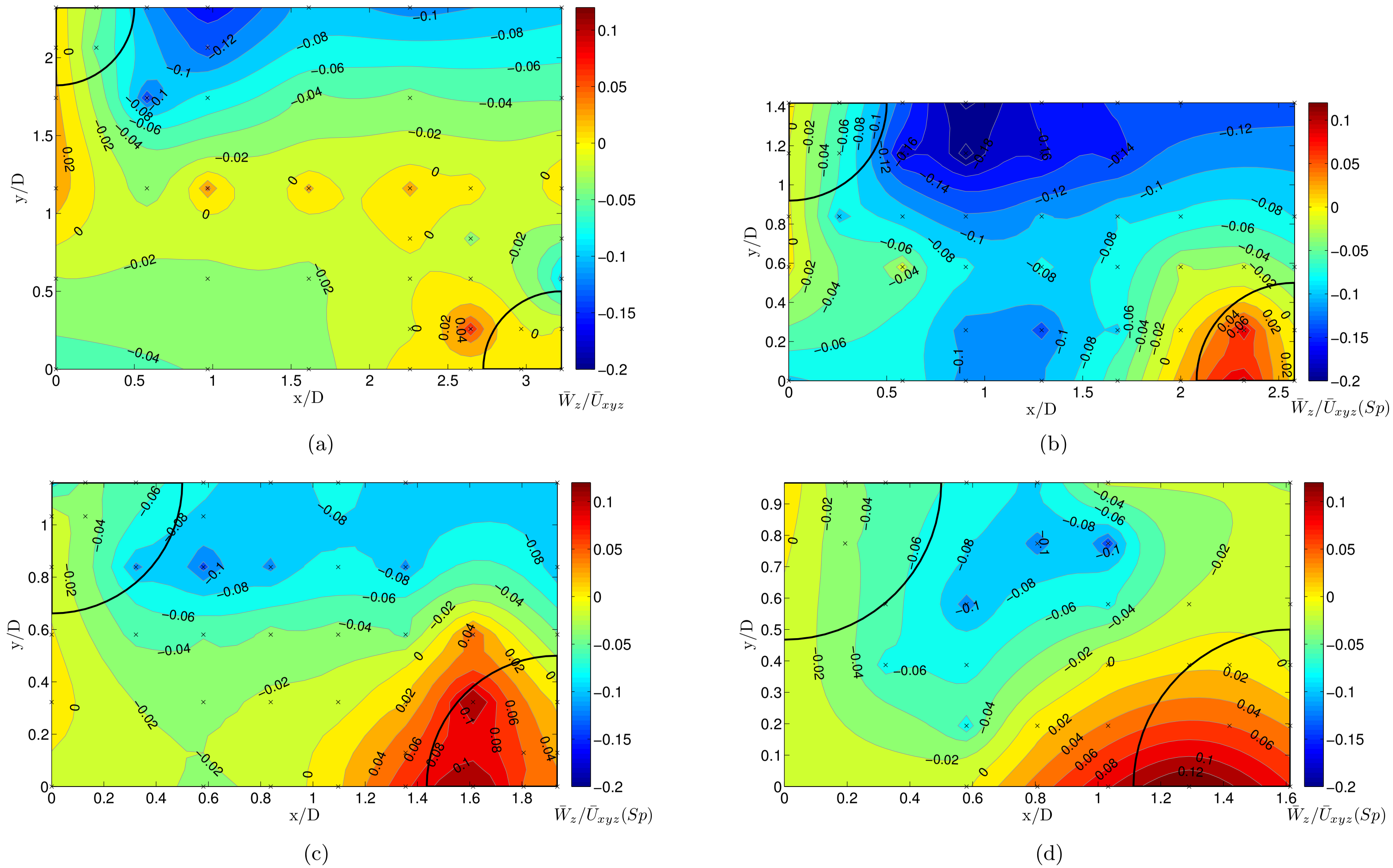

Figure 6.25. Plan view $(x-y)$ contour plot of depth-averaged vertical (w) velocities at a flow depth of 150mm for the boulder densities (a) Sparse, (b) Intermediate, (c) Dense and (d) Very dense. Velocities are normalised to the globally-averaged streamwise velocity for sparse density, $\bar{U}_{xyz}(Sp)$, at a flow depth of 150mm. Positive magnitude velocities indicate upward movement and negative indicates downward movement.

The strength of the vertical velocities in the wake at the intermediate density, in particular immediately behind the boulder, of up to 20% of the streamwise velocity indicate the dominance of the strong downward movement of the flow within this region. As the density increases the strength of the upward velocities over the front of the boulder increases, and the size of the region of high vertical velocities increases. This is accompanied with a decrease in the dominance of the downward motion of fluid particles in the wake region. It was thought that the shortening of the wake length was a result of the increased strength in the downward fluid motion over the boulder, however this is not shown in the depth-averaged profile. Examining Figure 6.18 confirms this and suggests that the strongest downward velocities behind the boulder are present at the intermediate density, which is confirmed by the depth-averaged profile. The depth-averaged profiles conform to the expected pattern due to the movement of the fluid over the boulder, suggesting that the secondary currents in the surface flow layer have little effect on the vertical velocities.

Figure 6.20 showed the difference in TKE between the boulder flow layer and surface flow layers, and therefore the two layers have been separated for the depth-averaged profile, so that the effect of the wake can be separated from the TKE associated with the secondary currents in the surface flow layer. Figures 6.26 and 6.27 present the boulder layer ($z/h < 1$) and surface layer ($z/h > 1$) depth-averaged contour plot of TKE respectively, for the four densities. The TKE was also normalised to the globally-averaged TKE for a flow depth of 150mm at the sparse density, $T\bar{K}E_{xyz}(Sp)$, for comparison. It would be expected that there is increased TKE magnitude in the wake region of the boulder. This is seen for the first three densities, with the magnitude of TKE increasing as the density increases, as well as the size of the region of increase magnitude. At the dense configuration, the increased TKE extends over the whole region between the boulders, but is highest at the downstream end point of the wake. At this density the downstream wake extended laterally, joining the dead-zone upstream of the boulder, and was found to be the greatest of all the densities, with the TKE profile exhibiting a similar pattern suggesting that the greater turbulence is associated with the interaction of the wakes. Examining the depth-averaged profiles of the three velocity components suggests that the high TKE region is associated with a gradient of cross-streamwise velocities where it changes from positive to negative. The higher magnitude of TKE at this density, and therefore momentum exchange, could be responsible for the lower than expected globally-averaged streamwise velocity. At the very dense configuration the TKE is consistent over the control volume, and is similar to the globally-averaged sparse TKE throughout.

The magnitude of TKE in the surface flow layer is much greater, where the maximum is four times that in the boulder layer flow; however at individual locations it can be seven or eight times greater. The TKE seen in the surface flow layer is associated with

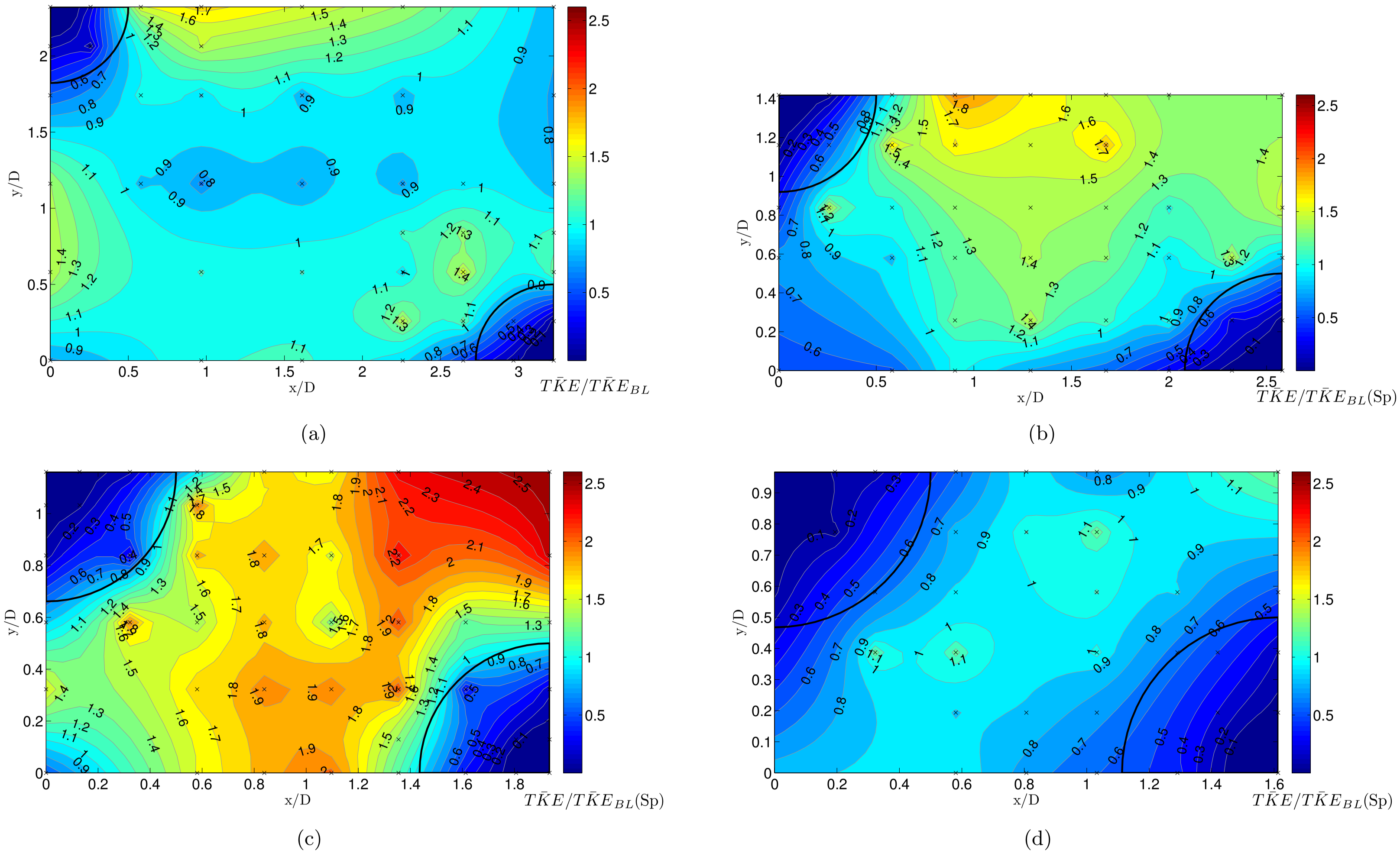

Figure 6.26. Plan view $(x-y)$ contour plot of boulder flow $(z/h<1)$ depth-averaged TKE at a flow depth of 150mm for the boulder densities (a) Sparse, (b) Intermediate, (c) Dense and (d) Very dense. Velocities are normalised to the globally-averaged TKE for sparse density, $T\bar{K}E_{xyz}(Sp)$, at a flow depth of 150mm.

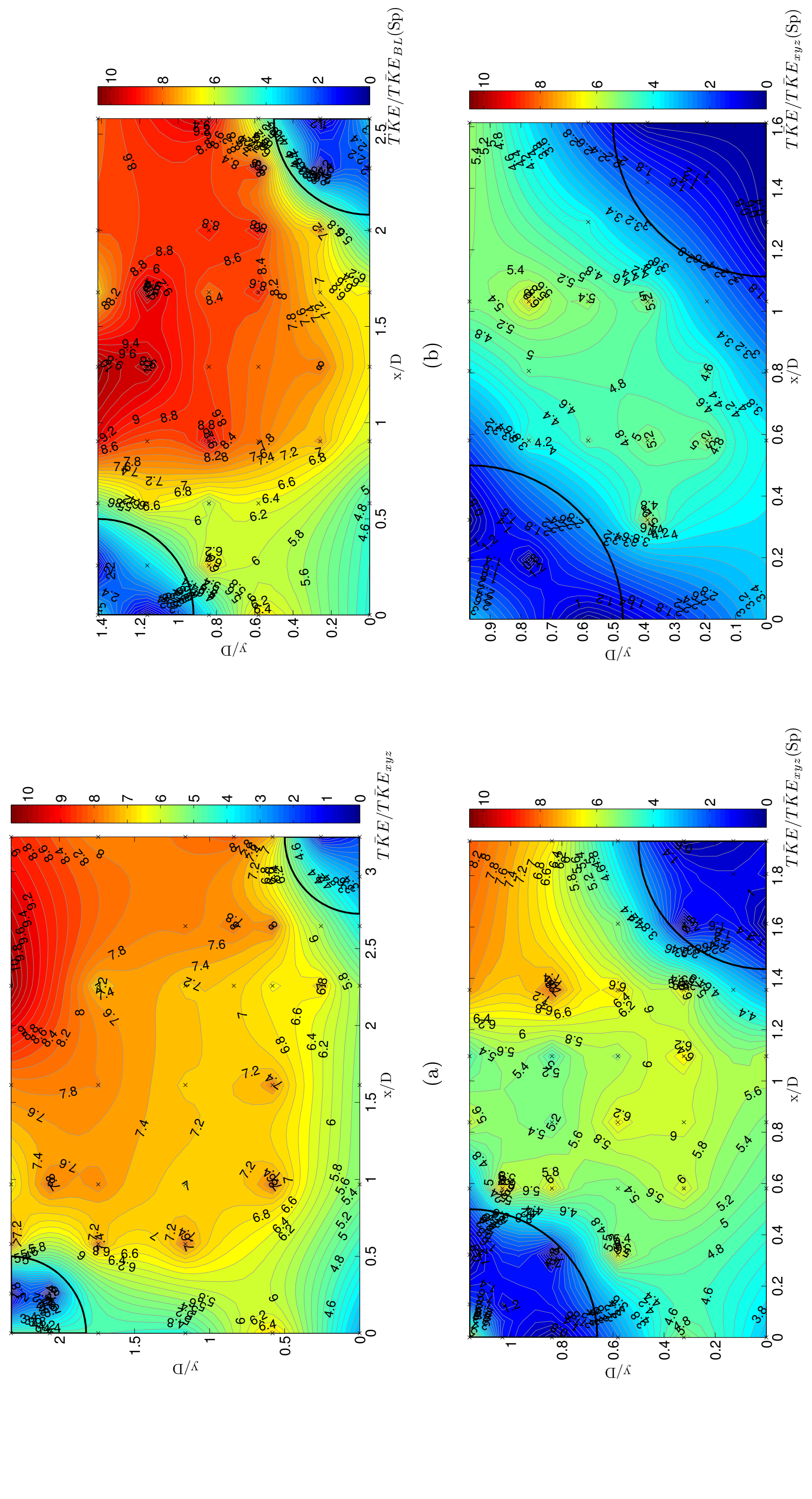

Figure 6.27. Plan view $(x - y)$ contour plot of surface layer $(z/h > 1)$ depth-averaged TKE at a flow depth of 150mm for the boulder densities (a) Sparse, (b) Intermediate, (c) Dense and (d) Very dense. Velocities are normalised to the globally-averaged TKE for sparse density $T\bar{K}E_{xyz}(Sp)$, at a flow depth of 150mm.

the free shear layer and secondary currents that were identified in Section 6.3.1, and the steep velocity gradients created by these. As has been suggested in the depth-averaged and spatially-averaged velocity profiles, these structures are strongest at the intermediate density, shown by the highest magnitude in TKE throughout the control volume. Again the lowest TKE is associated with the very dense density however the magnitude is still approximately five times that seen in the boulder layer.

This section has examined the effect of varying the longitudinal and lateral spacing of the boulders on the flow around the boulders and the size of the wake created at a constant flow depth of 150mm. A slight reduction in globally-averaged streamwise velocity was seen as the density increased which it was suggested was due to the blockage effect of increasing the number of boulders present. A number of flow features that were previously identified, were seen to be present in the spatially-averaged profiles, such as the upstream boundary layer, boulder wake, and secondary currents in the surface flow layer. The wake shortened with increased density and moved laterally to join the dead-zone upstream of the boulder face at the dense density, so that at this point the wakes of adjacent boulders were observed to be interacting. Interaction was seen at the highest density within the boulder layer flow, but not when the full measurement volume was considered. TKE increased in the boulder wake, and within the boulder layer flow was greatest at the dense configuration. The secondary currents identified in the surface flow layer, were seen to be dominant structures within the spatially and depth-averaged profiles, being strongest at the intermediate density. Therefore much greater TKE was present in the surface flow layer than the boulder flow layer. Although there was shortening of the wake, the area of wake in the control volume increased with increasing density, peaking at the dense density. The greatest wake at the dense configuration could be due to the lowest globally-averaged streamwise velocity associated with this density. Increased wake size was accompanied with increased lateral velocities as the flow was forced diagonally between the boulders, and increased velocities forcing the water over the top of the boulders. Quantifying the sizes of the wakes will be investigated in a later section.

6.3.5 Near-bed Turbulence Characteristics

As stated in Section 6.2, two point-specific methods based on the Reynolds stress and the TKE, were used to calculate the shear stress near the bed in order to examine the near-bed turbulence characteristics within the control volume. These were calculated using the measurements closest to the bed, and therefore represent the shear stress located 4mm above the bed. A comparison of the change in the near-bed turbulence with boulder density is presented in Figure 6.28 for the Reynolds stress method, and in Figure 6.29 for the TKE method. The global bed shear stress (Eq. (2.15)) was calculated as a comparison, gives a value of 1.176 N m^{-2}. Comparing this to the values presented in Figure 6.28 and Figure 6.29 shows that the local measurements of shear stress near the bed using both methods are much larger than the global value, in particular the TKE method has generated values upto 40 times greater. This suggests using these methods at these heigh are not good predictors of the bed shear stress, but can be used to evaluate the local shear stress near the bed.

As the density increases, the region of zero Reynolds shear stress that is immediately upstream of the boulder increases in size as a region of negative shear stress moves further upstream. The maximum near-bed shear stresses over the control volume are seen at the intermediate density. The region of high shear stress is associated with increased streamwise velocities at the bed, positive cross-streamwise velocities and negative vertical velocities. A region of high shear stress is also seen at the highest density, this is located at the intersection between negative and positive streamwise velocities and where downwards vertical velocities are present. The distribution of shear stress based on the TKE method is different (see Figure 6.29). At the sparse density the majority of the control volume has low shear stress near the bed, apart from a region upstream of the boulder, forming a steep gradient in the shear stress immediately upstream of this boulder. The strength of this gradient reduces as the density increases, but is at its lowest at the dense density where the shear stress over the full control volume is low. As with the Reynolds stress method, the highest stress shear using TKE method was seen at the intermediate density; however the region of high shear stress is related to the region in the boulder wake.

The retention of leaves was seen to occur on the upstream face of boulders. It is therefore proposed that the shear stress in this region might be linked to the retention of leaves. To investigate this proposed link, two regions were defined upstream of the boulder. These regions are rectangles that sit immediately upstream of the boulder, extending for the full diameter of the boulder laterally, and for a longitudinal length upstream of the boulder of 0.25D and 0.1D. These regions are designed to represent the possible retention locations of the boulders. For each boulder density, the spatially-averaged shear stress (using both methods) for the two different sized rectangles were calculated. Figure 6.30 shows the spatially-averaged shear stress based on both methods against the boulder volume fraction, for the two region sizes.

The two shear stress methods show the opposite relationship. The Reynolds stress method suggests that the shear stress increases, in fact changing from negative to positive, with increasing boulder volume fraction. It is possible that this change could be related to the presence of a horseshoe vortex upstream of the boulder, and the change in near-bed shear stress may relate to the strength or size of this vortex. The size of the upstream

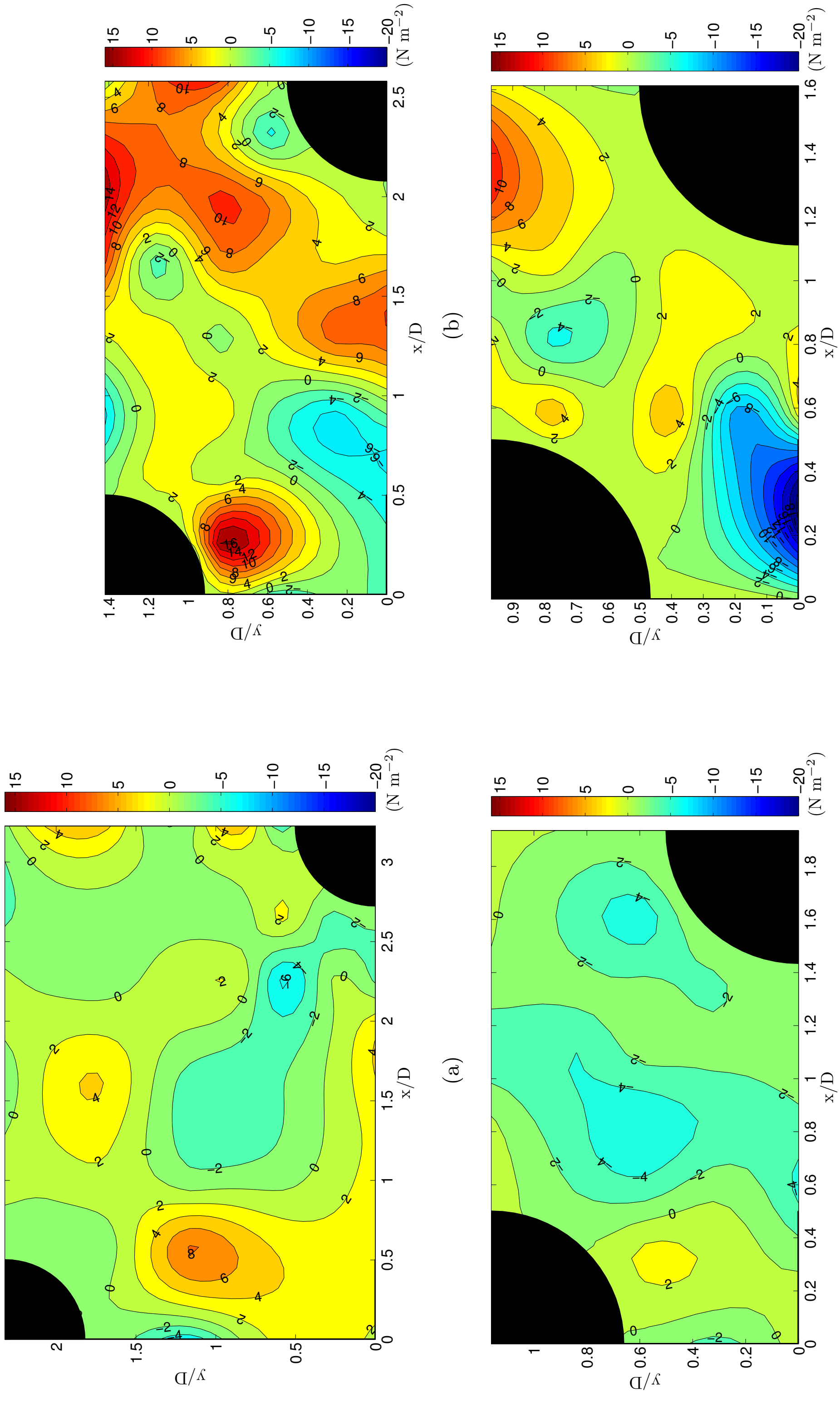

Figure 6.28. Plan view $(x-y)$ contour plot of the near-bed shear stress using the Reynolds stress method at the flow depth of 150mm for the boulder densities (a) Sparse, (b) Intermediate, (c) Dense and (d) Very Dense.

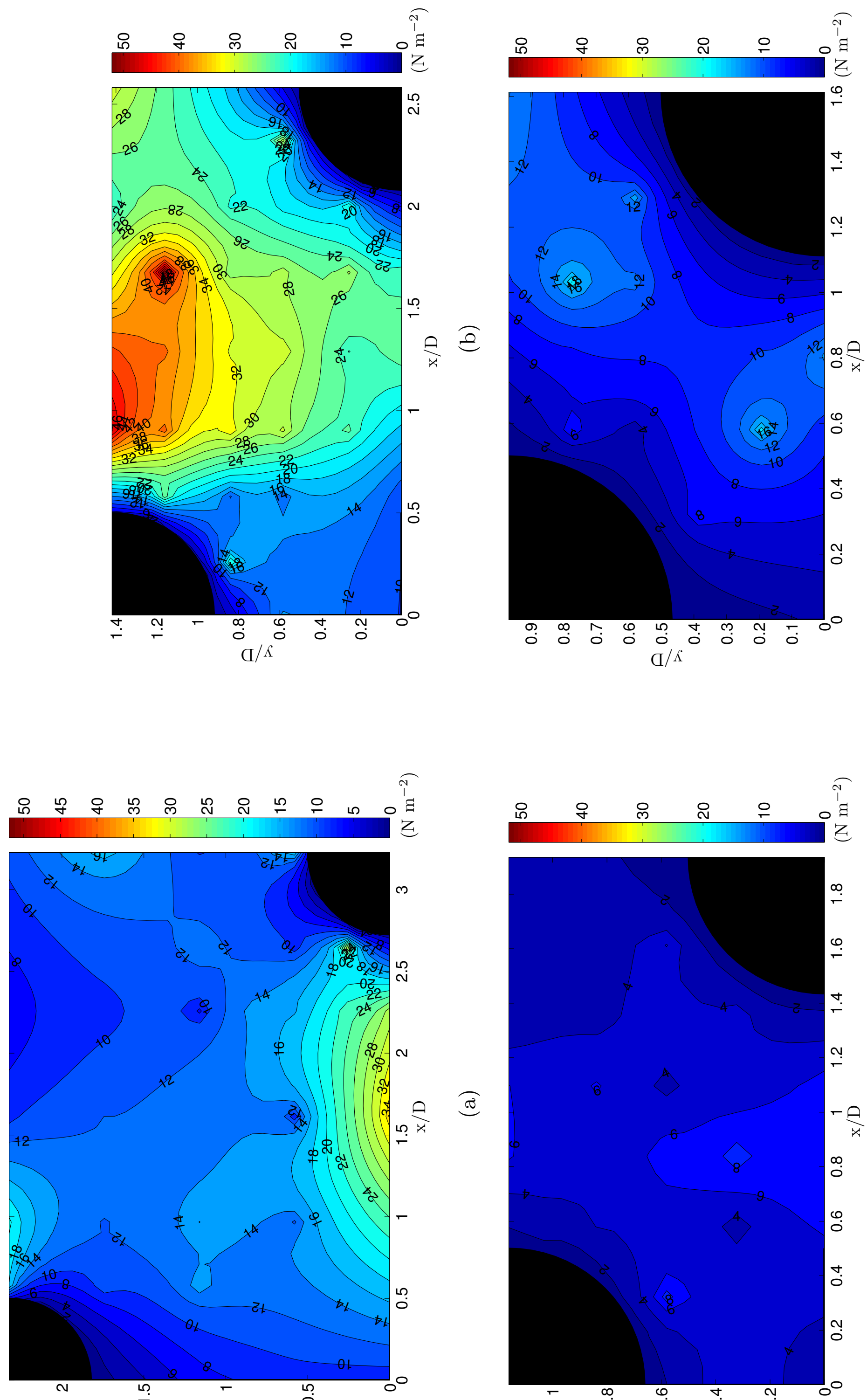

Figure 6.29. Plan view $(x - y)$ contour plot of the near-bed shear stress using the TKE method at the flow depth of 150mm for the boulder densities (a) Sparse, (b) Intermediate, (c) Dense and (d) Very Dense.

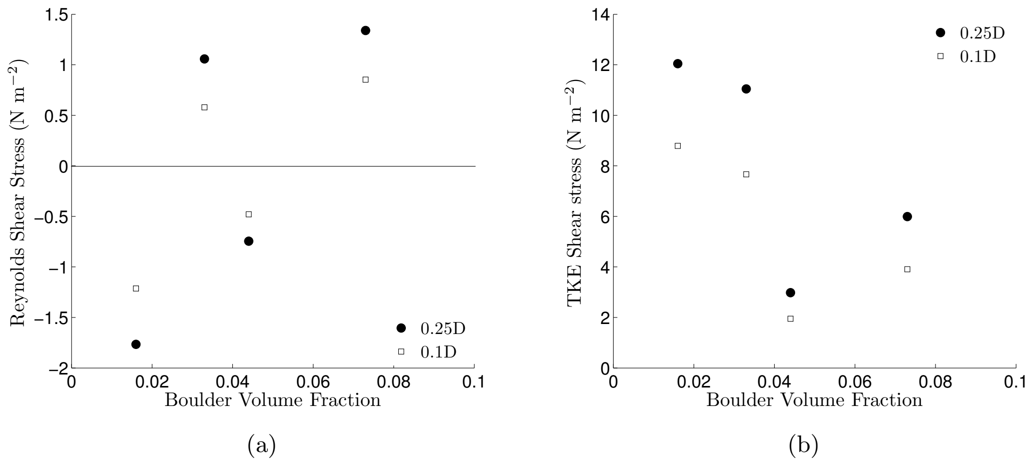

Figure 6.30. Plots of spatially-averaged near-bed shear stress against Boulder Volume Fraction for two region sizes upstream of the boulder ($0.25D \times D$ and $0.1D \times D$), using the two methods (a) the Reynolds stress and (b) the TKE method.

deadzone was seen to correspond to the estimated size of the horseshoe vortex in Section 6.3.1. However, examining Figure 6.18 does not suggest a relationship between the size of the upstream zone, and therefore inferred horseshoe vortex, and the shear stress near the bed based on the Reynolds stress method. For example, the greatest deadzone is observed at the dense configuration which does not correspond to the greatest magnitude of shear stress. However the spatially-averaged shear stress based on the TKE method decreases with increase in boulder volume fraction. For both methods the magnitude of spatially-averaged shear stress is smaller when considering the smaller region, which would be expected at this region considers stresses closer to the boulder. The link between these calculated values and retention will be discussed in Chapter 6.4.

This section has investigated the change in near-bed turbulence characteristics with boulder density, by examining the shear stress at 4mm above the bed using two point-specific methods. A lot of variation was seen between the two methods, and between the different densities. Generally shear stress values over the control volume were low, with isolated regions of higher shear stress. No clear patterns associated with change in density could be identified. However it is suggested that the magnitude or gradient of the shear stress immediately upstream of the boulder could be important in retention of leaves. The defining of regions upstream of the boulder to investigate this suggested different patterns for the two methods, with the Reynolds stress method showing a change from negative to positive, therefore an increase in shear stress with increasing boulder volume fraction. However, the TKE method indicates a decrease in the near-bed shear stress with increasing boulder volume fraction. The impact on leaf retention will be discussed in the next Chapter.

6.3.6 Wake Size

Nepf et al. (1997) suggested that the proportion of the flow that is considered to be in the wake zone affects the lateral dispersal characteristics of the flow field. Therefore it can be proposed that since wake zones trap solutes and contaminants they could also affect the ability of a stream to retain leaves. Two definitions were used to define the wake; (1) the time-averaged velocity defined wake, where the wake is defined as the region where streamwise velocities are 90% or less than the free stream velocity, and (2) the turbulence intensity defined wake where the turbulence intensity is within 10% of the free steam velocity; this definition is based on the one used by Zavistoski (1994) and Nepf et al. (1997). As previously stated, the globally-averaged streamwise velocity at the sparse density for the appropriate flow depth will be used in place of the free stream velocity.

Nepf et al. (1997) used the second wake definition to calculate a Wake Area Fraction (WAF) for randomly placed cylinders, which were used to represent emergent vegetation. The WAF is a two-dimensional measure of the wake area relative to the control volume area, which makes use of the depth-averaged profile. However, the previous sections have shown the three-dimensional nature of the flow suggesting that it is more applicable to calculate a Wake Volume Fraction (WVF). Wake volume fractions were investigated by Huthoff (2009), who coined the phrase 'wake filling factor'.

Secondary currents, and associated reduced streamwise velocities, have been shown to be dominant in the surface flow layer. Therefore, in order to isolate the boulder wake, the above methods will only be applied to the boulder flow layer ($z/h < 1$). Wake volume fractions were calculated by applying the thresholds of the two methods to the velocity and turbulence intensity measurements throughout the boulder layer. The volume of the wake was calculated relative to the control volume up to a relative height of 1. Figure 6.31 shows how the WVF varies with Boulder Volume Fraction (BVF), for the two methods; time-averaged velocity defined wake, and turbulence intensity defined wake, comparing between boulder submergence for the sparse density (Figure 6.31(a)) and boulder density for the 150mm flow depth (Figure 6.31(b)) separately.

Both figures show that the turbulence intensity method calculates much larger and consistent wake sizes than using the time-averaged velocity. There is a slight decrease in the wake size with increased density. However this is negligible and therefore this method suggests that the wake size is not affected by the boulder density or the flow depth. This is unlikely, as relationships between increase in obstacle density and increased wake size, have been reported (Nepf et al., 1997; Canovaro and Francalanci, 2008; Huthoff, 2009), suggesting that this method is reliant on averaging of the turbulence intensity over depth in

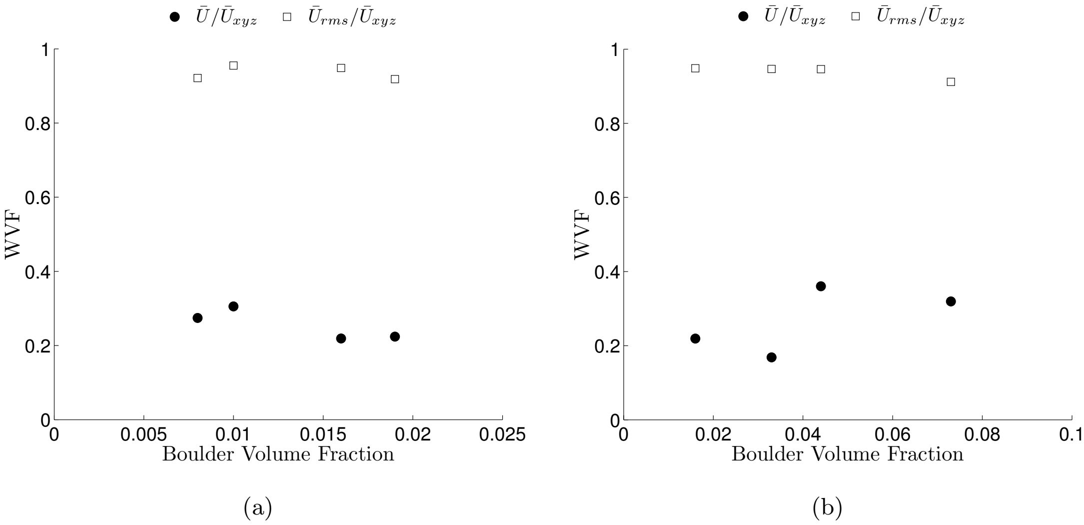

Figure 6.31. Wake volume fraction (WVF) calculated using two methods against the Boulder Volume Fraction comparing between (a) boulder submergence and (b) boulder density. Note the different x-axis scales.

order to produce a reliable estimate of the wake size. The time-averaged velocity method, however, produces more realistic estimates of the wake size. Comparing the change in WVF with boulder submergences suggests a general trend where an increase in boulder submergence results in a greater wake volume. This could be an artefact of the different velocities present at each flow depth due to the constant discharge, however efforts were made to remove this effect by using the globally-averaged streamwise velocity for each flow depth. A lot of variation is seen in the WVF values for the different boulder densities, making it not possible to determine a distinct relationship. However, there does appear to be an increase in the WVF with increase in boulder density.

Nepf et al. (1997) fitted an exponential model to the relationship between the stem area fraction and the wake area fraction, where the constant, M, represented the wake ratio (the area of wake relative to the area of the obstacle). It was suggested in previous sections that the two-dimensional wake size was been 2.73 and 4.83 at the sparse density for the 150mm flow depth. This same model was applied to the boulder volume fraction to WVF relationship, however, a fit could not be obtained.

The variation in the wake size over height was analysed by applying the thresholding for the two methods; time-averaged defined wake and turbulence intensity defined wake, and calculating the area of the wake relative to the area of the control volume at each height within the measurement profile. Comparisons between flow depths for the sparse density and between boulder densities at the 150mm flow depth for each method are presented in Figure 6.32.

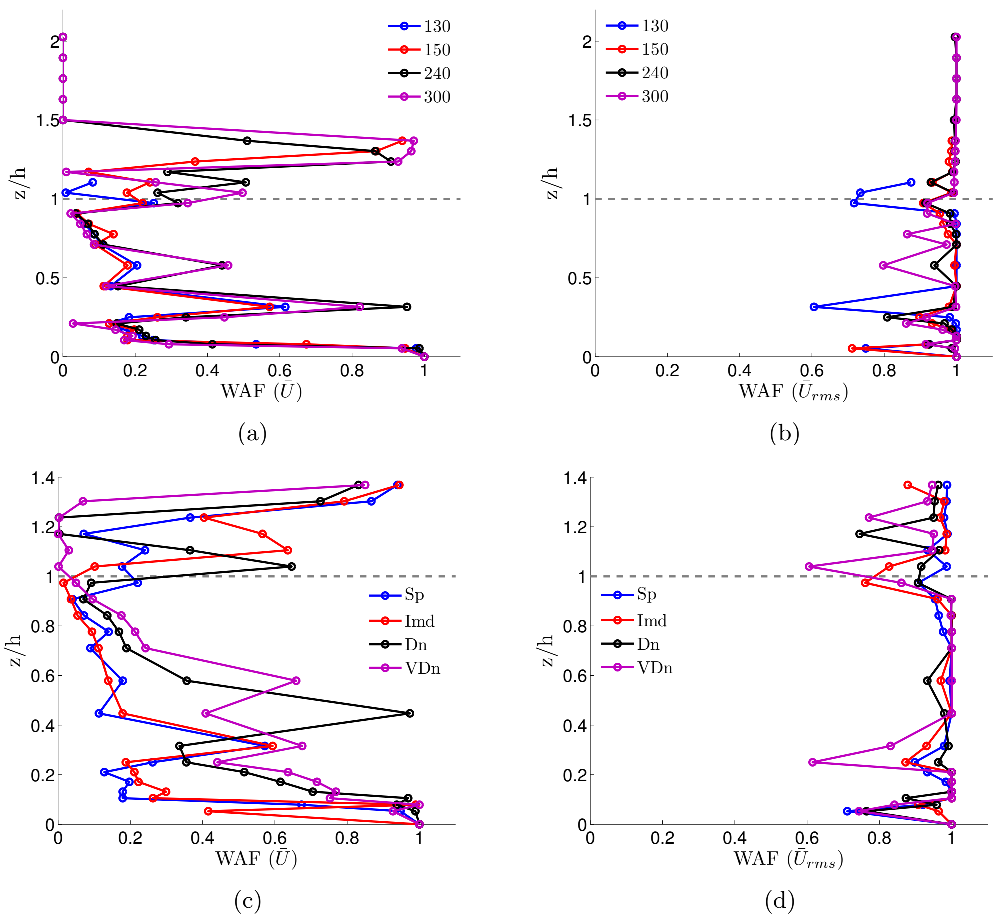

Figure 6.32. Wake Area Fraction calculated for each relative height (z/h) using two methods (a,c) $\leq$ 0.9 of streamwise u velocities normalised to the globally-averaged velocity and (b,d) $\leq$ 0.9 and $\geq$ 1.1 of the $Urms$ normalised to the globally-averaged streamwise velocity, comparing between (a,b) flow depths and (c,d) boulder densities, .

There is good agreement between the different flow depths, in particular when using the time-averaged velocity method (Figure 6.32(a)). There is a general trend of a decrease in WAF with increasing height from the bed. A number of peaks are present associated with structures that were identified in Section 6.3.1; the boundary layer (z/h <0.1), the boulder wake (z/h ≈0.4) within the boulder flow layer, and the free shear layer (z/h ≈1.1) and secondary currents (z/h ≈1.4) present in the surface flow layer. The wake can be seen to be associated with two peaks in the WAF profile, the first at a relative height of 0.4, and the second at approximately 0.6. The presence of the velocity deficit responsible for the latter peak was illustrated in Section 6.3.1, Figure 6.3(a) and is more easily seen in the schematic Figure 6.9 where the wake at this height extends all the way to the boundary of the control volume.

Comparing between the boulders densities shows that there is the same general trend as seen with the flow depths, where the WAF decreases with height over the bed. In the boulder flow layer, the highest WAF at each height is predominantly at the very dense density and the lowest is associated with the sparse density. This would be expected as the calculated WVF for the boulder flow layer exhibited a general trend of increasing with increase in density for the flow depth of 150mm. As with comparing the flow depths a number of structures that were previously identified are indicated by increases in the WAF at that height. Within the boulder layer the presence of the boundary layer and the boulder wake are visible, but less distinct than for comparing flow depth. As seen in the spatially averaged velocity profile (Figure 6.17), the peak associated with the wake for the dense density is significantly higher than the other densities. This could be due to the lower than expected globally-averaged streamwise velocity compared to the other densities. As when comparing the flow depths the very dense density has two peaks (z/h=0.4 and 0.6) associated with the boulder wake, but only one is seen at the other densities.

In the surface flow layer there is greater variation between the densities. At the very dense density there is minimal wake present in this layer apart from the single peak at a relative height of 1.4. This peak is associated with the secondary currents that were identified at this height, which were characterised by negative and reduced streamwise velocities, therefore generating a large WAF. This peak in WAF is present at all the densities. The intermediate density predominantly has the greatest WAF in the surface flow layer. At this density and the dense density there is another peak located just above the top of the boulder. These are related to the free shear layer that was identified downstream of the boulder crest, that was shown in Figure 6.3. Examining Figures 6.32(b) and 6.32(d), which show the turbulence intensity method of calculating WAF over height, illustrates why the WVF's were found to be extremely high, and not variable between the different depths and densities. There is a degree of consistency between the different flow depths, with the majority of heights having a WAF of 1.

This section has investigated how the area and volume of the wake varies with the boulder volume fraction and height for the different combinations of flow depth and boulder density. Two methods were used to define the wake; the time-averaged velocity method and the turbulence intensity method. The turbulence intensity was shown to be a poor estimator of wake size. Variation was seen in the WVF with boulder volume fraction, with a general trend of a increase in wake with increase in boulder submergence and density. Examining the WAF over height showed consistency between the different flow depths for the same density, but significant variation between the different densities for the same flow depth. Artefacts of the flow that were seen in the spatially-averaged velocity profiles were seen in the WAF profile, with a general trend of decreased wake size with increasing height.

6.4 Linking Hydraulics and Ecology

Applying the finding of the previous sections to the patterns of retention exhibited in Chapter 5 allows possible mechanisms of retentions to be suggested. A number of parameters have been calculated within this Chapter to describe the flow conditions for each of the configurations. However, leaf retention experiments were only carried out at three of the four densities, and velocity measurements were only taken at flow depth of 150mm for three densities. Therefore the conclusions of Chapters 5 can only be compared to the results of this chapter for four flow depths at the sparse density, and three densities (sparse, intermediate and dense) for a flow depth of 150mm.

A number of structures were identified within the flow structure (Section 6.3.1); a dead-zone upstream of the boulder, a wake and recirculation zone downstream of the boulder, a free-shear layer generated from the crest of the boulder and secondary currents in the surface flow layer. The secondary currents present within the surface flow layer were found to be the most dominant at the intermediate density, which also corresponds to the density of greatest retention. It is possible that retention could be affected by the surface layer flow however visual observation of the leaves observed them to travel more in the boulder layer flow, due to the decreased buoyancy. It was also suggested that the flow structure changed between the intermediate and dense density from where the boulders were acting in isolation, to wake-interfering flow. The increase in density was also associated with increased vertical and cross-streamwise velocities within the boulder layer. The change in flow structure could be responsible for the decrease in retention at the dense density, suggesting that retention might increase with the increase in the presence of boulders as long as they are acting in isolation, but when the density becomes such that they begin to interact the retention decreases again.

Two measures of retention calculated in Chapter 5 will be used to compared to the parameters calculated in the previous sections, firstly the retention efficiency per boulder, which removes the effect of increased boulder number isolating the effects of the boulder array and secondly, the retention coefficient as this allows the retention characteristic of the configuration, rather than the absolute retention, to be examined. It was suggested in Chapter 5 that the area mean velocity negatively affected leaf retention, however the analysis of the globally-averaged streamwise velocities showed them to be significantly lower than the $\bar{U}_{Blockage}$ for each of the flow depths and to vary between the different boulder densities. A negative relationship was identified between the $\bar{U}_{Blockage}$ and retention, but this relationship was only significant when the density was also considered. As the globally-averaged streamwise velocities were significantly different it would be prudent to examine the relationship of this parameter to retention. Figure 6.33 presents the the

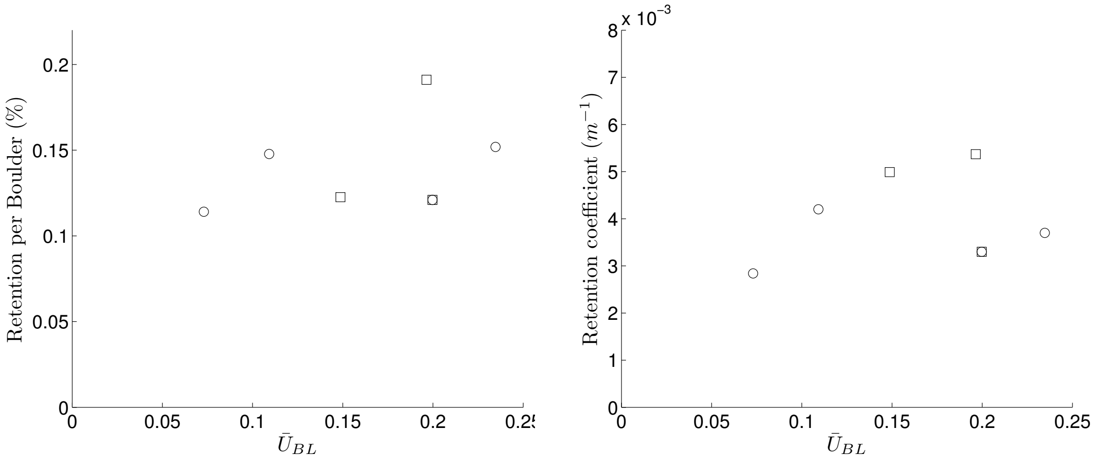

(a) (b)

Figure 6.33. Variation in retention defined by (a) the retention efficiency per boulder and (b) the retention coefficient k_R, with the boulder layer globally-averaged streamwise velocity $\bar{U}_{BL}$. The circles represent the points related to change in boulder submergence and the squares represent the change in boulder density.

variation in retention, using the two measures, with the boulder layer globally-averaged streamwise velocity.

Neither graph exhibits a definitive relationship. It can be suggested that retention may increase with increased boulder layer averaged velocity, however this is contradictory to the relationship exhibited with the area mean velocity and the reported relationship to discharge. The retention coefficient, suggests that a limiting relationship seems to be present, where an increase is seen until a maximum is reached, with the rate of increase decreasing as it gets closer to the maximum.

Chapter 5 suggested that the interaction between the boulders as the density increased initially aided retention and then, as the density increased further, a negative effect was induced, resulting in an optimum density for retention at the intermediate density. The wake volume fraction can be used as a measure of the interaction between the boulders within an array, and therefore might be able to describe the variation seen in retention. This comparison is given in Figure 6.34. Again a relationship between the WVF and the retention per boulder is not explicitly visible, although it could be suggested that there is a decrease in retention with increase in WVF. However, there does seem to be a relationship between the WVF and the retention coefficient. Initially the increase in WVF results in a decrease in the retention coefficient, reaching a minimum, after which the retention coefficient increases with further increase in the WVF. It was possible to fit a quadratic relationship to these data (R^2=83.9%);

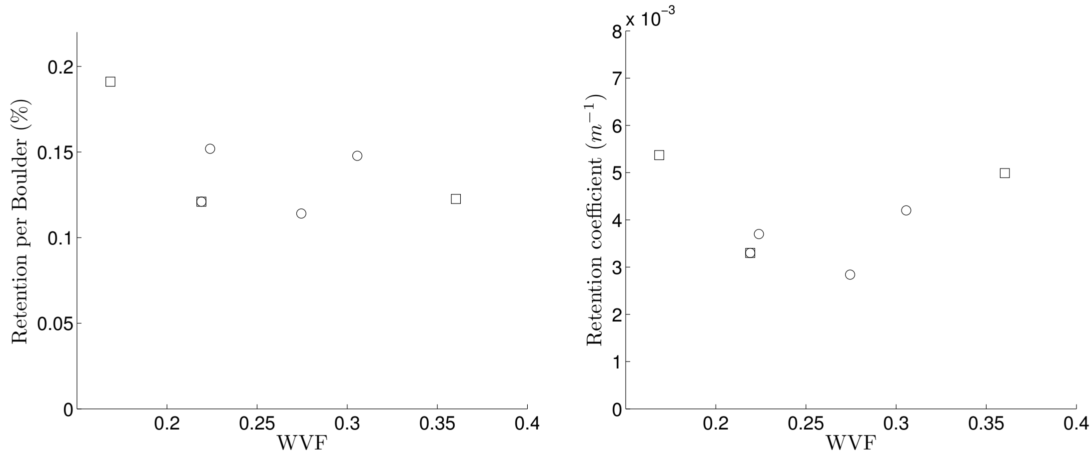

Figure 6.34. Variation in retention defined by (a) the retention efficiency per boulder and (b) the retention coefficient k_R, with the Wake Volume Fraction. The circles represent the points related to change in boulder submergence and the squares represent the change in boulder density.

$$k = 0.2259WVF^2 - 0.1192WVF + 0.0188 \tag{6.8}$$

This relationship suggests that the WVF where retention is least is 0.26. This relationship of a minimum retention at a given WVF is in contrast to the optimum density for retention, however no relationship between WVF and BVF was identified in Section 6.3.6. A reason for this relationship can not be suggested at present.

The presence and size of the wake would not be expected to be directly related to the retention of leaves, due to the wake being generated downstream of the boulder whereas the leaves were retained on the upstream face of the boulders. However the size of the wake is an indicator of the velocity field present and represents a region of reduced velocities. An increase in discharge and therefore velocity has been seen to negatively affect retention. Therefore it could be proposed that an increase in wake size, which represents a decrease in the velocities present within the boulder layer, would increase the retention.

Due to the leaves being retained on the upstream face of the boulder, it was suggested that the near-bed shear stress in this region might affect the ability for leaves to be retained. Two regions of different sizes were defined and spatially-averaged shear stress values were calculated for each of the region sizes and methods of calculating the shear stress near the bed (Figure 6.35). The relationship between retention and near-bed turbulence characteristics is very different for the two methods used. The TKE method appears to suggest that retention increases with increased shear stress for one measure of retention, but de-

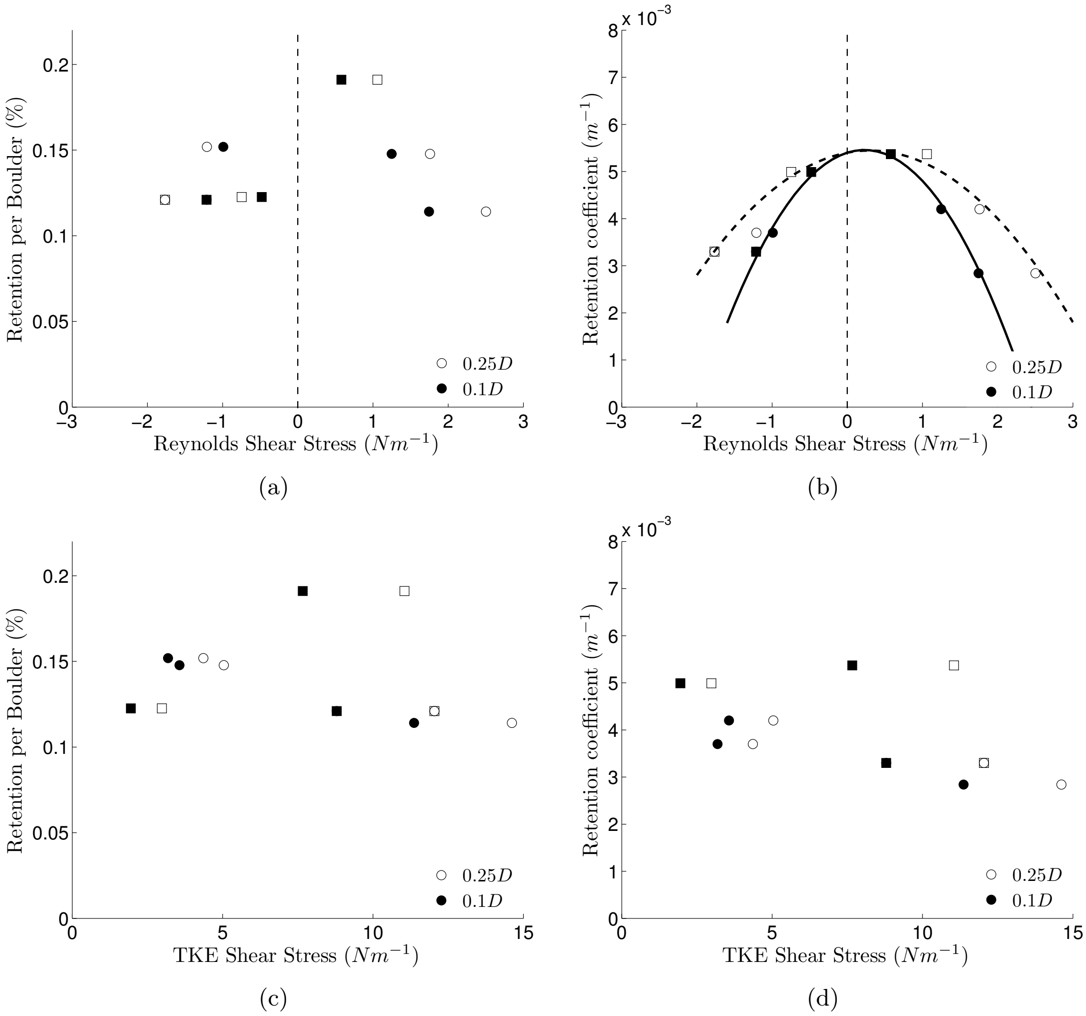

Figure 6.35. Variation in retention defined by (a,c) the retention efficiency per boulder and (b,d) the retention coefficient k_R, with the spatially-averaged bed shear stress calculated using the (a,b) Reynolds stress method and the (c,d) TKE method for two region sizes. The circles represent the points related to change in boulder submergence and the squares represent the change in boulder density.

creases with increased shear stress for the other. However, the Reynolds shear stress does appear to show a relationship with both measures of retention. Retention increases as the near-bed shear stress nears zero, with large positive and negative shear stresses reducing the retentive ability. A quadratic relationship can also be fitted to these relationships, in particular related to the retention coefficient for both regions, giving $R-sq$ of 99.1% and 92.5% for the $0.1D$ and $0.25D$ regions respectively. The distribution was wider for the larger region size as would be expected, however the relationship for the two regions had the same intercept and maximum, suggesting that this relationship has promise.

Drawing together the conclusions of Chapter 5 and with the results of this chapter allows possible mechanisms of leaf retention to be proposed. Maximum retention was present under isolated boulder flow conditions, where the wakes of adjacent boulders were distinct from each other. The change in condition to wake-interacting flow was associated with a decrease in retention suggesting that the interaction of the wake and dead-zone of adjacent boulders has a negative effect on retention. Comparison of the variation in retention with WVF suggested a value at which retention was at a minimum, with it increasing either side of this. For both this and an optimum density for retention to be true, a negative relationship would have to exist between WVF and BAF or BVF, which is unlikely as the WAF has been shown to increase towards one as the BAF increases (Nepf et al., 1997). The most promising explanation of retention is the local near-bed shear stress present upstream of the boulder in the leaf retention region. A strong relationship suggested that retention was greatest when the near-bed shear stress in that region was approximately zero and that both negative and positive shear stresses resulted in a reduction in retention.

6.5 Summary

Large protrusions, which are associated with gravel bed rivers, are important factors in describing the spatial distribution of ecology factors within a stream. The presence of protrusions affects properties of the flow such as velocities and the distribution of turbulence. These in turn have an effect on important processes such as particle interactions, and therefore, from an ecological point of view, predator-prey relationships (Lacey and Nikora, 2008), nutrient dispersal, niches for invertebrates (Hart et al., 1996) and resting regions for fish (Shamloo et al., 2001). The previous chapter suggested that characteristics related to the flow around the boulders may be able to explain the variation seen in retention at different boulder submergences and densities. This chapter presented a series of experiments that investigated how the flow around the boulders varied between four boulder submergences, and four boulder densities. Detailed velocity measurements were taken throughout a control volume, to allow full characterisation of changes in velocities and turbulence due to the boulders.

Previous research has characterised the formation of coherent structures as the result of different two-dimensional and three-dimensional obstacles, such as dunes, cylinders, and hemispheres, within the flow (e.g. Savory and Toy, 1986; Acarlar and Smith, 1987; Douglas et al., 2001; Stoesser et al., 2008). Approaching the boulder, a boundary layer was identified along with the presence of a dead-zone and stagnation point on the upstream boulder face. The size of the dead-zone was found to correspond to reported sizes of horseshoe vortices, which along with flow visualisation suggested its presence immediately upstream of the boulder. Downstream of the boulder a wake was characterised by a velocity deficit, which contained a recirculation zone of negative streamwise velocities. In the surface flow layer, a free shear layer was identified downstream of the boulder crest, and secondary currents characterised by reduced and negative streamwise velocities and strong cross-streamwise velocities were identified at the top of the measurement volume, ($z/h \approx$1.35).

Velocity components, TKE, turbulence intensities and near bed turbulence characteristics have been used to describe any variation present due to changes in the boulder submergence and density. The spatially-averaged profiles for all configurations showed the presence of the identified structures, indicating the dominance of these regions within the control volume. The close similarity between the spatially-averaged profiles for the different flow depths showed the consistency and repeatability of the results. The similarity between the profiles also showed that the coherent structures were not affected by flow depth. The greatest velocity deficit was associated with the secondary currents in the surface flow layer, illustrating the size, strength and extent over the control volume. The depth-averaged velocities showed that the wake shortened and increased laterally as the flow depth increased when considering only the boulder flow layer. Increased TKE was seen in the wake for the lower flow depths, but the extent was diminished with increase in flow depth due to the increasing depth of the surface flow layer.

The spatially-averaged profiles for the four densities showed a slight reduction with increase in density due to the blockage effect of increased boulders. Greater variation in the signatures of the identified structures in the profiles were seen between the densities, showing that the increase in density has an effect on the formation of these structures. The free shear layer located downstream of the boulder crest was not present at the very dense density and was found to be most pronounced at the sparse density, showing that that the increase in density reduced the formation of this structure. The depth-averaged velocities showed that as with the flow depth, the wake was seen to shorten and widen laterally with increased densities, leading to the interaction of adjacent wakes at the highest two densities, when considering the boulder flow layer. The greatest wake was seen at the dense configuration, due to the lowest globally-averaged streamwise velocity. The secondary currents within the surface flow layer were the most dominant structures within the control volume, illustrated by the greatest velocity deficit in the spatially-averaged profiles and the highest TKE values. These currents were most pronounced in the intermediate density. The TKE was increased in the boulder wake, and was again greatest at the dense configuration, when considering just the boulder flow layer. The increase in density was also associated with increased cross-streamwise and vertical velocities as the water is forced around the boulders.

Calculation of the near-bed shear stress using two methods showed great variation between the different densities, with predominantly low values over the area of the control volume, and isolated high stress regions, with no discernible pattern. A spatially-averaged shear stress near the bed was calculated for both methods for a defined region immediately upstream of the boulder, illustrating the proposed region of leaf retention. The Reynolds stress method suggested an increase in shear stress with increasing boulder volume fraction, however the TKE method suggests a decrease with increasing boulder volume fraction.

Wake volume fractions were calculated, using two methods for the boulder flow layer. The turbulence intensity method produced poor estimates of the wake size. The time-averaged velocity method showed variable results, however there was a general trend of an increase in wake size with increase in flow depth and boulder density. Consistency was seen between the flow depths when considering the WAF over height, however much greater variation was seen between the four densities. As with the spatially-averaged velocity profiles, the identified structures were visible in the WAF profiles, with a general trend of decreasing wake size with height.

A number of factors have been identified that have allowed the comparison of the effect of boulder submergence and boulder density on the flow structure around an array of boulders. Little variation was seen in the flow structure with change in flow depth, and the similarities showed good consistency in the results. Increase in boulder density was associated with increased wake size, increased turbulence within the boulder flow layer and increased time-averaged lateral and vertical velocities, suggesting that the flow structure changed as the density of the array increased. The sparse and intermediate densities exhibited isolated boulder flow, changing to wake-interacting flow at the dense and very dense setups.

The characterisation of the flow structure and the calculated parameters were applied to two measures of retention that were presented Chapter 5 in order to identify a possible mechanism of retention. Both the globally-averaged streamwise velocity within the boulder layer, and the WVF were poor predictors of retention, with no definitive relationships being suggested. The most positive predictor of retention was the spatially-averaged near-bed shear stress, although again the TKE method was a poor predictor, suggesting conflicting relationships with the two measures of retention. However a relationship with the spatially-averaged Reynolds shear stress was suggested, with retention increasing at the shear stress immediately upstream of the boulder nears zero, with positive and negative shear stresses resulting in a decrease in retention.

7

CONCLUSIONS

The previous chapters have presented a series of flume experiments that have investigated various physical and hydraulic factors suggested to affect the retention of leaves within streams. The seasonal dependence of temperate stream ecosystems on inputs of allochthonous matter, for both sources of carbon and nutrients, has been well researched. Therefore, it is surprising that the method of leaf retention has not been as well investigated. Studies have suggested links to both physical and hydraulic factors such as flow depth (e.g. Webster et al., 1994), gradient (e.g. Larrañaga et al., 2003) and the presence of retentive structures (e.g. Webster et al., 1987; Ehrman and Lambert, 1992), but only a relationship to discharge has been well reported (Webster et al., 1994; Larrañaga et al., 2003; Cordova et al., 2008; Hoover et al., 2006). The contribution of each of the presented experiments will be summarised and then ideas for future research will be discussed.

7.1 Introduction

A series of flume experiments have been presented that investigate how the retention of leaves and the flow structure vary with bed heterogeneity, boulder submergence and boulder density. Two differing experimental setups were used. The first investigated the leaf retention of a flat bed of two physically different substrates, sand and pebbles, placed in adjacent longitudinal strips under the same 'global' conditions. The second considered an idealised situation consisting of uniformly sized concrete hemispherical boulders placed in a staggered array directly on the glass flume bed. The boulders' submergence and density were varied systematically, for a constant discharge, allowing their affects on leaf retention to be identified. For each setup saturated leaves were added, with the number of leaves retained and their locations being recorded. Detailed three-dimensional velocity measurements were taken within a control volume allowing the flow structure to be characterised and the methods of retention to be proposed.

7.2 Effects of Bed Heterogeneity on Leaf Retention

Chapter 4 presented a comparison of leaf retention for two physically different bed materials, with the use of velocity measurements to identify in more detail the reason for retention at particular locations. Bed material significantly affects the retention of leaves, with greater substrate size leading to greater retention, due to the greater heterogeneity it provides even when a flat bed is considered. The small degree of variation within the bed profile due to the larger bed material was sufficient to enhance leaf retention. No single reason or method of retention could be identified for each of the four examined locations, with each having its own physical and hydraulic factor that aids retention. However, all the locations had an average flow depth greater than the global average.

The retention at two locations was attributed to the presence of distinct isolated protrusion. In this situation the flow was forced around the protrusion and over the top, creating a downward force that pushed the leaf or leaf pack onto the upstream face of the protrusion allowing it to be retained. At another location, a dead-zone was present due to the variation of bed, allowing the leaves to be retained. The last location exhibited the greatest variation within the bed height throughout the control volume, leading to this region having lower velocities throughout the velocity profile within the region of the leaf pack, which aided leaf retention. The presence of an isolated protrusion allowed the retention of larger leaf packs, illustrating the importance of these structures within streams. At all locations it is suggested that the downward force of the water flowing over the leaf pack aided retention. For one location secondary currents were observed above the leaf pack location; it is not suggested that these aid retention, but they will have consequences for other ecological distributions, for example, increased lateral diffusion of nutrients.

7.3 Effects of Boulder Submergence and Density on Leaf Retention

The importance of protrusions for retaining leaves was identified in Chapter 4, and therefore factors relative to protrusions were investigated to see how these varied leaf retention. Idealised boulders were used to represent boulders or pebble clusters in streams at known locations in order to simplify the variables present. Chapter 5 presented a series of flume experiments that systematically varied boulder submergence and boulder density, in order to analyse their effects on leaf retention. Leaf retention was significantly related to boulder density, with an optimum density for retention present. Although variation with flow depth was observed, it was found not to be significant. Density was significantly related to the retention coefficient and the mean transport distance. The area mean velocity and boulder volume fraction were both poor indicators of leaf retention; the presence of a maximum retention relationship was suggested but further investigation is required. However, when density was considered with the area mean velocity, both were significant, with the area mean velocity exhibiting a negative effect. This and the results of the flow depth experiments suggest that the well reported negative relationship between leaf retention and discharge, is more likely to be related to the associated increased velocity and not the increased flow depth.

If retention were purely due to the probability of contact with a retentive structure, then leaf retention would be a product of the boulders submergence and the number of structures present. An increase in flow depth did not harm retention, and although an increase in the number of boulders increased retention, when this effect was taken into consideration a relation between retention and boulder density was still present. Retention therefore is not purely dependent on the probability of contact. Although the number of boulders present has the ability to increase retention, the interaction between adjacent protrusions also has an effect. This interaction is not necessarily a direct effect, but is more probably due to the indirect effect on the velocity and turbulence fields that control the movements of leaves within the water column. The presence of an optimum density suggests that increased boulder density aids retention to a point, after which the interacting effect hinders retention.

7.4 Effects of Boulder Submergence and Density on Flow Structure and Wake Size

The presence of protrusions within the flow has an effect on the velocities and the distribution of turbulence within a stream. This in turn affects a number of ecological distributions, such as fish habitats (Shamloo et al., 2001), particle-particle interaction increasing nutrient dispersal and predator-prey interactions (Lacey and Nikora, 2008) and macroinvertebrate distributions (Bouckaert and Davis, 1998). Chapter 6 presented a series of flume experiments that analysed how the flow structure and turbulence field varied with boulder submergence and boulder density, comparing four flow depths and four boulder densities using detailed velocity measurements within a control volume.

The flow was divided into two layers, the boulder layer flow and the surface layer flow. In the boulder layer flow the presence of a horseshoe vortex upstream of the boulder was inferred from an upstream dead-zone, and the boulder created a wake downstream characterised by reduced streamwise velocities, and containing a recirculation zone of negative streamwise velocities. In the surface flow layer separation of the flow at the crest of the boulder generated a free shear layer including separation vortices, and near the top of the measurement volume, secondary currents characterised by strong cross-streamwise and reduced streamwise velocities were identified. The most dominant structure within the profile, and therefore the control volume for each of the flow depths and boulder density, was the secondary currents in the surface flow layer, illustrated by the greatest spatially-averaged velocity deficit and highest TKE. These currents were most pronounced in the intermediate density. The presence of the free shear layer was seen to decrease with increased boulder density, resulting in it not being present at the highest density, suggesting the formation of this structure was inhibited by increased boulder density.

The similarity between the spatially-averaged profiles of the four flow depths illustrated the repeatability in the results. However the greater variability with change in boulder density indicates a change in flow structure with increased boulder density. The presence of the secondary currents meant it was necessary to consider only the boulder flow layer when evaluating wake sizes. The wake was seen to shorten and increase laterally with increase in flow depth and boulder density. The effect was much more pronounced with change in boulder density, leading to interaction of the wake and dead-zone of adjacent boulders at the highest two densities. The increase in boulder density was also associated with increased cross-streamwise and vertical velocities due to the water being more tightly constrained by the boulders. Increased TKE was observed in the boulder wake, peaking at the dense density. Two regions upstream of the boulder were defined to create spatially-average bed shear stress values. The two methods, Reynolds stress and TKE, suggested contradictory relationships with boulder density, with the TKE method suggesting a decrease in bed shear stress with increasing boulder volume fraction, and the Reynolds method suggesting an increase. The time-averaged velocity definition provided a good estimate of wake volume, suggesting a general trend of increasing wake size with both boulder submergence and density, peaking at the dense density. The wake area generally decreased with height above the bed for both flow depth and boulder density.

Therefore an increase in boulder density was associated with an increase in wake volume, increased TKE within the wake, and increased cross-streamwise and vertical velocities. The flow structures within the surface layer flow decreased in strength with an increase in density, peaking at the intermediate density. The flow structure changed with density, with the boulders acting in isolation at the lower two densities, sparse and intermediate, and wake-interacting flow present at the higher two densities, dense and very dense.

7.5 Effects of physical and hydraulic factors on Leaf Retention

In order to suggest a possible mechanism of retention the results presented in Chapters 5 and 6 were drawn together. A number of parameters that were calculated to describe the flow conditions were investigated as possible predictors of retention. It was found that the globally-averaged streamwise velocity and the WVF were both poor predictors of retention, with no definitive relationship being visible, showing that a general characteristic of the flow structure could not be used to describe retention. The spatially-averaged Reynolds shear stress, that was calculated immediately upstream of the boulder, did prove to be a good predictor of the retention, with retention increasing as the shear stress neared zero, and decreasing with increased positive and negative shear stresses.

It is therefore concluded that the retention of leaves with streams is affected by a number of interacting factors. It has been shown that retention increases with increase bed heterogeneity, with only small changes in the substrate needed for increased retention. The importance of the presence of protrusions on retention has been illustrated, with an increase in the number of protrusions increasing retention. Retention is aided with increase in density while the protrusions remain independent, but interaction of the protrusions leads to a decrease in retention. The near-bed shear stress immediately upstream of the boulder affects retention, with large positive or negative shear stresses reducing retention.

7.6 Future Research

Leaf retention and velocity measurements were examined over a limited range of both boulder submergences and densities leading to a limited ability to infer direct relationships. Some interesting relationships have been identified, however each of these needs to be investigated further in order for more definite conclusions to be drawn. The retention of leaves needs to be investigated over a wider range of both flow depth and boulder density to identify if flow depth is a limiting relationship and whether there is an optimum density for retention. Velocity measurements should concentrate on upstream of the boulder, calculating the bed shear stress and also the shear stress present on the upstream face of the boulder, both of which can then be related to retention, to determine whether zero bed shear stress is optimal for retention. Analysis of the velocities over the whole control volume would allow indication of whether the optimum retention density did in fact correspond to limit at which the boulders are acting independently.

The transport of sediment is affected by its properties, and hydraulic characteristics, such as velocity, and is well described by the shields diagram. In order to understand how the hydraulic factors might control retention, a better understanding of how the leaf and water interact needs to be investigated. This would involve investigating the buoyancy of leaves, and how this changes with saturation. Also, the flexibility of the leaf, and therefore its ability to 'wrap' around a protrusion and be manipulated by the water. Visual observations during the experiments conducted in this thesis, found that saturated leaves travel near the flume bed, being rolled over by the water. If the leaf was travelling with the largest surface perpendicular to the bed, then the top of the leaf will be in a higher region of the velocity profile than the bottom, and therefore the top will be subject to higher velocities and forces, causing the leaf to roll. The investigation of this theory and the identification of the forces acting on a leaf will help understand the factors that will affect its retention.

Nepf et al. (1997) used a random walk model to model the diffusion of particles through an array of stems, using the wake area fraction to describe the degree of lateral movement. The use of the same model should be used to predict the retention of leaves for different boulder sizes and configurations. The use of different factors, such as the streamwise, cross-streamwise and vertical velocity in the wake region and in the free flow, the wake volume fraction, and bed shear stress, could be investigated. Being able to model the retention would give a better understanding of the factors that are important for leaves to be retained.

This thesis has concentrated on the hydraulic and physical factors that influence leaf retention at particular locations. The time series process of leaf pack formation was not considered. The formation of a leaf pack is an iterative process, as the retention of a single leaf will change the hydraulic and physical conditions at a location, which will then either increase or decrease the probability of another leaf being retained and so on. Analysis of the process of leaf pack formation will allow a better understand of the factors involved, whether that once one leaf has been retained, retention becomes easier or harder. This will have implications for river restoration, as to whether multiple regions capable of retaining just a few leaves is the best course of action, or a few regions that can support large leaf packs.

The results of this research not only pose future research questions for this field, but also might influence other areas of Ecohydraulics. Isolated boulders are important habitat features for fish within streams (Shamloo et al., 2001) providing feeding and resting opportunities. The characterisation of the flow structure in the presence of boulders suggested the presence of a free shear layer downstream of the crest of the boulder at the sparse density. This region of reduced and negative velocities was found to be approximately 300mm long and 70mm in height, which is in the region of the size of a brown trout (Armstrong et al., 2003). The presence of this region allows the fish to rest due to the reduced velocities, it has the ability to 'hide' from predators behind the boulder, and it provides a good feeding location as particulates within the flow will be forced up and over the boulder directly towards the fish. However the size, and degree of velocity reduction of this region was seen to be affected by boulder density, with a reduction in their presence with increased density. Therefore for river restoration and the restoration of fish habitats to be successful, further knowledge needs to be obtained as to the effects of boulder density on the presence of fish resting habitats.

BIBLIOGRAPHY

Aberle, J., Koll, K. and Dittrich, A. (2007), Analysis of form induced stresses over rough gravel-bed armour layers, *in* '33rd International Association of Hydraulic Research Congress'.

Acarlar, M. S. and Smith, C. R. (1987), 'A study of hairpin vortices in a laminar boundary layer. Part 1 hairpin vortices generated by a hemisphere protuberance', *Journal of Fluid Mechanics* **175**, 1–41.

Armstrong, J., Kempa, P., Kennedy, G., Ladle, M. and Milner, N. (2003), 'Habitat requirements of atlantic salmon and brown trout in rivers and streams', *Fisheries Research* **62**, 143–170.

Best, J. (2005), 'The fluid dynamics of river dunes: A review and some future research directions', *Journal of Geophysical Research* **110**, F04S02.

Biron, P. M., Lane, S. N., Roy, A. G., Bradbrook, K. F. and Richards, K. S. (1998), 'Sensitivity of bed shear stress estimated from vertical velocity profiles: The problem of sampling resolution', *Earth Surface Processes And Landforms* **23**, 133–139.

Biron, P. M., Robson, C., Lapointe, M. F. and Gaskin, S. J. (2004), 'Comparing different methods of bed shear stress estimates in simple and complex flow fields', *Earth Surface Processes and Landforms* **29**, 1403–1415.

Bocchiola, D., Rulli, M. C. and Rosso, R. (2006), 'Transport of large woody debris in the presence of obstacles', *Geomorphology* **76**, 166–178.

Bouckaert, F. W. and Davis, J. (1998), 'Microflow regimes and the distribution of macroinvertebrates around stream boulders', *Freshwater Biology* **40**, 77–86.

Buffin-Bélanger, T. and Roy, A. G. (1998), 'Effects of a pebble cluster on the turbulent structure of a depth-limited flow in a gravel-bed river', *Geomorphology* **25**, 249–267.

Canovaro, F. and Francalanci, S. (2008), Experimental observations of flow field around macro-scale roughness, *in* 'Proc. Int. Conf. on Fluvial Hydraulics River Flow 2008, 3-5 September 2008, Cesme, Turkey', pp. 419–424.

Canovaro, F., Paris, E. and Solari, L. (2007), 'Effects of macro-scale bed roughness geometry on flow resistance', *Water Resources Research* **43**(W10414), 1–17.

Chadwick, A., Morfett, J. and Borthwick, M. (2004), *Hydraulics in Civil and Environmental Engineering*, 4th edn, Spon Press.

Chow, V. T. (1959), *Open-Channel Hydraulics*, McGraw-Hill Book Company, Inc.

Cordova, J. M., Rosi-Marshall, E. J., Tank, J. L. and Lamberti, G. A. (2008), 'Coarse particulate organic matter transport in low-gradient streams of the Upper Peninsula of Michigan', *Journal of the North American Benthological Society* **27**(3), 760–771.

Cummins, K. W. (1974), 'Structure and function of stream ecosystems', *BioScience* **24**, 631–641.

Cummins, K. W., Cushing, C. E. and Minshall, G. W. (1995), An overview of stream ecosystems, *in* 'River and Stream Ecosystems', Elsevier.

Cummins, K. W., Petersen, R. C., Howard, F. O. and Wuycheck, J. C. (1973), 'The utilization of leaf litter by stream detritivores', *Ecology* **54**(2), 336–345.

Davis, J. A. and Barmuta, L. A. (1989), 'An ecologically useful classification of mean and near-bed flows in streams and rivers', *Freshwater Biology* **21**, 271–282.

Dolédec, S., Lamouroux, N., Fuchs, U. and Mérigoux, S. (2007), 'Modelling the hydraulic preferences of benthic macroinvertebrates in small European streams', *Freshwater Biology* **52**(1), 145–164.

Douglas, J., Gasiorek, J. M. and Swaffield, J. A. (2001), *Fluid Mechanics*, 4th edn, Prentice Hall.

Edington, J. M. (1968), 'Habitat preferences in net-spinning caddis larvae with special reference to the influence of water velocity', *The Journal of Animal Ecology* **37**(3), 675–692.

Ehrman, T. P. and Lambert, G. A. (1992), 'Hydraulic and particulate matter retention in a 3rd-order Indiana stream', *J. N. Am. Benthol. Soc.* **11**, 341–349.

Engel, P. (1981), 'Length of flow seperation over dunes', *Journal of the Hydraulics Division* **107**(10), 1133–1143.

Finelli, C. M., Hart, D. D. and Fonseca, D. M. (1999), 'Evaluating the spatial resolution of an acoustic doppler velocimeter and the consequences for measuring near-bed flows', *Limnology Oceanographer* **44**(7), 1793–1801.

Fisher, S. G. and Likens, G. E. (1973), 'Energy flow in Bear Brook, New Hampshire: An integrative approach to stream ecosystem metabolism', *Ecological Monographs* **43**(4), 421–439.

Gessner, M. O. and Chauvet, E. (1994), 'Importance of stream microfungi in controlling breakdown rates of leaf litter', *Ecology* **75**, 1807–1817.

Giller, P. S. and Malmqvist, B. (1998), *The Biology of Streams and Rivers*, Oxford Univeristy Press.

Hart, D., Clark, B. and Jasentuliyana, A. (1996), 'Fine-scale field measurement of benthic flow environments inhabited by stream invertebrates.', *Limnology and Oceanography* **41**, 297–308.

Hart, D. D. and Finelli, C. M. (1999), 'Physical-biological coupling in streams: The pervasive effects of flow on benthic organisms', *Annual Review of Ecological Systematics* **30**, 363–395.

Hladyz, S., Abjörnsson, K., Chauvet, E., Dobson, M., Elosegi, A., Ferreira, V., Fleituch, T., Gessner, M. O., Giller, P. S., Gulis, V., Hutton, S. A., Lacoursière, J. O., Lamothe, S., Lecerf, A., Malmqvist, B., Mckie, B. G., Nistorescu, M., Preda, E., Riipinen, M. P., Rîşnoveanu, G., Schindler, M., Tiegs, S. D., Vought, L. B.-M. and Woodward, G. (2011), 'Stream ecosystem functioning in an agricultural landscape: The importance of terrestrial-aquatic linkages', *Advances in Ecological Research* **44**, 211–276.

Hoover, T. M., Marczak, L. B., Richardson, J. S. and Yonemitsu, N. (2010), 'Transport and settlement of organic matter in small streams', *Freshwater Biology* **55**, 436–449.

Hoover, T. M., Richardson, J. S. and Yonemitsu, N. (2006), 'Flow-substrate interactions create and mediate leaf litter resource patches in streams', *Freshwater Biology* **51**, 435–447.

Huthoff, F. (2009), Estimating equivalent roughness lengths based on wake sizes, *in* 'Proc. 33rd IAHR Congress: Water Engineering for a Sustainable Environment, Vancouver, British Columbia, 9–14 August 2009.', pp. 1200–1207.

Hynes, H. B. N. (1970), *The Ecology of Running Waters*, Liverpool University Press.

James, A. B. W. and Henderson, I. M. (2005), 'Comparison of coarse particulate organic matter retention in meandering and straightened sections of a third-order New Zealand stream', *River Research and Applications* **21**, 641–650.

Jewett, J. W. and Serway, R. A. (2008), *Physics for Scientists and Engineers*, 7th edn, Thomson.

Kanani, A., Ahmari, H. and da Silva, A. M. F. (2010), Investigation of horizontal coherent structure in a shallow open-channel flow using velocity signal decomposition, *in* 'Proc. Int. Conf. on Fluvial Hydraulics River Flow 2010, September 8–10, Braunschweig, Germany', pp. 1059–1066.

Kim, S.-C., Friedrichs, C., Maa, J. P.-Y. and Wright, L. D. (2000), 'Estimating bottom stress in tidal boundary layer from acoustic doppler velocimeter data', *Journal Of Hydraulic Engineering* **126**(6), 399–406.

Lacey, R. and Nikora, V. I. (2008), Flow turbulence and characteristic length scales around an instream large roughness element, *in* 'Proc. Int. Conf. on Fluvial Hydraulics River Flow 2008, 3-5 September 2008, Cesme, Turkey', pp. 135–142.

Lacey, R. W. J. and Roy, A. G. (2007), ‘A comparative study of the turbulent flow field with and without a pebble cluster in a gravel bed river’, *Water Resources Research* **43**, W05502.

Lamouroux, N., Mérigoux, S., Capra, H., Dolédec, S., Jowett, I. G. and Statzner, B. (2010), ‘The generality of abundance-environment relationships in microhabitats: a comment on Lancaster and Downes (2009)’, *River Research And Applications* **26**(7), 915–920.

Lancaster, J. and Downes, B. J. (2010*a*), ‘Ecohydraulics needs to embrace ecology and sound science, and to avoid mathematical artefacts’, *River Research And Applications* **26**(7), 921–929.

Lancaster, J. and Downes, B. J. (2010*b*), ‘Linking the hydraulic world of individual organisms to ecological processes: Putting ecology into ecohydraulics’, *River Research and Applications* **26**(4), 385–403.

Larrañaga, S., Díez, J. R., Elosegi, A. and Pozo, J. (2003), ‘Leaf retention in streams of the Agüera basin (Northern Spain)’, *Aquatic Science* **65**, 158–166.

Li, R.-M. and Shen, H. W. (1973), ‘Effect of tall vegetation on flow and sediment’, *Journal of the Hydraulics Division* **99**(HY5), 793–814.

Lohrmann, A., Cabrera, R. and Kraus, N. C. (1994), Acoustic-Doppler Velocimeter (ADV) for laboratory use, *in* ‘Fundamentals and Advancements in Hydraulic Measurements and Experimentation, 1-5th August, Buffalo, New York’, pp. 351–365.

McLean, S., Nelson, J. and Wolfe, S. (1994), ‘Turbulence structure over two-dimensional bed forms: Implications for sediment transport’, *Journal of Geophysical Research* **99(6)**, 12729–12747.

Methods Of Test For Soils For Civil Engineering Purposes Part 2: Classification Tests BS1377-2 (1990).

Muotka, T. and Laasonen, P. (2002), ‘Ecosystem recovery in restored headwater streams the role of enhanced leaf retention’, *Journal of Applied Ecology* **39**, 145–156.

Nepf, H. M. (1999), ‘Drag, turbulence, and diffusion in flow through emergent vegetation’, *Water Resources Research* **35**(2), 479–489.

Nepf, H. M., Sullivan, J. A. and Zavistoski, R. A. (1997), ‘A model for diffusion within emergent vegetation’, *Limnology and Oceanography* **42**(8), 1735–1745.

Nezu, I. and Nakagawa, H. (1993), *Turbulence in Open-Channel Flows*, A.A. Balkema, Rotterdam, The Netherlands.

Nortek (2004), *Vectrino Velocimeter User Guide*, Nortek AS.

Petryk, S. (1969), Drag on cylinders in open channel flow, PhD thesis, Colorado State University, Fort Collins.

Poggi, D., Porporato, A., Ridolfi, L., Albertson, J. D. and Katul, G. G. (2004), ‘The effect of vegetation density on canopy sub-layer turbulence’, *Boundary-Layer Meteorology* **111**, 565–587.

Pokrajac, D., Campbell, L. J., Manes, C., Nikora, V. I. and McEwan, I. K. (2003), Spatially-averaged flow over ribbed roughness: A new application of quadrant analysis, *in* 'Proc. 30th IAHR Congress, Thessaloniki, Greece, 24-29 August', pp. 103–110.

Precht, E., Janssen, F. and Huettel, M. (2006), 'Near-bottom performance of the Acoustic Doppler Velocimeter (ADV) a comparative study', *Aquatic Ecology* **40**, 481–492.

Raupach, M. R. (1992), 'Drag and drag partition on rough surfaces', *Boundary-Layer Meteorology* **60**, 375–395.

Rice, S. P., Lancaster, J. and Kemp, P. (2010), 'Experimentation at the interface of fluvial geomorphology, stream ecology and hydraulic engineering and the development of an effective, interdisciplinary river science', *Earth Surface Processes and Landforms* **35**, 64–77.

Rice, S. P., Little, S., Wood, P. J., Moir, H. J. and Vericat, D. (2010), 'The relative contributions of ecology and hydraulics to ecohydraulics', *River Research and Applications* **26**, 363–366.

Rowinski, P. M., Aberle, J. and Mazurczyk, A. (2005), 'Shear velocity estimation in hydraulic research', *Acta Geophysica Polonica* **53**(4), 567 – 583.

Rusello, P. J., Lohrmann, A., Siegel, E. and Maddux, T. (2006), Improvements in acoustic doppler velocimetery, *in* 'Proc. 7th Int. Conf. on Hydroscience and Engineering, 10 - 13 Sep, Philadelphia, USA'.

Savory, E. and Toy, N. (1986), 'The flow regime in the turbulent near wake of a hemisphere', *Experiments in Fluids* **4**, 181–188.

Schlichting, H. and Gersten, K. (2000), *Boundary Layer Theory*, 8th edn, Springer.

Shamloo, H., Rajaratnam, N. and Katopodis, C. (2001), 'Hydraulics of simple habitat structures', *Journal of Hydraulic Research* **39**(4), 351–366.

Sontek (1997), *ADV Technical Documentation.*

Stoesser, T., Braun, C., Garca-Villalba, M. and Rodi, W. (2008), 'Turbulence structures in flow over two-dimensional dunes', *Journal Of Hydraulic Engineering* **134**(1), 42–55.

Tank, J. L., Rosi-Marshall, E. J., Griffiths, N. A., Entrekin, S. A. and Stephen, M. L. (2010), 'A review of allochthonous organic matter dynamics and metabolism in streams', *Journal of the North American Benthological Society* **29**(1), 118–416.

Tavakol, M., Yaghoubi, M. and Motlagh, M. M. (2010), 'Air flow aerodynamic on a wall-mounted hemisphere for various turbulent boundary layers', *Experimental Thermal and Fluid Science* **34**, 538–553.

Vannote, R., Minshall, G., Cummins, K., Sedell, J. and Cushing, C. (1980), 'The river continuum concept', *Canadian Journal of Fisheries and Aquatic Sciences* **37**, 130–137.

Vermass, D. A., Uijttewaal, W. S. J. and Hotitink, A. J. F. (2008), Effects of heterogeneous bed roughness on the momentum exchange in floodplains, *in* 'Proc. Int. Conf. on Fluvial Hydraulics River Flow 2008, 3-5 September 2008, Cesme, Turkey.', pp. 547–554.

Webster, J. R., Benfield, E. F., Ehrman, T. P., Schaeffer, M. A., Tank, J. L., Hutchens, J. J. and DAngelo, D. J. (1999), 'What happens to allochthonous material that falls into streams? A synthesis of new and published information from coweeta.', *Freshwater Biology* **41**, 687–705.

Webster, J. R., Benfield, E. F., Golladay, S. W., Hill, B. H., Hornick, L. E., Kazmierczak, R. F. and Perry, W. B. (1987), 'Experimental studies of physical factors affecting seston transport in streams', *Limnology Oceanographer* **32**(4), 848–863.

Webster, J. R., Covich, A. P., Tank, J. L. and Crockett, T. V. (1994), 'Retention of coarse organic particles in streams in the Southern Appalachian mountains', *J. N. Am. Benthol. Soc.* **13**, 140–150.

Young, S., Kovalak, W. P. and Signore, K. A. D. (1978), 'Distances travelled by autumn-shed leaves introduced into a woodland stream', *The American Midland Naturalist* **100**(1), 217–222.

Zavistoski, R. A. (1994), Hydrodynamic effects of surface piercing plants, Master's thesis, Massachusetts Institute of Technology.